



Durham E-Theses

High-resolution NMR studies of solid halogenated organic compounds

Carss, Steven Andrew

How to cite:

Carss, Steven Andrew (1995) *High-resolution NMR studies of solid halogenated organic compounds*, Durham theses, Durham University. Available at Durham E-Theses Online: <http://etheses.dur.ac.uk/5208/>

Use policy

The full-text may be used and/or reproduced, and given to third parties in any format or medium, without prior permission or charge, for personal research or study, educational, or not-for-profit purposes provided that:

- a full bibliographic reference is made to the original source
- a [link](#) is made to the metadata record in Durham E-Theses
- the full-text is not changed in any way

The full-text must not be sold in any format or medium without the formal permission of the copyright holders.

Please consult the [full Durham E-Theses policy](#) for further details.

High-resolution NMR Studies of Solid Halogenated Organic Compounds

by

Steven Andrew Carss, B.Sc.

A thesis submitted in partial fulfilment of the requirements for
the degree of Doctor of Philosophy

Department of Chemistry

University of Durham

1995

The copyright of this thesis rests with the author.
No quotation from it should be published without
his prior written consent and information derived
from it should be acknowledged.



18 MAR 1996

High-resolution NMR Studies of Solid Halogenated Organic Compounds

Steven Andrew Carss, B.Sc.

Abstract

This thesis is a study of solid halogenated organic compounds by Nuclear Magnetic Resonance Spectroscopy (NMR) in an attempt to extract previously inaccessible information.

The first part of the thesis is concerned with three fluorinated steroids, studied by observing ^1H , ^{13}C and ^{19}F nuclei. A number of experimental techniques are employed to verify solution-state and solid-state spectral assignments, and spectral anomalies are discussed. Both proton-coupled and proton-decoupled ^{19}F solid-state spectra, recorded using specially designed spectrometer hardware, are presented. The huge gain in resolution afforded by the implementation of proton decoupling allows static and MAS spectra to yield previously inaccessible information pertaining to various NMR parameters of the fluorine nuclei. Advantages of $^1\text{H} \rightarrow ^{19}\text{F}$ cross-polarisation experiments over ^{19}F single-pulse experiments are explained and rotational resonance, dipolar dephasing, T_1 measurement and spin-exchange experiments are presented from which information regarding phenomena such as spin diffusion and polymorphism is gleaned.

The second part of the thesis focusses on the topic of residual dipolar coupling, the transfer of quadrupolar effects to spin-1/2 nuclei via dipolar coupling and/or anisotropy in indirect coupling. Unexpected, field-dependent, multiplicities for signals in spectra of spin-1/2 nuclei are observed, which can be used to evaluate certain fundamental NMR parameters including the quadrupolar coupling constant and, in favourable cases, anisotropy in indirect coupling. The phenomenon is comprehensively studied for the ^{13}C , $^{35,37}\text{Cl}$ and ^{13}C , $^{79,81}\text{Br}$ spin-pairs in a range of solid halogenated compounds. Coupling to more than one halogen nucleus and long-range (non-bonded) coupling are considered. First-order perturbation, inverse first-order and "exact" theories, that allow the multiplet line positions to be predicted, are introduced and their results are subsequently compared to the experimentally observed line positions. Rapid molecular motion is shown to negate the effects of residual dipolar coupling and the phenomenon is analysed with the aid of NQR measurements.

Memorandum

The Research presented in this thesis has been carried out in the Department of Chemistry, University of Durham, between October 1992 and October 1995. Unless otherwise stated it is the original work of the author. None of this work has been submitted for any other degree.

The copyright of this thesis rests with the author. No quotation from it may be published without his prior consent and information derived from it should be acknowledged.

Acknowledgements

I would foremost like to thank my supervisor Professor R. K. Harris at the University of Durham for his constant guidance and support in all matters. I also thank Prof. A. C. Olivieri for his first-order perturbation theories, without which the research carried out on residual dipolar coupling would not have been possible, and Prof. K. D. M. Harris, and Drs. A. E. Aliev and S. H. Alarcon for their help in this field. Similarly I thank Dr. R. A. Fletton of Glaxo Wellcome for providing fluorinated steroid samples and valuable advice during a week of research conducted at Glaxo's headquarters. Technical expertise of a varying nature is greatly acknowledged from Barry Say, Dr. A. M. Kenwright, Dr D. C. Apperley, Drs. U. Scheler and R. Challoner, Nicola Davies and Julia Say.

On a more personal level I thank my fellow members of the Durham NMR group over the past three years for their friendship: Stefan, Elke, Graham, Abdul, Peter, Anna, Tim, Raouf, Se-Woung, Gary, Steve and Alison, the lads for stupendous crack, and Angela Gill for putting up with all my behavioural quirks and rugby.

Finally I acknowledge the financial support of The Durham University Isabel Fleck award, providing maintenance for the duration of my Ph. D., and The Engineering and Physical Sciences Research Council for research grants under which the NMR spectrometers were obtained.

Contents

1	Introduction	
1.1	Solid-state NMR as a Molecular Probe	1
1.2	NMR of Halogen Nuclei in the Solid State	1
1.3	Thesis Overview	3
PART I NMR Investigations of Three Pharmaceutical Fluorinated Steroids		
2	Difficulties Encountered in Retrieval of Information from ^1H, ^{13}C and ^{19}F NMR Spectra	
2.1	Introduction	8
2.2	Selective Averaging Techniques	9
2.2.1	Dipolar Coupling, High-power Proton Decoupling and Multiple-pulse Decoupling	10
2.2.2	Shielding Anisotropy and Magic-angle Spinning	12
2.2.3	Factors Affecting the Necessity to Implement Selective Averaging Techniques	14
2.3	Information Retrieval from ^1H and ^{13}C NMR Spectra	16
2.3.1	Characteristics of ^1H and ^{13}C Solution-state Spectroscopy	16
2.3.2	Aids to Spectral Assignment in ^1H and ^{13}C Solution-state NMR	17
2.3.3	Problems Inherent in ^1H and ^{13}C Solid-state NMR	21
2.3.4	Aids to Spectral Assignment in ^1H and ^{13}C Solid-state NMR	22
2.4	Information Retrieval from ^{19}F NMR Spectra	23
2.4.1	Properties of the ^{19}F Nucleus	23
2.5	Literature Review: ^{19}F Solid-state NMR	27
2.5.1	MAS-only Studies	27
2.5.2	^{19}F CRAMPS	29
2.5.3	High-power Proton Decoupling	30
3	Experimental	
3.1	Nuclei of Interest	35
3.1.1	Magnetic Properties of the Nuclei	35
3.2	Compounds	36
3.2.1	Numbering, Conformation and Stereochemistry	36
3.2.2	Nomenclature	38
3.3	Spectrometer Systems	38
3.3.1	Solution-state Spectrometers	39
3.3.2	Solid-state Spectrometers	39
3.4	Pulse Programs	40
3.4.1	Pulse Sequence Listing	40
3.4.2	Pulse Sequences Incorporating Composite Pulses	41
3.5	Spectral Considerations	43
3.5.1	Solvents and Chemical Shift References	43

3.5.2	Spectral Parameters	43
3.5.2.1	Solution-state NMR	43
3.5.2.2	Solid-state NMR	44
3.6	Spinning Sideband Analyses	45
4	^1H and ^{13}C NMR Studies	
4.1	Introduction	48
4.2	Solution-state Proton Spectra	48
4.2.1	One-dimensional Proton Spectra	48
4.2.2	Two-dimensional Proton Spectra	57
4.3	Carbon-13 Solution-state Spectra	62
4.3.1	One-dimensional Carbon-13 Spectra	62
4.3.2	Two-dimensional Carbon-13 Spectra	66
4.4	Solid-state Carbon-13 Spectra	69
4.4.1	Spectral Anomalies	70
4.4.1.1	Effects of (^1H , ^1H) Dipolar Coupling	70
4.4.1.2	Interplay of Dipolar and Shielding Tensors	71
4.4.1.3	Polymorphism Effects	74
4.5	Conclusions	75
5	^{19}F NMR Studies	
5.1	Introduction	78
5.2	Solution-state Fluorine-19 Spectra	80
5.3	Solid-state Fluorine-19 Spectra	83
5.3.1	The Effects of Proton Decoupling and MAS on Solid-state ^{19}F NMR spectra	83
5.3.2	Polymorphism	94
5.3.3	Single-pulse Excitation Versus Cross-polarisation	95
5.3.4	Shielding Tensors	97
5.3.5	Dipolar Dephasing	102
5.3.6	Spin-lattice Relaxation and Spin Diffusion	104
5.3.7	Rotational Resonance	110
5.4	Proton Solid-state NMR	112
5.4.1	Proton Single Pulse and Fluorine to Proton Cross-polarisation Experiments	112
5.5	Conclusions	114
6	^1H, ^{19}F, ^{13}C Solid-state Triple Resonance Studies	
6.1	Introduction	117
6.2	Proton to Carbon Cross-polarisation	117
6.3	Fluorine to Carbon Cross-polarisation	122
6.4	Conclusions	127

PART II Residual Dipolar Coupling Between Carbon-13 and Halogen Spins

7	Background and Theory of Residual Dipolar coupling	
7.1	Introduction	130
7.2	Factors Affecting, and the Appearance of, Lineshapes for	

	Spin-1/2 Nuclei Coupled to Quadrupolar Nuclei	134
7.3	Theoretical Predictions of the Lineshapes for Spin-1/2 Nuclei Coupled to Quadrupolar Nuclei	139
7.3.1	“Normal” First-order Theory	140
7.3.2	Application of “Normal” First-order Theory to (^{13}C , $^{35,37}\text{Cl}$) Residual Dipolar Coupling	142
7.3.3	The Exact Approach and its Application to (^{13}C , $^{35,37}\text{Cl}$) Residual Dipolar Coupling	143
7.3.4	“Inverse” First-order Theory: Application to (^{13}C , $^{79,81}\text{Br}$) Residual Dipolar Coupling	145
7.3.5	Comparison of Line Positions Predicted by Derived Analytical Equations and Full-matrix Diagonalisation	145
7.3.6	The Effects of Anisotropy in Indirect Coupling	149
7.4	“Self-decoupling”	149
7.5	Coupling to (Several) Remote Quadrupolar Nuclei	151
7.6	Background of Residual Dipolar Coupling	153
8	Experimental Aspects	
8.1	Nuclei of interest	160
8.1.1	Magnetic Properties of the Nuclei	160
8.2	Compounds	163
8.2.1	Properties and Numbering of Compounds Investigated for Second-order Quadrupolar (SOQ) Effects	163
8.3	Spectrometer Systems	165
8.4	Spectral Considerations	166
8.4.1	Solvents and Chemical Shift References	166
8.4.2	Spectral Parameters	166
8.5	Computer Lineshape Fitting and Simulations	167
9	(^{13}C, $^{35/37}\text{Cl}$) Residual Dipolar Coupling in Solid Sodium Chloroacetates	
9.1	Introduction	169
9.2	Variable-field Studies of Sodium Monochloroacetate	171
9.2.1	Experimental Results	171
9.2.2	Comparison of Experimentally Observed and Theoretically Predicted Splittings	174
9.2.2.1	Evaluation of Required Parameters	174
9.2.2.2	Comparison of Experimental and Predicted Results	176
9.3	Variable-field and Temperature Studies of Sodium Di- and Trichloroacetate	180
9.3.1	Predicted Appearance of Spectra	180
9.3.2	75.43 MHz Variable-temperature Spectra of Sodium Di- and Trichloroacetate	180
9.3.3	Motional Effects on (^{13}C , $^{35,37}\text{Cl}$) Residual Dipolar Coupling in Sodium Di- and Trichloroacetate	183
9.3.4	50.33 MHz Spectra of Sodium Di- and Trichloroacetate	184
9.3.5	Explanation of Absence of Expected Multiplicities in Spectra of Sodium Di- and Trichloroacetate	187

9.4	Conclusions	191
9.5	Acknowledgements	192
10	(¹³C, ^{79,81}Br/¹²⁷I) Residual Dipolar Coupling in Halogenated Aromatic and Related Compounds	
10.1	Introduction	194
10.2	(¹³ C, ^{79,81} Br) Residual Dipolar Coupling in 1,4-Dibromobenzene)	194
10.2.1	Fundamental Parameters	194
10.2.2	50.33 MHz Experimental Results	195
10.2.3	Theoretical Predictions of Line Positions	197
10.2.3.1	Inverse First-order Theory	197
10.2.3.2	Exact Theory	199
10.2.3.3	Fitting to Polynomial Expression	200
10.2.4	75.43 MHz Experimental Results	200
10.2.5	Theoretical Predictions of Line Positions	202
10.2.6	Comparisons and Explanation of Accuracy of Fit for Experimental and Calculated Line Positions	202
10.2.7	Simulation of Theoretical Powder Patterns and Factors Affecting the Accuracy of the Simulation	203
10.3	(¹³ C, ^{79,81} Br) Residual Dipolar Coupling in 1,3,5-Tri-, 1,2,4,5-Tetra- and Hexabromobenzene - The Effects of Remote Interactions	206
10.3.1	1,3,5-Tribromobenzene	206
10.3.2	1,2,4,5-Tetra- and Hexabromobenzene	208
10.4	Other Brominated Compounds	211
10.4.1	4-Bromo,-3,5-dimethylpyrazole	211
10.4.2	1-Bromo,4-chlorobenzene	213
10.5	Unfavourable Cases: Motion-induced Suppression of Predicted Multiplets	215
10.5.1	Sodium Monobromoacetate	215
10.5.2	1-Bromoadamantane	216
10.6	Iodinated Compounds	218
10.7	Conclusions	219
10.8	Acknowledgements	221

Chapter 1

Introduction

1.1 Solid-state NMR as a Molecular Probe

Nuclear magnetic resonance (NMR) spectroscopy of the solid-state has, over the years, developed into a powerful analytical tool, not only in the sense of molecular structure elucidation, but also as a means of determining the magnitude and sign of many internuclear interactions. Such information is only available where there exists, within the system under study, suitable nuclei to act as probes. Nowadays, a whole plethora of techniques are available to enable high-quality, high-resolution, and thus informative, spectra to be obtained from a wide variety of problematic nuclei. For example, pulsed FT NMR combined with cross-polarisation (CP)¹ and magic-angle spinning (MAS)² is now used routinely to overcome the problems posed by relatively NMR-insensitive nuclei such as ¹³C and ¹⁵N in solids. There still exists, however, certain areas of experimental difficulty, where extraction of informative data is arduous due to properties intrinsic to the nuclei or systems under study. Two such areas of experimental difficulty that arise concern the direct observation of nuclei of the elements contained in group 17 of the periodic table, the halogens.

1.2 NMR of Halogen Nuclei in the Solid State

Halogenated compounds display both great ubiquity and diversity in chemistry today, their uses ranging from synthetic pre-cursors to compounds of pharmaceutical importance. It is therefore unfortunate that the direct observation of the halogen nuclei in these compounds by NMR in the solid-state, and subsequent acquisition of valuable NMR parameters, is blighted by problems inherent to these nuclei. The



heavier halogen nuclei, chlorine, bromine and iodine, each possess a nuclear quadrupole moment, $S = 3/2$, $3/2$ and $5/2$ respectively, giving rise to a quadrupolar interaction which frequently exceeds the Zeeman interaction in magnitude, thus making their resonances broad and uninformative. Conversely, solid-state fluorine-19 NMR is plagued by problems arising due to the presence of strong dipolar interactions (both homonuclear and heteronuclear) between nuclei, leading to significant line broadening. Such interactions are commonplace in simple poly-fluorinated organic compounds. Averaging of these interactions to zero by rapid isotropic molecular tumbling, as experienced in the solution state, does not occur, since in the solid state molecules are held rigidly in the lattice, undergoing little motion. Consequently these large interactions overwhelm the fine structure of interest, similarly making spectra broad, featureless and uninformative. Suppression of homonuclear dipolar interactions, where there exists in the sample under study contiguous fluorine nuclei, can be achieved via combined rotation and multiple-pulse spectroscopy (CRAMPS)³, but suppression of (^1H , ^{19}F) heteronuclear dipolar interactions, in systems containing abundant protons, has been thought to be less straightforward. The usual method of suppressing analogous interactions in, for example, carbon-13 solid-state NMR, is to employ high-power proton decoupling (HPPD).⁴ For fluorine solid-state NMR, complications exist with the implementation of HPPD associated with the close proximity of the fluorine and proton resonance frequencies (approximately six percent apart) in conjunction with the large powers required. This imposes technically challenging constraints on the feasibility of acquiring proton-decoupled fluorine solid-state spectra.

As is apparent, therefore, the extraction of useful information from solid-state NMR spectra of either type of halogenated system by direct observation of the halogen nuclei is not a trivial matter.

1.3 Thesis Overview

This thesis is a record of the attempts made to extract data, previously either impossible or difficult to obtain, concerning various nuclear and internuclear parameters, from a selection of halogenated compounds. On the one hand, in the case of fluorinated systems, the problems associated with extraction of useful information directly from ^{19}F NMR have been overcome by technical advances in hardware design, whereas on the other hand, in the case of systems containing quadrupolar nuclei, these problems have been solved not by observing the quadrupolar nuclei directly, but via an indirect approach. The extraction of information is accomplished via the analysis of a phenomenon (only recently discovered for Cl, Br and I) in which the effects of quadrupolar nuclei are transmitted to other nearby nuclei. This phenomenon has been studied at length, and many articles existing in the literature provide an insight into it.^{5,6}

The thesis is sub-divided into two main parts, each part dealing with one of the two types of halogenated system mentioned above. The first half of the thesis is concerned with NMR studies, both in the solid state and solution state, of a group of structurally similar fluorinated steroids of pharmaceutical interest. Firstly, the routine observation of proton and carbon spectra are reported, and associated points of interest and anomalies in the spectra discussed. In particular, the difficulties encountered in obtaining accurate assignments of the carbon solution-state and solid-state spectra are highlighted. Spectra and tables of chemical shifts and indirect (J) coupling constants are given. Secondly, direct observation of the fluorine nucleus is considered along with both the origin and circumvention of the aforementioned problems in the solid state relating to the difficulties in implementing HPPD. As mentioned previously, specialised hardware, that has only recently become commercially available, is used to overcome these problems, the technical details of which are discussed. The systems studied have been deliberately chosen to contain fluorines which are well separated, so that there are only modest (^{19}F , ^{19}F) dipolar

interactions. This obviates the need for multiple-pulse operation, *i.e.* magic-angle rotation at modest speeds suffices to average such homonuclear coupling. Experimental techniques, for many years of scant value for such systems, but now worthwhile due to the improvement in resolution afforded by the implementation of HPPD, are subsequently discussed. Information from such spectra, which was previously unavailable given the poor resolution inherent in non-proton-decoupled fluorine spectra of compounds containing abundant protons, such as shielding information, is presented. Finally, research carried out using an HFX triple-resonance probe is presented. Observation of the carbon nucleus is investigated with cross-polarisation from both the protons and fluorine nuclei performed. For both methods of cross-polarisation single-channel decoupling of the fluorines and protons separately along with dual-channel decoupling is considered. Relevant spectra are presented and the results evaluated.

The second part of the thesis focuses on NMR of systems containing the heavier quadrupolar halogen nuclei. Information on certain internuclear parameters, inherently difficult to obtain, is accessed by observation of the phenomenon of second-order quadrupole effects transferred from the halogen nuclei chlorine, bromine and iodine, to the spin-1/2 nucleus carbon. The quadrupolar effects are transmitted via dipolar coupling, and anisotropy in indirect coupling. Consequently, with the correct analysis of the spectra, valuable information about direct and indirect coupling interactions between halogen and carbon nuclei can be gleaned. Information on halogen-carbon indirect coupling is particularly valuable since in the solution state all information is usually lost due to rapid motion causing fast quadrupole relaxation, and, in the solid state resolution is generally too poor to allow the observation of interactions of such a small magnitude.

Second-order effects of all three quadrupolar halogen nuclei are examined for a range of simple halogenated compounds, although, due to the properties of the individual nuclei, the research concentrates on the effects of chlorine and bromine. Various theories are presented to predict the splittings observed. Computer

simulations have been devised to evaluate the best fit of the direct and indirect coupling constants both in simple mono-halogenated compounds and in poly-halogenated systems. In some cases the effects of next-nearest neighbours on the carbon resonances have to be taken into consideration. Not all halogenated systems are suitable for such investigations due to a phenomenon termed "self-decoupling", where the expected splittings collapse due to fast quadrupolar relaxation, often as a result of some type of motion. "Self-decoupling" is more prevalent for the heavier nuclei, and these effects have been studied by variable-temperature NMR. In addition, a limited amount of work is presented on direct observation of the chlorine-35 nucleus.

At the start of each of the two parts, i.e. Chapters 2 and 7, is presented a brief introduction to the underlying theory applicable in addition to a literature review outlining research that has been carried out to date in similar fields. Chapters 3 and 8 then give a detailed account of the various experimental aspects of the work undertaken, such as the compounds studied, the spectrometer systems used, and the pulse sequences implemented, in both lines of research. Subsequent to the experimental chapters, chapters 4, 5 and 6 are concerned with work conducted on the fluorinated pharmaceutical steroids and make up the results and discussion section of part I of the thesis, whilst chapters 9 and 10 focus on compounds displaying halogen-carbon residual dipolar coupling, and make up the corresponding section in part II. At the end of each of the results and discussion chapters is contained a brief conclusions section recapitulating the fundamental points that have emerged.

References

1. A. Pines, M. G. Gibby and J. S. Waugh, *J. Chem. Phys.*, **59**, 569 (1973).
2. E. R. Andrew, A. Bradbury and R. G. Eades, *Nature*, **182**, 1659 (1958); **183**, 1802 (1959).
3. J. S. Waugh, L. M. Huber and U. Haeberlen, *Phys. Rev. Lett.*, **20**, 180 (1968).
4. D. E. Demco, J. Tegenfeld and J. S. Waugh, *Phys. Rev.*, *B* **11**, 4133 (1975).
5. P. Grondona and A. C. Olivieri, *Concepts in Magnetic Resonance*, **5**, 319 (1993).
6. A. C. Olivieri, *J. Magn. Reson.*, **81**, 201 (1989).

Part I

NMR Investigations of Three Pharmaceutical Fluorinated Steroids

Chapter 2

Difficulties Encountered in Retrieval of Information from ^1H , ^{13}C and ^{19}F NMR Spectra

2.1 Introduction

The NMR phenomenon is dependent on the property of nuclear spin, and it is transitions between the nuclear spin energy levels that give rise to the NMR signal. The exact energies of the transitions observed in NMR experiments are dependent upon the nuclear spin Hamiltonian, which contains terms that account for all internal and external interactions of the spin system under study, and can be represented by the following sum:

$$\mathcal{H} = \mathcal{H}_Z + \mathcal{H}_{\text{r.f.}} + \mathcal{H}_{\text{CS}} + \mathcal{H}_{\text{Q}} + \mathcal{H}_{\text{SR}} + \mathcal{H}_{\text{D}} + \mathcal{H}_{\text{J}} \quad (2.1.1)$$

In the above expression the first two terms, \mathcal{H}_Z and $\mathcal{H}_{\text{r.f.}}$ represent the influences of the (static) magnetic field (B_0) of the spectrometer and the r.f. magnetic field respectively, which are referred to as the external interactions, since they are under the control of the experimenter. The remaining terms pertain to, from left to right, interactions of nuclear spins with the induced magnetic fields due to orbital electronic motions (chemical shift), electric field gradients (quadrupolar coupling), the magnetic moments associated with molecular angular momentum (spin rotation) and each other directly through their magnetic dipole moments (dipolar coupling), and indirectly via electron spins (scalar J coupling). These terms make up the internal interactions, so named as they are an inherent property of the particular spin system. Some of them cause shifts whilst others cause broadening of the NMR lines.

In a liquid sample all interactions are averaged to their isotropic values due to rapid, isotropic, reorientational and translational molecular motion. The isotropic averages of anisotropic interactions such as shielding anisotropy, dipole-dipole interactions, quadrupole interactions etc. are zero, which means the internal Hamiltonian in a liquid sample is represented only by the interactions having non-zero isotropic averages, namely those of shielding and indirect spin-spin coupling. The averaging of the interactions occurs because, to first order, they all have the same orientation-dependence, of the form $(3 \cos^2 \theta - 1)$, the isotropic average of which can be shown to be zero, where θ represents the angle between B_0 and a local molecule-fixed direction. The outcome of this motional averaging is that, although the positions of the NMR lines in spectra of liquids can be measured with high precision, no information about any kind of anisotropic interaction of the spins, such as shielding anisotropy, is generally available, i.e. valuable information is lost. Spectral information concerning such anisotropic interactions can be obtained mainly from NMR spectra of solids, where no isotropic molecular motions are present. Unfortunately, however, the absence of such motion in the solid state itself means that lines in solid-state spectra are broad, primarily as a result of dipole-dipole interactions, and the desired information cannot be extracted. In order to access this information experimentally a number of ingenious schemes have been invented that rely on introducing 'motional averaging' not by isotropic motions, but by more specific anisotropic motions. Collectively these techniques are termed "selective averaging" since the aim is to selectively average those interactions that are not of interest whilst retaining those that are.

2.2 Selective Averaging Techniques

Of the techniques that exist today to selectively suppress the various interactions represented in equation 2.1.1, leading to the acquisition of high-resolution NMR spectra from solid samples, only those that have been implemented in

the research presented in this thesis, namely those to suppress heteronuclear dipolar interactions and shielding anisotropies, are discussed in any great detail in the following sections.

2.2.1 Dipolar Interactions, High-power Proton Decoupling and Multiple-pulse Decoupling

The dipolar interaction is an important interaction for NMR and especially in the context of this thesis, as its presence is vital to the success of a great number of experiments presented in the following chapters. Although the cross-polarisation, dipolar dephasing, 2-D spin-exchange and rotational resonance experiments are only possible due to the existence of dipolar interactions between nuclei, it is this interaction that is usually the one most responsible for spectral broadening in the solid state, a point mentioned in the previous section and emphasised by spectra presented in chapter 5.

A physical model of the internuclear dipolar interaction on a macroscopic scale would be the interaction between two small bar magnets. Each magnet has associated with it a magnetic field which can interact with the magnetic field of the other magnet. Any spinning charged particle (i.e. a nucleus) also acts as a magnet, generating a local magnetic field, which can similarly interact with dipolar fields of neighbouring nuclei. It is the interaction of these dipolar fields that is the prime cause of spectral broadening commonly encountered in solid-state NMR of microcrystalline powdered samples. Although dipolar broadening is useful when addressing questions involving molecular motion, its observation is generally a bane, since it obscures the structurally relevant chemical shift and indirect coupling information so useful in structure elucidation. It is therefore advantageous to be able to nullify its effects and allow high-resolution solid-state spectra to be acquired from which the relevant information can be easily extracted.

Dipolar coupling can be divided into two broad categories: Homonuclear dipolar coupling refers to coupling between like nuclei, (e.g. ^1H , ^1H), whereas

heteronuclear dipolar coupling occurs between nuclei of different isotopes or elements (e.g. ^1H , ^{13}C). It is of paramount importance to differentiate between these two modes since, although they arise from the same phenomenon, different selective averaging techniques must be implemented to effect their suppression.

Heteronuclear dipolar decoupling is effected by double-irradiation techniques, in much the same way as is commonly performed in solution-state NMR studies to decouple indirect (scalar) spin-spin interactions. However, the distinction between double-irradiation techniques in the two states should be clarified. Magnitudes of indirect spin-spin interactions are generally no larger than tens or hundreds of Hz, depending on the spin-pair, and efficient decoupling is possible using radiofrequency powers of the orders of 1-2 W. As mentioned previously, there is no manifestation of dipolar interactions in resonance frequencies for the solution state since they are averaged to zero by rapid isotropic motions. However, in the solid state the lack of motion means heteronuclear dipolar interactions predominate, and since they can frequently be of the order of tens of kHz much higher powers are required to suppress them. Heteronuclear dipolar interactions involving protons are amongst the largest encountered, and consequently for systems containing abundant protons, such as simple organic compounds, powers of 100-150 W are commonly needed to effect efficient decoupling. Hence the term High-Power Proton Decoupling (HPPD).

Achieving homonuclear dipolar decoupling is not so straightforward, as is apparent when consideration is given to the fact that trying to observe a proton signal whilst simultaneously decoupling at the same frequency is not feasible. Consequently, more ingenious techniques have been developed to suppress these homonuclear dipolar interactions. Multiple-pulse decoupling effects 'averaging in spin space' by manipulating the spin system using trains of r.f pulses having different but specific phases. At certain instances during the pulse sequence, referred to as detection points, the effect of the dipolar Hamiltonian on the magnetisation is zero and consequently homonuclear dipolar interactions are suppressed. There are many stringent criteria that must be fulfilled for the technique to work effectively, such as precision in the

powers and timing of the individual pulses, and for this reason it is a very technically demanding technique requiring the use of specialist equipment.

2.2.2 Shielding Anisotropy and Magic-angle Spinning

As was mentioned in section 2.1, the only manifestation of the shielding interaction in solution-state NMR spectra is through its isotropic value σ_{iso} . However, because the shielding interaction is generally anisotropic in the solid state, i.e. its value is orientation dependent, for a microcrystalline powder which contains all possible orientations of molecules distributed at random, not a single value of the chemical shift is observed but a range of shifts. The resultant bandshape is termed a shielding anisotropy powder pattern and contains information pertaining to the symmetry at the nuclear site. A nuclear environment can have its shielding characterised by three or less unique values. These three values refer to the principal components of the shielding tensor and can be extracted from the spectrum of a powdered sample. The orientation dependence of the shielding interaction can easily be understood in terms of the non-spherical distribution of electrons around the nucleus, contained in the various molecular orbitals. When there is cubic symmetry around the nuclear site, i.e. a spherical distribution of electrons, a distinctive sharp resonance is observed at the isotropic chemical shift. Figure 2.2.1 is a diagrammatic representation of the shielding anisotropy powder patterns that would be expected from nuclei in sites possessing no symmetry, axial symmetry and cubic symmetry.

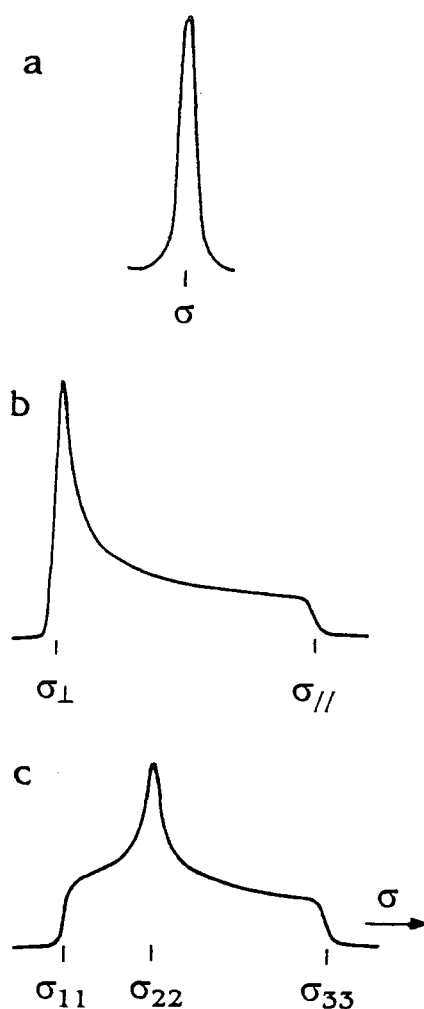


Figure 2.2.1 Diagrammatic representation of the powder patterns caused by shielding anisotropy for a nuclear site with (a) cubic symmetry, (b) axial symmetry, (c) lower symmetry.

As the shielding interaction displays a $(3 \cos^2 \theta - 1)$ geometric dependence it is possible to reduce the powder pattern arising from a static spectrum (i.e. the collection of every conceivable chemical shift arising from every possible molecular orientation) to its isotropic chemical shift by rapidly rotating the sample about an axis at an angle 54.7° to the static magnetic field B_0 , provided that the rate of rotation is greater than the width of the powder pattern. The angle 54.7° is known as the 'magic angle' and consequently the technique as magic-angle spinning. If rates less than this value are used (but greater than the intrinsic linewidth) the powder pattern will break

up into a spinning sideband manifold, that is a peak at the isotropic chemical shift and sidebands separated by integral values of the spinning rate from the centre. These spinning sidebands may extend slightly further than the apparent limits of the powder pattern in the static spectrum.

One other consequence of performing MAS is that because to first-order both homonuclear and heteronuclear dipolar interactions have a $(3 \cos^2 \theta - 1)$ geometric dependence these too are suppressed to some extent by the anisotropic motion. Ultimately, if it was possible to spin at rates greater than the static bandwidth of the dipolar coupled spectrum, which would mean spinning at rates approaching 40 kHz, suppression of these interactions would be observed. At the moment spinning at such rates is technically impossible, but spinning at rates substantially lower than these is known to have some effect on the strengths of the dipolar interactions operating between nuclei. This idea is further investigated in chapter 5.

2.2.3 Factors Affecting the Necessity to Implement Selective Averaging Techniques

It is important to realise that the selective averaging techniques presented in the previous section can be, and may need to be, implemented either separately or concurrently, depending on the type of information required and the nature of the system under investigation. Invariably in solid-state NMR the goal is to achieve as high a degree of resolution as is possible, perhaps in order to differentiate between nuclei in very similar chemical environments, and in such cases the simultaneous application of a number of the selective averaging techniques would be the approach adopted. However, if information regarding the principal components of the shielding tensor for a particular nucleus was required then one would acquire the spectrum with a static sample, implementing only HPPD and/or multiple pulse decoupling to suppress dipolar interactions. These considerations are demonstrated in chapter 5, where ^{19}F solid-state NMR spectra of the three pharmaceutical steroids are presented using different combinations of selective averaging techniques.

The importance of the chemical nature of the compound can be explained as follows. If a compound contains, let's say, carbon atoms together with abundant protons, as is generally the case with most organic compounds, to obtain a high-resolution ^{13}C solid-state NMR spectrum HPPD would normally be carried out in conjunction with MAS to suppress (^{13}C , ^1H) heteronuclear dipolar interactions and ^{13}C shielding anisotropies respectively. There would be no need to apply homonuclear dipolar decoupling in the form of multiple-pulse sequences on the ^{13}C channel, because (^{13}C , ^{13}C) dipolar coupling is generally weak because of the low natural abundance of ^{13}C . However, situations may arise where heteronuclear dipolar interactions are averaged by some kind of molecular motion, as may occur in many polymeric species, and in these instances it may not even be necessary to apply HPPD, but only MAS, in order to obtain a high-resolution spectrum.

These selective averaging techniques are widely applicable, and assist greatly in the extraction of information from systems containing a wide variety of different nuclei, in NMR of the solid state today. In carbon-13 solid-state NMR their implementation poses no major problems and they are now performed routinely. Proton solid-state NMR experiments generally require the implementation of multiple-pulse sequences to suppress homonuclear dipolar interactions and although this technique is technically demanding, as was stated previously, such experiments are performed, albeit less frequently. In the case of fluorine solid-state NMR, however, things are not so straightforward. An unforeseen difficulty arises concerning the implementation of one particular selective averaging technique due to properties intrinsic to the fluorine nucleus. This difficulty has meant very little solid-state ^{19}F NMR employing HPPD has been performed to date. The nature, origin and circumvention of the difficulty is considered in detail later in the chapter, but first somewhat more general problems, encumbering the retrieval of information from NMR spectra of all directly observed nuclei discussed in chapters 4, 5 and 6 and pertaining to both solid-state and solution-state NMR studies, are addressed.

2.3 Information Retrieval from ^1H and ^{13}C NMR Spectra

2.3.1 Characteristics of ^1H and ^{13}C Solution-state NMR Spectroscopy

In the solution state, acquisition of simple proton NMR spectra is relatively straightforward and quick and, due to the indirect coupling interactions that exist between protons, a large amount of structural information is contained therein. However, unfortunately, for structurally complex molecules, the small chemical shift range experienced by the proton leads to frequent signal overlap, making the deciphering of such information difficult. The situation is eased somewhat in these instances by integrating signal intensities to ascertain how many overlapping resonances are contained in any region of the spectrum, but detailed analyses of multiplet structures are still sometimes rendered problematic. Integration of peaks that are not obscured is also of great use in the assignment of proton spectra, due to the propensity for protons to display magnetic equivalence, for example in methyl groups.

Conversely, carbon solution-state NMR is much more time consuming, and (^{13}C , ^{13}C) indirect coupling is usually unobservable in routine ^{13}C NMR due to the low natural abundance of the isotope. (^1H , ^{13}C) Heteronuclear indirect coupling is however ubiquitous in most organic compounds, and provided spectra are recorded in proton-coupled mode information concerning the types of neighbouring carbon atoms can be gleaned from the complex splittings manifest in the carbon resonances. Unfortunately, such coupling can lead to large reductions in signal heights in these spectra, making the peaks less readily discernible from background noise. It is therefore advantageous to acquire ^{13}C solution-state spectra under conditions of proton decoupling to optimise signal intensity. In addition, proton decoupling is known to have other important implications on signal intensity, which can be used to advantage in spectral assignment. If the predominant mechanism for relaxation of the carbon nuclei involves dipole-dipole interactions, which is generally the case in simple organic compounds, the nuclear Overhauser effect^{1,2} can act so as to enhance the

intensities of certain resonances. The largest source of dipole-dipole relaxation is usually between carbons and adjacent protons. Consequently, enhancement is seen for CH, CH₂ and CH₃ carbons, but not so much for quaternary carbons. Another factor implicit in the above discussion is the fact that less effective dipole-dipole relaxation for quaternary carbons leads to increased relaxation times for these carbons which is similarly manifest in lower signal intensities if sufficient recycle delays are not left between pulses. Both these factors can assist in the recognition of signals arising from quaternary carbons. One slight drawback to the distortion of signal intensities is that they are now no longer proportional to the number of equivalent nuclei and therefore signal integration is of little use in spectral assignment of proton-decoupled carbon spectra. Since magnetic equivalence in carbon nuclei is less prevalent than in protons, especially in structurally complex molecules, this is of minor consequence.

Clearly peak assignment in proton-decoupled carbon spectra of complex molecules, where all signals appear as singlets and congestion may be extensive, is far from easy and, unless other techniques are implemented, these spectra may be impossible to fully assign.

2.3.2 Aids to Spectral Assignment in ¹H and ¹³C Solution-state NMR

The correct assignments of carbon and proton solution-state spectra go hand in hand. A vast array of experimental techniques exists today that simplify spectral assignment, but obtaining accurate assignment of proton and carbon spectra of complicated molecules often requires that a concurrent examination of all spectral data available, gathered from a variety of different experiments observing both protons and carbon nuclei, be carried out. In addition to data obtained from experimental work, assignment of spectra can also be aided by other sources. Frequently the literature contains work previously performed on similar systems. In our case the early comprehensive review by Blunt and Stothers³ of steroid solution-state chemical shifts proved to be of great assistance as did numerous others.⁴⁻¹¹ NMR

structural databases form another alternative. Chemical shifts in the spectrum of the object molecule are compared to those found in spectra of structurally similar compounds, or compounds containing similar structural units, contained in the database, and estimations of the expected values of the chemical shifts for each nucleus in the structure are made on this basis.

In the case of carbon-13 NMR in the solution state various ingenious spectroscopic techniques are available which effectively discriminate between different types of carbon atoms. Spectral-editing procedures such as APT¹² (attached proton test), INEPT¹³⁻¹⁵ (Insensitive Nuclei Enhanced by Polarisation Transfer) and DEPT¹⁶ (Distortionless Enhancement by Polarisation Transfer) are three such techniques, the later two of which are effectively able to distinguish between resonances arising from methyl, methylene, methine and quaternary carbons. However, these techniques are unfortunately unable to differentiate between carbons of the same type in a system, which may present problems in certain cases. The fluorinated steroids, which form the basis of the NMR studies presented in chapters 5-7 are one such case, since some of the structures contain a number of structurally very similar methylene carbons, the signals of which occur within a 10 ppm chemical shift range. To obtain unambiguous assignments of these resonances there are a number of techniques available, most of which rely upon the existence of internuclear interactions, such as the dipolar and indirect coupling between different nuclei, to determine the exact location of any given nucleus in the structure.

One solution is to enter the realms of two-dimensional NMR. Here the problem of overcrowding is not such a handicap, since now information is divided into two dimensions. INADEQUATE^{17,18} (Incredible Natural Abundance Double-Quantum Transfer Experiment) is one such two-dimensional experiment. It is undoubtedly one of the most powerful techniques available for assignment of carbon solution-state spectra and relies upon the observation of carbon-carbon indirect coupling between neighbouring nuclei in order ascertain their connectivity, thus permitting the molecular framework to be deduced. Given the low natural abundance

of carbon-13, these interactions are barely detectable and the experiment relies heavily on computational techniques. Consequently it is hugely time consuming and therefore not really a viable option for routine carbon-13 NMR. Generally the most widely used method of achieving assignments with a high degree of certainty is to perform a 2-D ^1H - ^{13}C HETCOR¹⁹⁻²¹ experiment. If this experiment is performed in conjunction with a 2-D ^1H COSY²²⁻²⁴ experiment, then assignments can be made to a much higher degree of confidence. These experiments rely on proton-carbon and proton-proton indirect couplings respectively, which result in correlations between the two dimensions. For the ^1H - ^{13}C HETCOR experiment, conditions can be optimised to detect either $^1J_{\text{CH}}$ coupling, leading to correlations between directly bonded carbon nuclei and protons, or to detect $^2J_{\text{CH}}$ and $^3J_{\text{CH}}$ coupling, giving information revealing the identity of neighbouring or next nearest neighbouring nuclei.

Homonuclear²⁵ and heteronuclear²⁶⁻²⁸ 2-D 'J-resolved' spectra may also be utilised. These experiments contain chemical shift information in one dimension and information concerning any relevant indirect coupling present in the other, thereby removing problems that may be encountered regarding signal overlap of complex multiplets. Detailed analyses of signal multiplicity are then possible, resulting in the determination of all coupling constants. Not only do the magnitudes of coupling constants provide valuable clues to spectral assignment, but they can also be used to predict the particular stereochemistry displayed, and conformation adopted, by molecules (see section 4.3).

One further technique available to assist assignment of proton spectra is the NOE difference experiment, which works due to the strong dipolar coupling present between nuclei in close proximity to one another. A resonance that is not overlapped by any other signals is strongly irradiated and perturbations in the intensities of other resonances in the spectrum are observed, usually by recording difference spectra. The resonance from any nucleus that is near (usually within two or three bond distances) to the one being irradiated is subject to a change in intensity. This procedure is repeated for a number of other resonances until the topology of the molecule can be

established. An extension of this experiment is the two-dimensional NOESY^{29,30} experiment which finds extensive use in the rapidly expanding field of biological NMR. Molecular structures of biological systems are frequently extremely complicated, and attempts to obtain meaningful structural information from simple NMR experiments invariably prove futile. The experiment works by correlating resonances from nuclei that undergo cross-relaxation (i.e. that are close enough to display significant dipolar coupling to one another) and is thus a very powerful tool in structure elucidation. One drawback of the NOESY experiment is the difficulty encountered in differentiating between chemical exchange and cross-relaxation effects, although this can be circumvented by application of the ROESY³¹ experiment (Rotating Frame Overhauser Effect Spectroscopy). It is important to stress the fact that unlike both COSY and HETCOR experiments, which operate through indirect coupling interactions and are consequently transmitted via chemical bonds, the NOE difference, ROESY and NOESY experiments work via dipolar coupling which acts 'through-space'. They do not, therefore, require nuclei to be a few atoms removed in terms of bond distances, but need only for them to be close in space to experience coupling to one another and display perturbations in signal intensities or correlations in the second dimension. Consequently not only topological, but also stereochemical and conformational information is available from such experiments.

The particular approach that was adopted in assignment of the carbon and proton solution-state spectra presented in chapter 4 of this thesis was to use two-dimensional COSY-45 and short-range HETCOR experiments. The detailed mechanics of the assignment of these spectra are contained therein.

2.3.3 Problems Inherent in ¹H and ¹³C Solid-state NMR

Carbon-13 NMR suffers from the poor receptivity of the nucleus arising from, in the most part, the low natural abundance of this isotope. This is not such a hindrance in solution-state spectra, but in the solid state the problem becomes more

acute. Experiments can become inhibitive long in the solid state due to the apparent loss in sensitivity as a result of linebroadening effects such as field inhomogeneities and incompletely averaged internuclear interactions. The intensity of a signal in the solid state is distributed over a larger range of frequencies than in the solution state, rendering resonances less discernible from the background noise and inherently more difficult to detect. Increased relaxation times in the solid state, necessitating the need for longer recycle delays, may also be a factor contributing to increased acquisition times. This has been largely overcome by the advent of the proton-to-carbon cross-polarisation experiment, where proton spins are excited and subsequently magnetisation is transferred to the carbon spins. The advantages of such a technique are twofold. Not only are recycle delays usually reduced, since we are now concerned with spin-lattice relaxation of the proton nuclei, which generally proceeds faster than carbon relaxation, but also there is an inherent gain in signal intensity of up to four times.

As mentioned previously, in the solid state, since molecules are generally held rigidly in the lattice, dipolar interactions are not averaged to zero by rapid isotropic molecular tumbling. This is of little consequence in carbon-13 solid-state NMR, where (^{13}C , ^{13}C) dipolar interactions are negligible and (^{13}C , ^1H) heteronuclear dipolar interactions are easily suppressed by HPPD and MAS. For solid-state proton NMR of compounds containing abundant protons HPPD is not a viable option as it is not feasible to observe and decouple at the same frequency. However, H,H dipolar interactions are the strongest in existence, commonly of the order of 40 kHz, and suppression of these interactions is imperative if any discernible resolution is to be observed, especially given the small chemical shift range displayed by the proton. Without the implementation of multiple-pulse sequences broad featureless spectra, from which little valuable information can be gleaned, are generally obtained. This limitation is expressly demonstrated in chapter 4.

2.3.4 Aids to Spectral Assignment in ^1H and ^{13}C Solid-state NMR

In the solid state, where resolution is inferior due to the incomplete averaging of dipolar interactions and shielding anisotropy, experiments such as COSY and HETCOR are of limited use. Proton spectra in particular, even with the implementation of multiple-pulse sequences are practically impossible to fully assign for complex molecules.

The assignment of solid-state carbon spectra can be aided by comparison to the corresponding solution-state spectra, since generally chemical shift differences of only a few ppm are observed between the two phases. Information that distinguishes quaternary and (usually) methyl carbons from methine and methylene carbons is available from dipolar dephasing experiments. This experiment is basically the simple cross-polarisation experiment with a window inserted in the proton decoupling prior to acquisition of the signal (usually 40-60 μs). It works on the principle that quaternary and methyl carbon nuclei generally display weaker dipolar interactions to protons than do methylene and methine carbons. In the case of the quaternary carbon this is due to the remoteness from any protons, and for the methyl group this is as a consequence of rapid rotation reducing the magnitude of the dipolar interaction locally. Signals from carbons that are strongly dipolar coupled are broader than signals from other carbons (cf. CH_2 vs CH_3), which leads to a more rapid decay of transverse magnetisation, and consequently there is little signal left from these carbons to acquire at the end of the decoupling window. In addition, chemical shifts can be compared to those observed for related compounds, and although solid-state NMR of steroids has been less well documented than for steroid solutions a number of papers have published containing relevant information.³²⁻³⁹

2.4 Information Retrieval from ^{19}F NMR Spectra

2.4.1 Properties of the ^{19}F Nucleus

In principle, the fluorine nucleus is an ideal one with which to probe molecular structure, having a natural abundance of 100% and a large gyromagnetic ratio, leading to a receptivity second only to that of the proton. In addition, the fluorine nucleus has a much larger chemical shift range than that displayed by the proton. For instance, chemical shifts have been observed from -448 ppm (relative to CFCl_3) to +865 ppm for FOOF .⁴⁰ In organic fluorinated systems chemical shift ranges are more usually limited to the 0 to -200 ppm, although this is still ten times the -5 to 15 ppm range exhibited by protons in similar systems. This increased chemical shift range leads to a greater ability to differentiate between chemically inequivalent nuclei compared to proton NMR, making fluorine-19 NMR an analytical technique of considerable utility.

Indeed, in the solution state this ideality is borne out by the potential to acquire spectra quickly and simply. However, in the solid state certain complications arise that need to be surmounted before fluorine spectra can be obtained routinely. The two principal effects which hinder the acquisition of fluorine-19 high-resolution spectra of normal fluorinated organic compounds in solids containing abundant spins (protons) are dipolar coupling (both homonuclear and heteronuclear) and shielding anisotropies. The fluorine nucleus possesses the third highest gyromagnetic ratio (behind the hydrogen and tritium nuclei) and consequently dipolar interactions in a fluorinated organic compounds containing abundant fluorines and/or protons can be expected to be large. Similarly the large chemical shift range displayed by ^{19}F nuclei means anisotropies are correspondingly large. Since both of these interactions can lead to significant line broadening the need for the concurrent use of selective averaging techniques is paramount if any meaningful analysis of ^{19}F NMR spectra obtained from solid organic compounds containing fluorines and protons is to be possible.

As outlined in section 2.2.1 shielding anisotropies can be averaged to their isotropic values by spinning at the magic angle. For fluorine fairly modest speeds suffice (~ 5 kHz), although this may result in the production of spinning sidebands at integral multiples of the spinning rate on either side of the isotropic resonance. Nowadays probes designed for the acquisition of ^{19}F solid-state spectra frequently incorporate spinning modules capable of spinning at rates up to 20 kHz, which is easily able to effect efficient suppression of these interactions and aids interpretation of spectra by giving rise to fewer spinning sidebands.

As experienced in proton solid-state NMR, if like nuclei in the molecule are sufficiently contiguous for homonuclear dipolar coupling to be significant, then the use of multiple-pulse sequences may be necessary to effect efficient homonuclear dipolar decoupling and produce the desired high degree of resolution in the spectrum. By combining such a multiple-pulse sequence and MAS, CRAMPS⁴¹ (Combined Rotation And Multiple-Pulse Spectroscopy) offers a reliable method of suppressing both homonuclear dipolar interactions and shielding anisotropies, and although the set-up procedure is lengthy and the technique is technically demanding, a large number of ^{19}F solid-state spectra have been acquired successfully for compounds containing abundant fluorines using multiple-pulse sequences such as WAHUA,⁴² MREV-8^{43,44} and BR-24.⁴⁵

The pharmaceutical steroids investigated were deliberately chosen so as to possess well-separated fluorines and hence display only modest (^{19}F , ^{19}F) dipolar interactions. Consequently magic-angle spinning at moderate speed was sufficient to average these homonuclear interactions, and the need to implement multiple-pulse operation on the fluorine channel was rendered superfluous. However, this still leaves heteronuclear dipolar coupling to be taken into consideration. These compounds contain a plethora of protons in close proximity to the fluorine(s), and consequently large dipolar interactions are present. Plainly these heteronuclear dipolar interactions must be suppressed, if any fine structure is to be observed, and it is this facet of fluorine solid-state NMR that creates difficulties.

As stated in section 2.2.1 heteronuclear dipolar coupling effects are commonly suppressed by means of double resonance techniques, which, for simple organic compounds (where generally it can be assumed that the abundant spins will be protons) amounts to HPPD. For carbon-hydrogen, nitrogen-hydrogen and numerous other spin-pairs this does not present a problem. However, for the fluorine-hydrogen spin-pair difficulties arise pertaining to the close proximity of the ^{19}F and ^1H resonant frequencies (188.29 MHz versus 200.13 MHz at 4.7 T). This six percent difference represents a significant technical challenge to the practicality of achieving high-power proton decoupling. The inability of the usual narrowband pass filters used in multinuclear spectrometers to efficiently discriminate between frequencies that display such a small disparity necessitates the use of high-specification filters, which have only become commercially available in recent years. In addition, the requirement for a specially-designed HF probe, possessing two narrowband channels for fixed frequencies, imparts constraints on the ease with which such work can be undertaken. These problems have been successfully surmounted by the acquisition of such a probe at Durham.

Another problem that besets solid-state fluorine-19 NMR studies of organic fluorinated systems is the inhibitive long longitudinal relaxation times commonly found in rigid systems. If there exists, within the system of study, any kind of motion, as for example is experienced in fluorinated polymers, then longitudinal relaxation times may be significantly reduced. This effect was in evidence for one of the fluorinated steroids. As for the case of carbon solid-state NMR, this drawback can be alleviated to some extent by the implementation of cross-polarisation from protons.

It is for the reasons stated in the previous paragraphs that high-resolution ^{19}F solid-state investigations of fluorinated compounds containing abundant protons have attracted scant attention to date.

One can envisage a kind of hierarchy of fluorinated compounds which, as one progresses higher up the hierarchy, impart more and more stringent constraints on the ease of obtaining high-resolution spectra by the necessity to apply a combination of

the aforementioned selective averaging techniques. This point is illustrated in Table 2.3.1.

^{19}F		^1H		Technique
Dilute	Abundant	Dilute	Abundant	
✓		✓		MAS
	✓	✓		CRAMPS
✓			✓	HPPD/MAS
	✓		✓	HPPD/CRAMPS

Table 2.3.1 Summary of selective averaging techniques required to obtain high-resolution ^{19}F solid-state NMR spectra of fluorinated organic compounds.

In table 2.3.1 the term dilute is used when referring to a nuclei that is dilute enough so as to display negligible homonuclear dipolar coupling, and the term abundant implies the presence of such dipolar couplings. The information contained in table 2.3.1 gives a very simplified picture and, as was the case for ^{13}C solid-state NMR, considered in section 2.3, there are many exceptions to the rule. For instance one area of research carried out has focused on polymer chemistry where once again, aided by substantial molecular-level motion, fast magic-angle spinning may cause sufficient suppression of dipolar couplings to enable observation of individual resonances without the need for multiple-pulse sequences or HPPD. However, the fact still remains that examples of the successful implementation of HPPD for observation of ^{19}F in the solid-state are few and far between. The following section reviews the work conducted in the area of solid-state ^{19}F NMR, taking examples from the realms of both organic and inorganic chemistry. Fluorine containing compounds are cited that cover each of the four categories of compound listed in table 2.2.1.

2.5 Literature Review: ^{19}F Solid-state NMR

2.5.1 MAS-only Studies

Compounds for which MAS alone has been found to give rise to high-resolution spectra have generally been either inorganic materials containing dilute fluorines and very few or no protons, or polymer species that exhibit some kind of motion. These polymer species can be characterised further by their mobility.

Highly mobile polymers can give rise to high-resolution spectra even at low spinning speeds (< 4 kHz). Unambiguous assignment of the resonances of the side-chain $-\text{O}-\text{CH}_2-\text{CF}_2-\text{CF}_2-\text{CF}_2-\text{CF}_3$ in a sample of a proton-containing fluorinated polyphosphazene was achieved by Zumbulyadis and co-workers from high-resolution ^{19}F MAS/NOESY spectra.⁴⁶

With the implementation of more rapid spinning (16.8 kHz) three distinct resonances were clearly identified in samples of the rigid polymer poly(chlorotrifluoroethene), $-(\text{CF}_2-\text{CFCl})_n-$, trade name Kel-F.⁴⁷ Spectral narrowing, however, was only observed at spinning speeds in excess of 8.5 kHz. In addition a variety of co- and terpolymers containing vinylidene fluoride, (CFCH_2) in conjunction with: (a) hexa-fluoropropene $(\text{CF}_2\text{CFCF}_3)$, (b) hexafluoropropene and tetrafluoroethene (CF_2CF_2) , and (c) chlorotrifluoroethene (CF_2CFCl) have been studied, requiring spinning at rates between 18.0 and 20.1 kHz to obtain chemically resolved peaks.⁴⁸ The degree of resolution obtained at such high spinning rates allows the deduction of polymer microstructure out to five-carbon chain sequences. Fast-spinning MAS has also been used to study more complex polymeric species produced by plasma polymerisation.

One area of research where slow-spinning ^{19}F MAS NMR has proved useful for inorganic compounds is in the study of the fluorination of dentally important apatites.⁴⁹⁻⁵¹ MAS rates of 3-4 kHz have been used to observe the increase in ^{19}F signal intensities of fluoroapatite (FAP) $(\text{Ca}_5(\text{PO}_4)_3\text{F})$ and fluorohydroxyapatite (FHAP) $(\text{Ca}_5(\text{PO}_4)_3(\text{OH})_{1-x}\text{F}_x)$, formed from the exposure of hydroxyapatite to F^-

solutions. Also, since the homogeneously broadened signals of CaF_2 also present are not narrowed by spinning at such slow rates the differentiation of types of fluoride present has been possible. Slow-spinning MAS has also been used to identify and quantify the presence and location of antimony activators in a range of doped FAP samples (phosphors) finding use in the manufacture of fluorescent lights. ^{19}F spectra showing shifted peaks and shoulders attributable to substitution and correlating with increasing antimony content have been recorded. ^{19}F NMR with MAS at 3.5 kHz has been used by Raudsepp et al.⁵² to study differences in fluorine sites, especially in their local symmetry, in the synthetic minerals tremolite and fluoroscandium pargasite. Clark et al.⁵³ have studied a range of ionic fluorides by ^{19}F MAS incorporating spinning rates of ~ 3 kHz. These have included LiF , NaF , KF , RbF , CsF , Et_4NF and Bu_4NF . A wider range of F^- environments exists in the solid state compared to the solution state, and consequently an increased chemical shift range has been observed. Some of the samples have been deposited onto calcium fluoride and alumina surfaces as a precursor to work on catalysis, and in this latter case strong hydrogen bonding to surface hydroxyl protons has resulted in large chemical shift changes.

The above work has been extended to study the adsorption of fluoride-containing species onto silica⁵⁴ and montmorillonite clay,⁵⁵ for which a range of complex fluorides have been formed by adsorbing MF species ($\text{M} = \text{NH}_4, \text{Na}, \text{K}, \text{Rb}, \text{Cs}$) onto montmorillonite K10 at various loadings and drying the resultant samples at a range of temperatures. Some of the resonances in the MAS spectra have been assigned to known species, such as SiF_6^{2-} and AlF_6^{3-} , whereas other resonances could not be unambiguously assigned.

Fast-spinning techniques have been used by Kreinbrink et al.⁵⁶ to improve the quantification of FAP/CaF_2 mixtures by observing spectra displaying narrow lines from each species and not just FAP, and greater line narrowing has been observed for simple inorganic fluorides such as those studied by Clark et al. at speeds of up to 15.5 kHz.

2.5.2 ^{19}F CRAMPS

Where samples contain abundant fluorines, but are either totally devoid of protons or contain only dilute protons, the use of multiple-pulse sequences (where small anisotropies exist) or CRAMPS is necessary to achieve a suitably high degree of resolution. Initial ^{19}F experiments using multiple-pulse sequences to suppress (^{19}F , ^{19}F) homonuclear dipolar coupling were performed on a single crystal of CaF_2 , for which the cubic symmetry around the fluorine nuclei meant no shielding anisotropy was observed.⁴² Consequently this compound gave a good indication of the efficiency of the technique and served as a standard against which to compare resolution in further studies of other compounds. The later combination of multiple-pulse sequences with MAS meant samples containing numerous fluorines in anisotropic environments, such as in perfluorinated organic compounds, could be studied. The acquisition of ^{19}F NMR spectra in the CRAMPS mode of operation led to a huge increase in resolution for a sample of perfluoronaphthalene compared to MAS only operation.⁵⁷ From such spectra it was possible to discern the four inequivalent fluorines in this molecule. Other perfluorinated solids investigated have included the linear fluorocarbon $\text{C}_8\text{F}_{17}\text{SO}_3\text{Na}^+$,⁵⁸ for which by spinning at 4 kHz it has been possible to identify four resonances from CF_3CF_2^- , $-(\text{CF}_2)_n-$ and $-\text{CF}_2\text{SO}_3^-$ moieties, and a saturated fluorocarbon $\text{C}_{14}\text{F}_{30}$.⁵⁹ The CRAMPS technique has also been applied to the study of the aforementioned calcium fluoride / fluoroapatite mixtures.⁶⁰

As regards examples of CRAMPS used on polymeric samples, the very first example of the technique was in observing the ^{19}F signal from the polymer Kel-F.⁶¹ Two ^{19}F resonances, separated by 23 ppm, with an intensity ratio of 2:1 were assigned to the CF_2 and CFCl fluorines. However, the number of examples of the technique in polymer science still remains relatively low.

The novel material $-(\text{C}(\text{CF}_3)=\text{C}(\text{CF}_3))_n-$ has been studied at Durham,⁵⁹ and the morphology and orientation has been probed in static samples of polytetrafluoroethane.⁶²⁻⁶⁶

2.5.3 High-power Proton Decoupling

For compounds which contain abundant protons, and little suppression of (^1H , ^{19}F) dipolar interactions due to molecular motions is seen, it is necessary to employ HPPD. Very few examples of the successful implementation of HPPD from fluorines exist. However, proton-decoupled ^{19}F NMR spectra for proton-containing fluorinated polymers and copolymers, such as poly(vinylidene fluoride) (PVF_2), poly(fluoromethylene) (PFM), poly(vinyl fluoride) (PVF) and poly(trifluoroethylene) (PF_3E) involving ^{19}F T_1 measurements,⁶⁷ and investigations into conformational characteristics have also been recorded.⁶⁸ Simultaneous irradiation at both proton and fluorine resonant frequencies has been reported by Kendrick et al. consisting of dual-channel decoupling of ^1H and ^{19}F from ^{13}C in the ^{13}C spectrum of a fluoroanthenyl radical cation salt.⁶⁹ Hagaman et al.^{70,71} have measured ^{19}F T_2 values using proton decoupling in simple monofluorinated organic substances, including one steroid very similar in structure to a compound studied in our investigations. $^1\text{H} \rightarrow ^{19}\text{F}$ cross-polarisation has previously been successfully implemented in ^1H , ^{19}F , ^{13}C triple-resonance experiments to investigate miscibility in poly(methylmethacrylate) / poly(vinylidene fluoride) blends.^{72,73}

References

1. R. Kaiser, *J. Chem. Phys.*, **42**, 1838 (1965).
2. F. A. L. Anet and A. J. R. Bourn, *J. Chem. Soc.*, **87**, 5250 (1965).
3. J. W. Blunt and J. B. Stothers, *Org. Magn. Reson.*, **9**, 439 (1977).
4. H. J. Reich, M. Jautelat, M. T. Messe, F. J. Weigert, and J. D. Roberts, *J. Am. Chem. Soc.*, **91**, 7445 (1969).
5. N. S. Bhacca, D. D. Giannini, W. S. Jankowski, and M. E. Wolff, *J. Am. Chem. Soc.*, **95**, 8421 (1973).
6. D. D. Giannini, P. A. Kollman, N. S. Bhacca, and M. E. Wolff, *J. Am. Chem. Soc.*, **96**, 5462 (1974).
7. J. R. Hanson and M. Siverns, *J. Chem. Soc. Perkin I*, 1956 (1976).
8. G. Lukacs, X. Lusinchi, E. W. Hagaman, B. L. Buckwalter, F. M. Schell and E. Wenkert, *C. R. Acad. Sci.*, **C 274**, 1458 (1972).
9. W. B. Smith, *Annu. Rep. NMR Spectrosc.*, **8**, 199 (1978).
10. J. P. Hickey, I. S. Butler and G. Pouskouleli, *J. Magn. Reson.*, **38**, 501 (1980).
11. J. T. Nelson and L. J. Kurz, *Magnet. Res. Chem.*, **31**, 203 (1993).
12. M. R. Bendall, D. M. Doddrell and D. T. Pegg, *J. Am. Chem. Soc.*, **103**, 4603 (1981).
13. G. A. Morris and R. Freeman, *J. Am. Chem. Soc.*, **101**, 760 (1979).
14. G. A. Morris, *J. Am. Chem. Soc.*, **102**, 429 (1980).
15. D. P. Burum and R. R. Ernst, *J. Magn. Reson.*, **39**, 163 (1980).
16. D. M. Doddrell, D. T. Pegg and M. R. Bendall, *J. Magn. Reson.*, **48**, 323 (1982).
17. A. Bax, R. Freeman, T. A. Frenkiel and M. H. Levitt, *J. Magn. Reson.*, **43**, 478 (1981).
18. A. Minoretti, W. P. Aue, M. Reinhold and R. R. Ernst, *J. Magn. Reson.*, **40**, 175 (1980).
19. A. A. Mandsley and R. R. Ernst, *Chem. Phys. Lett.*, **50**, 368 (1977).
20. G. Bodenhausen and R. Freeman, *J. Magn. Reson.*, **28**, 471 (1977).
21. A. Bax and G. A. Morris, *J. Magn. Reson.*, **42**, 501 (1981).

22. J. Jeneer, *Proceedings of the Ampère International Summer School*, Basko Polji, Yugoslavia (1971).
23. R. Freeman and G. Morris, *J. Magn. Reson.*, **42**, 164 (1981).
24. A. Bax and R. Freeman, *J. Magn. Reson.*, **44**, 542 (1981).
25. W. P. Aue, J. Karhan and R. R. Ernst, *J. Chem. Phys.*, **64**, 4226 (1976).
26. L. Müller, A. Kumar and R. R. Ernst, *J. Chem. Phys.*, **63**, 5490 (1975).
27. G. Bodenhausen, R. Freeman and D. L. Turner, *J. Chem. Phys.*, **65**, 839 (1976).
28. L. Müller, A. Kumar and R. R. Ernst, *J. Magn. Reson.*, **25**, 383 (1977).
29. A. Kumar, G. Wagner, R. R. Ernst and K. Wüthrich, *J. Am. Chem. Soc.*, **103**, 3654 (1981).
30. A. Kumar, R. R. Ernst and K. Wüthrich, *Biochem. Biophys. Res. Commun.*, **95**, 1 (1980).
31. H Kessler, M. Gehrke and C. Griesinger, *Angew. Chem. Intl. Edn. Engl.*, **27**, 490 (1988).
32. R. A. Fletton, R. K. Harris, A. M. Kenwright, R. W. Lancaster, K. J. Packer and N. Sheppard, *Spectrochim. Acta*, **43A**, 1111 (1987).
33. R. A. Fletton, R. K. Harris, B. J. Say, R. R. Yeung, R. W. Lancaster, *Spectrochim. Acta*, **45A**, 465 (1989).
34. R. K. Harris, A. M. Kenwright, B. J. Say, R. R. Yeung, R. A. Fletton, R. W. Lancaster and G. L. Hardgrove, Jr., *Spectrochim. Acta*, **46A**, 927 (1990).
35. E. A. Christopher, R. K. Harris and R. A. Fletton, *Solid State NMR*, **1**, 93 (1992).
36. S. R. Byrn, P. A. Sutton, B. Tobias, J. Frye and P. Main, *J. Am. Chem. Soc.*, **110**, 1609 (1988).
37. P. J. Saindon, N. S. Cauchon, P. A. Sutton, C.-j. Chang, G. E. Peck and S. R. Byrn, *Pharm. Res.*, **10**, (2) 197 (1993).
38. E. W. Hagaman, *J. Magn. Reson.*, **A 104**, 125 (1993).
39. E. W. Hagaman and J. H. Burns, *Fuel*, **72**, 1239 (1993).
40. J. W. Emsley and L. Phillips, *Progress in Nuclear Magnetic Resonance Spectroscopy*, Pergamon, Oxford, **Vol 7** (1971).
41. L. M. Ryan, R. E. Taylor, A. J. Paff and B. C. Gerstein, *J. Chem. Phys.*, **72**, 508 (1980).

42. J. S. Waugh, L. M. Huber and U. Haeberlen, *Phys. Rev. Lett.*, **20**, 180 (1968).
43. P. Mansfield, *J. Phys. Chem.*, **4**, 1444 (1971).
44. W. -K. Rhim, D. D. Elleman and R. W. Vaughan, *J. Chem. Phys.*, **58**, 1772 (1973); **59**, 3740 (1973).
45. D. P. Burum and W. -K. Rhim, *J. Chem. Phys.*, **55**, 746 (1971).
46. N. Zumbulyadis, P. M. Roberts and WT. Ferrar, *J. Magn. Reson.*, **72**, 388 (1987).
47. S. F. Dec, R. A. Wind, G. E. Maciel and F. E. Anthonio, *J. Magn. Reson.*, **70**, 355 (1986).
48. S. F. Dec, R. A. Wind and G. E. Maciel, *Macromol.*, **20**, 2754 (1987).
49. J. P. Yesinowski and M. J. Mobley, *J. Am. Chem. Soc.*, **105**, 6191 (1983).
50. D. J. White, W. D. Bowman, R. V. Faller, M. J. Mobley, R. A. Wolfgang and J. P. Yesinowski, *Acta. Odotol. Scand.*, **46**, 375 (1989).
51. J. P. Yesinowski, R. A. Wolfgang and M. J. Mobley, *Adsorption on and Surface Chemistry of Hydroxyapatite*, Plenum, New York, p 157 (1983).
52. M. Raudsepp, A. C. Turnock, F. C. Hawthorne, B. L. Sheriff and J. S. Hartmann, *Am. Mineral.*, **17**, 580 (1987).
53. J. H. Clark, E. M. Goodman, D. K. Smith, S. J. Brown and J. M. Miller, *J. Chem. Soc., Chem. Commun.*, 657 (1986).
54. C. V. A. Duke, J. M. Miller, J. H. Clark and A. P. Kybett, *Spectrochim. Acta*, **46A**, 1381 (1990).
55. F. M. Asseid, C. V. A. Duke and J. M. Miller, *Can. J. Chem.*, **68**, 1420 (1990).
56. A. T. Kreinbrink, C. D. Sazavsky, J. W. Pyrz, D. G. A. Nelson and R. S. Honkonen, *J. Magn. Reson.*, **88**, 267 (1990).
57. R. K. Harris, P. Jackson, and G. J. Nesbitt, *J. Magn. Reson.*, **85**, 294 (1989).
58. R. K. Harris, P. Jackson, L. H. Merwin, B. J. Say and G. J. Haegele, *J. Chem. Soc. Faraday Trans.*, **84**, 3649 (1988).
59. P. Jackson, Ph.D. Thesis, University of Durham (1987).
60. K. A. Smith and D. P. Burum, *J. Magn. Reson.*, **84**, 85 (1989).
61. B. C. Gerstein, R. G. Pembleton, R. C. Wilson and L. M. Ryan, *J. Chem. Phys.*, **66**, 361 (1977).
62. A. D. English and A. J. Vega, *Macromol.*, **12**, 353 (1979).

63. A. J. Vega and A. D. English, *Macromol.*, **13**, 1635 (1980).
64. A. J. Brandolini, K. J. Rocco and C. Dybowski, *Macromol.*, **17**, 1455 (1984).
65. A. J. Brandolini, T. M. Apple and C. Dybowski, *Polymer*, **23**, 39 (1982).
66. A. J. Brandolini and C. Dybowski, *J. Polym. Sci., Polym. Lett. Ed.*, **21**, 423 (1983).
67. B. R. McGarvey and S. Schlick, *Macromol.*, **17**, 2392 (1984)
68. A. E. Tonelli, F. C. Schilling and R. E. Cais, *J. Am. Chem. Soc.*, **25**, 441 (1983).
69. R. D. Kendrick and C. S. Yannoni, *J. Magn. Reson.*, **75**, 506 (1987).
70. E. W. Hagaman, *J. Magn. Reson.*, **A 104**, 125 (1993).
71. E. W. Hagaman and J. H. Burns, *Fuel*, **72**, 1239 (1992).
72. W. E. J. R. Maas, W. A. C. van der Heijden, W. S. Veeman, J. M. J. Vankan and G. H. Werumeus Buning, *J. Chem. Phys.*, **95**, 4698 (1991).
73. A. P. A. M. Eijkelenboom, W. E. J. R. Maas, W. S. Veeman, G. H. Werumeus Buning and J. M. J. Vankan, *Macromol.*, **25**, 4511 (1992).

Chapter 3

Experimental

3.1 Nuclei of Interest

3.1.1 Magnetic Properties of the Nuclei

Information regarding the fundamental NMR parameters of all nuclei, which have been directly observed in research carried out on the fluorinated steroids, is contained in table 3.1.1.

Nucleus	Spin, I	Natural Abundance (%)	Gyromagnetic Ratio, γ ($10^7\text{T}^{-1}\text{s}^{-1}$)	Receptivity ^a (Relative to ^1H)
^1H	1/2	99.98	26.7522	1.00
^{13}C	1/2	1.11	6.7283	1.76×10^{-4}
^{19}F	1/2	100	25.1815	0.83

^a Product of natural abundance and sensitivity.

Table 3.1.1 NMR properties of nuclei directly observed.¹

Larger magnetogyric ratios and higher natural abundances displayed by the proton and fluorine nuclei compared to that of the carbon nucleus are manifest in substantially larger receptivities, which means NMR spectra can be acquired much more quickly for the two former nuclei. The different values of the magnetogyric ratios also have important implications on aspects of the cross-polarisation

experiments between proton and carbon, fluorine and carbon, and proton and fluorine nuclei.

3.2 Compounds

The pharmaceutical steroids investigated consisted of three structurally similar compounds containing one, two and three fluorine atoms respectively.

3.2.1 Numbering, Conformation and Stereochemistry

As with all qualitative NMR spectra involving complex structures a numbering system is a necessity in spectral assignment. The fluorinated steroids suitably demonstrate this, as each contains in excess of twenty carbon atoms. The numbering system adopted is that which is conventionally used.² A steroid by definition is a compound containing four fused rings of carbon atoms, three of which contain six atoms and one of which contains five. These rings are lettered left to right A to D. Numbering commences with the atoms contained in ring A, followed by B, then C, and finally the five-membered ring D.³ Certain methyl substituents are also present, attached to C-13 and C-10. The numbering scheme is depicted in figure 3.2.1.

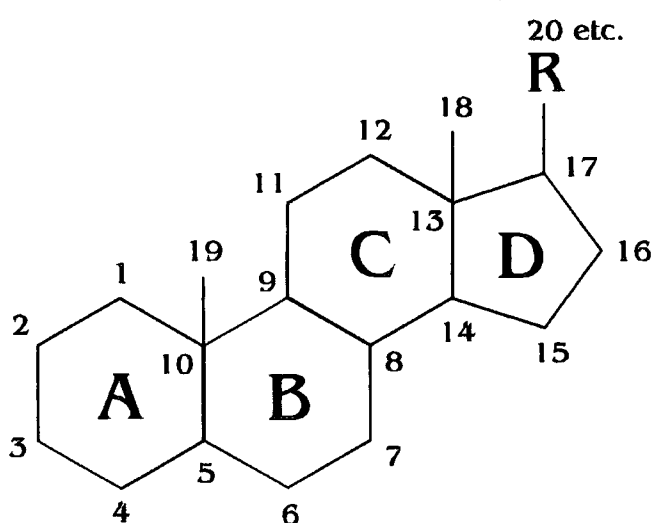


Figure 3.2.1 Conventional numbering scheme for steroids.

This tetra-cyclic structure is a prerequisite if a compound is to be classed as a steroid. However, a great deal of variation, both in substituents (on for example C-20), and hybridisation of carbon atoms is permitted. This is apparent when we consider the three particular pharmaceutical steroids that we have investigated. Their structures are illustrated in figure 3.2.2.

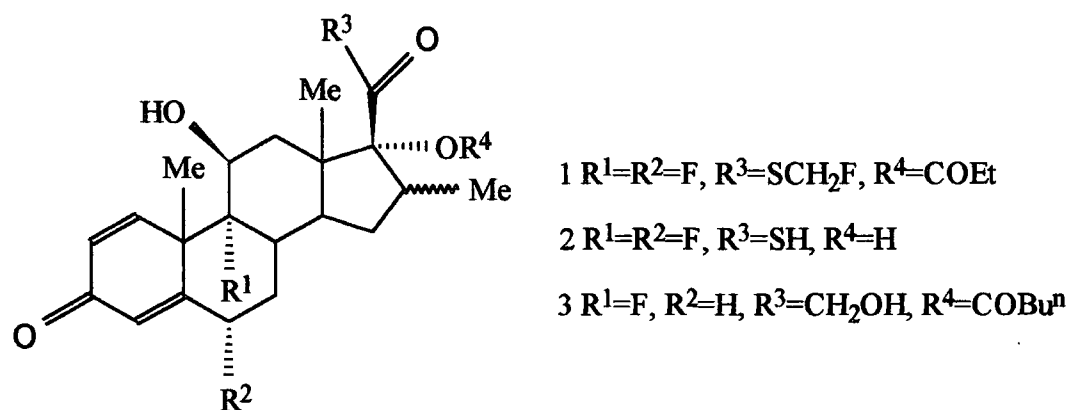


Figure 3.2.2 Molecular structures of the three pharmaceutical steroids studied. The conventional numbering system, as discussed in the text, is adopted.

One structural feature evident in our compounds, from figure 3.2.2, is that ring A is not aliphatic. The sp^2 hybridisation of the carbon atoms in ring A introduces some conformational constraints on the molecular structure. In the case of steroids made up entirely of aliphatic carbons, there are two types of conformation exhibited; the A and B rings can be either *cis* or *trans* fused.³ However, in systems such as ours, conjugation in the A ring leads to a unique stereochemistry. The carbonyl carbon C-3 and the four alkene carbons C-1, C-2, C-4 and C-5 must all lie in (or near) a plane and the conformation is locked in a manner that can be described neither as *cis* nor *trans* fused. In figure 3.2.2 the stereochemistry of the substituents is represented by wedges for β -bonds, coming out of the plane of the paper and dashed lines for α -bonds, going behind the plane of the paper. The undefined stereochemistry represented by the wavy line for C-16 Me is due to the fact that in compounds 1 and 2 the methyl is α , whereas

in compound 3 the methyl is β . In the instances where we have long chain substituents R_3 and R_4 , attached to C-17 and C-20 respectively, the numbering system of the steroid backbone is extended to these atoms, with those atoms along R_3 numbered prior to those contained in R_4 . Protons and fluorines in these compounds are referred to in the text by the same numbering system adopted for the carbons i.e. they are referred to as F-6, F-9, H-1, H-11 OH, H-16 Me etc.

In addition to the aforementioned stereochemical considerations, compound 2 was known to exhibit polymorphism (the existence of two or more crystal forms of a compound).⁴ Three different samples were obtained, which each contained different proportions of two polymorphs in a macroscopic mix.

3.2.2 Nomenclature

The importance of the universal numbering scheme introduced in the previous section can also be appreciated by considering nomenclature of these compounds. The names, both trivial and IUPAC, of the above compounds 1-3, each of which appeared as a fine white powder, are listed below:

(1) Androsta-1,4-diene-17-carbothioic acid, 6α , 9α -difluoro- 11β -hydroxy- 16α -methyl-3-oxo- 17α -(1-oxopropoxy)-*S*-(fluoromethyl)ester trivial name (fluticasone propionate).

(2) Androsta-1,4-diene, -6α , 9α -difluoro- 11β , 17α -dihydroxy- 16α -methyl,3-oxo-17-carbothioic acid.

(3) Pregna-1,4-diene, -9α -fluoro- 11β ,21-dihydroxy- 16β -methyl- 17α -[(1-oxopentyl)oxy]-(-3,20-dione) trivial name (betamethasone-17-valerate).

3.3 Spectrometer Systems

A variety of spectrometers and probes has been used during the course of these studies. What follows is a resume of all aspects regarding spectrometer hardware.

3.3.1 Solution-state Spectrometers

All solution-state spectra, i.e. proton, carbon and fluorine, including 2-D ^1H COSY and ^1H - ^{13}C HETCOR, were recorded on a Varian VXR-400S spectrometer using a four-nucleus switchable Varian 5mm probe.

3.3.2 Solid-state Spectrometers

Most solid-state spectra of the fluorinated compounds were performed either on a Bruker CXP-200 spectrometer or, latterly, on a Chemagnetics CMX-200H spectrometer, both equipped with a 4.7 T wide-bore (89.5 mm) Oxford Instruments superconducting magnet. Simple proton-to-carbon cross-polarisation spectra carried out on the CXP-200 spectrometer were acquired using a Bruker double air-bearing probe accepting 7 mm ceramic rotors, with fluted Kel-F tops. Similar carbon spectra acquired on the CMX-200H used a dual-channel HX double-bearing probe. 7.5 mm zirconia pencil rotors were used in conjunction with vespel drive tips and PTFE spacers and end caps. Spinning speeds of up to 7 kHz were readily attainable, and stable spinning was not so critically dependent on uniform packing as it was for the Bruker rotors. The triple resonance work was conducted on the CMX-200, although one of the old Bruker amplifiers was used on the fluorine channel. A special HFX triple resonance probe was used that accepted similar rotors to those used in conjunction with the HX probe. Tuning of this probe was not trivial given the number of variables in the tuning circuit.

Proton and fluorine spectra were acquired with an HF Double-Resonance APEX probe with narrow-band channels for both fluorine and protons. The Chemagnetics stator accepted 4mm zirconia pencil rotors. The system was capable of achieving MAS rates of 17 kHz. To surmount problems arising from background signals caused by rotor drive tips, spacers and end caps, for the acquisition of fluorine-19 spectra Vespel was used for all, whilst for the acquisition of proton spectra drive tips made of Kel-F and rotor inserts made of teflon were used.

The CMX-200H was equipped with an automatic speed controller which was capable of stabilising the spinning speed to within ± 1 Hz under optimum conditions.

A small number of proton relaxation-time measurements were carried out on a home-built spectrometer operating at 60 MHz. This spectrometer was equipped with an electromagnet and was only capable of accepting static samples.

3.4 Pulse Programs

3.4.1 Pulse Sequence Listing

The majority of pulse sequences implemented in the course of this work are straightforward. The mechanics of these pulse sequences are well-documented in the literature so I do not intend to dwell on their experimental aspects. All the pulse sequences that have been implemented are listed in table 3.4.1.

EXPERIMENT	ACRONYM
Single-pulse	SPE
Cross-polarisation	CP
Proton 2-D correlation	^1H COSY
Proton-carbon heteronuclear correlation	^1H - ^{13}C HETCOR
Insensitive nuclei enhanced by polarisation transfer	INEPT
Dipolar dephasing	DD
Spinning sideband suppression	TOSS
Longitudinal relaxation time measurement by inversion recovery	T_1 ir
2-D spin-exchange experiment	EXSY

Table 3.4.1 List of pulse programs.

3.4.2 Pulse Sequences Incorporating Composite Pulses

Two of the pulse sequences listed in table 3.4.1 included composite pulses. A background suppression pulse sequence was used in the fluorine solid-state work to eliminate signals arising from materials used in the construction of the probe. This pulse sequence is illustrated in figure 3.4.2.

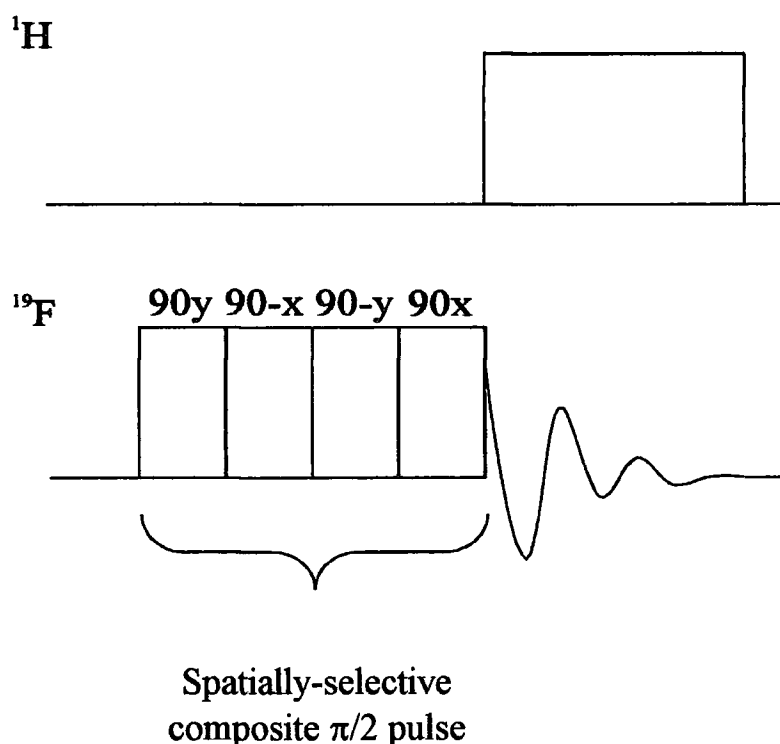


Figure 3.4.2 Background suppression pulse sequence.

This particular pulse sequence, developed by Bax,⁵ is spatially selective. The composite pulse contained therein consists of a continuous train of four pulses each phase shifted 90 degrees from the previous pulse. It relies on the fact that the intensity of the B_1 field rapidly falls away with distance from the homogeneous region in the centre of the coils. Consequently spins that are outside the rotor experience a magnetic field strength reduced in magnitude and therefore undergo a tip angle of less than 90 degrees. The pulse sequence discriminates against spins experiencing a tip

angle of less than 90 degrees, therefore effectively limiting the sample volume to within the confines of the rotor.

The second composite pulse was used in an inversion-recovery pulse sequence and is depicted in figure 3.4.3.

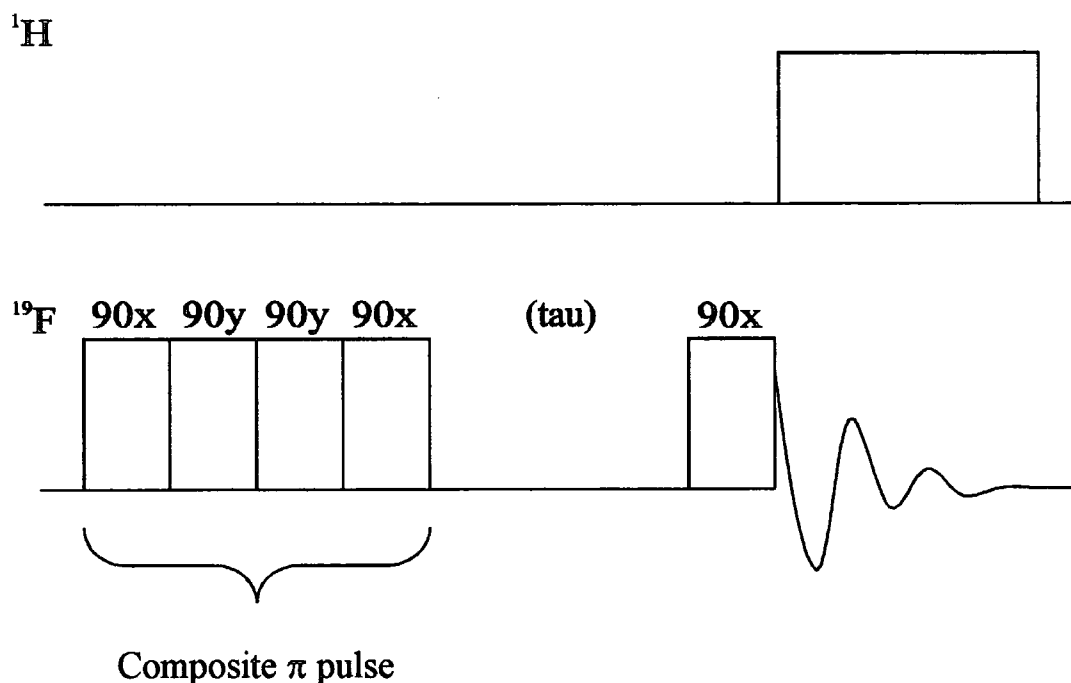


Figure 3.4.3 T_1 inversion-recovery pulse sequence with compensated π -pulse.

A similar four-pulse composite pulse is incorporated, but in this instance the phases of the individual pulses are altered such that a π pulse and not a $\pi/2$ pulse results. The effect of this pulse sequence is to nullify as greatly as possible the consequences of having an incorrectly set π -pulse duration or, likewise, the existence of differential tip angles throughout the sample as a result of B_1 field inhomogeneities.⁶ As with any inversion-recovery experiment, the π pulse is followed by a $\pi/2$ read pulse.

3.5 Spectral Considerations

3.5.1 Solvents and Chemical Shift References

In the solution state solvents used were either CDCl_3 , DMSO-d_6 , or acetone- d_6 , depending on solubility. The particular solvent used for any given steroid is disclosed in the tables of chemical shifts listed in chapters 4 and 5. Carbon spectra were referenced internally using the conventional value of the solvent peaks with respect to TMS (77 ppm for CDCl_3 , 43 ppm for DMSO-d_6 , and 30 ppm for acetone- d_6).⁷ Proton spectra were also referenced externally to TMS at 0 ppm. The fluorine reference was internal CFCl_3 at 0 ppm.

In the solid state chemical shifts were referenced externally (i.e. by replacement rotor). Carbon spectra were referenced with respect to the high frequency signal of adamantane at 38.4 ppm, proton spectra were again referenced to TMS at 0 ppm. In all fluorine experiments spectra were referenced to CFCl_3 at 0 ppm using a static replacement rotor, whilst chlorine solid-state NMR spectra were referenced to the resonance of 1 M NaCl solution at 0 ppm.

3.5.2 Spectral Parameters

3.5.2.1 Solution-state NMR

Solution-state carbon, proton and fluorine spectra, including the ^1H 2-D COSY and ^1H - ^{13}C HETCOR performed on the fluorinated steroids, were recorded at 100.58 MHz, 399.97 MHz and 376.27 MHz respectively. Carbon spectra were recorded with a 25 kHz spectral width and employed a 10 μs pulse duration in conjunction with a 2-3 s recycle delay. Proton spectra were acquired over a 5 kHz spectral width, using approximately a 6.2 μs pulse duration. It is assumed that in most simple organic compounds the longitudinal relaxation times are of the order of 1-2 s. This was indeed borne out by relaxation time measurements. Thus, an acquisition time of 4 seconds obviated the need to employ a recycle delay. Proton COSY 2-D experiments used the standard COSY-45 pulse sequence, employing a 45° read pulse.

A 18.5 μs 90° pulse duration was used in conjunction with a 1.0 s recycle delay. 32 or 16 transients were recorded for each of at least 256 FID's containing 1024 data points each. A spectral width of not more than 4 kHz in F2 was implemented in each case. Zero-filling to 1024 in both dimensions was carried out before a 2-D Fourier transformation using sine bell squared apodisation. ^1H - ^{13}C HETCOR spectra were acquired using a 20-25 kHz spectral width in 2K data points for F2 and a spectral-width of not less than 4 kHz in 1K data points for F1. Before 2-D Fourier Transformation a shifted sine bell squared exponential multiplication was applied to both dimensions (-0.026 seconds in F2, -0.046 seconds in F1). Fluorine solution-state spectra were recorded with spectral widths of 11550 Hz, 10304 Hz and 1978 Hz respectively for compounds 1-3. A pulse duration of 8 μs was implemented with a recycle delay of 2 or 4 s. In each case 64 transients were acquired. For the carbon-13 spectra of the chlorinated and brominated compounds similar spectral parameters were used as for those conducted on the fluorinated steroids.

3.5.2.2 Solid-state NMR

The solid-state ^{13}C NMR spectra of the pharmaceutical steroids were acquired at 50.33 MHz on the CMX-200H and 50.32 MHz on the CXP-200. High-resolution spectra were obtained using combined High-Power Proton Decoupling, Cross-Polarisation employing a flipback pulse on the proton channel, and MAS at speeds up to 5.0 kHz. Spectral conditions were as follows: Spectral width 20 kHz., contact time 2-3 ms, recycle delay 5 s, with in excess of 10 000 transients generally recorded. 2K data points were collected in each FID and zero-filled twice to give an 8K Fourier transform, which was executed with a 10 Hz exponential line broadening factor applied. Dipolar-dephasing experiments conducted on the Bruker CXP-200 spectrometer used a 50-60 μs window in proton decoupling prior to data acquisition.

Fluorine solid-state spectra were recorded at 188.29 MHz. Single-pulse (SP) experiments were performed under the following operating conditions: spectral width 50 kHz; pulse duration 1.8 μs ; recycle delay 60 s; number of transients 16 (each

consisting of 1024 data points). Cross-polarisation experiments employed a flip-back pulse on the proton channel, a contact time of 1 ms, and a recycle delay of 10 s, all other spectral parameters being as for SP operation. MAS speeds were *ca.* 10 kHz for fast-spinning experiments and varied between *ca.* 1 kHz and *ca.* 3 kHz for slow-spinning experiments. Data processing generally involved zero-filling once to 2K data points and a 20 Hz exponential apodisation before Fourier transformation. Dipolar dephasing experiments conducted on compound 1 were acquired using an echo to refocus chemical shifts, under conditions of rotor synchronisation. The window in the decoupling is for the pre-refocussing time. Values between 100 μ s and 800 μ s were used. Different rotational resonance conditions were met for compound 1 by spinning the rotor at 4220 Hz and 5005 Hz. The two-dimensional spin-exchange experiment performed on compound 1 used CP preparation, consisting of a 5.0 μ s $\pi/2$ pulse duration and a 1.0 ms contact time. A mixing time of 50 ms was implemented, and a 50 μ s increment in t_1 was used. 256 FID's were recorded, each containing 1024 data points and consisting of 48 transients. All spectra were recorded at ambient temperature, *ca.* 298 K.

Solid-state proton single-pulse and fluorine-to-proton cross-polarisation experiments were conducted with the spectrometer operating at a frequency of 200.13 MHz. Samples were spun at MAS rates of 10 kHz in both experiments, and a 3.2 μ s pulse duration in conjunction with a 1 ms contact time was implemented for cross-polarisation experiments.

3.6 Spining Sideband Analyses

In order to access information concerning the various shielding tensor components of the fluorine nuclei, spinning sideband fitting computer programs were implemented. One of these was developed at Durham, whilst the other was a new Varian software package. Both these computer programs are based on the same mathematical expression for the intensities of spinning sidebands derived by Maricq

and Waugh.⁸ Details of the programs can be found elsewhere,^{9, 10} and I wish only to mention briefly their experimental aspects.

Certain parameters are estimated visually from a close inspection of relevant slow-spinning or static proton-decoupled spectra. These data are then entered into the program, which processes them to give an estimation of the relevant shielding parameters, along with a level of confidence of these parameters, displayed by means of a sum of differences squared. The information necessary as an input to the program is as follows; Larmor frequency, spinning speed, number of sidebands, spinning sideband intensities and estimations of the anisotropy and asymmetry. Accurate evaluation of spinning sideband intensities is achieved via peak integration packages contained in the CMX-200H software. The program operates by converging at the best fit for the data entered. Certain deficiencies are known to exist in the program for cases where the asymmetry parameter is low (< 0.2) i.e. close to axial symmetry,⁹⁻¹¹ although given the high asymmetry parameters displayed by the fluorines in our samples these problems were of no consequence. One proviso on the success of such fitting programs applied to slow-spinning spectra is the ability to keep the MAS rate constant. Otherwise, the higher-order spinning sidebands are spread out over a range of frequencies such that they are indistinguishable from the background noise. Using the "HF" probe with its 4 mm O.D. rotors some difficulties were experienced in this area when it was necessary to spin at speeds of the order of 800 Hz. These were largely overcome by manual control of the spinning speed via adjustment of the bearing air pressure during the acquisition.

References

1. R. K. Harris, *Nuclear Magnetic Resonance Spectroscopy*, John Wiley and Sons (1983).
2. IUPAC In *Pure and Applied Chemistry*, Butterworth, vol 31, (1972).
3. R. T. Morrison and R. N. Boyd, *Organic Chemistry*, Allyn and Bacon Inc., 3rd Edn., (1973).
4. M. C. Etter, R. C. Hoye and G. M. Vojta, *Cryst. Reviews*, 1, 281 (1988).
5. A. Bax, *J. Magn. Reson.*, 65, 142 (1985).
6. R. Freeman, S. P. Kempell and M. H. Levitt, *J. Magn. Reson.*, 38, 453 (1980).
7. W. Kemp, *Organic Spectroscopy*, Macmillan, 2nd Edn. (1989).
8. M. M. Maricq and J. S. Waugh, *J. Chem. Phys.*, 70, 3300 (1979).
9. H. Bai, *Ph.D. Thesis*, University of Durham (1991).
10. L. Merwin, *Ph.D. Thesis*, University of Durham (1987).
11. R. K. Harris, P. Jackson, L. H. Merwin, B. J. Say and G. Hägel, *J. Chem. Soc., Faraday Trans. I*, 84, 3649 (1988).

Chapter 4

^1H and ^{13}C NMR Studies

4.1 Introduction

Carbon and hydrogen are, by definition, generally the most abundant elemental constituents in organic compounds. Therefore it is of little surprise that carbon and proton NMR play a prominent role in the analysis and characterisation of such compounds. The fact that a solution-state proton NMR experiment can usually be carried out with the utmost ease means that this is usually the logical starting point for an NMR investigation of any organic compound.

4.2 Solution-state Proton Spectra

4.2.1 One-dimensional Proton Spectra

The ^1H solution-state spectrum of compound 1, the trifluorinated steroid, is shown in figure 4.2.1. The properties of the proton (high receptivity and short spin-lattice relaxation time) combined favourably to result in this spectrum taking only four minutes to acquire.

Proton chemical shifts for all three steroids are listed in table 4.2.1, along with assignments of homonuclear and (^1H , ^{19}F) heteronuclear indirect coupling constants. (^1H , ^{19}F) couplings, where identified, are listed in bold type. The letters d,t,q and m refer to the multiplicity of the signal and represent doublet, triplet, quartet and multiplet respectively. Obsc. represents a signal obscured by other resonance.

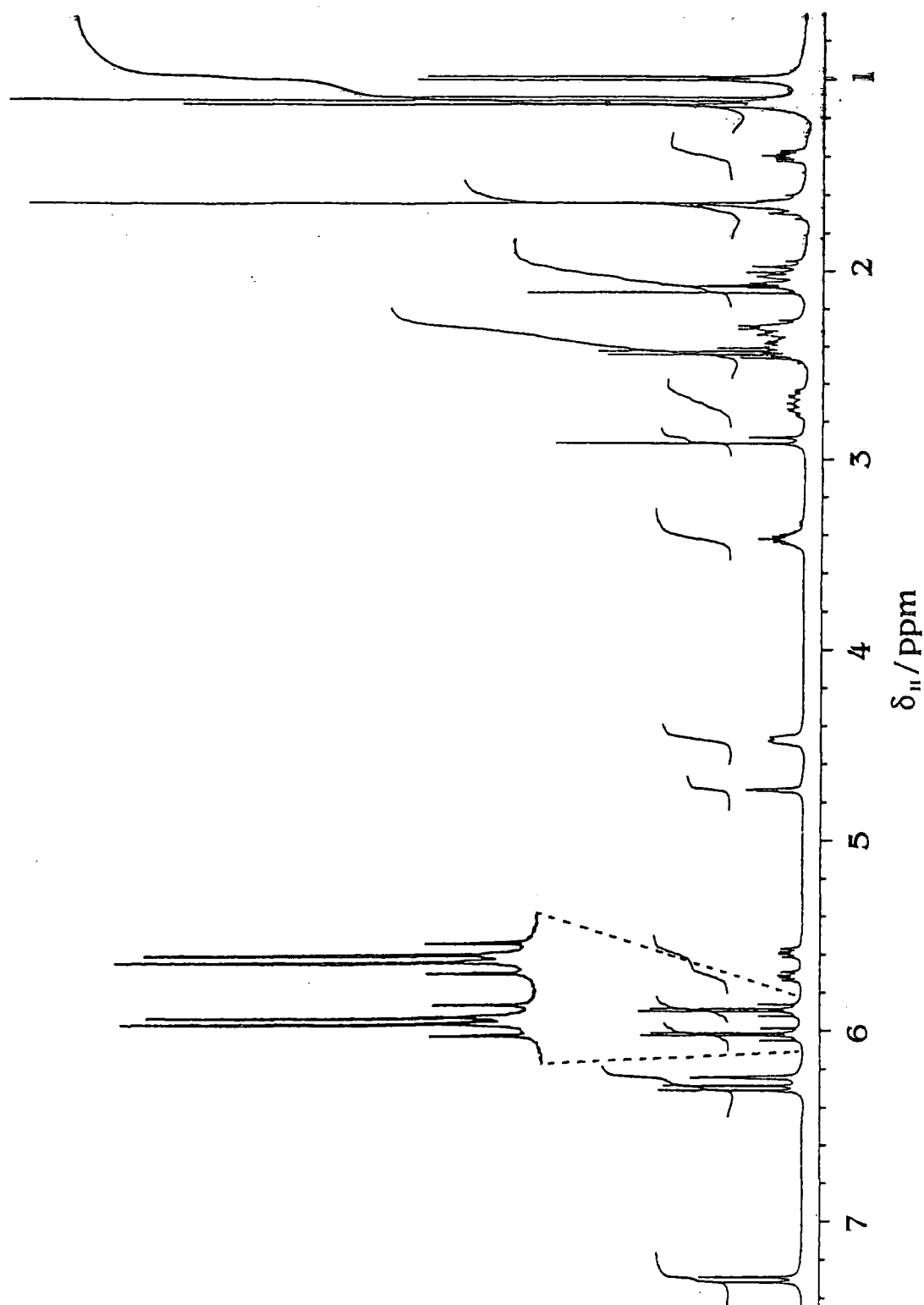


Figure 4.2.1 399.95 MHz solution-state proton spectrum of compound 1. Inset is an enlargement of the resonance due to H-21a and b. Spectral parameters were as follows: spectral width 5.0 kHz, acquisition time 3.7 s (0 s recycle delay), pulse duration 4.5 μs , number of transients 64.

Hydrogen	1 ^a	Compound 2 ^b	3 ^c
1	7.31 dd (10.4, 1.6)	7.27 d (10.0)	7.28 d (10.4)
2	6.30 dd (10.4, 2.0)	6.29 dd (10.0, 1.6)	6.32 dd (10.4, 1.2)
4	6.24 dd (2.8, 1.6)	6.1	6.11
6 α	-	-	2.38 m (obsc)
6 β	5.64 dddd (48.8, 11.2, 4.4, 1.7)	5.67 ddd (48.8, 10.0, 4.8)	2.62 ddd (13.2, 13.2, 3.2)
7 α	2.38 m (obsc.)	1.47 m (obsc.)	1.55 m (obsc.)
7 β	1.66 m (obsc.)	2.20 m (obsc.)	1.92 m (obsc.)
8	2.71 dddd (28.8, 11.8, 11.8, 5.0 1.7)	2.48 m	2.43 dddd (32.4, 11.2, 11.2, 4.7)
11	4.47 m	4.11 m	4.39 d (8.4)
11-OH	4.74 dd (3.6, 2.4)	5.55 (obsc.)	3.46 (broad)
12 α	2.32 m (~13)	2.15 d (13.6)(broad)	2.38 d (13.6)
12 β	2.04 m (~13)	1.82 d (13.6)(broad)	1.50 m (obsc.)
14	2.30 ddd (12.0, 11.8, 8.0)	2.18 m (obsc.)	1.94 m (obsc.)
15 α	1.40 ddd (12.0, 8.0, 3.8)	1.14 m (12.2, 7.6, 3.8)	1.20 d (11.6)(broad)
15 β	1.99 dddd (12.0, 12.0, 11.1, 2.0)	1.67 m	1.90 m (obsc.) (11.6)
16	3.42 dqd (11.1, 7.3, 3.8)	2.87 m (broad)	2.12 q (broad) (7.2)
17-OH	-	6.0 (broad)	-
18	1.14	0.94	0.93
19	1.65	1.49	1.54
20-SH	-	5.38	-
21a	5.95 dd (46.4, 9.6)	-	4.03 d (17.2)
21b	5.98 dd (46.4, 9.6)	-	4.00 d (17.2)
21-OH	-	-	3.46 (broad)
23	2.44 q (7.6)	-	2.29 t (7.2)
24	1.12 t (7.6)	-	1.54 s
25	-	-	1.30 q (7.2)
26	-	-	0.87 t (7.2)
H-16 Me	1.00 d (7.3)	0.85 d (7.2)	1.36 d (7.2)

In ^ad₆-acetone, ^bd₆-DMSO and ^cCDCl₃.

^d Chemical shifts in ppm.

^e Coupling constants in Hz given in parentheses.

Table 4.2.1 ¹H NMR chemical shifts^d and coupling constants^e for steroids 1-3.

The variation in chemical shifts displayed by particular nuclei in the three compounds can easily be explained in terms of the influence of different substituents. For instance the shift observed for H-6 β in compound 3 is much lower than those observed for the analogous protons in compounds 1 and 2, which reflects the absence of fluorination at the C-6 position in the former compound. The electronegative substituent fluorine pulls electron density towards itself, causing the H-6 β proton to be deshielded (i.e. the effective magnetic field at the H-6 β proton is stronger in compounds 1 and 2 than in compound 3). These effects are also apparent, albeit less conspicuously, from comparisons of the shifts observed for H-7 α in the three compounds. Less dramatic effects are observed for H-4, because it is more distant from F-6, and for H-8 because all three steroids are fluorinated at C-9. It is important to remember when making such comparisons of chemical shifts that in each of the three spectra recorded a different solvent was used giving rise to slight variations in chemical shift due to the differences in polarity and magnetic susceptibility of these solvents. Although the difference in chemical shift experienced by a proton on changing solvent is not usually large, except where substantial hydrogen bonding is possible, for example with hydroxyl protons, this point should not be overlooked.

The signals enlarged and inset in figure 4.2.1, arising from protons H-21a and H-21b, highlight two interesting points. Firstly, the presence of a clearly visible large proton-fluorine coupling of approximately 50 Hz underlines a vital aspect of assignment of proton spectra for our compounds. The presence of fluorine nuclei in these structures leads to substantial proton-fluorine coupling constants. $^2J_{\text{HF}}$ coupling constants are far greater in magnitude than $^2J_{\text{HH}}$ coupling constants, and are therefore instantly recognisable. Add to this the fact that coupling to fluorine frequently occurs over large distances (up to five bonds under favourable conditions), and it can be appreciated that this property of the fluorine nucleus is a great aid in spectral assignment of signals arising from nuclei in close proximity to fluorine atoms.

The second point of interest is that the intensities of these resonances are perturbed. Their intensities are distorted as a result of second-order indirect coupling

effects. Describing the fluoromethyl group as an ABX spin system, representing HHF respectively, the distortion is attributed to the fact that the difference in resonant frequencies of the two spins ($\nu_A - \nu_B$) is of the same order of magnitude as the coupling constant between them (J_{AB}). Fortunately J_{AX} and J_{BX} are of very similar magnitudes, as would be expected within such a fluoromethyl group, and are, in addition, much greater than J_{AB} . If J_{AX} and J_{BX} were of the same order as J_{AB} then further complications would arise and the coupling pattern would be harder to interpret. Figure 4.2.2 (a) is a diagrammatic representation of the situation arising due to coupling within the CH_2F group, assuming $J_{AX} = J_{BX}$. If we first neglect the effects of coupling to the fluorine (X) nucleus we can depict the situation as in figure 4.2.2 (b).

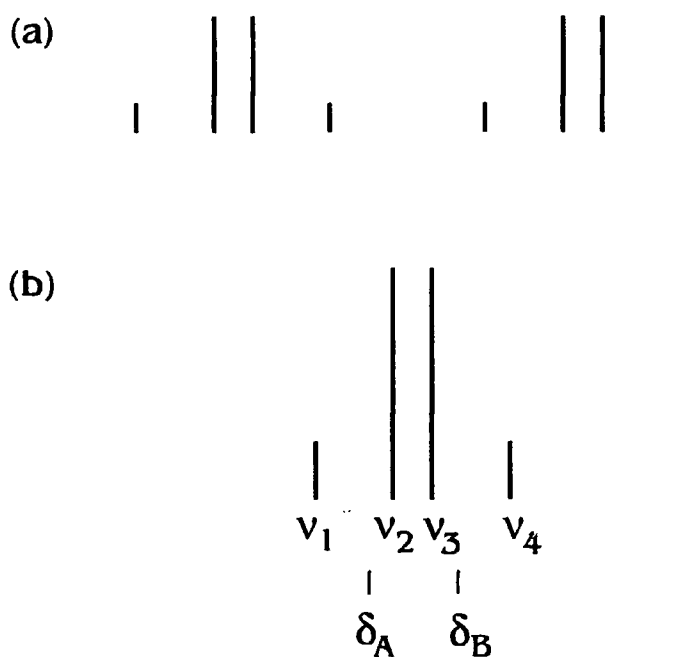


Figure 4.2.2 Diagrammatic representation of second-order indirect coupling effects.

In figure 4.2.2 (b) the true chemical shifts of a and b (H-21a and H-21b) no longer lie at the mid-points of the doublets, but at approximately the 'centre of gravity' of the doublets, as denoted by δ_A and δ_B . The four components of the resonances are labeled ν_1 to ν_4 from high frequency to low frequency respectively,

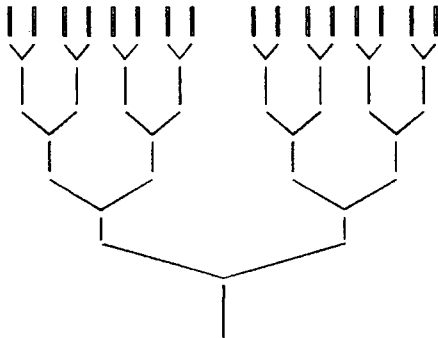
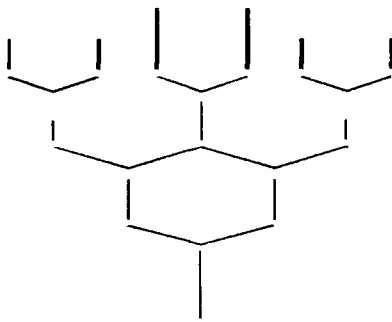
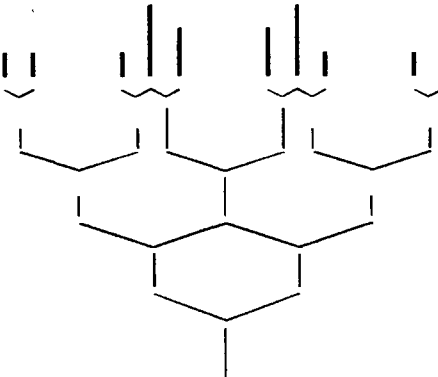
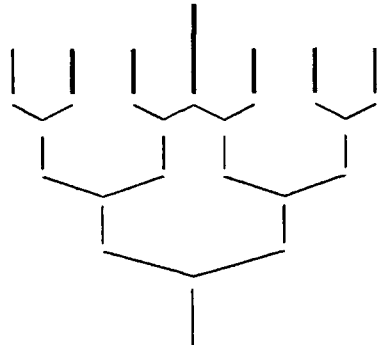
where ν_1 and ν_2 are due (in the limit) to spin A and ν_3 and ν_4 are due to spin B. True chemical shifts can be calculated using equation 4.2.1.

$$\delta_A - \delta_B = 10^6 [(\nu_1 - \nu_4)(\nu_2 - \nu_3)]^{1/2} / \nu_0 \quad (4.2.1)$$

This equation was used to calculate the chemical shifts for H-21a and b in compounds 1 and 3, which both contain geminal protons attached to C-21, and that only show a small disparity in chemical shift from one another. In compound 3 these geminal protons are part of a CH₂OH functional group, and a similar second-order effect is observed.

One striking feature of the data contained in table 4.2.1 and the spectrum illustrated in figure 4.2.1 is the large number of couplings displayed by various signals. As stated in the introduction, because some of these signals are obscured by others, a detailed analysis of all multiplet structures is not always possible, a point exemplified by the signals arising from the geminal protons attached to C-7 and C-12 in all three steroids. However, for the signals that are not obscured a great deal of information can be gleaned from the multiplet fine structure that assists in spectral assignment.

Take for example the signal arising from H-8 in the spectrum of compound 1 (figure 4.2.1). In all, twenty-two individual components are visible in this multiplet due to a variety of homonuclear and heteronuclear, long-range and short-range indirect couplings. The value of the information attainable from a detailed analysis of coupling constants in such a multiplet structure is demonstrated in table 4.2.2, which documents in detail the magnitude and origin of the coupling constants observed in the spectrum of compound 1, for some of the more complex multiplets, that are not obscured by other signals.

Proton	Multiplet Structure	Magnitude of Coupling Constants	Assignment
H-6 β		1.7 Hz	$^4J_{H,H}$ (H-8)
		4.4 Hz	$^3J_{H,H}$ gauche (H-7 β)
		11.2 Hz	$^3J_{H,H}$ trans (H-7 α)
		48.8 Hz	$^2J_{H,F}$ (F-6)
H-14		8.0 Hz	$^3J_{H,H}$ (H-15 α)
		11.8 Hz	$^3J_{H,H}$ trans (H-8)
		12.0 Hz	$^3J_{H,H}$ (H-15 β)
H-15 β		2 Hz	$^4J_{H,H}$ (H-16Me)
		11.1 Hz	$^3J_{H,H}$ cis (H-16)
		12.0 Hz	$^2J_{H,H}$ (H-15 α)
		12.0 Hz	$^3J_{H,H}$ (H-14)
H-15 α		3.8 Hz	$^3J_{H,H}$ (H-16)
		8.0 Hz	$^3J_{H,H}$ (H-14)
		12.0 Hz	$^2J_{H,H}$ (H-15 β)

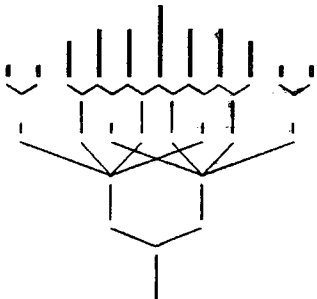
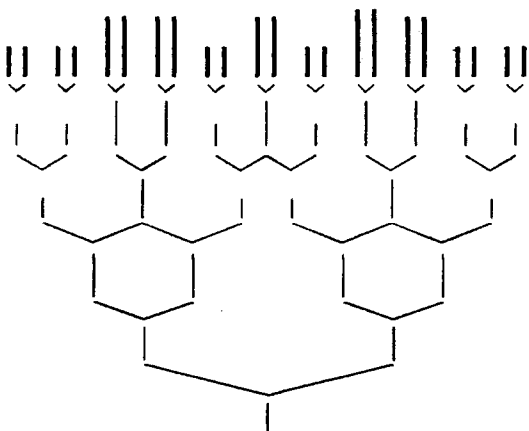
H-16		3.8 Hz	${}^3J_{\text{H,H}} (\text{H-15}\alpha)$
		7.3 Hz	${}^3J_{\text{H,H}} (\text{H-16Me})$
		11.1 Hz	${}^3J_{\text{H,H}} \text{ cis } (\text{H-15}\beta)$
H-8		1.7 Hz	${}^4J_{\text{H,H}} (\text{H-6}\beta)$
		5.0 Hz	${}^3J_{\text{H,H}} \text{ gauche } (\text{H-7}\beta)$
		11.8 Hz	${}^3J_{\text{H,H}} \text{ trans } (\text{H-7}\alpha)$
		11.8 Hz	${}^3J_{\text{H,H}} \text{ trans } (\text{H-14})$
		28.8 Hz	${}^3J_{\text{H,F}} (\text{F-9})$

Table 4.2.2 Assignment of coupling constants observed in the proton solution-state spectrum of compound 1.

A great number of the coupling constants listed in table 4.2.2 are vicinal proton-proton couplings, the magnitudes of which are well known to be dependent on a number of factors. In particular the size of the dihedral angle is known to affect substantially the values of vicinal coupling constants. The variation of ${}^3J_{\text{vic}}$ with dihedral angle is well documented and understood,¹ and can be used to advantage in spectral assignment to determine the stereochemistry of the molecule under study. Conversely, if the stereochemistry is already known the magnitude of the coupling constants can be used as an aid to spectral assignment. Figure 4.2.3 is a simple diagrammatic representation of the variation in J_{vic} with dihedral angle.

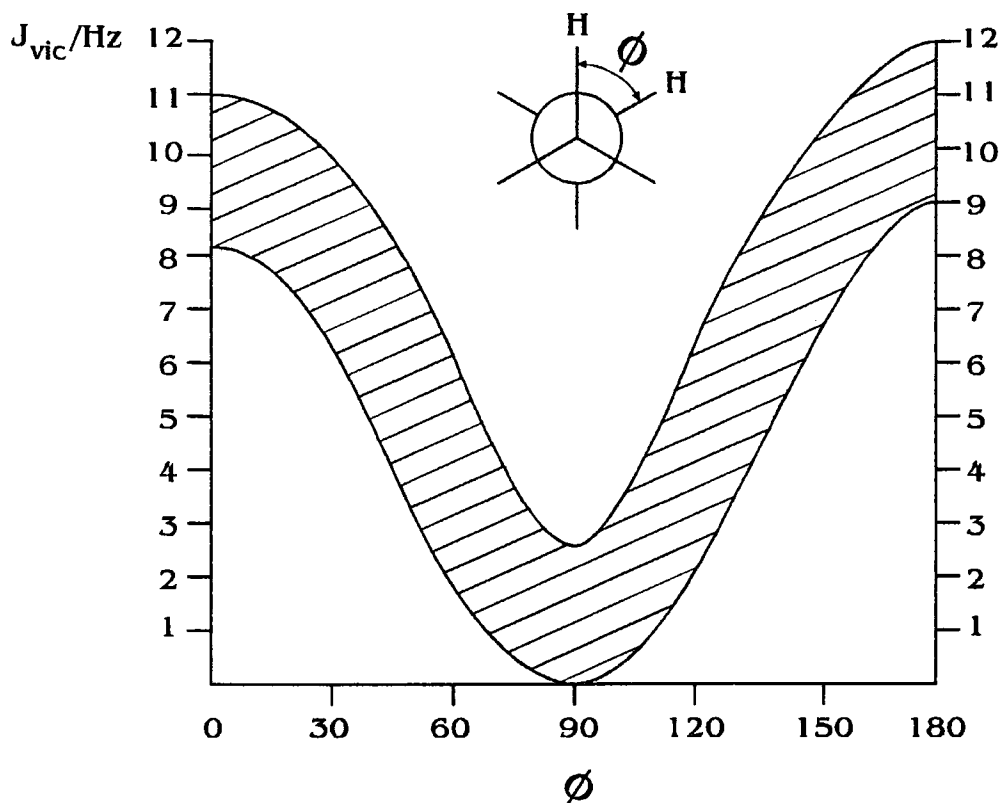


Figure 4.2.3 Variation of proton-proton vicinal coupling constants with dihedral angle ϕ .

The low-energy conformations usually adopted in simple unstrained alkanes correspond to dihedral angles of 60° (gauche+), 300° (gauche-), and 180° , (trans). Figure 4.2.4 is a representation of the conformation adopted by compound 1, and can be used in conjunction with table 4.2.2 to verify the magnitudes of the vicinal couplings observed in all areas of the structure. If we consider the conformation adopted in the region around C-14, C-15 and C-16, due to the presence of the cyclopentyl ring, ring strain gives rise to dihedral angles differing from those for the optimum, low-energy states. Dihedral angles of approximately 30° , 110° and 150° cause coupling constants of unexpected magnitudes.

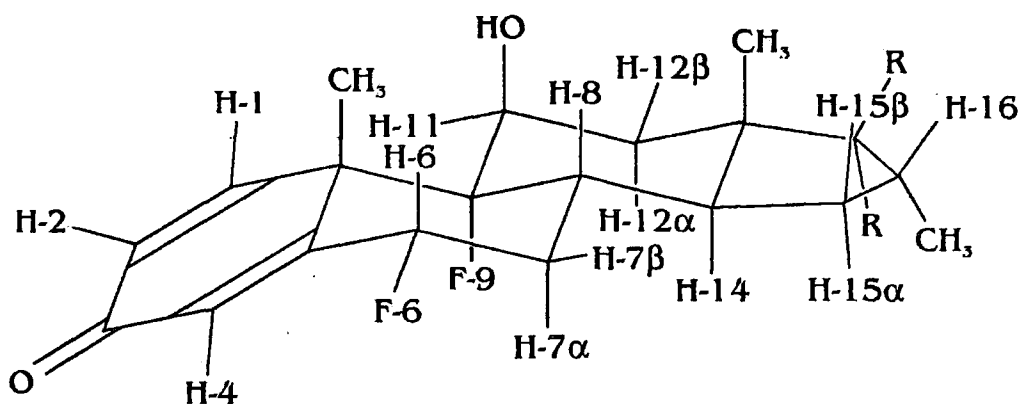


Figure 4.2.4 Representation of the conformation adopted by compound 1.

4.2.2 Two-dimensional Proton Spectra

Information available from the magnitude of homonuclear indirect coupling constants can be of great use in the assignment of proton spectra, but has its limitations. Where a multitude of similar couplings exist it may be difficult to account for their exact origin. To identify exactly which nuclei couple to which other nuclei a COSY-45 experiment can be performed. The results of such an experiment conducted on compound 1 are presented in figure 4.2.5. Of the most intense off-diagonal peaks, three can be assumed to occur from geminal coupling between the methylene protons attached to C-7, C-12 and C-15. Other large cross-peaks occur due to coupling between the H-1 and H-2 protons and H-16 and H-16 Me. These peaks were the starting point for the other assignments, the details of which are outlined below.

The two double doublets at 7.31 ppm and 6.30 ppm couple to each other. In addition, the low-frequency signal also couples to a double doublet at 6.24 ppm. All three signals are in the region where we expect alkene protons to appear and therefore can be confidently assigned to the protons around ring A. Their particular assignments are verified as H-1 (7.31 ppm), H-2 (6.30 ppm) and H-4 (6.24 ppm). For this group of nuclei the coupling pattern is very difficult to interpret and assign.

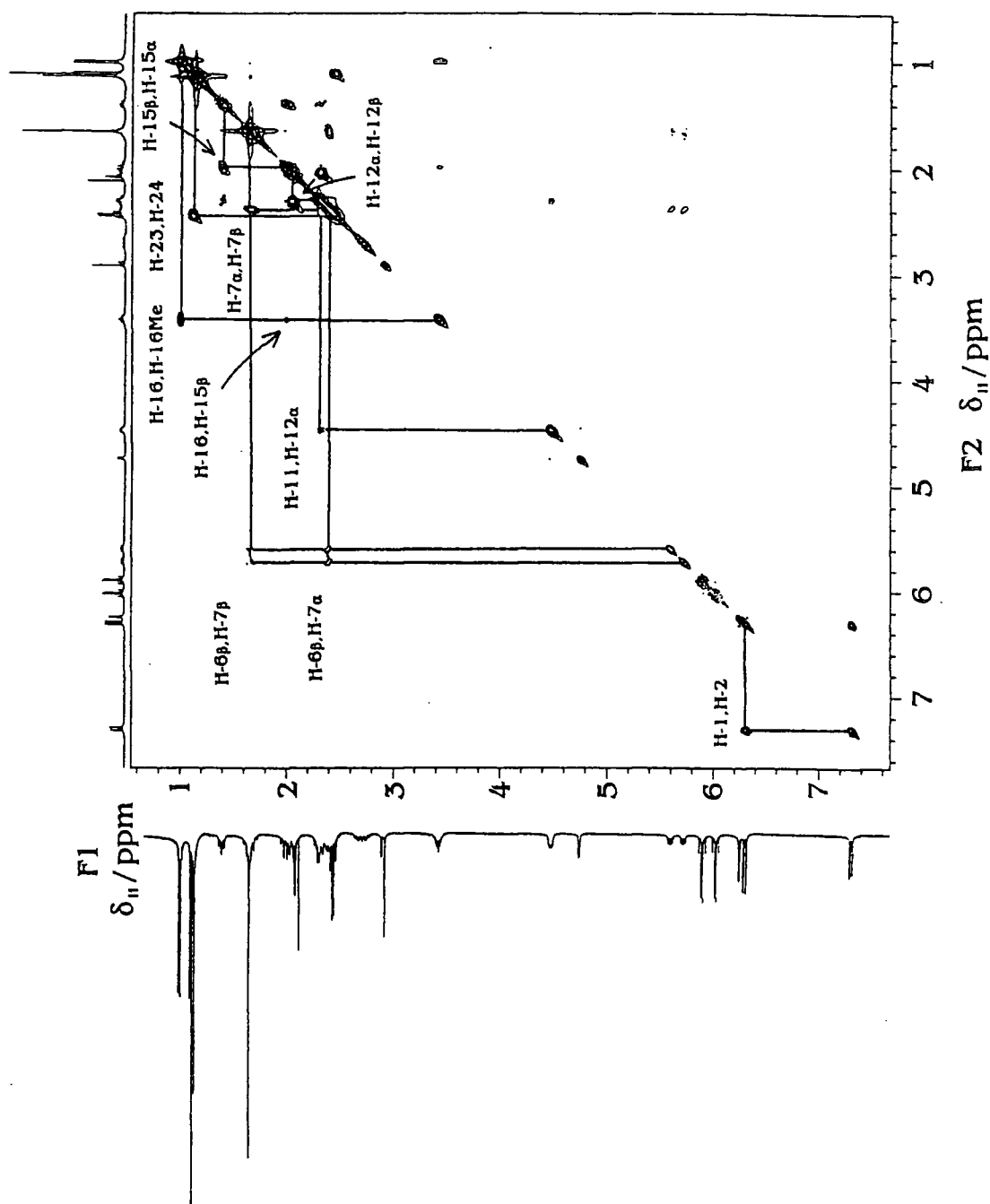


Figure 4.2.5

Contour plot of the 100.577 MHz ^1H COSY-45 spectrum of steroid 1, recorded for a solution in acetone- d_6 , showing some of the correlations. The following spectral parameters were used: spectral width 2907 Hz (both dimensions), pulse duration 18.5 μs , recycle delay 1 s, number of transients 16 incremented 242 times.

Only a coupling between H-1 and H-2 and a coupling between H-4 and H-2 are visible in the COSY spectrum.

However, on inspection of the 1-D spectrum (figure 4.2.1), all three signals show two couplings, one large and one small. The reason that the other fine couplings in these signals remain undetected in the COSY could be either because they are due to long-range coupling to fluorine nuclei present on ring B, or, conversely that these are proton-proton couplings that are too small to detect. For the fine splitting in H-1 either coupling to F-9 through the 'W' pathway, well known for efficient transmission of indirect coupling effects, or a five-bond coupling to H-4, afforded efficient by the presence of a conjugated system between these nuclei could be responsible. Similarly, the fine structure in the signal from H-4 at 6.24 ppm could be due to coupling to H-1, H-2 or F-6.

The signals at 4.74 ppm and 4.47 ppm display a weak coupling to one another in the COSY spectrum. A one-dimensional proton spectrum repeated on compound 1 using d_6 DMSO as the solvent revealed that the signal at 4.74 ppm was found to shift to high frequency to 5.55 ppm. Such a large dependence of chemical shift on solvent is indicative of a hydroxyl proton, as was discussed in section 4.2.1. For this reason the signal at 4.74 ppm was assigned to H-11 OH and that at 4.47 ppm to H-11. This assignment was further validated by the correlation of H-11 to one of a pair of geminal protons at 2.04 ppm (H-12 β).

The signal at 3.42 ppm similarly displays a coupling to one of a pair of geminal protons in addition to coupling to a signal at 1.00 ppm, which, given its chemical shift and integral value, must belong to a set of magnetically equivalent methyl protons. The only methyl protons in the system that could exhibit such a strong coupling are those of H-16 Me. This also explains the coupling to the two geminal protons (12.0 Hz to H-15 β at 1.99 ppm and 3.8 Hz to H-15 α at 1.40 ppm). It is interesting to note that of these two couplings, again only the larger coupling to H-15 β is observed in the COSY spectrum.

Other correlations that were useful in assignment were those of H-14 with H-15 α and H-15 β , H-23a and b with the methyl protons H-24, and H-6 at 5.64 ppm to the geminal protons H-7 α and H-7 β at 2.38 and 1.66 ppm respectively. This final assignment was particularly valuable since, as mentioned previously, the signals from the two H-7 geminal protons are obscured by other resonances, thus eliminating the chance of gleaned assignment information from the magnitude of couplings in their multiplet structure.

The above discussions have centred on compound **1**, since this was the most suitable to demonstrate the value of a detailed analysis of the coupling constants exhibited by particular resonances in the one-dimensional experiment and the importance of the COSY-45 spectrum to establish the origin of these coupling constants so as to achieve accurate spectral assignment. However, for compounds **2** and **3** individual resonances, and consequently splittings arising from indirect coupling between nuclei, are less discernible due either to signal overlap or signal broadening. In these instances the information available from a simple one-dimensional experiment is less informative, and assignment on the basis of such an experiment alone would leave many highly ambiguous assignments. A spectrum recorded at a higher field strength would help to reduce the cluttering of the spectrum, but this would only be of limited use. This is where the true value of the COSY-45 spectra to authenticate assignments can be appreciated.

The low-frequency region of the COSY-45 spectrum of compound **3** is shown in figure 4.2.6. Where severe signal overlap was a major problem in the one-dimensional spectrum, the second dimension clarifies which signals overlap with which and, assignments can now be made with a much higher degree of accuracy. All relevant correlations between signals are highlighted in figure 4.2.6.

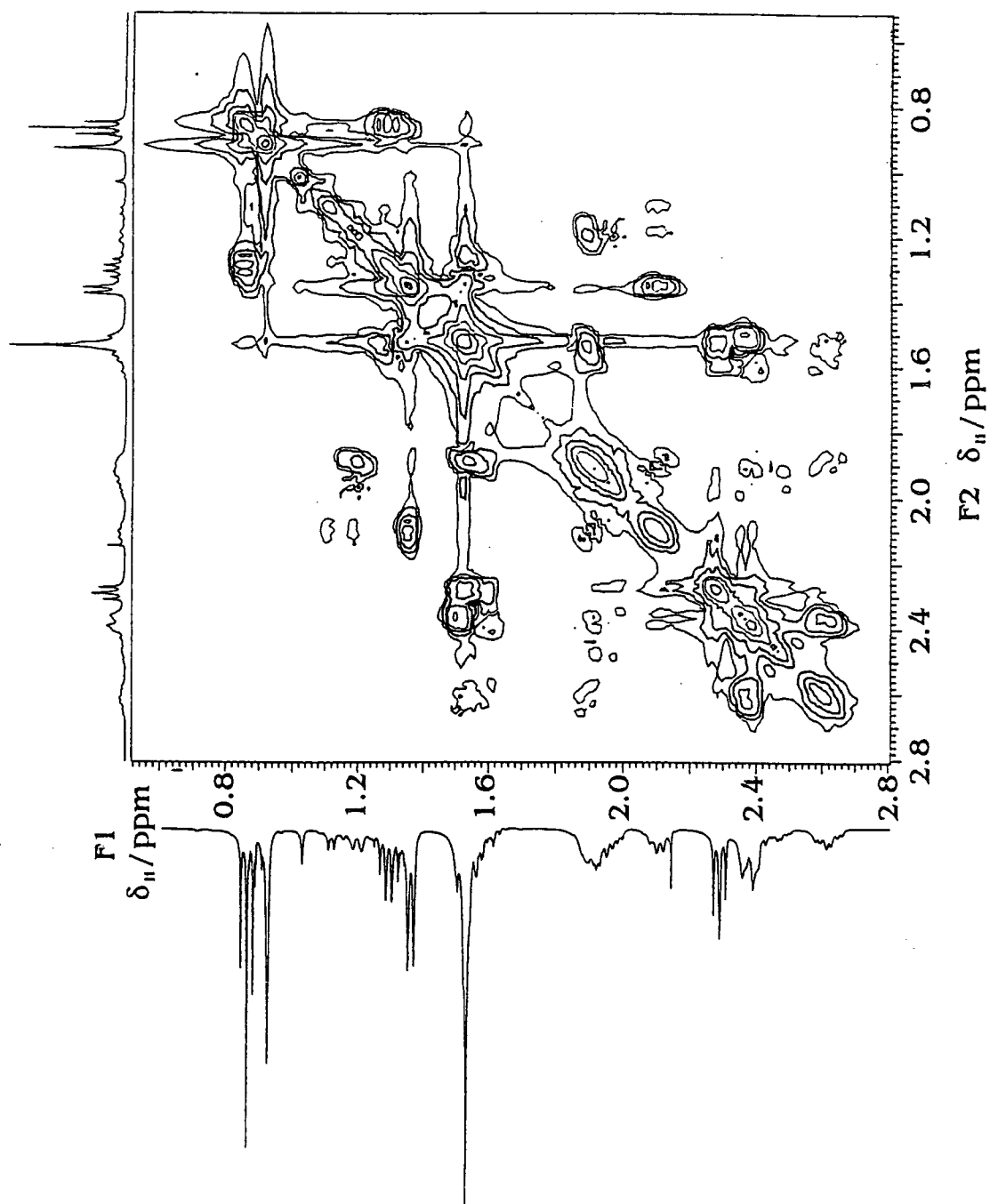


Figure 4.2.6

Expansion of the low-frequency region of the 100.577 MHz proton COSY-45 spectrum of compound 3, using spectral conditions identical to those used in figure 4.2.5.

The problem of overlapping peaks is epitomised by the regions of the spectrum corresponding to ~ 1.5 , ~ 1.9 and ~ 2.4 ppm. These areas each contain signals from three protons, all of which display numerous couplings, and naturally overlap is severe. However, with the second dimension, all correlations become clearly visible, and this enables assignments to be made with a much higher degree of accuracy.

One point of interest arising from figure 4.2.6, that has already been mentioned in section 4.2.1, is the apparent low-frequency shift of the H-16 proton at 2.12 ppm compared to the corresponding proton in the spectrum of compound 1, which resonates at 3.42 ppm. Initially, when assigning this resonance using only the one-dimensional proton spectrum, this disparity led to some confusion in ascertaining the true identity of this peak. Inspection of the COSY-45 spectrum reveals categorically that this signal arises from H-16 since it displays a strong correlation to H-16Me at 1.36 ppm. The large chemical shift difference has already been explained as being a consequence of the fact that for compound 1 the H-16 proton is on the β face (see figure 4.2.4), whereas in compound 3 the proton is on the α face of the molecule.

4.3 Carbon Solution-state Spectra

4.3.1 One-dimensional Carbon Spectra

All carbon spectra were acquired under conditions of proton decoupling for reasons discussed previously, and as was found for the proton spectra certain resonances were much easier to assign than others. This can be appreciated by considering the appearance of the low-frequency and high-frequency regions of the proton decoupled carbon-13 solution-state spectrum of compound 1 shown in figure 4.3.1.

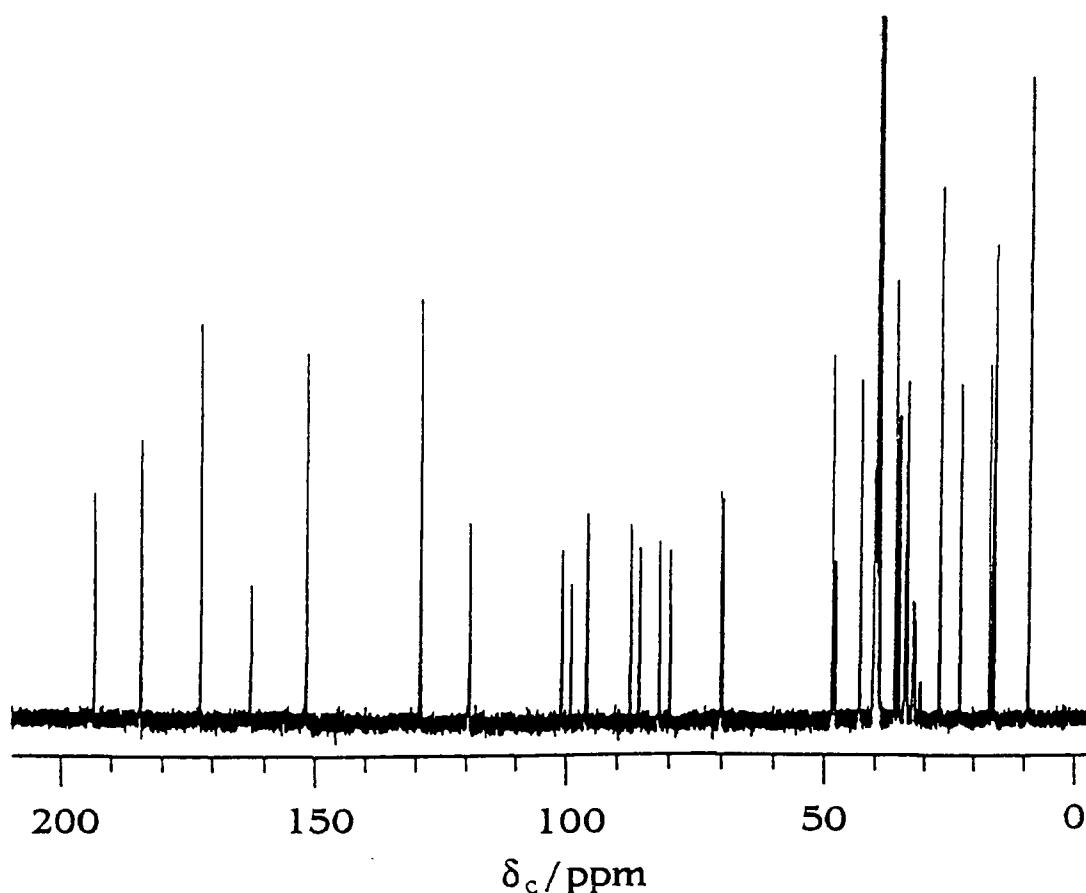


Figure 4.3.1 100.58 MHz proton-decoupled carbon-13 solution-state spectrum of compound 1. Operating conditions were as follows: Spectral width 25 kHz, recycle delay 2 s, pulse duration 10 μ s, number of transients 1024.

Again, the presence of splittings in some of the signals due to indirect coupling to fluorine was a major help in spectral assignment for these compounds, especially compound 1. Unmistakably large 1J (^{13}C , ^{19}F) indirect couplings are observed in the signals at 86.73 ppm, 99.84 ppm, and 81.01 ppm in figure 4.3.1. Finer splittings due to 2J or 3J couplings are visible in signals occurring at 119.44 ppm, 162.69 ppm and in the region between 20 ppm and 50 ppm. In fact two of these signals (at 31.97 ppm and 47.88 ppm) are double doublets, indicative of coupling to two fluorine nuclei. The only carbon nuclei that could display such a coupling are C-7, C-8, C-5 or C-10. C-5 was eliminated on the basis that an alkene carbon was

unlikely to display such a low chemical shift. The high-frequency signal was postulated to belong to the quaternary C-10, again due to its chemical shift. However, to verify the assignment of this resonance, and the one at 31.97 ppm, further information was needed, which was obtained from a DEPT experiment. The individual sub-spectra from the DEPT experiment are displayed in figure 4.3.2.

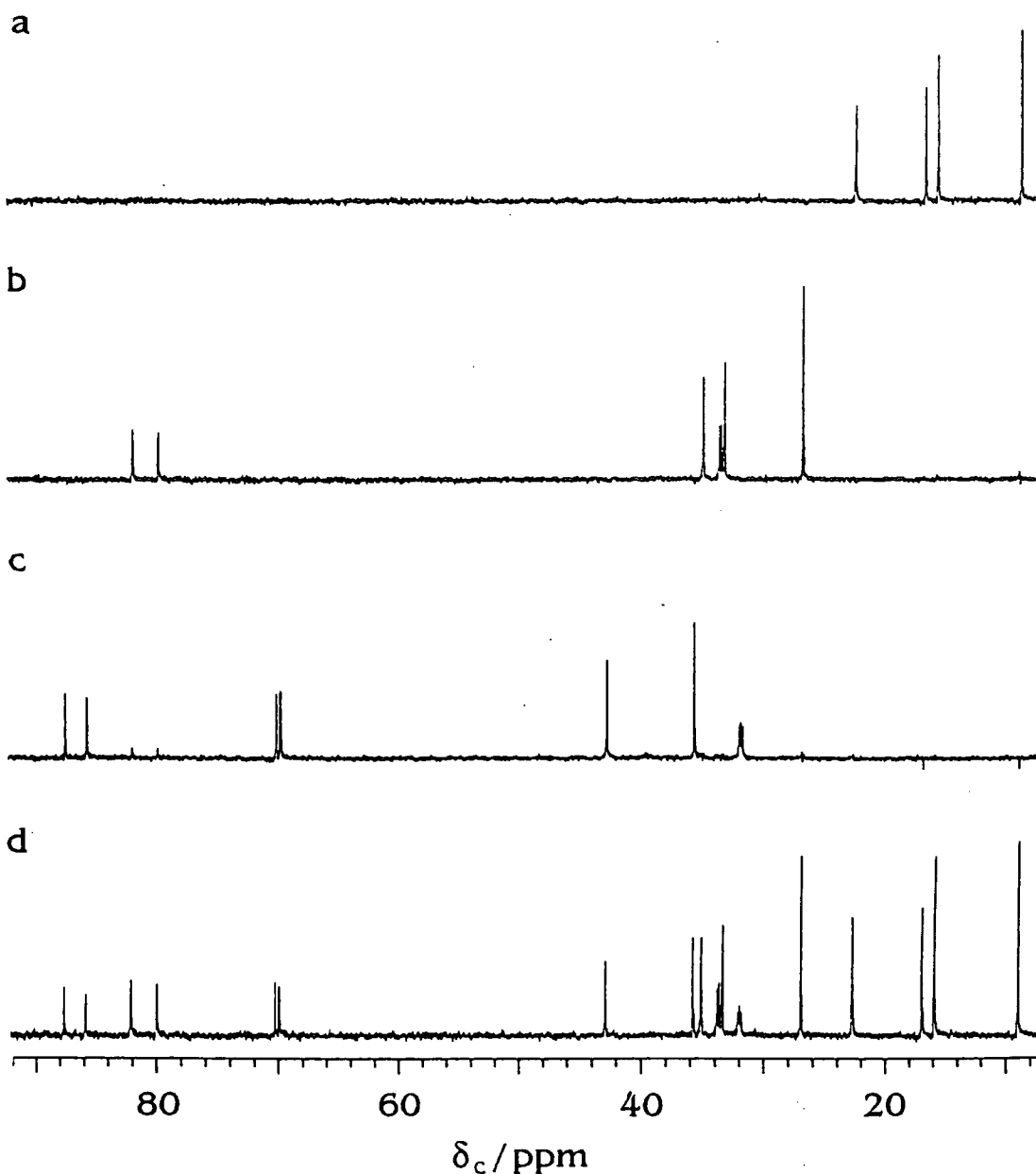


Figure 4.3.2 High-frequency region of the carbon-13 DEPT spectra of compound 1. Sub-spectra show (a) CH₃ carbons only, (b) CH₂ carbons only, (c) CH carbons only and (d) all protonated carbons.

It is immediately apparent that our assignment problem, along with many others, is solved, since the signal at 47.88 ppm does not appear in any of the sub-spectra, and must consequently arise from a quaternary carbon (C-10). In addition, the signal at 31.97 ppm, displaying the two couplings, appears in the CH sub-spectrum and not the CH₂. This must therefore arise from C-8 and not C-7. Other assignments verified by information contained in the DEPT spectra were as follows: the signal at 81.01 ppm is from C-21 (appears in sub-spectrum (b)), the one at 99.84 ppm is from C-9 (does not appear in any sub-spectra) and that at 86.73 ppm is from C-6 (appears in sub-spectrum (c)). The doublet at 33.72 ppm arising from a methylene carbon must be due to C-7 and the methyl resonance at 22.71 ppm, also a doublet, must be due to C-19, since these are the only two nuclei of their kind in close enough proximity to a fluorine nucleus for coupling to be feasible.

The complete list of carbon solution-state assignments of all three steroids and carbon-fluorine indirect coupling constants is contained in table 4.3.1.

Carbon	1 ^b	Compound 2 ^b	3 ^c
1	151.67	151.87 (9.6)	152.58
2	129.15	129.06	129.56
3	184.35	184.40	186.75
4	119.44 (12.6)	119.40 (13.0)	124.87
5	162.69 (13.4)	162.97 (13.4)	166.66
6	86.73 (180.0)	86.82 (180.0)	30.92
7	33.72 (18.9)	33.92 (18.3)	27.59
8	31.97 (18.7, 11.1)	32.14 (18.7, 11.1)	33.67 (19.5)
9	99.84 (177.0)	100.23 (177.4)	100.18 (176.0)
10	47.88 (22.1, 3.4)	48.06 (22.2, 4.5)	48.19 (22.1)
11	70.07 (35.5)	70.21 (35.8)	71.46 (37.4)
12	35.10	35.28	37.25
13	48.42	48.88	47.45
14	42.86	43.08(11.1)	43.60
15	33.38	31.98	34.81
16	35.74	37.33	47.02
17	96.10	92.30	93.89
18	15.89	16.02	17.04
19	22.71 (5.0)	22.83 (5.3)	22.92 (5.7)
20	193.24	197.90	205.43
21	81.01 (212.0)		67.30
22	172.41		174.17
23	26.92		34.28
24	8.96		26.49
25			22.18
26			13.58
C-16Me	16.89	15.04	19.44

^a Chemical shifts listed as δ_C (ppm), with coupling constants in Hz given in parentheses.

^b In DMSO- d_6

^c In CDCl₃

Table 4.3.1 Carbon-13 solution-state chemical shifts and indirect (¹³C, ¹⁹F) spin-spin coupling constants^a for steroids 1- 3.

4.3.2 Two-dimensional Carbon Spectra

As was mentioned in section 4.1, the biggest failing of the DEPT experiment is its inability to differentiate between nuclei of the same type within a structure. To efficiently do this necessitates the use of the HETCOR experiment, which allows us

to correlate carbon resonances to proton resonances, whose identities are already known to a high degree of reliability from analyses of the one-dimensional and COSY-45 spectra. For compound **1** the HETCOR spectrum allowed us to correctly assign the otherwise virtually indistinguishable C-12 and C-15 methylene carbons. The two proton signals at 2.32 ppm and 2.04 ppm, assigned to H-12 α and H-12 β respectively, were found to correlate to $\delta_{\text{C}} = 36.39$ ppm, unambiguously assigning this peak to C-12. Likewise, the two signals at 1.40 ppm and 1.99 ppm assigned to the geminal H-15 protons correlated to a resonance at 34.53 ppm (C-15).

For compound **3**, the monofluorinated steroid, as was the case for the COSY-45 spectrum, the HETCOR spectrum was of increased importance. There were a number of reasons for this. Firstly, fewer instances of (^{13}C , ^{19}F) indirect coupling arose to provide valuable clues in the assignment of peaks in the carbon spectrum. Secondly, this is the largest structure, containing twenty-seven carbon atoms, seven of which are chemically similar methylene carbons, already known to present assignment problems in these compounds. Lastly, as previously mentioned in section 4.2, the proton spectrum of compound **3** contained a large number of overlapping resonances. The high-frequency area of the HETCOR spectrum of compound **3** is shown in figure 4.3.3.

The severe overlap in the proton spectrum around 2.4 ppm, making assignment difficult, is no longer a problem since it is instantly apparent to which carbon the signals are correlated, and hence how many resonances are overlapping.

From the COSY-45 spectrum, the methylene proton resonances had been provisionally assigned. Using the HETCOR spectrum the signals arising at 1.30 ppm, 1.54 ppm, 1.55/1.92 ppm, 2.38/2.62 ppm, 2.29 ppm, 1.20/1.90 ppm, 1.50/2.38 ppm were assigned to H-25a and b, H-24a and b, H-7 α /H-7 β , H-6 α /H-6 β , H-23a and b, H-15 β / H-15 α and H-12 β / H-12 α respectively.

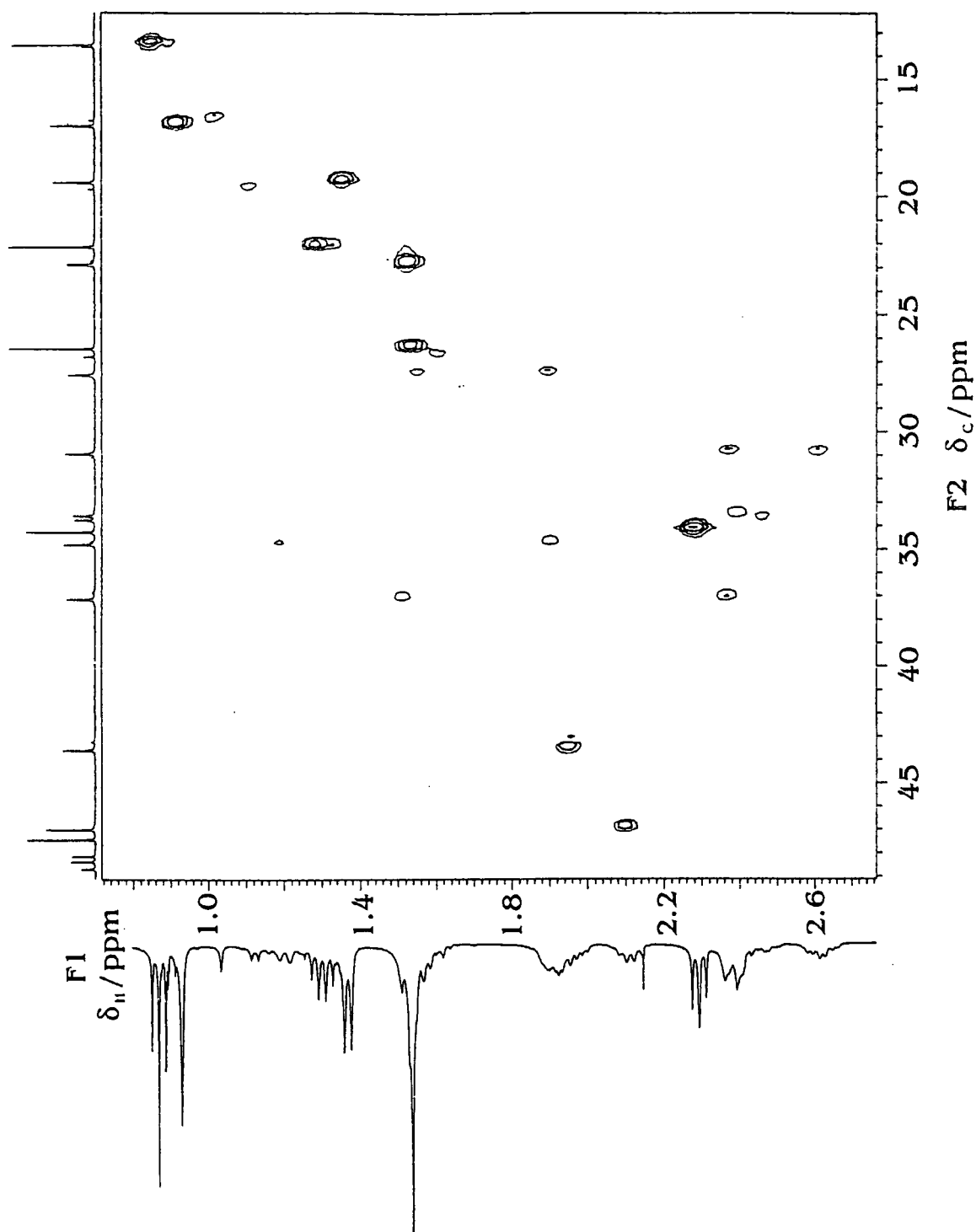


Figure 4.3.3 Contour plot of the high-frequency area of the 100.58 MHz short-range ^1H - ^{13}C HETCOR spectrum of compound 3. The following spectral parameters were used: Spectral width 20325 Hz (2907 Hz in second dimension), recycle delay 1 s, pulse duration 17.0 μs , number of transients 256, incremented 256 times.

4.4 Solid-state Carbon-13 Spectra

The carbon-13 solid-state chemical shifts of compounds 1-3 and observable carbon-fluorine indirect coupling constants are listed in table 4.4.1.

Carbon	Compound			
	1	2(i)	2(ii)	3
1	156.6	154.6	155.0	155.9
2	130.0	129.9	131.3	129.7
3	188.7	187.2	185.3	187.5
4	119.3	120.6	122.9	124.9
5	169.5	164.3	162.8	169.7
6	87.7 (189)	^c	^c	31.9
7	34.4	34.1	33.1	27.7
8	34.4	34.1	34.0	34.4
9	101.3 (185)	101.3 (~ 192 ^d)	102.5 ^c	100.9 (189)
10	50.7	49.7	50.3	48.1
11	73.2	72.5	72.8	72.5
12	37.2	36.0	36.4	38.3
13	50.7	50.3	50.3	49.7
14	43.6	45.0	44.8	43.8
15	34.4	34.1	34.0	35.1
16	36.6	38.1	38.6	46.5
17	95.5	92.7	93.2	94.6
18	18.6	18.3	18.9	19.7
19	22.8	26.9	25.1	23.4
20	193.9	204.9	203.3	205.6
21	^c			68.2
22	172.1			174.6
23	28.6			34.4
24	11.5			26.2
25				23.2
26				15.7
C-16Me	15.9	16.0	16.0	19.9

^a Chemical shifts listed as δ_c / ppm. They are accurate to ± 0.3 ppm, but within one spectrum the relative shifts are more accurate than this.

^b Coupling constants in Hz given in parentheses.

^c Not clearly observed.

^d Values subject to error arising from signal overlap.

Table 4.4.1 Carbon-13 solid-state chemical shifts^a and scalar (¹³C, ¹⁹F) spin-spin coupling constants^b for steroids 1- 3.

4.4.1 Spectral Anomalies

4.4.1.1 Effects of (^1H , ^1H) Dipolar Coupling

From table 4.4.1 it is apparent that the only instances of carbon-fluorine indirect coupling observable are ^1J couplings. No ^2J or ^3J couplings are seen in the spectra as a consequence of the reduced resolution in the solid-state. The ^1J coupling constants observed compare favourably with those seen in the solution state ($\pm < 10\%$). However, of these fluorinated carbon resonances it is apparent that no entries appear for the chemical shifts of the carbons C-6 in either polymorphic form of compound **2** or for that of C-21 in compound **1**. The solution-state chemical shifts of these fluorinated carbons are 86.73, 99.84 and 81.01 ppm for C-6 (CF), C-9 (CHF) and C-21 (CH_2F) respectively, which appear as clearly discernible doublets in figure 4.3.1. In the corresponding region of the solid-state $^1\text{H} \rightarrow ^{13}\text{C}$ cross-polarisation MAS spectrum of compound **1** (figure 4.4.1), which is expanded in the inset, only two resonances are clearly visible, both displaying ^1J (^{13}C , ^{19}F) scalar coupling. The third resonance arising from C-21 is lost in a broad 'hump'. Add to this the fact that the signal from C-6 is less readily observed than that from C-9, and we can postulate with a high degree of certainty that the effect is due to the hydrogens bonded to carbons (cf. C-6 in compounds **2(i)** and **2(ii)**). Residual homonuclear (^1H , ^1H) dipolar interactions, perhaps as a result of inadequate strength decoupling fields, influencing the fluorine behaviour are most likely to be the cause of such broadening. The situation is not helped by the diminution of the centreband intensities due to the spinning sidebands.

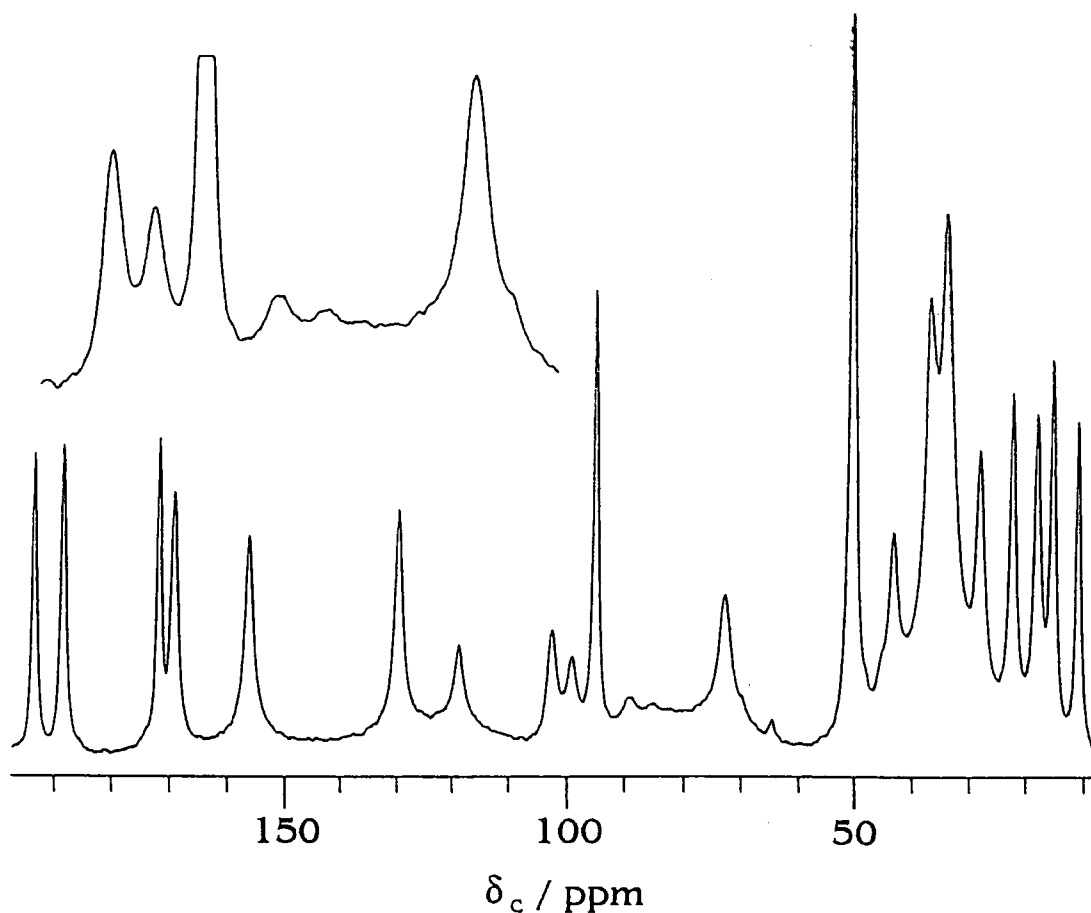


Figure 4.4.1 50.33 MHz CP/MAS spectrum of compound 1. The spectrum was recorded from 11,444 transients, employing a 2 ms contact time. Spectral width was 20 kHz and a recycle delay of 5 s was used in conjunction with a $4.0 \mu\text{s}$ $\pi/2$ pulse duration.

4.4.1.2 Interplay of Dipolar and Shielding Tensors

One peculiarity apparent in the signals arising from the C-9 resonance in the above spectrum, and indeed in the solid-state spectra of all these compounds, is that the two components of the doublet differ in intensity. This aspect of the C-9 resonance is better understood with closer inspection of the associated spinning-sideband manifold in the $^1\text{H} \rightarrow ^{13}\text{C}$ cross-polarisation MAS spectrum of compound 3, shown in figure 4.4.2, in which the spinning rate was increased to ~ 5 kHz to ensure that the first-order low-frequency spinning sideband was clear of the methyl resonances.

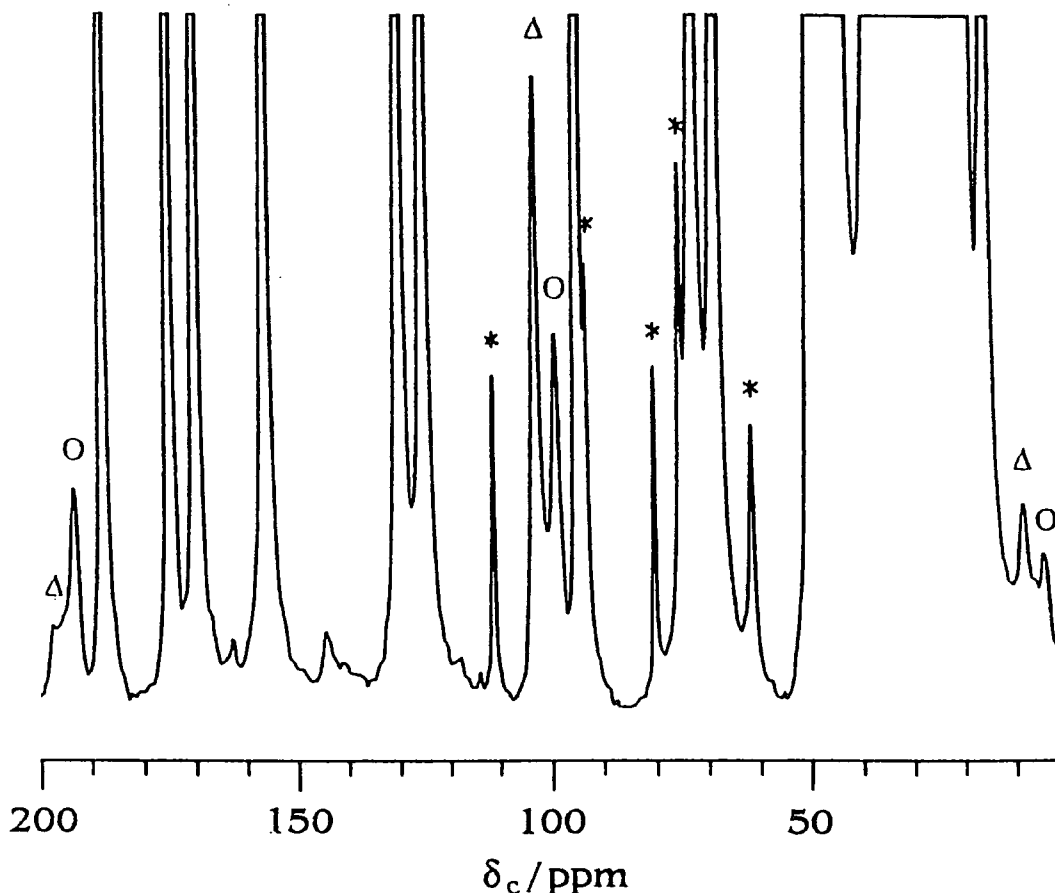


Figure 4.4.2 Expansion of the 50.33 MHz ^{13}C CP / MAS spectrum of Betamethasone-17-valerate highlighting, via the unequal intensity distribution in the spinning side-band manifold of the C-9 resonance, the combined effect of (^{13}C , ^{19}F) heteronuclear dipolar coupling and ^{13}C shielding anisotropy. The three bands marked O forms one spinning-sideband manifold, and those marked Δ another such manifold. The centrebands of these two manifolds are separated by $^1J_{\text{FC}}$. Asterisks denote spinning sidebands.

A reversal in intensity of the two components is observed in the high-frequency spinning sideband compared to the centreband. Furthermore, the weak low-frequency centreband (indicated by a circle) is associated with strong wide-ranging spinning sidebands, whereas the stronger centreband has weaker, less wide-ranging sidebands. It is found that summing the total intensity for each of the components across the whole frequency range of the spinning-sideband manifolds results in equality in intensity for the two components. A phenomenon is occurring which is stretching the shielding anisotropy powder pattern for one component of the

doublet whilst compressing it for the other component of the doublet. The observation can be attributed to the joint effect of (^{13}C , ^{19}F) dipolar coupling and ^{13}C shielding anisotropy, for which the scalar coupling acts to distinguish signals involving different fluorine spin states. Information regarding the magnitudes and signs of the scalar coupling, shielding anisotropy and dipolar coupling interactions can be accessed from suitable analyses of spectra. Such a phenomenon has been reported before for the (^{13}C , ^{31}P) nuclear pair in phosphonium iodide² and for the (^{19}F , ^{31}P) nuclear pair in polycrystalline fluorophosphates,³ but to the best of our knowledge has not been previously reported in C-F systems.

To carry out an analysis of the spectral data presented in figure 4.4.2 it is preferable to consider the C-F spin-pair as an AX spin system, where the A represents the observed nucleus ^{13}C , and X the nucleus to which it is coupled ^{19}F . (^{19}F , ^{13}C) 1J coupling constants are well documented in the literature as being negative in sign, which means that the low-frequency component of the C-9 centreband, having the weaker intensity, must arise from the A transition when the X nucleus is β . In addition, because this centreband is weak, as was previously discussed, it also must arise from the spin state having the 'stretched' shielding anisotropy. Similarly the high-frequency A transition ($X = \alpha$) must possess the 'compressed' anisotropy. The effective anisotropy in such cases of interplay between shielding anisotropy and dipolar coupling is given by equation 4.4.1.

$$\lambda' = \lambda - 2D'm_X/v_A \quad (4.4.1)$$

where λ represents the actual value of the shielding anisotropy and λ' its effective value. For the low-frequency centreband ($X = \beta$) the $2D'm_X/v_A$ term is negative which, if we assume that the anisotropy is positive, gives us an increased effective anisotropy. This result is consistent with the experimental observation of strong wide-ranging spinning sidebands, and it can therefore be categorically stated that this

particular carbon nucleus displays a negative $^1J(^{19}\text{F}, ^{13}\text{C})$ coupling constant and a positive shielding anisotropy.

4.4.1.3 Polymorphism Effects

As mentioned previously, steroid 2 exists in two crystal forms. This became apparent when a doubling of peaks was observed in the solid-state spectra of this compound (see figure 4.4.3). The two samples are estimated to contain 85 % of polymorph (i) and 15 % polymorph (ii) (upper spectrum) and 10 % polymorph (i) and 90 % polymorph (ii) (lower spectrum) by weight. As can be seen from table 4.4.1 and as is depicted in figure 4.4.3, carbonyl carbon atoms and unsaturated carbon atoms in conjugation with these exhibit the greatest variation in chemical shift between the forms. The phenomenon can be attributed to hydrogen bonding effects, and depends on the distance O-H---O. Less significant chemical shift variations of other carbon atoms are a consequence of slight differences in crystal packing and/or molecular geometry variations (especially conformation). The steroids 1 and 3 exhibit no such doubling of peaks in the solid-state spectra, (see figure 4.4.1 and 4.4.2) which is indicative of there being only one molecule in the asymmetric unit. There may be specific hydrogen bonding effects on chemical shifts for the solid state, since carbonyl carbon atoms and unsaturated carbon atoms in conjugation with these, along with hydroxyl carbon atoms, experience some of the largest variations in chemical shift on going from the solution-state to the solid-state. However, there also appear to be some non-specific "solvent effects", as attested by the fact that nearly all the solution → solid changes in shift are positive.

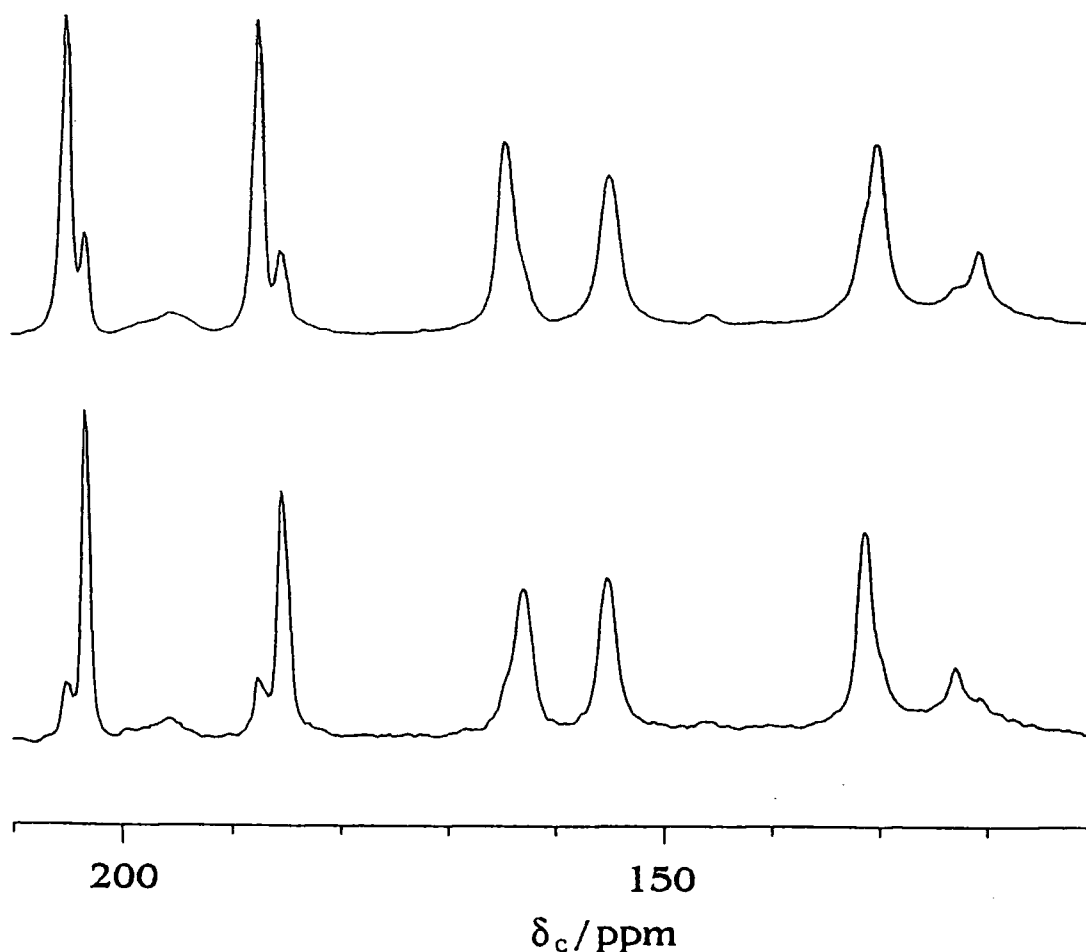


Figure 4.4.3 High-frequency region of the 50.33 MHz ^{13}C CP/MAS spectrum of two samples of compound 2, showing two resonances (with different intensities for the two samples) for several carbons, which is attributed to the occurrence of polymorphic forms.

4.5 Conclusions

Results presented in this chapter have outlined one of the many routes available to the NMR spectroscopist in the assignment of proton and carbon spectra. The wealth of information available not only from complicated two-dimensional experiments, consisting of numerous pulses with varying phases, but also from simple one-dimensional experiments has been underlined. In particular, structurally complex

molecules, possessing crowded spectra, have been used to highlight the vital role the study of the effects of nuclear interactions have in the assignment of NMR spectra and in furthering our understanding of both the properties of these compounds at a molecular level and associated NMR phenomena.

In the solution state indirect coupling interactions have been used to ascertain topologies and stereochemistries of these molecules. Via solid-state NMR investigations the occurrence of polymorphism has been detected in one of the compounds studied and has been traced to arise either from hydrogen-bonding or crystal packing and/or molecular geometry variations. The effects of interplay between dipolar and shielding tensors resulting in doublets of unequal intensities for signals arising from fluorinated carbons have been observed.

References

1. W. Kemp, *NMR in Chemistry*, Macmillan (1986).
2. R. K. Harris, K. J. Packer, and A. M. Thayer, *J. Magn. Reson.*, **62**, 284 (1985).
3. U. Haubenreisser, U. Sternberg and A. R. Grimmer, *Mol. Phys.*, **60**, 151 (1987).

Chapter 5

^{19}F NMR Studies

5.1 Introduction

Despite the problems inherent in the acquisition of high-resolution solid-state fluorine spectra, other properties intrinsic in the fluorine nucleus, discussed in section 2.4.1, combine to make it an excellent nucleus with which to observe the NMR phenomena. These properties can be more readily appreciated in the solution state, where random molecular tumbling negates many of the problems that blight solid-state fluorine-19 NMR. The strong dipolar interactions are suppressed by the rapid motion and consequently it is no longer imperative to implement proton decoupling in order to obtain good resolution. Indeed proton decoupling is often omitted in order to observe strong (^1H , ^{19}F) indirect couplings, which can extend over a significant number of bond lengths, and which can prove so useful in structure determination. Such clues to molecular structure are lost in the solid state with the necessity to implement HPPD to achieve a satisfactory degree of resolution, since HPPD suppresses not only (^1H , ^{19}F) dipolar interactions, but also (^1H , ^{19}F) indirect (scalar) interactions. Although it is possible to selectively suppress the (^1H , ^{19}F) dipolar interactions whilst retaining (^1H , ^{19}F) indirect coupling by use of suitable multiple-pulse decoupling sequences, these tend to be technically demanding and, furthermore, it is still questionable whether indirect couplings would be observable in solid state spectra given the inherent reduction in achievable resolution in the solid state. The maximum resolution possible in the solid state is generally far below that found in the solution state because the rate of motion witnessed by molecules in solution is invariably so rapid that it suppresses dipolar interactions to a far greater extent than would be possible using any selective averaging technique.

The resultant inherent gain in resolution in the solution state not only allows us to detect (^1H , ^{19}F) indirect couplings, and gives an apparent improved signal-to-noise ratio, but also improves our ability to distinguish nuclei displaying only small magnetic inequivalences. This can be likened to the way the advent of higher and higher field spectrometers has improved our ability to differentiate such signals, although the reasons are very different.

Another consequence of the rapid molecular motion seen in solutions is that longitudinal relaxation times are greatly reduced. For rigid systems fluorine T_1 times can be minutes rather than seconds in the solid state. Consequently spectra can be acquired much more quickly and simply for solutions.

In this chapter a proton coupled ^{19}F solution-state spectra of compound 1 is presented, and chemical shifts for all three fluorinated steroids are tabulated, along with (^1H , ^{19}F) indirect coupling constants. Furthermore it is demonstrated that ^{19}F NMR of the solid state employing high-power proton decoupling is not only feasible, given the correct apparatus, but also that the gain in resolution afforded by the successful implementation of proton decoupling allows a whole host of experimental techniques, long since regarded as routine in solid-state carbon-13 NMR, to be applied to the more technically demanding case of solid-state fluorine-19 NMR. The fluorinated steroids give, for the first time, proton-decoupled MAS fluorine spectra of organic compounds of pharmaceutical interest involving more than one fluorine atom per molecule.^{1,2}

Single-pulse and $^1\text{H} \rightarrow ^{19}\text{F}$ cross-polarisation experiments have been performed on both spinning and static samples, with and without proton decoupling, and have highlighted certain advantages inherent in the CP mode of operation. Chemical shifts are compared with those seen in the solution state. Although the steroids are chemically quite similar, they have been found to possess subtle differences in properties that manifest themselves in the NMR investigations. Decoupled static and slow-spinning experiments have been used to access information regarding the relevant shielding tensors, which has yielded some interesting results. Dipolar

dephasing³ and rotational resonance^{4,5} effects have been demonstrated for the trifluorinated steroid **1**, and have been used to make qualitative estimations about the magnitude of the relevant dipolar interactions present between nuclei. Fluorine spin-lattice relaxation times, measured by means of the inversion-recovery pulse sequence, have indicated that spin diffusion between the fluorine nuclei in compound **1** is efficient. This has been verified, and the dynamics of this spin diffusion investigated, by 2-D EXSY⁶ experiments performed with variable mixing times. The occurrence of polymorphism in steroid **2**, already detected by carbon-13 solid-state NMR studies, has been confirmed and monitored by observation of the fluorine nucleus. For completeness, the reverse cross-polarisation ($^{19}\text{F} \rightarrow ^1\text{H}$) experiment has also been carried out.

It is important to appreciate the relative merits and shortcomings of solid-state NMR over solution-state NMR. Although solution-state spectra generally display greater resolution than solid-state spectra, which leads to an increased ease of extraction of information, ultimately less information is available from solution-state spectra. In the solid state we are hindered only by our inability to access this wealth of information due ultimately to technological constraints. The experiments outlined in the previous paragraph highlight the increased volume of information solid state NMR gives. Furthermore, much of this relies on the fact that internuclear interactions are not averaged to their isotropic values in the solid state by molecular motion, as occurs in solution, and these spectra can be used to extract information regarding the nature of such interactions, which is lost in the solution state.

5.2 Solution-state Fluorine-19 Spectra

The problem intrinsic in the acquisition of solid-state fluorine-19 NMR spectra pertaining to the feasibility of implementing HPPD as a result of close proximity of the proton and fluorine resonant frequencies and the resultant need for effective isolation of these frequencies has been discussed in chapter 2. However, the question

arises as to why proton-decoupled ^{19}F spectra can be acquired in the solution state apparently without any great difficulty. To understand this it is necessary to consider once again the relative powers needed to effectively decouple protons in the two states. As was mentioned in chapter 2, in the solution state dipolar interactions are suppressed by the rapid molecular motion, and consequently in fluorinated compounds proton decoupling only amounts to suppression of the smaller (^1H , ^{19}F) indirect coupling interactions. The magnitudes of such interactions rarely exceed 50 Hz, the suppression of which only requires powers of the order of 1-2 W. However, in the solid state (^1H , ^1H) homonuclear and (^1H , ^{19}F) heteronuclear dipolar interactions must also be suppressed and, because these are known to be up to 20 kHz in magnitude, much higher-strength decoupling fields are needed, utilising powers in excess of 100 W. It is the isolation of the proton and fluorine resonant frequencies at this increased power that presents the problems. Such isolation is much easier at the lower powers adequate for solution-state fluorine-19 NMR.

The fluorine-19 proton-coupled solution-state spectrum of compound 1, the trifluorinated steroid, is shown in figure 5.2.1. The total acquisition time was seven minutes. As was the case in the carbon-13 spectrum of this compound (figure 4.3.1) the clearly visible splittings in the signals, which are a consequence of (^1H , ^{19}F) indirect coupling, provide valuable clues to the assignment of this spectrum. The signal at -191.72 ppm is a triplet, indicative of coupling to two equivalent protons, and is therefore assigned to the fluorine of the fluoromethyl group. The magnitude of the ^2J (^1H , ^{19}F) coupling is of the order of 50 Hz, which is in good agreement with literature values for related compounds.^{7,8} Further definitive assignments can be made on the basis of the magnitude of the coupling constants displayed by each of the two remaining resonances. Both signals are double doublets, the largest (^1H , ^{19}F) indirect coupling constant being displayed by that at -187.38 ppm, and this is again approximately 50 Hz. We can predict therefore that this signal is most likely to arise from F-6, the only other fluorine attached to a proton-bearing carbon.

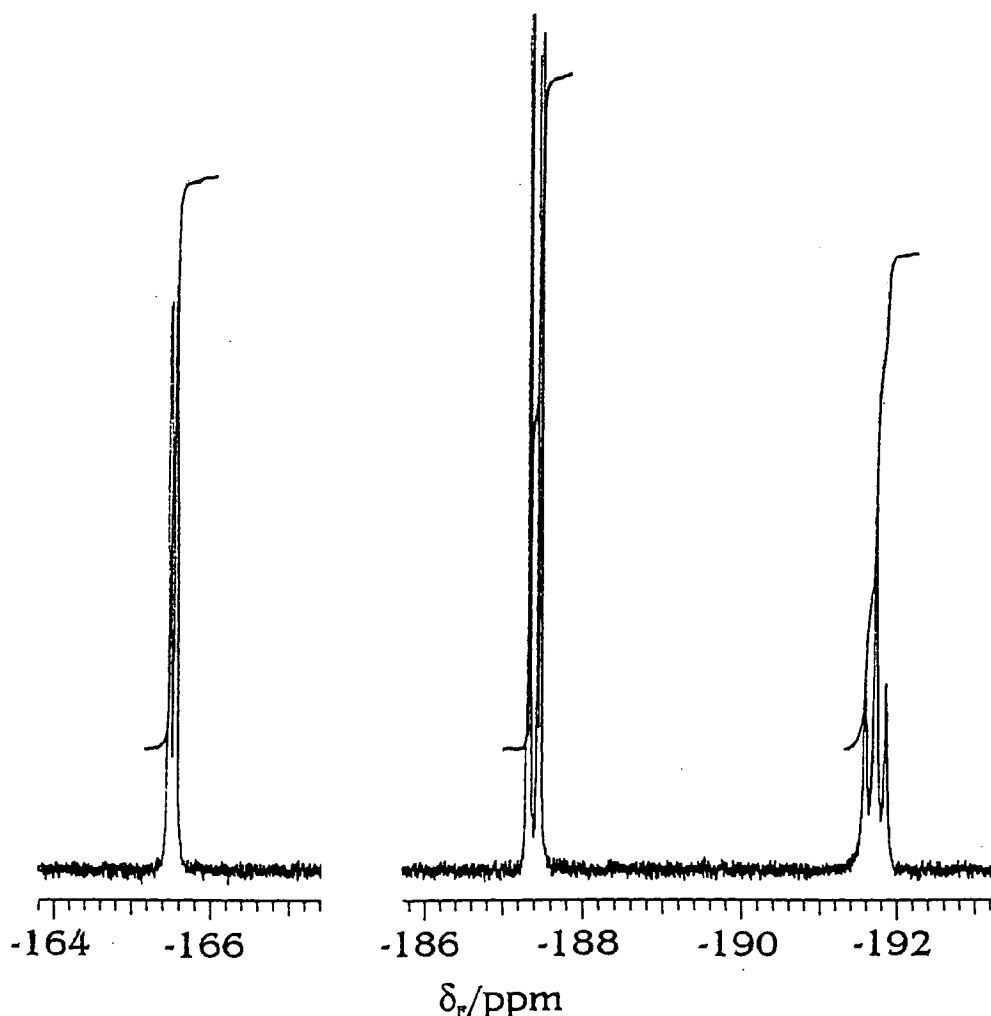


Figure 5.2.1 376.27 MHz proton-coupled ^{19}F solution-state spectrum of compound 1. A $8.0\ \mu\text{s}$ pulse duration was used in conjunction with a 4 s recycle delay. 64 transients were acquired using a spectral width of 11.5 kHz.

The smaller (~ 30 Hz) coupling in the signal at -165.52 is close to the expected value for a $^3\text{J} (^1\text{H}, ^{19}\text{F})$ coupling and the resonance is assigned to F-9. It is, of course, possible to cross-check these assignments by referring to the detailed analyses of coupling constants displayed by the adjacent proton resonances, the results of which were presented in the previous chapter. Both H-8 and H-6 are found to display coupling constants of the correct magnitude to verify these assignments. In addition, the smaller couplings in each of the signals arise from ^3J (from F-6) and ^4J (from F-9) ($^1\text{H}, ^{19}\text{F}$) coupling to H-7 β and H-7 α respectively. The sizable four-bond coupling displayed by F-9 is again afforded by the 'W' pathway. Close inspection of figure

5.2.1 also solves one last coupling constant assignment problem. In chapter 4 it was postulated that the fine splitting seen in the resonance of H-1 could be due either to long-range coupling to fluorine or to coupling to another proton. No such splitting of 1.6 Hz is visible in the fluorine spectrum, even though the digital resolution is 0.33 Hz. This categorically proves that the splitting of H-1 is due to (^1H , ^1H) indirect coupling, to the proton attached to C-4.

Similar considerations apply to spectra of compounds 2 and 3. Table 5.2.1 lists all relevant solution-state data for each of the three steroids studied.

Compound	δ_{F} /ppm	(^1H , ^{19}F) Indirect Coupling Constants / Hz	Assignment
1 ^a	-165.52	8.6, 27.8	CF
	-187.38	13.9, 48.5	CHF
	-191.72	49.3	CH ₂ F
2 ^b	-163.87	10.5, 29.7	CF
	-186.08	13.9, 48.5	CFH
3 ^a	-166.75	7.5, 29.0	CF

^a In CDCl₃

^b In d₆DMSO

Table 5.2.1. Fluorine-19 solution-state NMR data for compounds 1-3

5.3 Solid-state fluorine-19 Spectra

5.3.1 The Effects of Proton Decoupling and MAS on Solid-state ^{19}F NMR Spectra

When considering the effects of HPPD and MAS on the appearance of solid-state fluorine spectra there are a number of factors that have to be taken into consideration. The selective suppression of the various internuclear interactions

present allows us to access valuable information. For the trifluorinated steroid the interactions of relevance are (^1H , ^1H) and (^{19}F , ^{19}F) homonuclear dipolar coupling, (^1H , ^{19}F) heteronuclear dipolar coupling, shielding anisotropies and indirect coupling. If any fine structure arising from chemical shifts and/or indirect coupling is to be observed suppression of the large dipolar interactions is imperative. Similarly, given the large chemical shifts displayed by the fluorine nucleus it can be postulated that associated anisotropies will be substantial and these must also be suppressed to obtain chemical shifts accurately. (^{19}F , ^{19}F) dipolar coupling can be neglected in our compounds due to the dilute nature of the fluorine nuclei. This obviates the need for multiple-pulse operation at the observe frequency, i.e. CRAMPS, and avoids the technical difficulties associated with this technique. (^1H , ^{19}F) heteronuclear and (^1H , ^1H) homonuclear dipolar interactions are suppressed by HPPD, which allows us to determine solid-state ^{19}F chemical shifts with a much higher degree of accuracy and to detect indirect coupling to any magnetic nuclei other than protons, providing of course that the natural abundance of the heteroatom is high enough, and coupling constants large enough, to be observed given the inherently poorer resolution in the solid state compared to the solution state.

MAS is used to suppress shielding anisotropies, but a slight complication arises in that in addition to suppressing shielding anisotropies, MAS is also known to suppress dipolar couplings due to the similar $(3 \cos^2\theta - 1)$ geometrical dependence. Ultimately therefore, if MAS without proton decoupling is performed suppression of both shielding anisotropies and dipolar coupling occurs. The extent of suppression is governed by the rate of sample rotation and, if it were possible to spin at rates similar in magnitude to the interaction itself, the broadening effects of dipolar couplings, both (^1H , ^{19}F) heteronuclear and (^1H , ^1H) homonuclear, on the NMR signal could, in theory, be totally negated. Indeed such effects have already been observed for different compounds, in instances where dipolar coupling is not so strong, by spinning at speeds of the order of 24 kHz, as was discussed in chapter 2 (see references 8 and 9). Unfortunately the magnitude of the (^1H , ^{19}F) and (^1H , ^1H) dipolar interactions

present in our compounds implies attaining the speeds necessary to effect total suppression of these interactions is technically impossible at the present time, but some degree of suppression may still occur for spinning at rates of up to 15 kHz. Consequently, when comparing bandwidths for static coupled and spinning coupled spectra, to what degree the reduction in bandwidth is due to the suppression of (^1H , ^{19}F) dipolar coupling by HPPD and to what extent it is due to averaging of shielding anisotropies by MAS is unknown. Figure 5.3.1 illustrates the effects of implementing HPPD and the fluorine-19 solid-state NMR spectrum of compound 3. The static proton-coupled spectrum (a), vividly demonstrates spectral broadening due to the combined effects of shielding anisotropies and dipolar couplings, which renders the spectrum of little worth. The identical spectrum but for the implementation of MAS is shown in spectrum (b). The overall reduction observed in the bandwidth is large (up to 20 times) as a result of the implementation of MAS. However, as mentioned previously, what is not clear is to what extent this reduction is due to the collapse of the powder pattern (suppression of shielding anisotropies) and to what extent it is due to suppression of heteronuclear (^1H , ^{19}F) dipolar coupling. Put another way, is the broadening in 5.3.1 (b) due to remaining heteronuclear dipolar coupling, ubiquitous strong (^1H , ^1H) homonuclear dipolar coupling or weak (^{19}F , ^{19}F) dipolar coupling. One way to investigate further such ambiguities would be to employ a suitable multiple-pulse proton-decoupling sequence to retain heteronuclear dipolar coupling and suppress homonuclear dipolar coupling. Spectrum (c) is the static spectrum acquired under conditions of proton-decoupling. Because MAS is known to suppress dipolar interactions in addition to shielding anisotropies, when considering the effects of HPPD on the form of fluorine solid-state spectra it is more worthwhile to compare static spectra. The bandwidth of spectrum (c) is far less that of the static proton-coupled spectrum(a), due to total suppression of (^1H , ^{19}F) heteronuclear and (^1H , ^1H) homonuclear dipolar coupling, but the substantial broadening effect of the shielding anisotropy displayed by the fluorine nucleus still remains and is manifest in a relatively broad powder pattern.

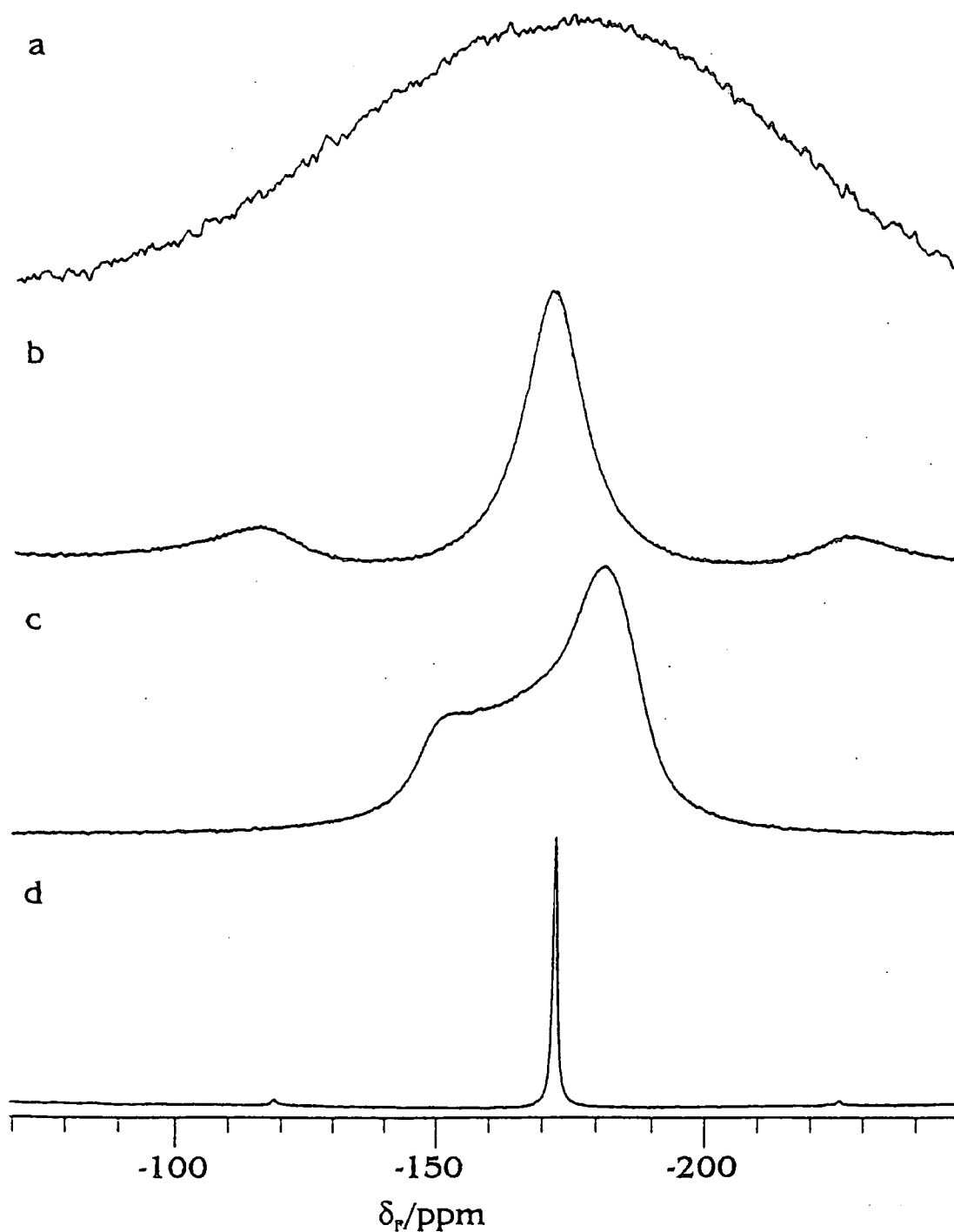


Figure 5.3.1 Comparison of the (a) static proton-coupled, (b) MAS proton-coupled, (c) static proton-decoupled and (d) MAS proton-decoupled $^1\text{H} \rightarrow ^{19}\text{F}$ cross-polarisation spectra of compound 3. Each spectrum was acquired using a spectral width of 50 kHz, a recycle delay of 10s, a $1.8 \mu\text{s}$ pulse duration and a 1 ms contact time. The number of transients were 2880, 1024, 4000 and 16 for spectra a - d respectively. For spectra c and d decoupling fields were of the order of 100 kHz, whereas in spectra a and b MAS rates of 10 kHz were employed.

Whatever the exact nature of the suppression of these interactions by the various selective averaging techniques, as can be seen from figure 5.3.1 (d), the concurrent application of MAS and HPPD causes a substantial reduction in linewidth to a value that is small compared to the ^{19}F chemical shift range. This allows us to differentiate much more effectively between nuclei in similar chemical environments. The residual linewidth is approximately 200 Hz. Although a linewidth of 200 Hz represents a significant gain in resolution, if we compare this to linewidths found in the corresponding ^{19}F solution-state spectrum this value represents an increase of some thirty times. Therefore, although great improvements in resolution are possible by simultaneous application of selective averaging techniques, the level of resolution achievable in the solid state is still very much inferior to that possible in the solution state.

For compound **3**, and other monofluorinated compounds, the requisite for good resolution in the solid state is not of paramount importance in order to obtain accurate chemical shifts. However, for molecules containing a greater number of fluorine atoms the necessity for the application of such techniques to observe separate resonances becomes more important. This point is emphasised in figures 5.3.2 and 5.3.3. Figure 5.3.2 is a comparison of (a) the static CP coupled and (b) the static CP decoupled spectra of compound **1**. Again, without proton decoupling a broad featureless spectrum is obtained, the bandwidth of which is some 40 kHz. The implementation of HPPD reduces this bandwidth appreciably, although the resultant spectrum is still broad due to the superposition of three powder patterns. Figure 5.3.3 compares resolution obtained in (a) the CP/MAS proton-coupled and (b) the CP/MAS proton-decoupled spectra of compound **1** (note the enlarged scale compared to figure 5.3.2).

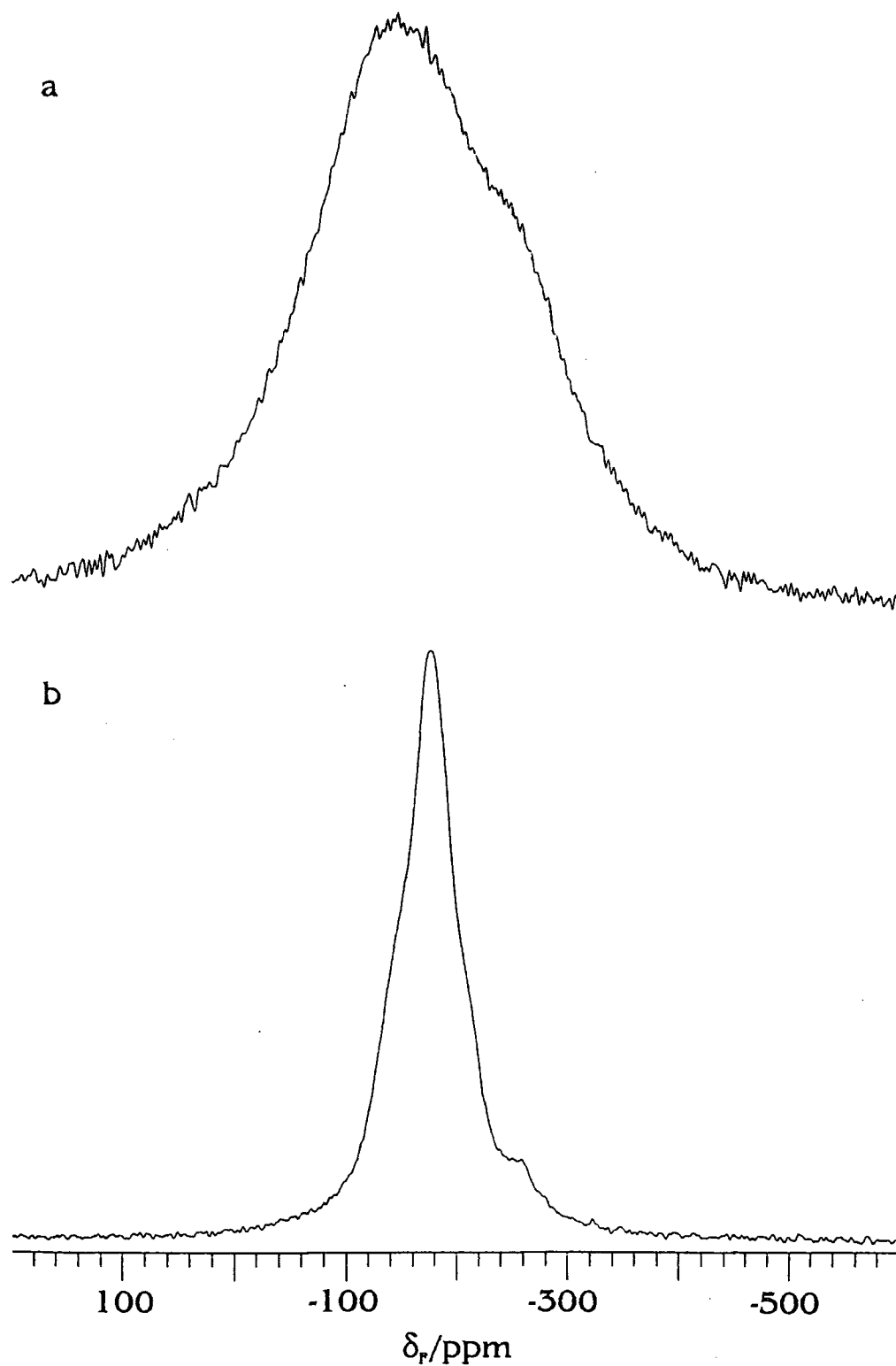


Figure 5.3.2. The static proton-coupled (a) and proton-decoupled (b) 188.28 MHz ^{19}F solid-state CP spectra of compound 1. Experimental conditions were as follows : Pulse duration 2.5 μs , contact time 1 ms, recycle delay 2 s, spectral width 200 kHz, number of transients 3584.

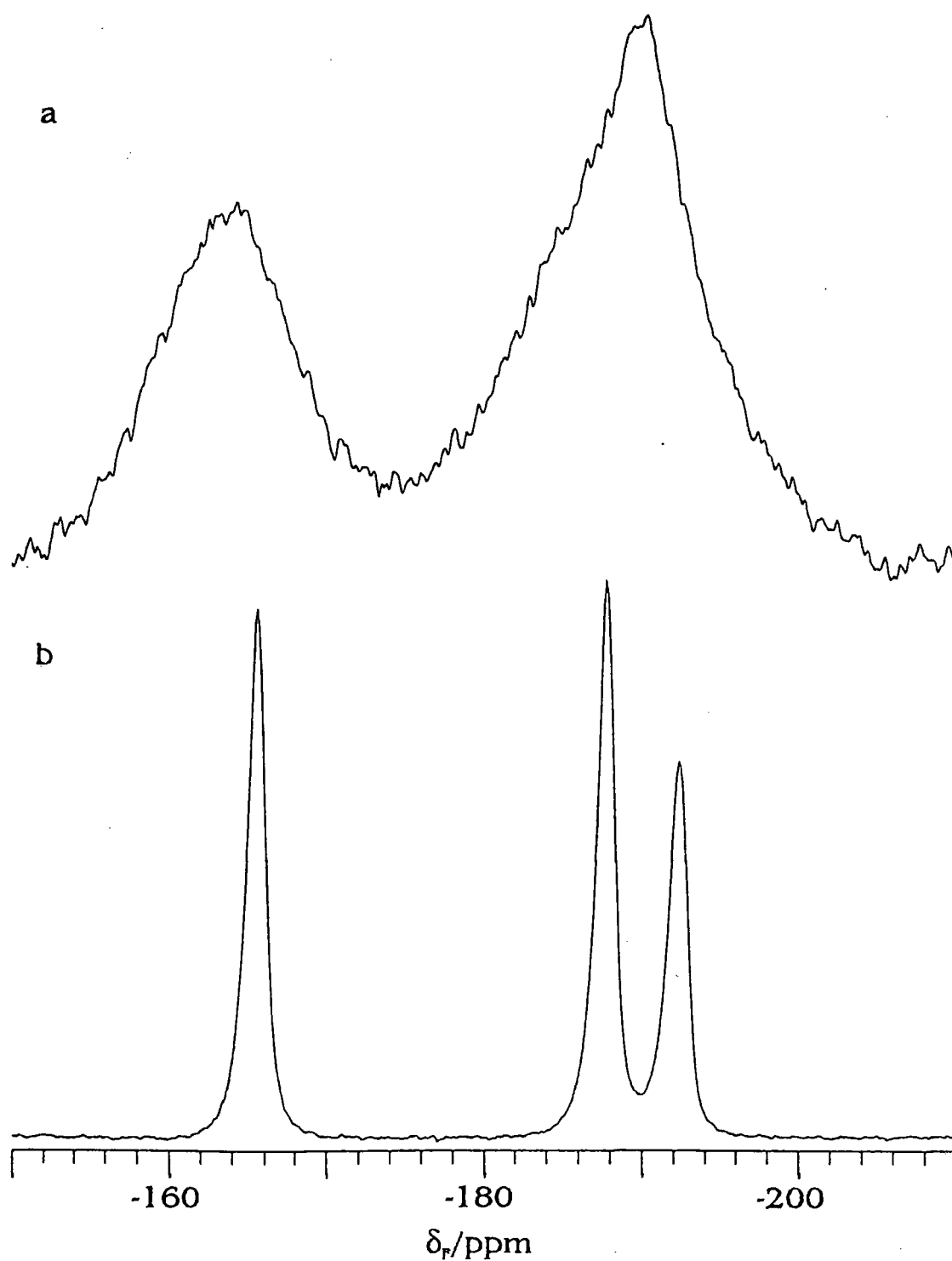


Figure 5.3.3. The 188.28 MHz ^{19}F CPMAS proton-coupled (a) and proton-decoupled (b) solid-state spectra of compound 1. A 2.5 μs pulse duration was used in conjunction with a 1 ms contact time and 2 s recycle delay. 3584 transients were acquired over a spectral width of 50 kHz. The MAS rate was 10 kHz.

Figure 5.3.3 plainly illustrates the increased ability to differentiate resonances separated by only a few ppm by the concurrent application of proton decoupling and MAS. The improvement in resolution afforded by the successful implementation of proton decoupling enables us for the first time to record fluorine chemical shifts of the three fluorinated steroids in the solid-state. Table 5.3.1 lists these shifts (referenced to CFCl_3 at 0 ppm) and the linewidths for all three steroids.

Compound	$\delta_{\text{F}}/\text{ppm}$	Linewidth/Hz	Assignment
1	-165.6	197	CF
	-187.9	200	CHF
	-192.3	200	CH_2F
2	-165.2	210	CF
	-166.5 ^a	^b	CF
	-180.1 ^a	240	CHF
	-183.4	222	CHF
3	-171.4	143	CF

^a Weak peaks assigned to a polymorphic form.

^b Shoulder.

Table 5.3.1 Fluorine-19 solid-state NMR data for compounds 1-3.

For compound 1 the linewidths of the three fluorine resonances are very similar, demonstrating that proton decoupling is effective for fluorines contained in both CFH groups and CH_2F groups. Proton decoupling can therefore be deemed to be efficient for fluorines of all types, and consequently the technical difficulties associated with decoupling at a frequency close to the observe frequency would appear to have been circumvented. However, in this instance it may be argued that rapid rotation of the fluoromethyl group in compound 1, analogous to the rapid rotation of methyl groups seen in simple organic compounds, could be causing the heteronuclear dipolar interactions between the fluorine and protons to be partially

suppressed and therefore that statements regarding comparisons of the effectiveness of proton decoupling for fluorine nuclei in different chemical environments cannot be so simply made. In order to investigate such a hypothesis, and the effectiveness of proton decoupling as a whole, a number of experiments were conducted using varying decoupling field strengths for all three steroids, which unearthed some interesting results. Initial MAS experiments performed on compound 1 revealed that in the absence of proton decoupling, no noticeable difference in linewidth was evident for the fluoromethyl resonance compared to the other two signals, thus proving that motion-induced averaging of coupling is not a significant factor for the CH_2F group. However, more interestingly, the experiment revealed that maximum linewidths for the resonances did not necessarily occur at zero decoupler field. The intensities of the resonances were found to die away before recovering slightly. This phenomenon is illustrated in figure 5.3.4 which is a stacked plot of the spectra obtained under conditions of varying decoupler field strength for a sample spinning at 10 kHz. It was surmised that the dip in intensity of the resonances at a particular proton decoupling field strength could only be due to an interaction of some kind with the decoupling field. The three factors to consider in these experiments are the MAS rate, the decoupling field strength and the rate of any internal motion occurring in the molecule. It was already known that the fluoromethyl group was expected to undergo rapid rotation in this particular compound, and if the frequency of such a rotation was similar to the strength of the decoupler field it could be the interaction of these two effects causing the observed dip in signal intensity. Consequently a set of similar experiments were conducted on this compound at varying temperatures, the hope being that if internal motion accounts for the dip in intensity the reduction and increase in rate of rotation of the fluoromethyl group afforded by the decrease and increase in temperature respectively would result in the minimum signal intensity shifting to lower and higher decoupler field strengths respectively. Varying the temperature had little effect on the strength of decoupling field at which the dip occurred and so it was concluded internal motion could not be responsible.

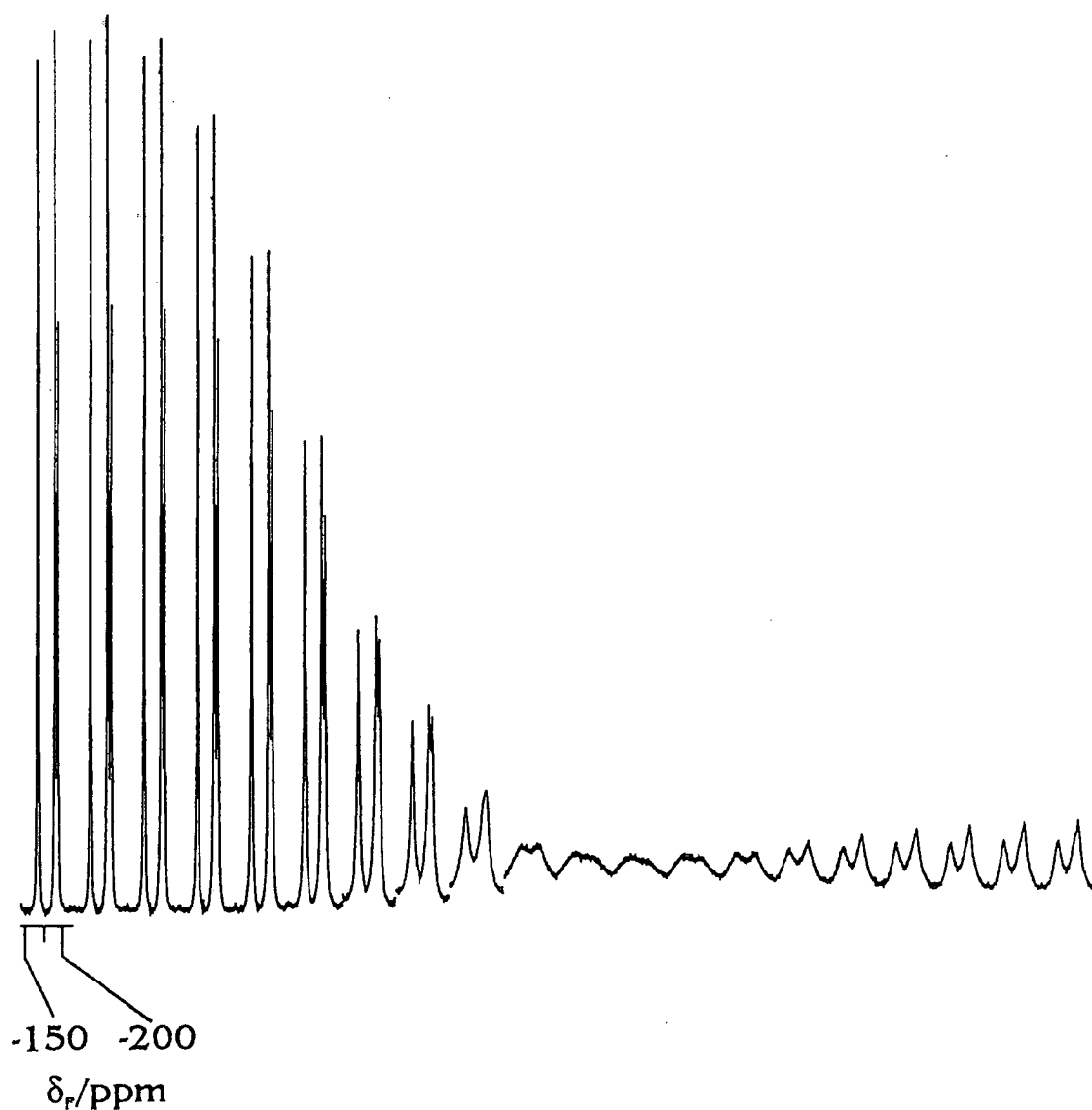


Figure 5.3.4 Stacked plot of the spectra obtained from a 188.28 MHz CP/MAS spectrum of compound 1 using varying decoupler powers. Spectral parameters are as for figure 5.3.3, except that a MAS rate of 14 kHz was used. Maximum decoupling power corresponds to a 3 μ s proton pulse duration (\approx 83 kHz decoupling field). Subsequent field strengths are, from left to right, equivalent to 73.4, 64.9, 55.5, 46.3, 39.0, 31.6, 25.0, 19.5, 15.2, 11.4, 8.3, 6.1, 4.2, 2.9, 2.2, 1.9, \sim 1.0, \sim 0.5, and 0 kHz respectively.

This conclusion was further supported by the results obtained from experiments conducted on the mono- and di- fluorinated steroids, which contained no fluoromethyl group and yet still displayed a similar reduction in signal intensity at the same decoupler field strength. If internal motion was not the cause, then could it be surmised that perhaps external motion (i.e. the MAS rate) could account for the

effect. Experiments were conducted spinning at 14 kHz, 12 kHz, 10 kHz, 8 kHz, 6 kHz, and 3 kHz and on a static sample. As the spinning speed was reduced to 3 kHz the minimum intensity was found to shift to lower decoupling powers. Decoupling field strengths were calculated for each of the settings used in the experiment and the power at which minimum intensity was observed was found to be in good agreement with the MAS rate. In addition an identical experiment conducted on a static sample displayed no such dip in intensity. It was therefore concluded that the observed phenomenon was an effect produced by the interaction of the decoupling field with the MAS rate. When the MAS rate is of the same order of magnitude as the decoupler field strength the two frequencies interact and the resultant spectrum is in effect similar to one recorded static and proton-coupled i.e. one in which dipolar couplings and shielding anisotropies remain and combine to give a broad featureless spectrum.

One further point of interest that arose from the variable decoupling experiments was an apparent shift to higher frequency of all resonances as the decoupler field strength was increased. This behaviour is not so noticeable from figure 5.3.4, but can be more readily observed by referring to figure 5.3.3. A similar shift was observed in comparing the proton-coupled and proton-decoupled spectra of the monofluorinated steroid (figures 5.3.1. b and d respectively). In both cases the magnitude of the shift experienced by the signals under conditions of proton decoupling is one of approximately 1 ppm to lower frequency. These shifts are due to a phenomenon known as the Bloch-Siegert effect.^{9,10} Shifts of up to 7 ppm have been experienced when observing the fluorine nucleus,¹¹ and the fact that the change in chemical shift for our samples is only some 1 ppm may reflect the strength of the decoupling field. This theory could also explain the anomaly that a larger chemical shift difference was displayed by the signal of the monofluorinated steroid (3) on going from the solution state to the solid state, compared to the trifluorinated steroid (1). Here the chemical shift difference is nearer the value of 7 ppm, expected for Bloch-Siegert shifts in this experiment, and it could well be that the reference spectrum (CFCl₃) was acquired using a smaller decoupling field than was used for the

spectrum of compound 3. This is one disadvantage of referencing chemical shifts using a replacement rotor.

5.3.2 Polymorphism

In chapter 4 solid-state carbon-13 spectra revealed the presence of two polymorphs of compound 2. This property was also detected in the solid-state fluorine-19 spectrum of two different samples of compound 2, each containing different proportions of the two polymorphs. These spectra are shown in figure 5.3.5 and demonstrate that fluorine-19 solid-state NMR is a viable alternative to carbon-13 solid-state NMR for the detection of polymorphism in fluorinated organic compounds, with the added advantage of increased sensitivity.

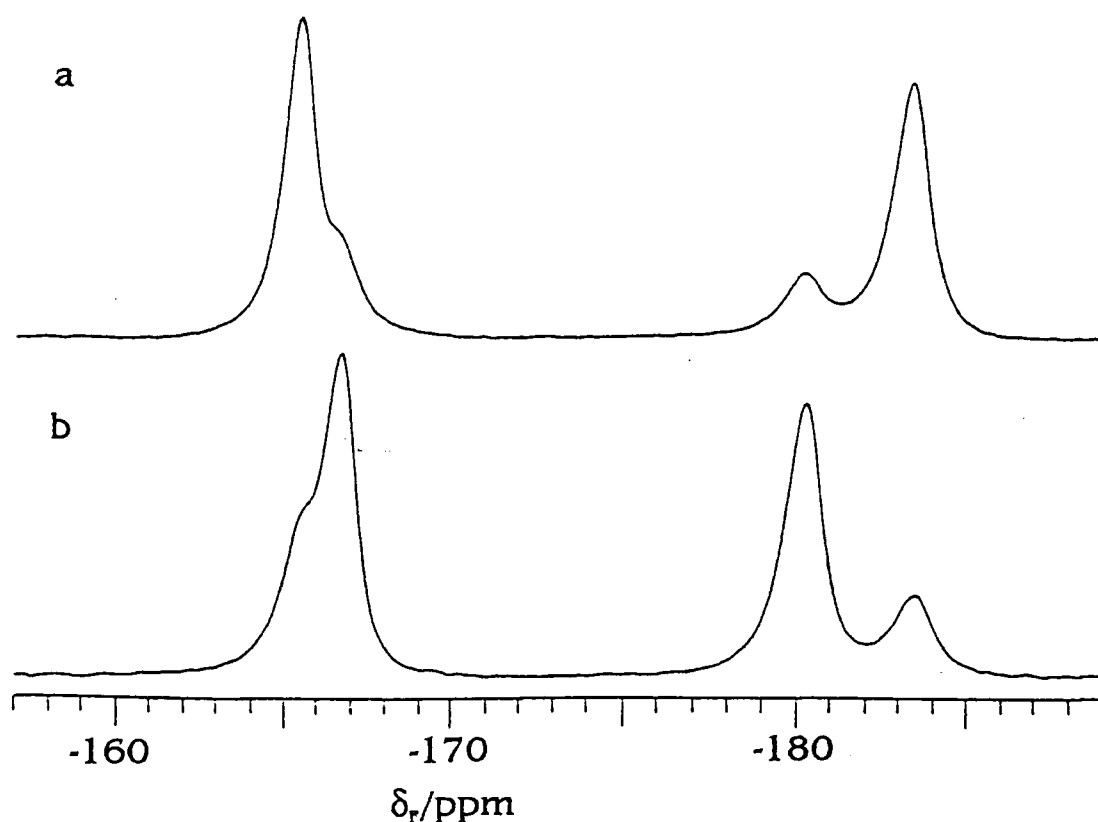


Figure 5.3.5 188.28 MHz fluorine-19 single-pulse proton-decoupled spectra of two samples of compound (2), containing different proportions of two polymorphs. Spectral parameters: Spectral width 100 kHz, pulse delay 60s, pulse duration 1.9 μ s, number of transients 32.

5.3.3 Single Pulse Excitation Versus Cross-polarisation

It has been known for some time that long longitudinal relaxation times for fluorine nuclei in rigid systems can inhibit the celerity at which ^{19}F solid-state spectra can be acquired. This aspect of fluorine solid-state NMR is epitomised by the monofluorinated steroid (3) and the difluorinated steroid (2), for which it was found that long recycle delays (up to 100 s) were necessary to allow full relaxation before the application of another pulse in simple single-pulse experiments.

The problem of prohibitively long spin-lattice relaxation times is encountered for many nuclei in the solid-state. In ^{13}C solid-state spectra of organic compounds this tends to go largely unnoticed due to the inclination to acquire in the cross-polarisation mode of operation, which can be carried out using much shorter recycle delays. The reason for this is that under conditions of proton spin-locking, due to the much lower spin-temperature of the protons compared to the carbons, the loss of proton magnetisation is very small during any given 'contact', analogous to a pulse in the SPE experiment, allowing a large number of contacts to be made before the total magnetisation is appreciably reduced. Put another way, immediately after the FID has been acquired the remaining ^{13}C magnetisation is practically zero, but the proton magnetisation has scarcely been reduced, allowing the immediate application of another contact. Implicit in the above discussion is the fact that the magnitude of T_1 (^{13}C) is irrelevant, and it is $T_{1\rho}$ (^1H) (the spin-lattice relaxation time under conditions of spin-locking) that is the vital criterion. Ideally $T_{1\rho}$ (^1H) should be long (allowing many contacts to be made before appreciable reduction in ^1H magnetisation occurs) and T_1 (^1H) should be short so that when the proton magnetisation does have to be replenished it does not take too long.

The magnetic properties of the protons in our samples were known to be favourable, since $^1\text{H} \rightarrow ^{13}\text{C}$ cross-polarisation experiments had already been carried out with high levels of success. This suggested that, in practice at least, the analogous ^{19}F experiment would be feasible and prove to be of great use in the reduction of

experiment time. As predicted, under conditions of $^1\text{H} \rightarrow ^{19}\text{F}$ cross-polarisation much shorter recycle delays were found to suffice, resulting in large time savings.

One less-favourable aspect of $^1\text{H} \rightarrow ^{19}\text{F}$ cross-polarisation compared to the analogous carbon-13 experiment is that little inherent gain in signal intensity (up to 4 times for ^{13}C) is observed for the fluorine nucleus as a consequence of the small disparity in magnetogyric ratios of the fluorine nucleus and the proton, but such a property is largely inconsequential due to the high receptivity of the fluorine nucleus.

An additional inherent advantage was unearthed with the successful implementation of cross polarisation. Spectra acquired in the single-pulse mode of operation were found to contain a broad 'hump' at approximately -135 ppm, which was attributed to signals arising from fluorine-containing polymers used in the manufacture of certain probe components. These polymers, identified as PTFE and Kel-F, are devoid of protons and consequently were insensitive to cross-polarisation experiments. The minimisation of such background signals is clearly visible in figure 5.3.6, a comparison of $^1\text{H} \rightarrow ^{19}\text{F}$ cross-polarisation and ^{19}F single-pulse spectra for compound 3 (betamethasone-17-valerate).

Satisfactory suppression of the signals arising from the background was also achieved by the use of special pulse sequences developed by Bax, relying on spatially-selective 90° pulses to limit the effective volume of excitation to within the confines of the rotor (see figure 3.4.2). Both single-pulse and cross-polarisation versions of the Bax experiment were performed even though for our samples their only real worth was in demonstrating their feasibility as a method of efficient background suppression, since the single-pulse analogue required large recycle delays for compounds 2 and 3, and the cross-polarisation version was rendered redundant as simple CP operation already gave background-free spectra. Undoubtedly the use of such sequences would prove invaluable in the case of compounds insensitive to cross-polarisation.

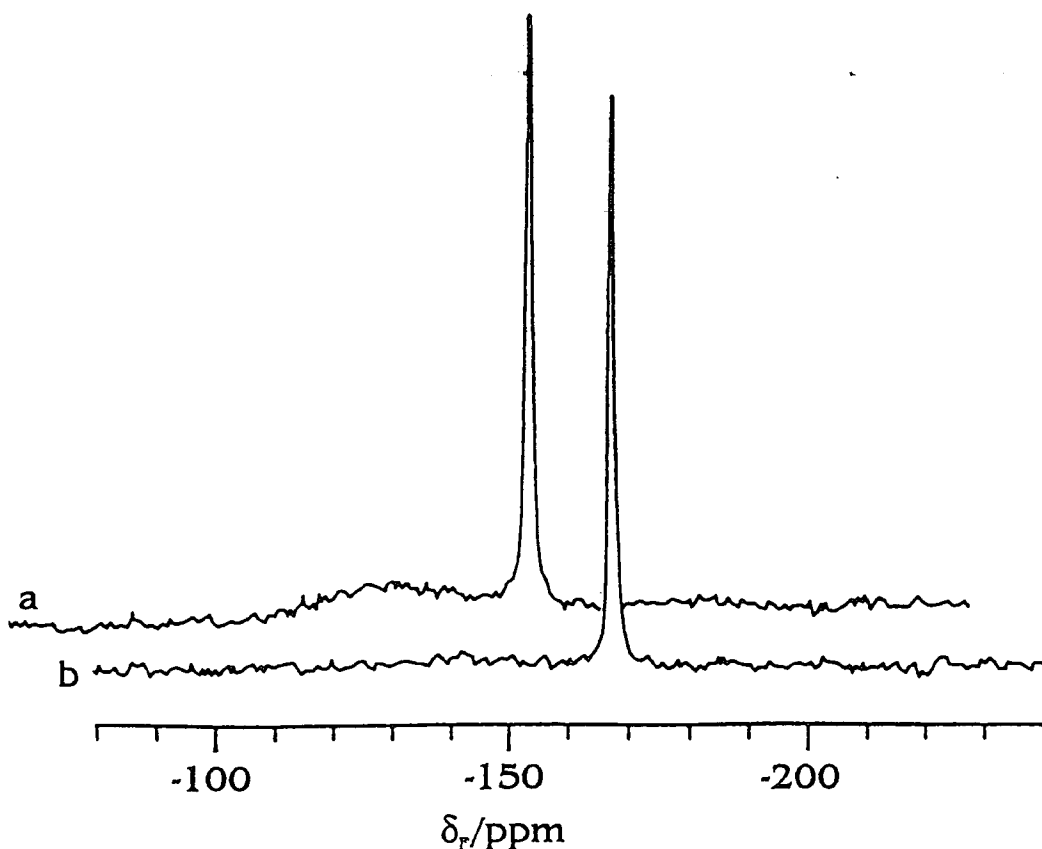


Figure 5.3.6 Comparison of the (a) ^{19}F single-pulse and (b) $^1\text{H} \rightarrow ^{19}\text{F}$ cross-polarisation spectra of betamethasone-17-valerate (**3**). Signals arising from the background in the single pulse experiment, occurring as a broad hump centred on ~ 135 ppm, are absent in the CP mode of operation. Spectrum a employed a recycle delay of 60 s, whereas one of 10 s was used for spectrum b.

5.3.4 Shielding Tensors

The dramatic effect of MAS on solid-state fluorine-19 NMR spectra has already been demonstrated, with the powder patterns observed in the static decoupled spectra of compound **1** and **3** being substantially broader than the sharp resonances seen in the corresponding MAS decoupled spectra. Moreover, spinning sidebands are present for the latter. The static spectrum can be used to estimate the principal values of the shielding tensor σ_{xx} , σ_{yy} and σ_{zz} and the anisotropy, for this particular fluorine, via a bandshape analysis computer program. Here we use the widely accepted convention $|\sigma_{zz} - \sigma_{iso}| > |\sigma_{xx} - \sigma_{iso}| > |\sigma_{yy} - \sigma_{iso}|$. These estimations were compared to results obtained from analyses of intensities in the spinning sideband manifolds

using a computer fitting program, discussed in chapter 3, conducted on slow-spinning cross-polarisation spectra of compound **3**. A comparison of the CP/MAS static and slow-spinning spectra of compound **3** is illustrated in figure 5.3.7.

Similar analyses of slow-spinning sideband manifolds were carried out on compound **1**, at two spinning speeds, although in the case of this particular steroid the increase in the number of fluorine nuclei in the molecule, combined with residual linewidths of ~ 200 Hz, meant that a spinning speed of ~ 1800 Hz was the slowest that could be implemented before overlap of spinning sidebands complicated the spectrum to a degree that made interpretation impossible. The static powder pattern of the trifluorinated steroid (**1**) was also difficult to interpret due to signal overlap, and consequently no meaningful analysis of the static powder pattern was possible. Figure 5.3.8 is a comparison of the static and slow-spinning CP/MAS spectra of compound **1**, which highlights the difficulty in accessing information from the static spectrum due to the overlap of powder patterns, but which illustrates that analysis of the spinning sideband manifolds is still feasible.

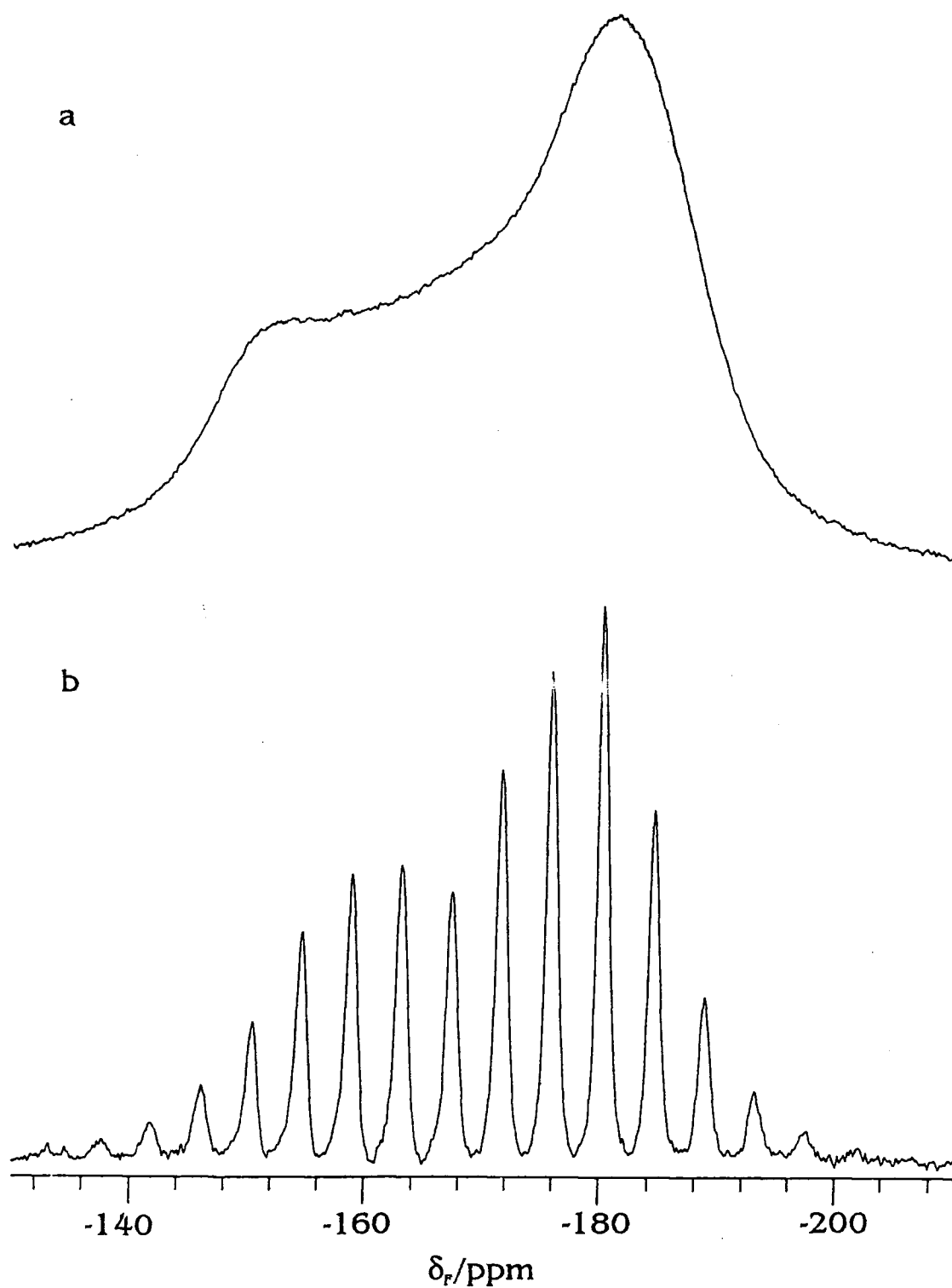


Figure 5.3.7 Comparison of the 188.28 MHz CP/MAS static (a) and slow-spinning (800 Hz) (b) spectra of compound 3. Spectrum (a) was acquired from 4000 transients whereas spectrum (b) was obtained from 32 transients.

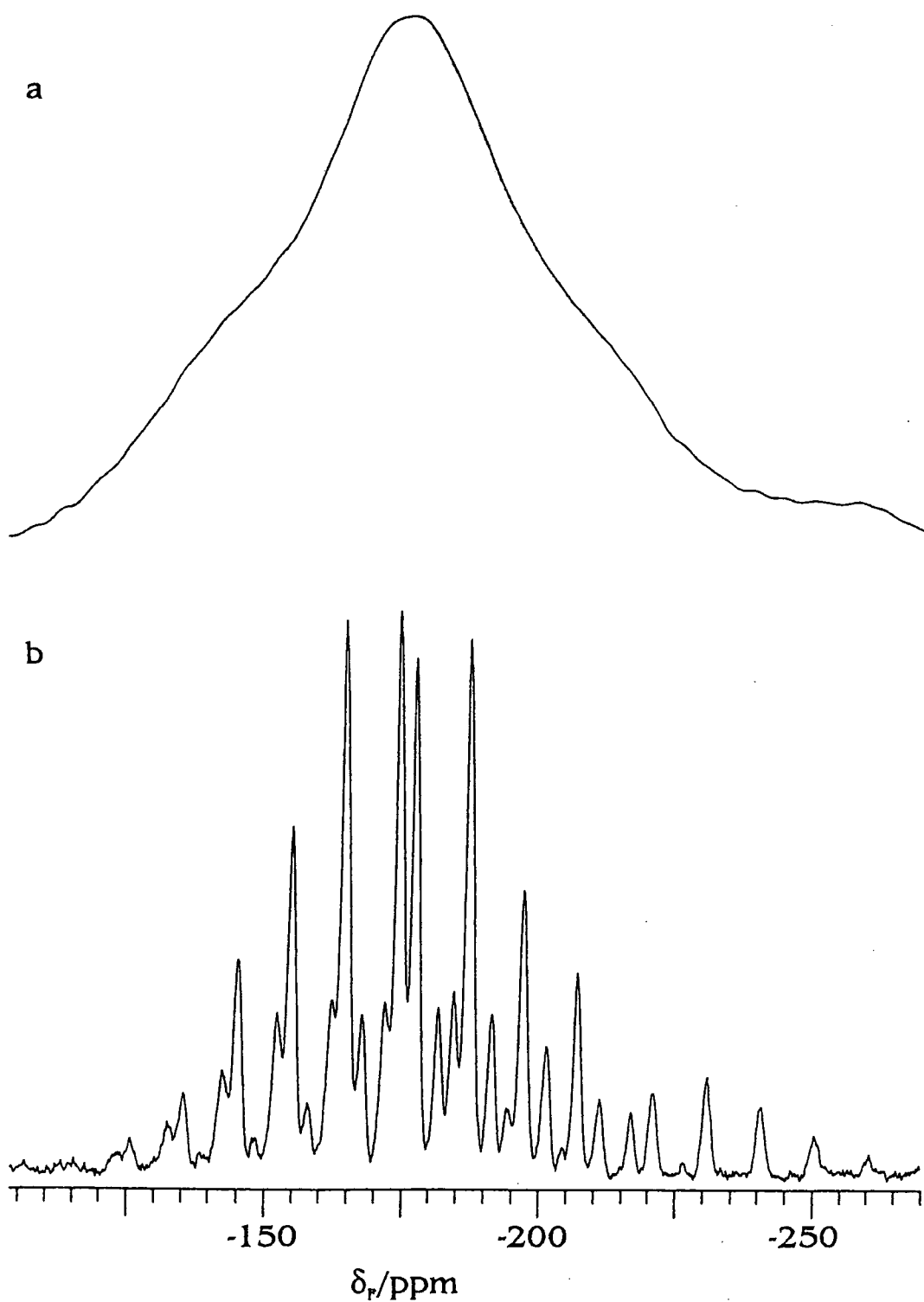


Figure 5.3.8 Comparison of the 188.28 MHz CP/MAS static (a) and slow-spinning (1860 Hz) (b) spectra of compound 1. 3584 transients were recorded for spectrum (a) and 32 for spectrum (b).

In compound 3 it can be assumed that the chemical environment of the fluorine C-9 is very similar to that of the corresponding fluorine in compound 1. Therefore it was expected that these two fluorines would display similar values of shielding tensor components. Shielding tensor information for compounds 1 and 3 are contained in table 5.3.2, from which a number of interesting points can be drawn.

Compound 1, slow-spinning (1860Hz.)

Fluorine	$(\sigma_{XX}-\sigma_{iso})/\text{ppm}$	$(\sigma_{YY}-\sigma_{iso})/\text{ppm}$	$(\sigma_{ZZ}-\sigma_{iso})/\text{ppm}$	λ/ppm	η
CF	-24	-5	28	28	0.66
CHF	22	6	-28	-28	0.58
CH ₂ F	58	16	-75	-75	0.56

Compound 3, slow-spinning (800Hz.)

Fluorine	$(\sigma_{XX}-\sigma_{iso})/\text{ppm}$	$(\sigma_{YY}-\sigma_{iso})/\text{ppm}$	$(\sigma_{ZZ}-\sigma_{iso})/\text{ppm}$	λ/ppm	η
CF	-19	-6	24	24	0.55

Compound 3, static

Fluorine	$(\sigma_{XX}-\sigma_{iso})/\text{ppm}$	$(\sigma_{YY}-\sigma_{iso})/\text{ppm}$	$(\sigma_{ZZ}-\sigma_{iso})/\text{ppm}$	λ/ppm	η
CF	-19	-7	23	23	0.55

Table 5.3.2 Shielding tensor information for compounds 1 and 3.



Firstly, the values obtained for the principal components of the shielding tensors and anisotropies of the CF fluorines in compound **1** and **3** do exhibit close agreement. Secondly, in the trifluorinated steroid, (**1**), the CF fluorine displays an anisotropy approximately equal in magnitude but opposite in sign to that displayed by the CHF fluorine (the sign of the anisotropy is also opposite to that displayed by the CH₂F fluorine). Thirdly, the magnitude obtained for the anisotropy of the CH₂F fluorine is more than twice the value obtained for the CF and CFH fluorines. Lastly, all three fluorine nuclei display similar, substantial, values for the asymmetry parameter η , which is surprising given the different local chemical environment of each fluorine and the rapid rotation of the fluoromethyl group. None of the groups approaches axial symmetry in its shielding.

Errors in the fitting procedure were calculated as a sum of the differences squared from the slow spinning spectra and ranged from ~ 6 for the CF fluorine to ~ 22 for the CH₂F fluorine. The increased error for the CH₂F may be attributed to the mobility of the fluoromethyl group.

5.3.5 Dipolar Dephasing

Dipolar dephasing experiments conducted on compound **3**, under conditions of rotor synchronisation, employed an echo in the pulse sequence to refocus chemical shifts. This was necessitated by the large ¹⁹F chemical shift range in conjunction with long dephasing times needed to effect any noticeable suppression of the resonances. In each experiment the decoupling window was inserted only prior to the 180 (F) pulse and was varied from 0 μ s to 800 μ s in 100 μ s increments. The pre and post refocussing time was 1 ms. Figure 5.3.9 illustrates the results obtained from the dipolar dephasing experiments in the form of a stacked plot.

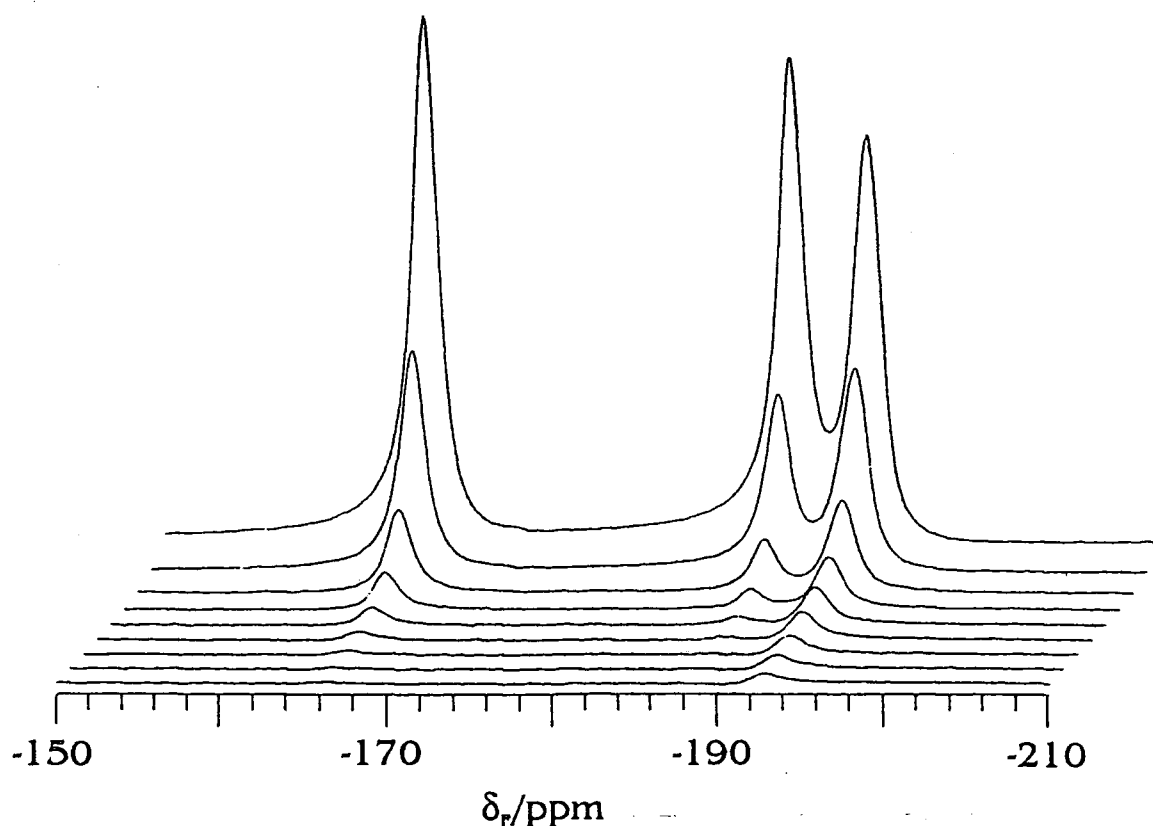


Figure 5.3.9 Spectra from the dipolar dephasing experiments conducted on compound (1). The dephasing times employed are between 0 and 800 μs in 100 μs steps (top spectrum to bottom). The number of transients acquired for each spectrum was 3200.

As the dephasing time is successively increased the CHF resonance is the first to become suppressed, followed by the CF signal. However, even after a dephasing time of 800 μs the fluoromethyl resonance is still visible. This behaviour parallels that seen in carbon-13 dipolar-dephasing experiments, where methine carbons are suppressed before methyl and quaternary carbons, and it is again due directly to the efficiency of the dipole-dipole relaxation mechanism. The quicker dephasing of the CHF fluorine is afforded by a relatively high rate of dipole-dipole relaxation. This suggests a stronger (^1H , ^{19}F) dipolar interaction for F-6 compared to F-9, which is not unreasonable given the close proximity of the proton geminal to this fluorine and the absence of any contiguous protons for F-9. Likewise the slower dephasing of the CH_2F fluorine can be attributed to a reduced rate of dipolar relaxation, due to rapid rotation about the S-C bond partially averaging local dipolar interactions.

The much longer dephasing times needed to effect satisfactory suppression of the signals compared to the times needed in analogous carbon-13 experiments suggest that dipolar interactions between protons and fluorine nuclei are less than between protons and carbon nuclei in our molecule. At first sight this is surprising given the larger value of the magnetogyric ratio for the fluorine nucleus compared to that of the carbon nucleus, but not when the proportionality of the dipolar interaction to r^{-3} is taken into account. If we consider the carbon nucleus of C-6, using bond distances of C-H = 112 pm and C-F = 142 pm and a bond angle of 108° , which gives the distance F-H to be ~ 205 pm, the values of the dipolar interactions within this group of nuclei can be calculated from equation 5.3.1.

$$D = (\mu_0/4\pi) \gamma_I \gamma_S h / 4\pi^2 r^3 \quad (5.3.1)$$

The calculated values are as follows: C-H ≈ 21.5 kHz, C-F ≈ 9.9 kHz and H-F ≈ 12.9 kHz. It is clearly apparent that even though the product of the magnetogyric ratios for the proton and the fluorine nucleus is some four times that for the proton and the carbon nucleus, the distance term is the dominant factor. The increased internuclear distance for the former nuclear pair reduces the resultant dipolar coupling constant by a factor of almost two. Consequently we would expect dipolar dephasing to take longer between protons and fluorine nuclei than between protons and carbon nuclei.

5.3.6 Spin-lattice Relaxation and Spin Diffusion

It was stated in section 5.3.4 that the acquisition of the single-pulse spectra of compounds **2** and **3** required considerable recycle delays to allow the fluorine nuclei to relax back to equilibrium. The optimum delay was of the order of 100 s, although a value of 60 s was found to give satisfactory results. When the analogous experiment was conducted on the trifluorinated steroid, (**1**), it was found it was possible to use

much shorter recycle delays (*ca.* 20 s), and still obtain spectra of comparable signal-to-noise ratios to those recorded for the mono- and difluorinated steroid. Relaxation of the fluorines appeared to be occurring much more rapidly. Compound **1** was the only steroid to contain a monofluoromethyl group, which could reasonably be expected to undergo rapid rotation about the S-C bond, in much the same way as methyl groups in simple organic compounds. If the rate of this motion is suitable, a reduction in the longitudinal relaxation time of this particular fluorine can be expected. In addition, if dipolar interactions with other fluorines in the molecule are substantial this fluoromethyl group can act as a relaxation sink, via spin diffusion. From a simple estimation of the internuclear distance, it is possible to evaluate the magnitude of the (^{19}F , ^{19}F) homonuclear dipolar couplings between the fluorine nuclei in the molecule using equation 5.3.1. Using this equation we obtain the following values: $F6 - F21 = 200$ Hz, $F9 - F21 = 250$ Hz and $F6 - F9 = 1600$ Hz. It is therefore reasonable to assume that significant spin diffusion between the fluorine nuclei is possible. Hence it was surmised that the departure from the need for a long recycle delay observed for compound **1** was most probably due to spin-diffusion effects. T_1 experiments undertaken using the standard inversion-recovery pulse sequence for compounds **1** and **3**, were conducted on compound **3** to test such a hypothesis. For compound **3** the CF resonance was found to have a longitudinal relaxation time in the region of 68 s, whereas all three chemically different fluorine nuclei in compound **1** exhibited the same T_1 value of approximately 6.8 s. Figure 5.3.10 is a comparison of the stacked plots obtained from the two inversion-recovery T_1 experiments performed on compounds **1** and **3**, which emphasises the marked difference in longitudinal relaxation times for the analogous CF fluorines in the two compounds.

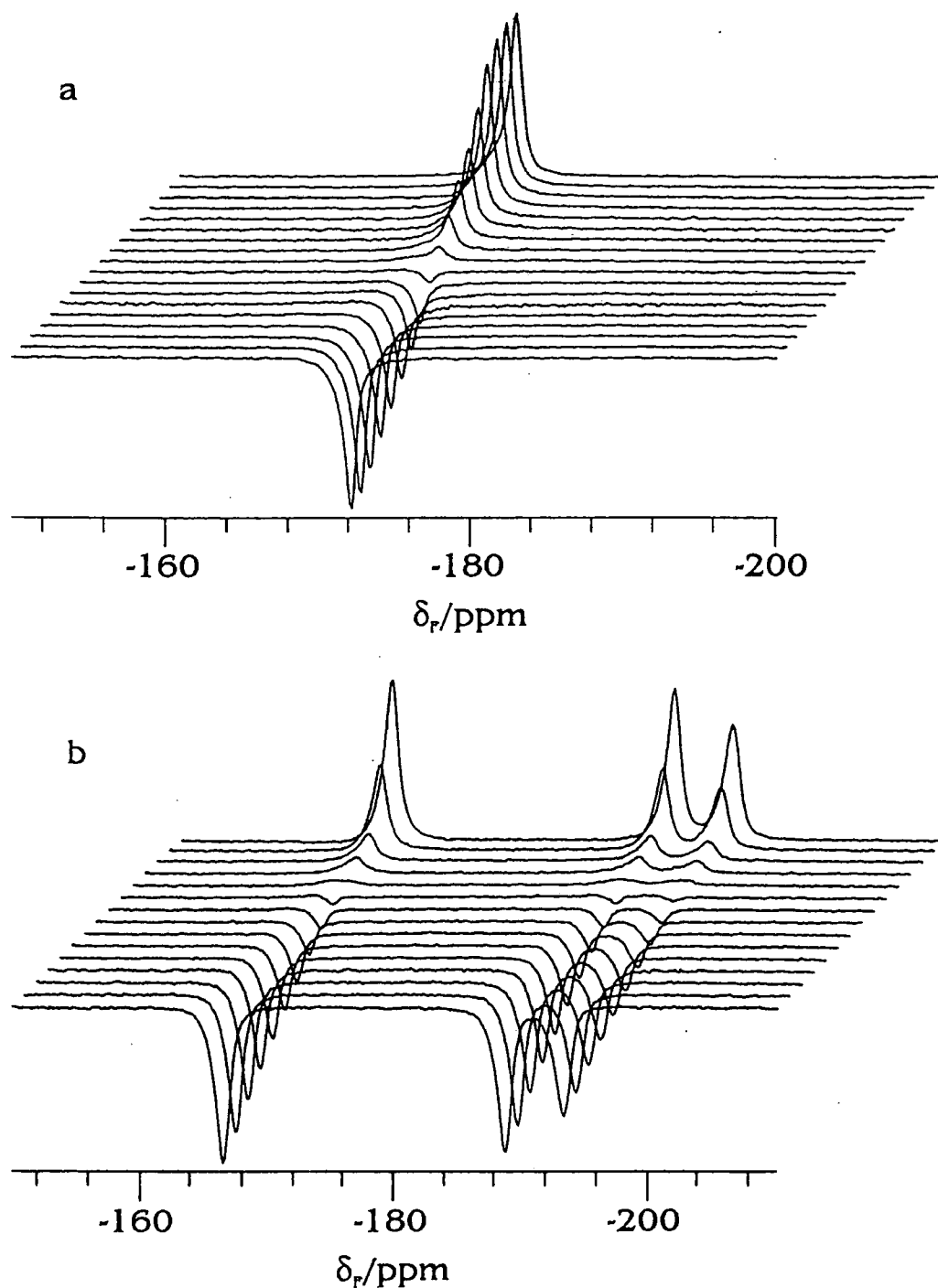


Figure 5.3.10 Stacked plots obtained from the inversion-recovery experiments conducted on (a) compound 3 and (b) compound 1. A $2.9 \mu\text{s}$ pulse duration was implemented and recovery times used were as follows (from front to back): For compound 1; 0.1, 0.5, 1.0, 1.5, 2.0, 2.5, 3.0, 3.5, 4.0, 4.5, 5.0, 5.5, 6.0, 10.0, and 30.0 seconds. For compound 3; 1, 2, 5, 10, 15, 20, 25, 30, 40, 50, 60, 75, 90, 120, 180, 250, 400 and 600 seconds.

To further validate the idea that spin diffusion was in operation in the trifluorinated steroid a 2-D spin-exchange (EXSY) experiment was performed. The pulse sequence of Jeener et al.¹² was implemented, with a cross-polarisation preparation and proton decoupling during both evolution and detection times (but not during the mixing time). A contour plot of the data collected is shown in figure 5.3.11

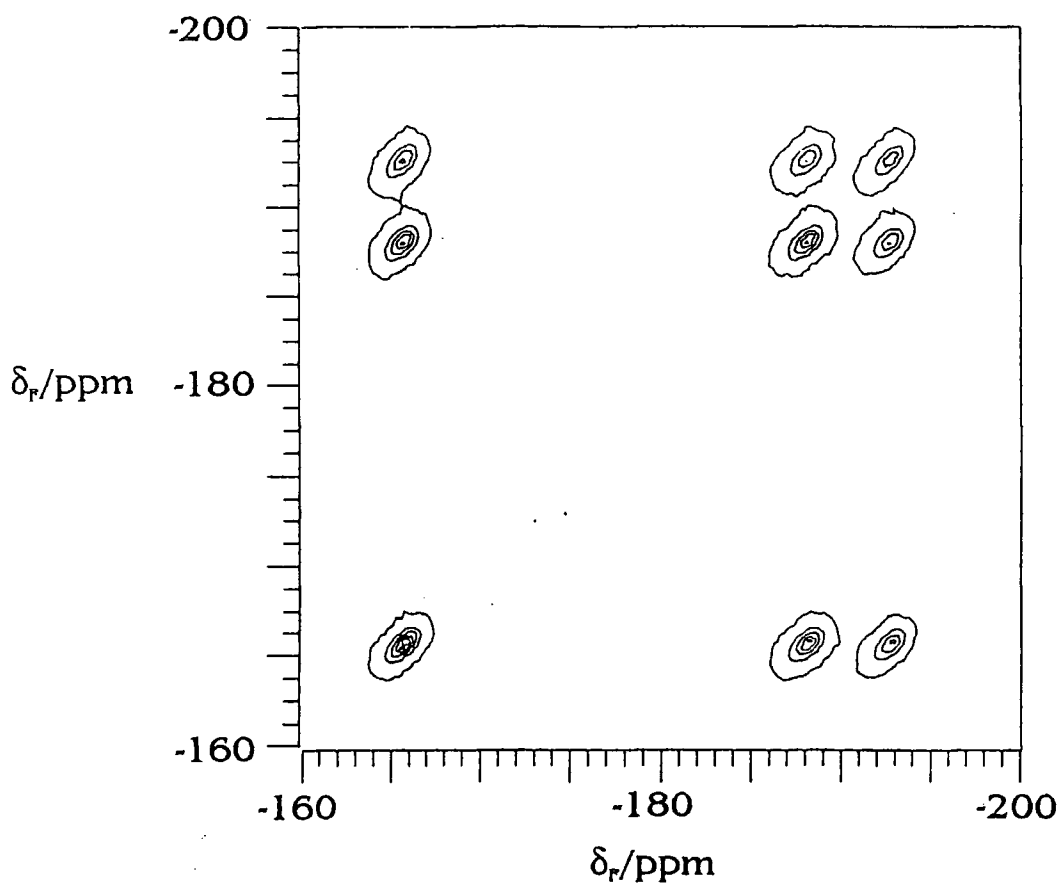


Figure 5.3.11 Contour plot of the 188.28 MHz ^{19}F 2-D spin-exchange experiment carried out on the trifluorinated steroid 1, using CP preparation. Experimental conditions: ^1H pulse duration 2.6 μs , ^{19}F pulse duration 2.9 μs , contact time 2 ms, recycle delay 2 s, spectral width in both dimensions 20 kHz, 50 μs increment in t_1 over 128 increments using a mixing time of 50 ms.

The presence of cross-peaks at high intensity for every conceivable position amongst the fluorines of compound 3 demonstrates that spin diffusion is prevalent between all the fluorines within the molecule and is rapid on a timescale within 50 ms.

Although it is difficult to differentiate between spin diffusion and chemical exchange effects using the 2-D EXSY experiment, unless one implements homonuclear dipolar coupling during the mixing time, we conclude that the occurrence of off-diagonal peaks in the spectrum must be due to spin diffusion, the probability of chemical exchange occurring within such a system being negligible. One interesting feature of this spectrum is the peak occurring at ~ -171 ppm. This resonance displays no correlation with any of the other peaks, and is almost certainly due to an impurity of remnants of compound **3** still left in the rotor. This illustrates that no spin diffusion is present between the two different sample domains contained in the rotor.

To investigate further the dynamics of spin diffusion, the 2-D spin-exchange experiment was repeated for a number of different mixing times, and analyses made of the intensity of the off-diagonal peaks occurring in these spectra. This series of spectra are shown in stacked plot form in figure 5.3.12

In Figure 5.3.12 the height of the most intense peak has been kept constant for each of the stacked plots, and consequently the apparent noise level can be seen to decrease with decreasing mixing time as the cross peaks become less intense. Apart from the obvious reduction in intensities of the cross-peaks as we proceed to shorter mixing times, other more subtle differences in relative intensities of the three cross-peaks are apparent. The larger cross-peaks tend to occur between the CF and CFH fluorines. This is not surprising since the distance between these two nuclei is the smallest (the nuclei being both on the α -face of the steroid, assuming the 3 and 6 positions on ring B of the steroid).

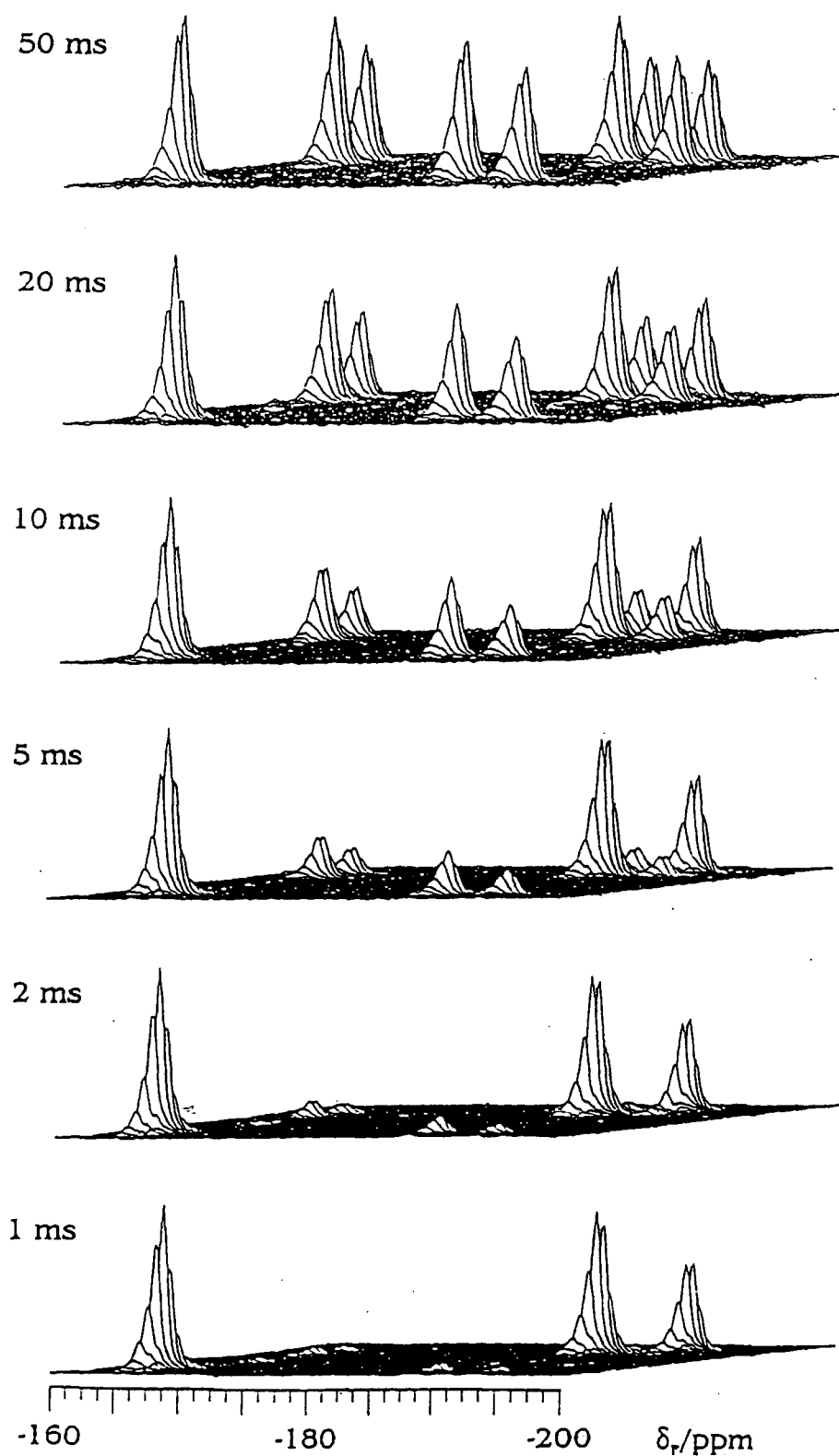


Figure 5.3.12 Stack of stacked plots obtained from the 2-D spin-exchange experiment with variable mixing time conducted on compound 1, using mixing times as indicated, highlighting the reduction in cross-peak signal intensity. All other spectral parameters are as in figure 5.3.11.

5.3.7 Rotational Resonance

A comparison of two rotational resonance spectra and the fast-spinning spectrum of compound 1 is contained in figure 5.3.13. For these experiments, which were conducted using the single-pulse mode of operation, at two of the spinning speeds where first-order rotational resonance conditions were met, broadening of the resonances amounted to an approximate doubling of the linewidths to 500 Hz. No fine structure of the signals was observed in either spectrum. The dilute nature of the fluorine nuclei and the presence of proton decoupling acting so as to essentially convert the fluorines into isolated spin pairs, in conjunction with the substantial difference in chemical shifts allowing easy detection of any broadening seemed to suggest that these systems would be ideal systems in which to observe rotational resonance effects. The existence of substantial line broadening induced by rotational resonance is consistent with the observation of spin-diffusion.

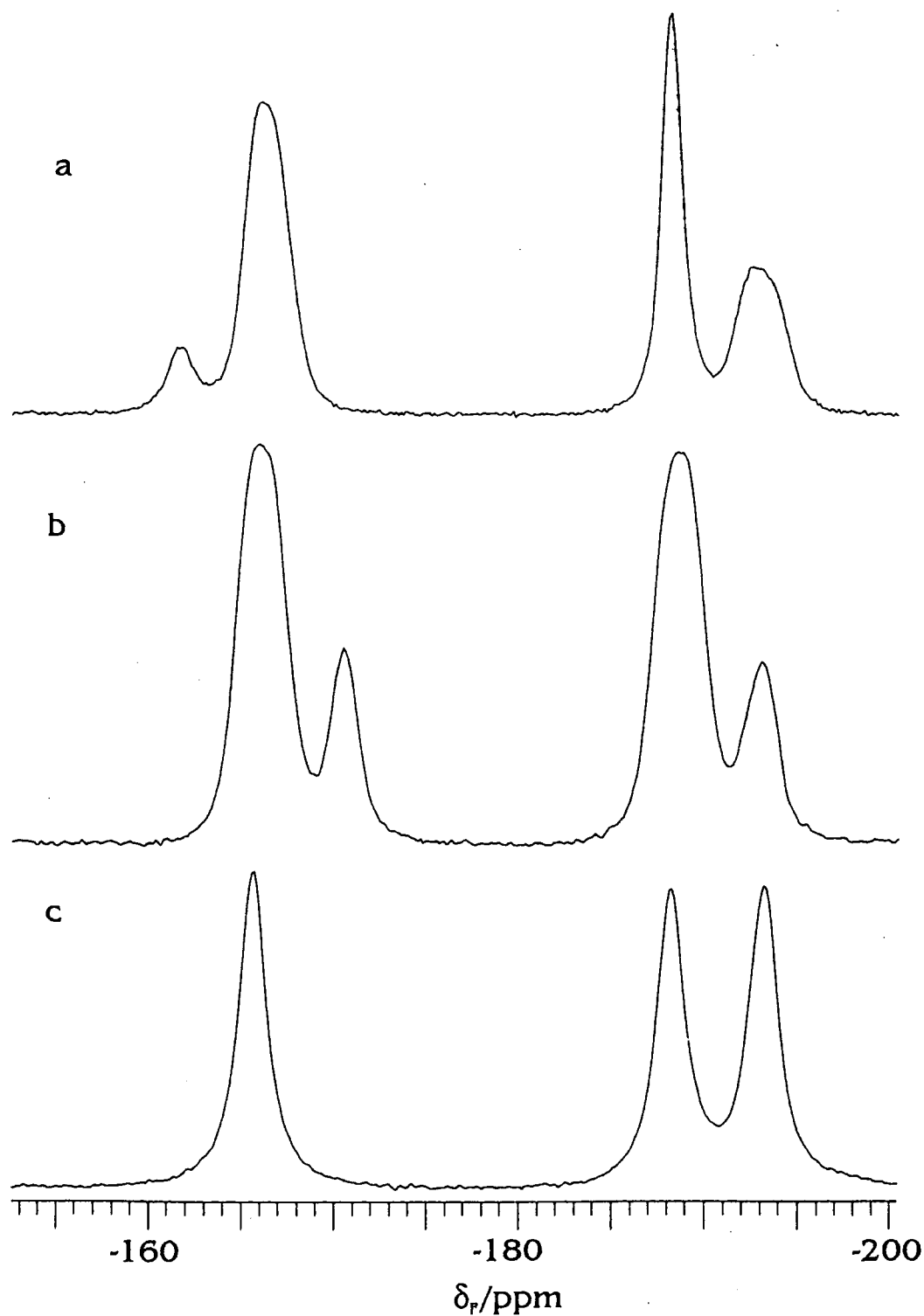


Figure 5.3.13 Comparison of two rotational resonance spectra (spun at (a) 5005 Hz and (b) 4220 Hz) and (c) fast-spinning fluorine-19 CP/MAS spectrum of compound 1, clearly displaying broadening of resonances under conditions of rotational resonance.

5.4 Proton Solid-state NMR

5.4.1 Proton Single-pulse and Fluorine to Proton Cross-polarisation Experiments

A proton single-pulse MAS experiment, with fluorine decoupling, conducted on compound 1 gave, as expected, a relatively broad spectrum, although some structure was visible, the resonance consisting of a broad peak superimposed onto a sharper peak. In addition some low-intensity spinning sidebands were also visible. This single-pulse spectrum is shown in figure 5.4.1.

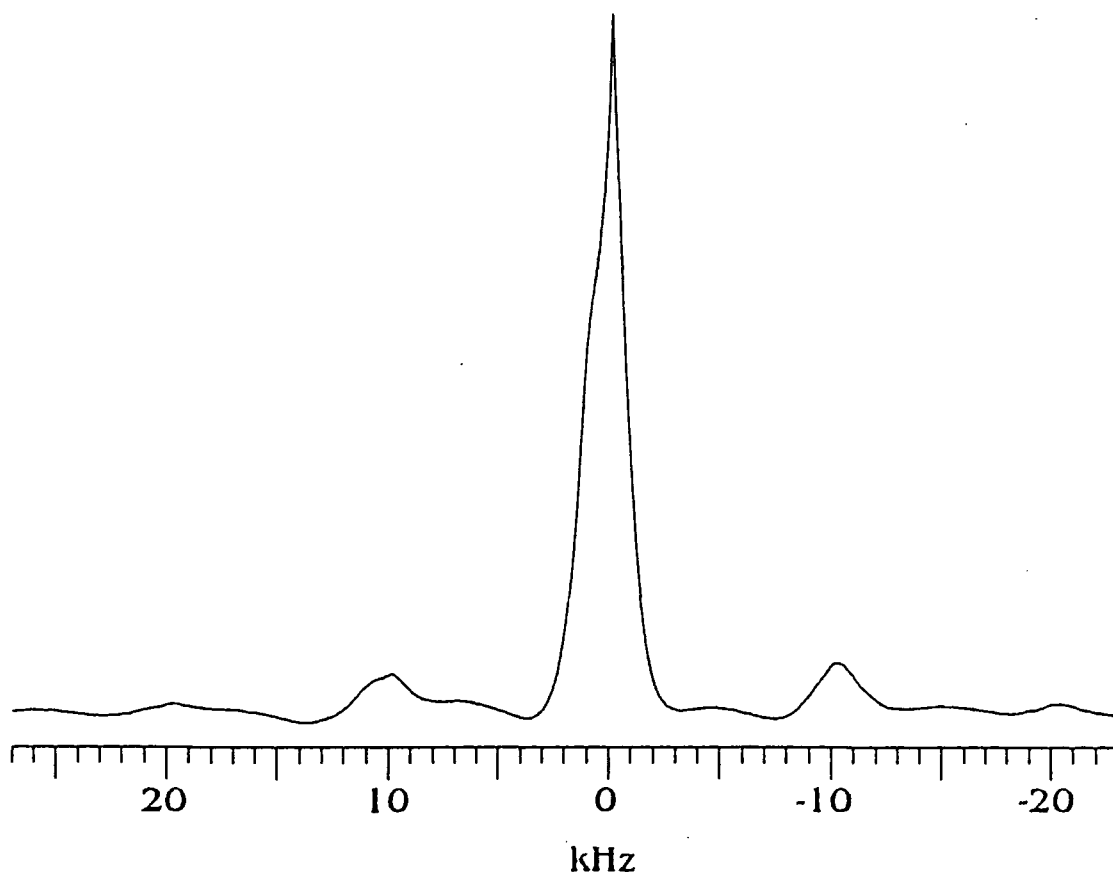


Figure 5.4.1 Single-pulse 200.13 MHz proton spectrum of compound 1. Operating conditions: Spectral width 50 kHz, pulse duration 3.2 μ s, recycle delay 2 s, number of transients 32, spinning rate 10 kHz.

The total bandwidth in figure 5.4.1 is approximately 2 kHz, and the spectrum is of little analytical use. If this spectrum is compared to the $^{19}\text{F} \rightarrow ^1\text{H}$ cross-polarisation experiment, performed employing fluorine decoupling, (figure 5.4.2) it is noticeable that a slightly broader linewidth (approximately 2.5 kHz) is encountered and less definition is visible than in the simple single-pulse proton spectrum.

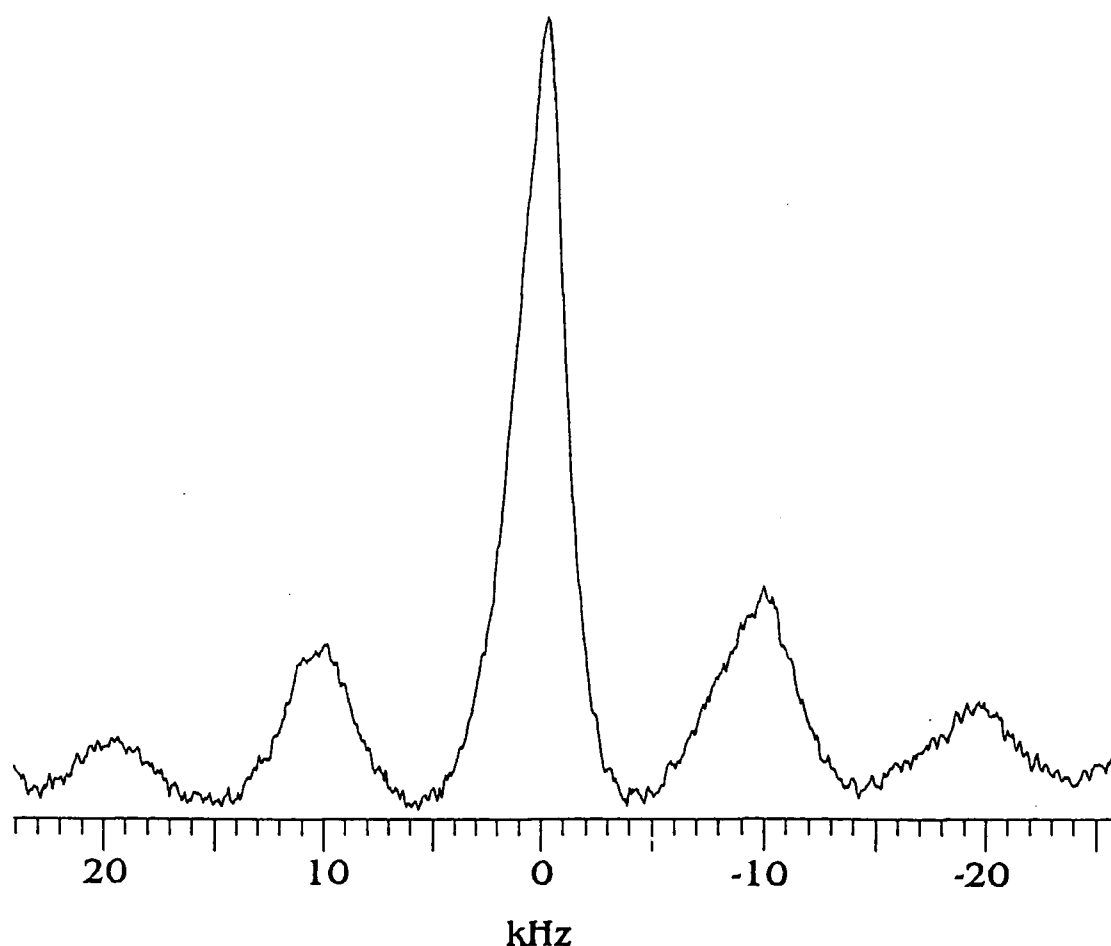


Figure 5.4.2 200.13 MHz proton spectrum of compound 1 with fluorine-to-proton cross-polarisation. Operating conditions were identical to those used in figure 5.4.1, except that a 60 s recycle delay was used. In addition a 1.0 ms contact time was implemented.

In addition, due to the dearth of fluorines in our compounds, the signal to noise ratio was considerably reduced compared to that seen in figure 5.4.1. Although

fluorine decoupling was employed during proton detection, the linewidth still remains broad because of the absence of multiple-pulse operation on the proton channel to suppress homonuclear dipolar interactions. The cross-polarisation pulse sequence again suppressed any signals arising from the materials of the probe, for similar reasons to those stated earlier. Pulsing at intervals of two seconds was possible for compound **1**, since spin-diffusion substantially reduced the longitudinal relaxation times of the fluorines contained in this system. However, similar fluorine-to-proton cross-polarisation experiments performed on compounds **2** and **3** naturally were inefficient because of the inherently long T_1 values of the fluorines in these systems. For this reason such experiments are of little practical value for rigid systems except when used to investigate properties such as cross-polarisation dynamics, which allow estimations of the strengths of dipolar couplings to be made, or in cases where differentiation is required between domains in a sample which contain fluorine nuclei in abundance and domains which are bereft of fluorines.

5.5 Conclusions

It has been demonstrated that the difficulties associated with the acquisition of high-resolution fluorine-19 solid-state NMR spectra of compounds containing abundant protons, relating to the close proximity of the proton and fluorine resonant frequencies, have been overcome. A variety of experimental techniques employing proton decoupling have been successfully implemented for the fluorine nucleus, in a series of proton-containing fluorinated steroids, via the use of a Chemagnetics doubly tunable probe with narrowband ^{19}F and ^1H channels. Favourable properties for our systems have enabled us to carry out cross polarisation from protons to fluorine, and it has been demonstrated that acquiring fluorine-19 solid-state spectra in this mode of operation, if possible, can lead to large time savings. The negation of inhibitive long longitudinal relaxation times for the fluorines that CP effects, and the vast improvement in resolution of the fluorine signals under conditions of proton

decoupling for such compounds, have enabled us to study phenomena such as dipolar dephasing, rotational resonance and spin diffusion. From simple estimations of the relevant dipolar coupling constants, both homonuclear and heteronuclear, between nuclei in the compounds, we have been able to explain fully the manifestations of the aforementioned phenomena and have been able to ascertain information regarding mobility within the structures.

References

1. S. A. Carss, U. Scheler, R. K. Harris, P. Holstein, and R. A. Fletton, *J. Chem. Soc., Chem. Commun.*, 2407 (1994).
2. S. A. Carss, R. K. Harris, P. Holstein, B. J. Say, and R. A. Fletton, *Magn. Reson. Chem.*, (in press).
3. S. J. Opella and M. H. Fry, *J. Am. Chem. Soc.*, **101**, 5854 (1979).
4. E. R. Andrew, A. Bradbury, R. G. Eades and V. T. Wynn, *Phys. Letters*, **4**, 99 (1963); E. R. Andrew, S. Clough, F. F. Farnell, T. D. Gledhill and I. Roberts, *Phys. Letters*, **21**, 505 (1966)
5. R. Challoner and R. K. Harris, *Chem. Phys Letters*, **228**, 589 (1994).
6. J. Jeener, B. H. Meier, P. Bachmann, R. R. Ernst, *J. Chem. Phys.*, **71**, 4546 (1979).
7. E. F. Mooney, *An Introduction to ^{19}F NMR Spectroscopy*, Heyden/Sadtler, (1970).
8. J. W. Emsley, L. Phillips and V. Wray, *Fluorine Coupling Constants*, Pergamon Press (1977).
9. F. Bloch and A. Siegert, *Phys. Rev.*, **57**, 522 (1940).
10. N. F. Ramsey, *Phys. Rev.*, **100**, 1191 (1955).
11. A. Vierkötter, *Private Communication*, 36th Experimental NMR Conference, Boston, March 26-30 (1995).
12. J. Jeneer, B. H. Meier, P. Bachmann and R. R. Ernst, *J. Chem. Phys.*, **71**, 4546 (1979).

Chapter 6

^1H , ^{19}F , ^{13}C Solid-State Triple Resonance Studies

6.1 Introduction

After the feasibility of simultaneous irradiation at the proton and fluorine resonant frequencies with our equipment had been proven, the possibility of performing ^1H , ^{19}F , ^{13}C triple-resonance experiments was the next logical step. A second special development probe was commissioned from Chemagnetics (HFX) that allowed observation of typical low- γ nuclei such as ^{13}C or ^{15}N whilst performing either selective or concurrent decoupling at the fluorine and proton resonant frequencies. Furthermore, since the fluorine nucleus exhibits a magnetogyric ratio reduced by only six percent compared to the proton, this too should prove a suitable nucleus from which to cross-polarise. $^1\text{H} \rightarrow ^{13}\text{C}$, $^1\text{H} \rightarrow ^{19}\text{F}$ and $^{19}\text{F} \rightarrow ^1\text{H}$ cross-polarisations had already successfully been carried out on the three fluorinated steroids, and therefore no problems were immediately foreseeable. With this in mind one can envisage that there exists, in total, six modes of operation open to us. Cross-polarisation may be performed from either the protons or fluorine nuclei contained in the steroids whilst decoupling during the acquisition of the ^{13}C signal on both or either of the proton and fluorine channels. Each of these experiments was conducted on the trifluorinated steroid (compound 3) and the results are presented in the succeeding sections.

6.2 Proton to Carbon Cross-polarisation

The first of these experiments in which we cross-polarise from protons to carbon, whilst decoupling only on the proton channel during acquisition, is analogous

to the experiment described in section 4.4.2.1, the spectrum of which was shown in figure 4.4.1. A very similar spectrum was obtained using the HFX probe, although since only 256 transients were acquired the signal-to-noise ratio is far poorer. Figure 6.2.1 shows the spectrum acquired in the $^1\text{H} \rightarrow ^{13}\text{C}$ CP $\{^1\text{H}\}$ mode of operation using the HFX probe.

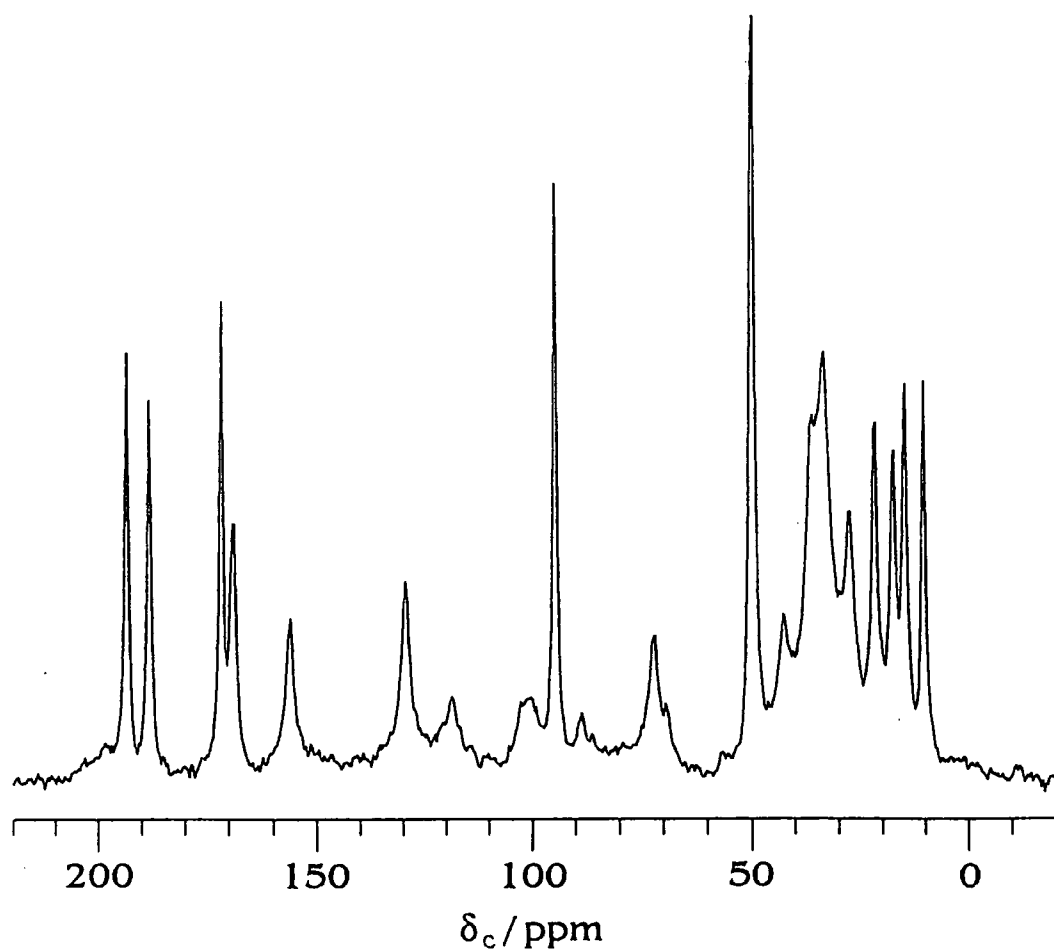


Figure 6.2.1 50.33 MHz $^1\text{H} \rightarrow ^{13}\text{C}$ $\{^1\text{H}\}$ CP spectrum of fluticasone propionate (1). Operating conditions: Spectral width 20 kHz; pulse duration 5 μs ; contact time 2 ms; recycle delay 5 s; number of acquisitions 1024.

Although the signal-to-noise ratio is far worse than that seen in figure 4.4.1, it can be seen that the signal arising from C-21 is similarly lost in the background noise. The signals from C-6 and C-9 appear, as expected, at 87.7 and 101.3 ppm

respectively, although the doublet structure, due to (^{13}C , ^{19}F) indirect coupling is only clearly discernible in the signal arising from C-6. If we now consider the same experiment, but employing simultaneous decoupling of proton and fluorine spins during acquisition of the FID, not only are all three of the fluorinated carbons clearly visible above the noise level but they all appear as singlets (see figure 6.2.2).

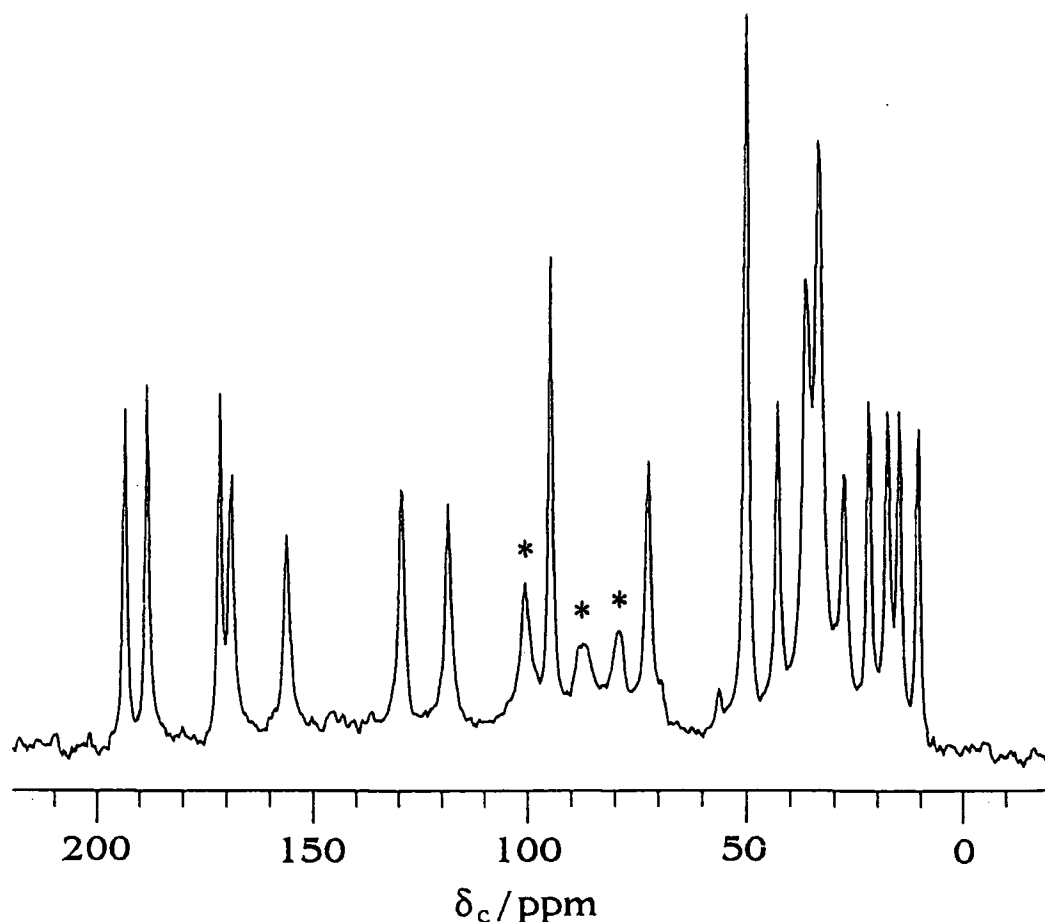


Figure 6.2.2 50.33 MHz $^1\text{H} \rightarrow ^{13}\text{C}$ $\{^1\text{H}, ^{19}\text{F}\}$ CP spectrum of fluticasone propionate (1). Operating conditions: Spectral width 20 kHz; pulse duration 5 μs ; contact time 3.2 ms; recycle delay 5 s; number of acquisitions 256. The peaks arising from the fluorinated carbons are indicated by an asterisk.

The manifestation of the fluorinated carbon signals as singlets is not surprising given that the application of high-power fluorine decoupling suppresses not only (^{13}C , ^{19}F) dipolar coupling, but also (^{13}C , ^{19}F) indirect coupling. The collapse of the doublet

structure also explains the apparent increase in intensity of these signals compared to the spectrum acquired using only HPPD. One additional point worthy of note is that the linewidths of the resonances arising from the fluorinated carbons in figure 6.2.2 are substantially larger than those of the other carbons in this spectrum. This is especially true of the carbon resonance of the CFH group at 87.7 ppm and is thought to arise from relatively ineffective decoupling of the fluorines.

If we now consider the experiment conducted using decoupling only on the fluorine channel during acquisition of the signal (i.e. $^1\text{H} \rightarrow ^{13}\text{C} \{^{19}\text{F}\}$) the spectrum obtained displays very poor resolution due to the presence both of proton homonuclear dipolar coupling and (^1H , ^{13}C) heteronuclear dipolar coupling. The spectrum is shown in figure 6.2.3.

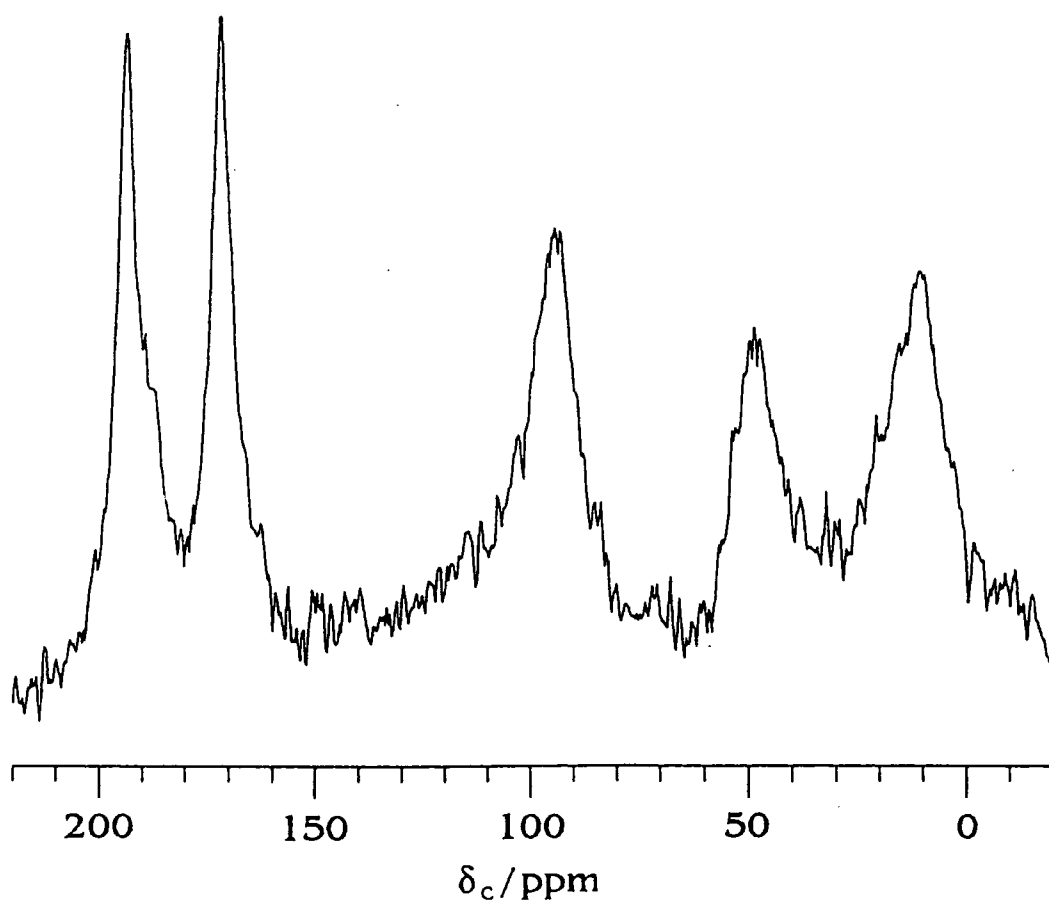


Figure 6.2.3 50.33 MHz $^1\text{H} \rightarrow ^{13}\text{C} \{^{19}\text{F}\}$ CP spectrum of fluticasone propionate (1). Operating conditions: Spectral width 20 kHz; pulse duration 5 μs ; contact time 2.0 ms; recycle delay 5 s; number of acquisitions 1024.

Five broad resonances are clearly visible, centred on approximately 193, 172, 93, 49 and 10 ppm. If one refers to table 4.4.1, it becomes apparent that these signals are centred around regions of the spectrum where signals from carbon nuclei that we would expect to possess small (^1H , ^{13}C) dipolar coupling constants are to be found (i.e. quaternary carbons and methyl carbons). For example, 193 ppm is close to the chemical shift of C-20 (quaternary), 172 ppm to the chemical shift of C-22 (quaternary), 93 ppm to the chemical shift of C-17 (quaternary), 49 ppm to the chemical shift of C-10 and C-13 (both quaternary), and 10 ppm to the chemical shift of C-24 (methyl). It is well known that the efficiency of cross-polarisation is dependent on the magnitude of dipolar interactions between the two nuclei in question. This explains why cross-polarisation is ineffective in the solution state, or for certain types of solid-state samples such as mobile polymers, where molecular motion averages the dipolar interactions. Therefore, where it may originally have been envisaged that these quaternary and methyl carbon nuclei would not cross-polarise efficiently due to the fact that they possess weak (^1H , ^{13}C) dipolar interactions it became obvious from the experimental results that although this was true it could not be the dominant effect. The phenomenon can be explained thus: for all protonated carbons, except the rapidly rotating methyl carbons, significant (^1H , ^{13}C) heteronuclear dipolar coupling exists. Since no high-power proton decoupling was applied when acquiring the spectrum shown in figure 6.2.3, signals from any such carbons are broadened by the effects of this coupling to a degree where they are indistinguishable from the baseline. For a carbon more remote from protons the strength of the dipolar interactions is less, and consequently its signal does not disappear. However, such carbons would be expected to display less efficient CP and therefore their signals would appear less intense. We have a situation of two opposing effects. If the magnitudes of the dipolar interactions are too large the signal is broadened, but the signal does not appear unless there is some degree of dipolar coupling. It turns out that provided a sufficient dipolar interaction exists a carbon spin will gain magnetisation by CP, in time, especially if there is, as in our compounds, an

abundance of protons (a large proton 'spin-bath'). Cross-polarisation may become a less practical mode of acquisition if only a small number of protons are contained in the system. Such an effect is considered for the (^{13}C , ^{19}F) spin-pair in the following section.

6.3 Fluorine to Carbon Cross-polarisation

Our samples were known to be fairly rigid, and since cross-polarisation had already been carried out with a large degree of success, from proton to both carbon and fluorine, and from fluorine to proton, there was no reason to expect that cross-polarisation from fluorine to carbon would present any problems.

However, as was mentioned in the previous section, certain problems arise when there exists in the system very few nuclei from which you are cross-polarising. For $^{19}\text{F} \rightarrow ^{13}\text{C}$ cross-polarisation such a situation arises in compound 1, which contains only three fluorine nuclei. It might be expected therefore that the intensity of a carbon signal in a $^{19}\text{F} \rightarrow ^{13}\text{C}$ CP spectrum will reflect the proximity of the carbon nucleus giving rise to that signal to a fluorine nucleus. This prediction was borne out in the results obtained from experiments conducted using this mode of cross-polarisation, and the experiments revealed interesting details that were consistent with information gleaned from earlier proton experiments regarding conformation. The fluorine-to-carbon cross-polarisation spectrum of compound 1, employing decoupling on only the proton channel, is shown in figure 6.3.1.

Although the signal-to-noise ratio is far poorer than that seen in figure 6.2.1, the signal arising from C-6 is still a doublet, that from C-9 is still a broad singlet and that from C-21 is again lost in the baseline. These fluorinated carbon signals now have an enhanced intensity compared to the other signals, as a direct consequence of their proximity to the dilute fluorine nuclei leading to a stronger (^{13}C , ^1H) dipolar coupling and therefore a greater rate of cross-polarisation. However, other more subtle differences in intensity are visible.

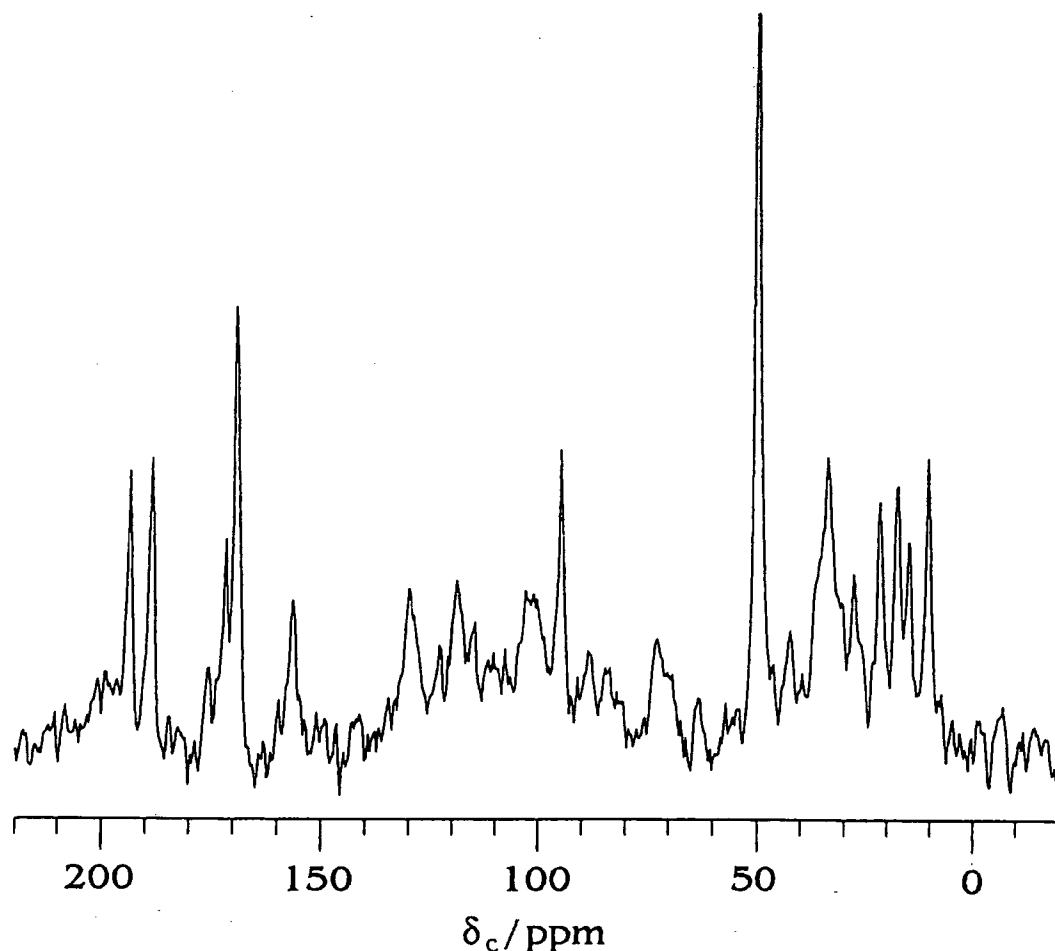


Figure 6.3.1 50.33 MHz $^{19}\text{F} \rightarrow ^{13}\text{C}$ $\{^1\text{H}\}$ CP spectrum of fluticasone propionate (1). Operating conditions: Spectral width 20 kHz; pulse duration 5 μs ; contact time 3.0 ms; recycle delay 5 s; number of acquisitions 1024.

In the analogous proton-decoupled spectrum recorded using $^1\text{H} \rightarrow ^{13}\text{C}$ cross-polarisation (figure 6.2.1), the signal assigned to C-22 at 172.1 ppm is more intense than that assigned to C-5 at 169.5 ppm. In the corresponding $^{19}\text{F} \rightarrow ^{13}\text{C}$ cross-polarisation spectrum the intensities of these signals are reversed, with the C-5 resonance now being the most intense. This is attributed to the closer proximity of C-5 to the fluorine F-6 compared to C-22, leading to a larger (^{13}C , ^{19}F) dipolar coupling and consequently more efficient cross-polarisation. Similarly the intensity of the signal from C-4 at 119.3 ppm is now greater than that from C-2 at 130.0 ppm for the same reason. Finally, and most interestingly, the intensity of the C-16Me resonance at 15.9 ppm is significantly reduced compared to that in the spectrum acquired cross-

polarising from protons, since this carbon is on the α face of the steroid, the opposite face to C-21 and is therefore remote from any of the fluorine nuclei in the same molecule.

The $^{19}\text{F} \rightarrow ^{13}\text{C}$ CP spectrum acquired using dual-channel ^1H and ^{19}F decoupling is shown in figure 6.3.2. It is worth noting that a cross-polarisation time of 15 ms was implemented in this experiment to ensure that as many carbon signals as possible appeared in the spectrum.

Now, with the familiar collapse of the doublet structures for the fluorinated carbon signals, all three signals are clearly visible.

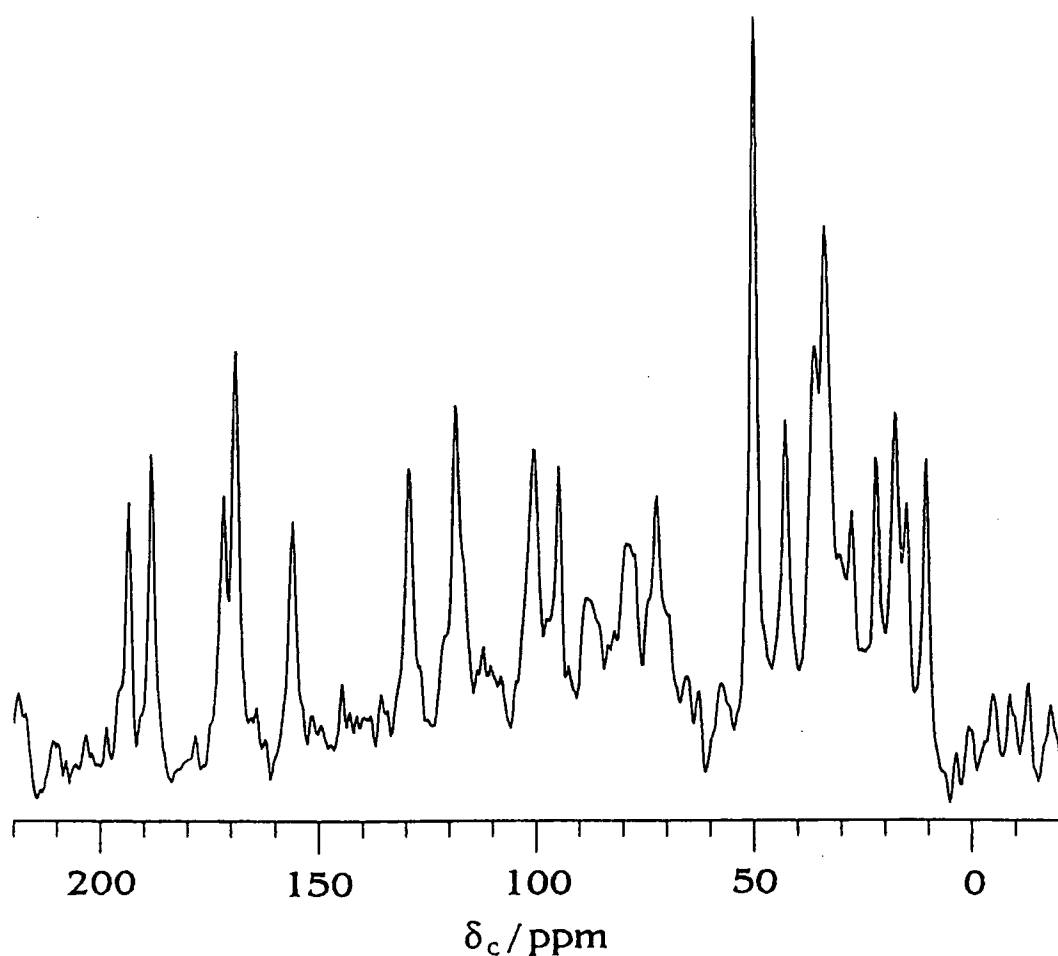


Figure 6.3.2 50.33 MHz $^{19}\text{F} \rightarrow ^{13}\text{C}$ $\{^1\text{H}, ^{19}\text{F}\}$ CP spectrum of fluticasone propionate (1). Operating conditions: Spectral width 20 kHz; pulse duration 5 μs ; contact time 15 ms; recycle delay 5 s; number of acquisitions 256.

The collapse of the doublet structures coupled to the increased rates of cross-polarisation for these carbons, as a consequence of their close proximity to fluorine nuclei, results in the signal from the C-9 carbon being more intense than that arising from C-17 at 95.5 ppm, which was one of the most intense signals in the spectrum when cross-polarisation was carried out from the protons. Once again all three fluorinated carbon signals are broader than the non-fluorinated ones.

To test the hypothesis that cross-polarisation is most efficient for carbons in close proximity to the fluorine nuclei an identical experiment was performed, but this time using a contact time of 0.4 ms. This spectrum is depicted in figure 6.3.3.

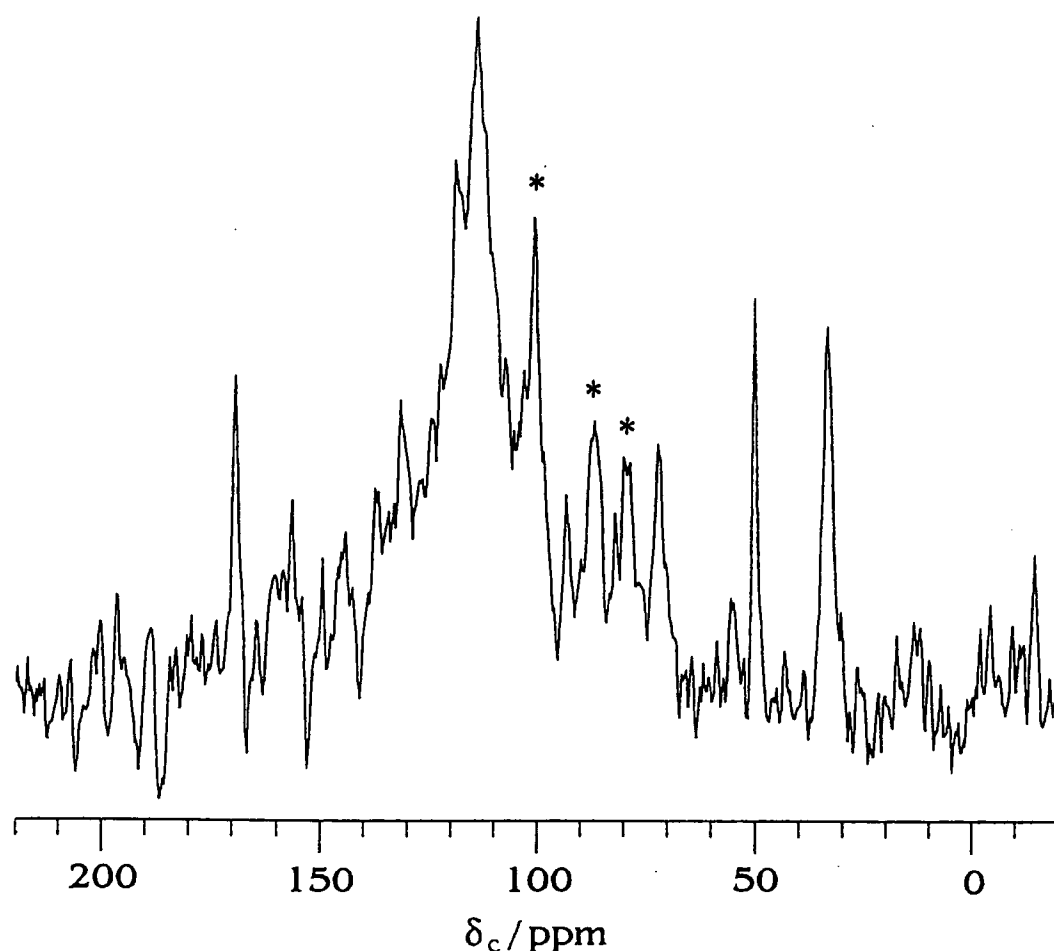


Figure 6.3.3 50.33 MHz $^{19}\text{F} \rightarrow ^{13}\text{C}$ (^1H , ^{19}F) CP spectrum of fluticasone propionate (1). Operating conditions same as for figure 6.3.2 except contact time 0.4 ms. The fluorinated carbons signals are indicated by an asterisk.

Although the noise level in this spectrum is high it contains far fewer resonances than figure 6.3.2. The peaks arising from the fluorinated carbons are among the most intense, a property epitomised by the C-9 resonance, which is the second most intense. The broad peak, clearly observable, centred on approximately 120 ppm, is easily explained. As was mentioned in chapter 5, the probe design incorporates numerous components that are manufactured out of perfluorinated polymers such as Teflon and Kel-F. Although such materials are insensitive to $^1\text{H} \rightarrow ^{13}\text{C}$ cross-polarisation they are not insensitive to $^{19}\text{F} \rightarrow ^{13}\text{C}$ cross-polarisation and consequently this large signal can be attributed to these materials. Other resonances that are also visible are those arising from C-22, C-10, C-7 and C-8, i.e. non-fluorinated carbons that are in close proximity to fluorine nuclei. Such behaviour is consistent with the conjecture of increased rates of cross-polarisation for such carbon nuclei.

Finally, the spectrum acquired implementing only fluorine decoupling is shown in figure 6.3.4. Unfortunately, once again the level of noise in the spectrum is very high, but above this noise the broad peak centred on approximately 120 ppm, arising from Teflon and Kel-F, can be clearly observed. In addition, a shoulder can be detected on this large peak, to lower frequency. After the results presented in section 6.2 we would expect to observe, in addition, only the signal from C-9, the non-protonated carbon. However, in reality the feasibility of any attempt to obtain a definitive interpretation of the shoulder at ~ 100 ppm has to be questioned.

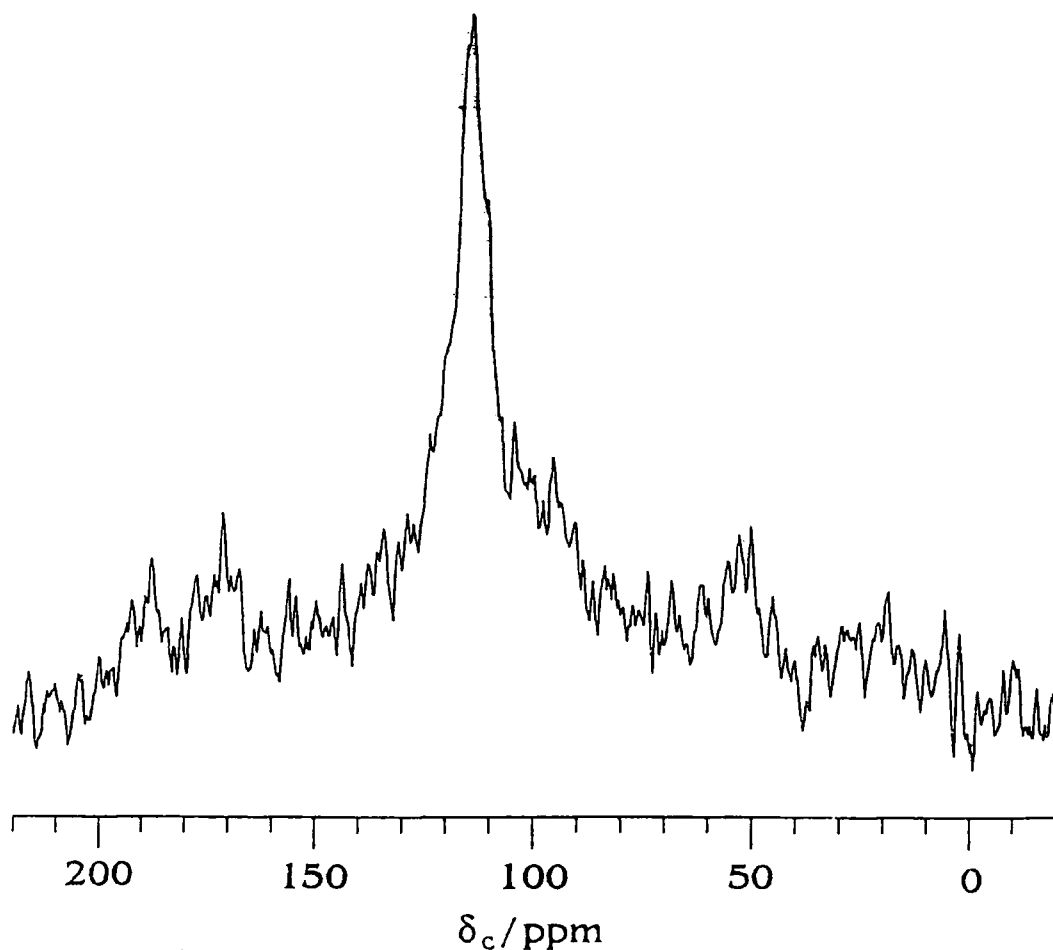


Figure 6.3.4 50.33 MHz $^{19}\text{F} \rightarrow ^{13}\text{C}$ $\{^{19}\text{F}\}$ CP spectrum of fluticasone propionate (1). Operating conditions: Spectral width 20 kHz; pulse duration 5 μs ; contact time 3 ms; recycle delay 5 s; number of acquisitions 1024.

6.4 Conclusions

It has been demonstrated that both $^1\text{H} \rightarrow ^{13}\text{C}$ and $^{19}\text{F} \rightarrow ^{13}\text{C}$ cross-polarisation experiments, performed in conjunction with either separate or concurrent decoupling at the proton and fluorine resonant frequencies, are feasible. With the concurrent application of proton and fluorine decoupling has come the ability to detect the signal arising from the fluoromethyl carbon in the trifluorinated steroid (1). Splittings observed in the CF and CFH signals of this compound due to (^{13}C , ^{19}F) indirect coupling have been removed. The strength of the respective dipolar interactions

between nuclei, which is dependent on the internuclear separation, has been shown to have a major influence on the intensity of signals in the $^{19}\text{F} \rightarrow ^{13}\text{C}$ cross-polarisation experiments due to the dilute nature of the fluorines, by performing an experiment using a short contact time when only signals arising from carbons in close proximity to fluorines have been observed. Such observations have led to confirmations of the conformation adopted by this compound.

In the future it is hoped that developments will be made to enable $^1\text{H} \rightarrow ^{19}\text{F} \rightarrow ^{13}\text{C}$ double-cross-polarisation and related experiments to be performed.

Part II

Residual Dipolar Coupling Between Carbon-13 and Halogen Spins

Chapter 7

Background and Theory of Residual Dipolar Coupling

7.1 Introduction

The selective averaging techniques presented in chapter 2 have been shown to provide an effective method for narrowing solid-state resonances. MAS spatially averages shielding anisotropies, and broadening arising from dipolar interactions can be suppressed by spin decoupling or multiple-pulse sequences. In most cases this averaging is possible because the Zeeman interaction (typically 20-500 MHz for modern spectrometers) far exceeds any shielding anisotropies or dipolar interactions (usually less than 100 kHz), and only the leading term of the relevant Hamiltonians need be considered. However, where quadrupolar nuclei are concerned, these may experience large anisotropic interactions with local electric field gradients, which can be of the order of hundreds of MHz depending on the type of nucleus and the symmetry of the nuclear site. Now Hamiltonian terms other than the leading ones need to be taken into consideration, having angular dependencies differing from $(3\cos^2\theta - 1)$ which are not therefore averaged by MAS, but scaled by a factor dependent on the quadrupolar coupling constant χ ($\chi = e^2Qq_{zz}/h$). Consequently the powder patterns usually observed for the central $1/2 \leftrightarrow -1/2$ transition of quadrupolar nuclei are not totally suppressed by MAS but similarly only scaled, and bandwidths observed in solid-state MAS NMR spectra of quadrupolar nuclei can frequently still be very large. All fine structure of interest arising from chemical shifts and indirect coupling is lost. It is for this reason that quadrupolar nuclei often lend themselves more to study by NQR spectroscopy than by NMR. The excessive spectral broadening commonly found in NMR spectra of quadrupolar nuclei is expressly

demonstrated by the ^{35}Cl solid-state MAS NMR spectrum of 3-chlorobenzoic acid shown in figure 7.1.1.

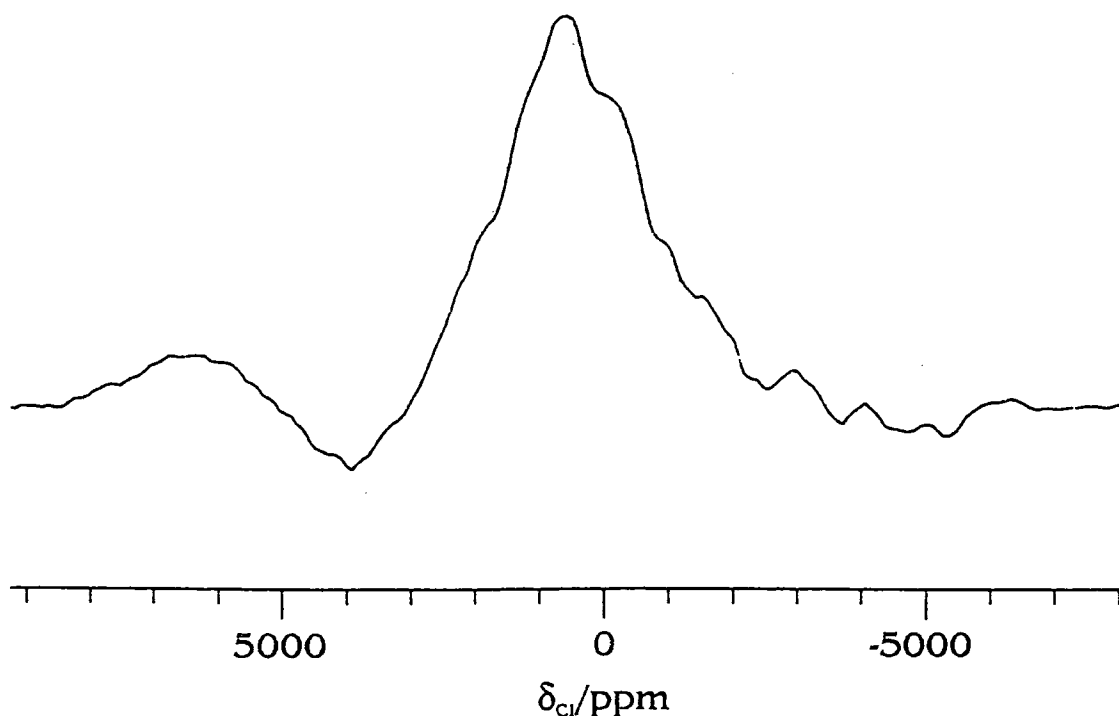


Figure 7.1.1 19.623 MHz MAS spectrum of 3-chlorobenzoic acid. Spectral parameters: spectral width 500 kHz, pulse duration 5 μs , recycle delay 2 s, number of transients 128.

The presence of a large quadrupole coupling constant of approximately 70 MHz, some three and a half times the size of the Zeeman interaction, broadens the signal to such a degree that retrieval of information concerning the fundamental NMR parameters is practically impossible. The situation is all the more exasperating since the chlorine-35 nucleus possesses a high receptivity, is known to display a large chemical shift range, and would therefore be very useful in structural analysis were it possible to suppress the large quadrupolar interactions. Fortunately, there do exist today experimental techniques which, when implemented, can suppress quadrupolar interactions and allow meaningful NMR data to be obtained. DOR (Double Rotation) and DAS (Dynamic Angle Spinning) are two such techniques, but these are

technically demanding and therefore expensive. However, in some instances, for example if the nucleus concerned is contained in an environment of high symmetry, no quadrupolar broadening occurs and sharp resonances can be observed. Such a proviso for high symmetry is known to exist in the cubic structured lattices of alkali metal halides. Numerous solid-state NMR experiments have been conducted on metal halides,¹ involving observation of ^{35}Cl , ^{37}Cl , ^{79}Br , ^{81}Br and ^{127}I nuclei.^{3,4} Arguably the simplest of these compounds is NaCl. Figure 7.1.2 demonstrates the dramatic effects of increased symmetry at the nuclear site on the resolution obtained in ^{35}Cl solid-state NMR spectra.

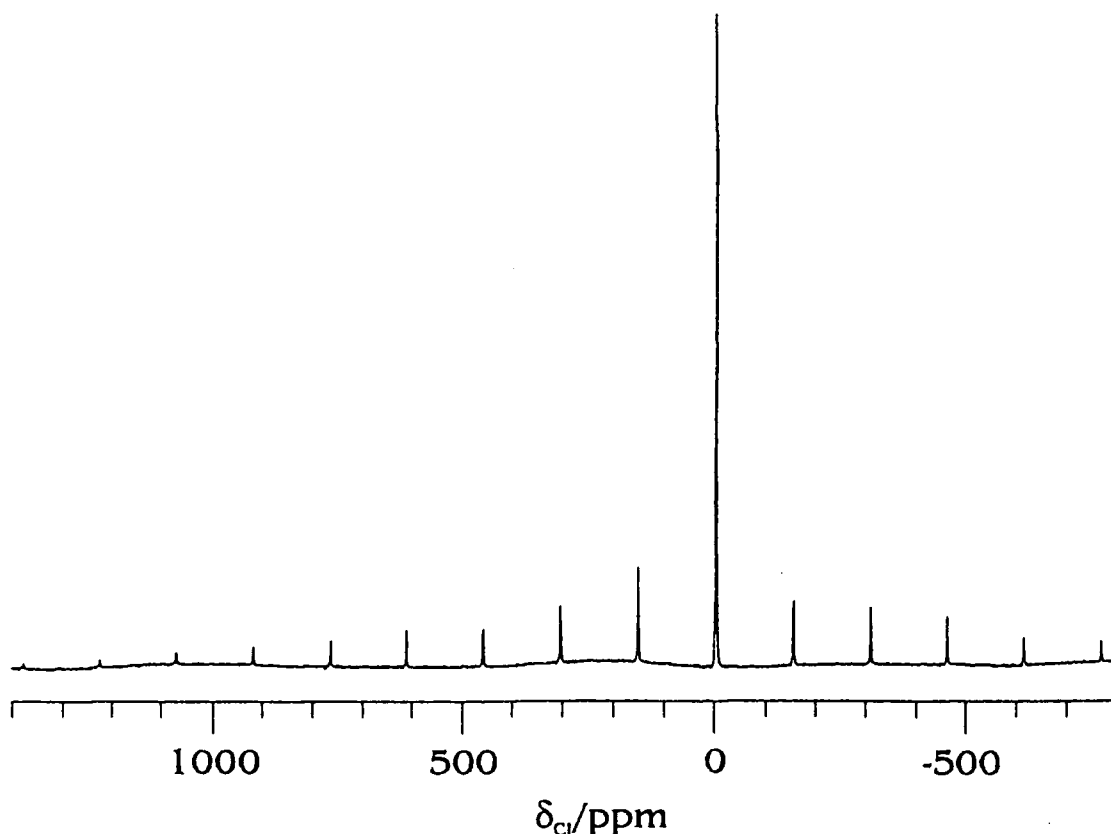


Figure 7.1.2 19.623-MHz MAS spectrum of NaCl. Spectral parameters: spectral width 50 kHz, pulse duration 5 μs , recycle delay 20s, number of transients 16.

The absence of quadrupolar broadening combines with the favourable properties of the chlorine-35 nucleus to produce a high-resolution NMR spectrum.

Good signal-to-noise ratio, narrow resonances and clearly discernible spinning sideband manifolds allow easy extraction of information regarding chemical shifts and shielding anisotropies. Unfortunately, although such high symmetry is commonly found in ionic lattices it is rarely encountered in organic compounds. Consequently examples of chlorine-35 MAS spectra of chlorinated organic compounds, displaying such a high resolution, are few and far between. Once again information retrieval, and hence evaluation of fundamental NMR parameters for such systems by direct observation of the quadrupolar nucleus, is rendered virtually impossible. It is therefore pertinent to ask if it is possible to access information pertaining to such parameters for quadrupolar nuclei by means other than the direct observation of the quadrupolar nucleus.

In 1979 it was first postulated that quadrupolar effects could be transmitted to spin-1/2 nuclei,⁵ and soon afterwards this was confirmed when strange splittings were reported in the signals arising from carbon nuclei directly bonded to nitrogen in CP/MAS spectra of nitrogen containing organic compounds.⁶⁻⁸ Powder patterns consisting of 2:1 or 1:2 doublets were seen, whose splittings (expressed in Hz) were inversely proportional to the static magnetic field strength. This inverse proportionality of the magnitude of the splittings ruled out the possibility that they could be originating from indirect coupling effects, which are invariant to the static field strength. The phenomenon is now known to arise from the transfer of quadrupolar effects to the spin-1/2 nucleus via incompletely averaged dipolar coupling or anisotropy in indirect coupling. MAS is again unable to eliminate the heteronuclear dipolar interactions in these cases due to the presence of a quadrupolar coupling constant comparable in magnitude to the Zeeman interaction. It is for this reason that the phenomenon is considered a second-order effect. The phenomenon, which has been termed residual dipolar coupling, has been well documented in the literature for a wide variety of quadrupolar-spin-1/2 spin-pairs,⁹⁻¹¹ the exact identities of which are considered in more detail in section 7.6. The interaction of the nuclear quadrupole causes mixing of the Zeeman states for the spin-1/2 nucleus which is

manifest in unexpected multiplicities in its signal. Initially only splittings in resonances of spin $1/2$ nuclei directly bonded to the quadrupolar nucleus were observed, but more recently the effects have also been seen to arise between nuclei that are not bonded. This is a consequence of the fact that the phenomenon is mainly transmitted via dipolar coupling. If the spin- $1/2$ nucleus is physically in close enough proximity to the quadrupolar nucleus to undergo dipolar coupling to it, residual dipolar coupling effects may be observable. This introduces the possibility of intermolecular residual dipolar coupling if the molecular configuration in the crystal structure is favourable. The information transferred to the spin- $1/2$ nucleus is a kind of fingerprint of the quadrupolar nucleus, relating directly to the various internuclear interactions present. These fundamental NMR parameters can be extracted by analysis of the bandshapes seen for signals in the MAS spectra of the spin- $1/2$ nucleus. A number of such methods of analysis exist which range from lengthy exact theories, necessitating full-matrix diagonalisation of the Zeeman-quadrupole Hamiltonian, to simpler, more amenable, theories only recently developed. The latest theories are based on a perturbation approach and lead to more manageable analytical equations that can be applied with greater ease. There are three such theories, and which of the three methods is most suitably applied is dictated by certain conditions including the strength of the static magnetic field B_0 and the properties intrinsic to the quadrupolar nucleus. The theory of all three of these bandshape analysis techniques is discussed in detail later in this chapter, with special attention paid to the information pertaining to internuclear parameters that can be extracted.

7.2 Factors Affecting, and the Appearance of, Lineshapes for Spin- $1/2$ Nuclei Coupled to Quadrupolar Nuclei

Lineshapes observed in the spectra of the spin- $1/2$ (I) nucleus due to the second-order interaction with a quadrupolar spin (S) are dependent on a number of factors, some of which are intrinsic in the compound under study. These include the Larmor frequency of the S quadrupolar nucleus ν_s ; the S quadrupole coupling

constant ($\chi = e^2Qq_{zz}/h$); the isotropic indirect I,S spin-spin coupling constant J ; the anisotropy of the J tensor which is assumed to be axially symmetric, ($\Delta J = J_{||} - J_{\perp}$) and the angles β' and α' which define the orientation of the unique axis of the J tensor in the principal axis system (PAS) of the electric field gradient (EFG) tensor; the dipolar I,S coupling constant ($D = (\mu_0/4\pi)\gamma_I\gamma_S h/4\pi^2 r_{IS}^3$), or more precisely the effective dipolar coupling constant, D' , which incorporates D and ΔJ into one term, providing the J and D tensors are co-axial ($D' = D - \Delta J/3$); the polar (β^D) and azimuthal (α^D) angles defining the location of the I,S internuclear vector, r_{IS} , in the (PAS) of the (EFG) tensor; the asymmetry parameter (η) of the EFG tensor at S . As will be demonstrated, in certain cases where there is coupling to more than one quadrupolar nucleus it is necessary to take into account the effects of these nuclei concurrently. Some of these quadrupolar nuclei, as mentioned previously, may not be directly bonded to the I nucleus, and therefore consideration of intermolecular interactions from quadrupolar nuclei in neighbouring molecules, as well as intramolecular interactions, may be required. Of the dependencies listed above, one of the most fundamental, when considering second order quadrupolar effects, is that of the Larmor frequency of the quadrupolar nucleus ν_s , which is of course directly proportional to the static magnetic field strength B_0 . For a given quadrupolar-spin-1/2 spin-pair it is the ratio of the quadrupole coupling constant, multiplied by the effective dipolar coupling constant, to the Larmor frequency of the quadrupolar nucleus, $\chi D'/\nu_s$, that primarily determines the magnitude of the second-order shift that influences the form of the multiplet observed. For any given spin-pair, the effective dipolar coupling constant is invariant, and therefore splittings can conveniently be expressed in units of D' , so that they are only dependent on the factor χ/ν_s . For simplicity, this factor will be referred to as R throughout the following discussions.

Coupling to the quadrupolar nucleus causes the spin-1/2 I signal to be split into $2S + 1$ lines (for any given molecular orientation in the magnetic field). The innermost lines of the I spin multiplet caused by the perturbation of the Zeeman energy levels by the quadrupolar interaction will always be shifted in the opposite

direction to the outermost line(s). This is a salient point, since if the value of $\chi D'/\nu_s$ becomes sufficiently high some of the lines can begin to cross over. For set values of D' and χ , this occurs more readily for low values of S , a point which is highlighted in figure 7.2.1, which is a diagrammatic representation of the influence of the parameter $\chi D'/\nu_s$ on the spectra of spin-1/2 nuclei coupled to quadrupolar spins of increasing spin quantum number.

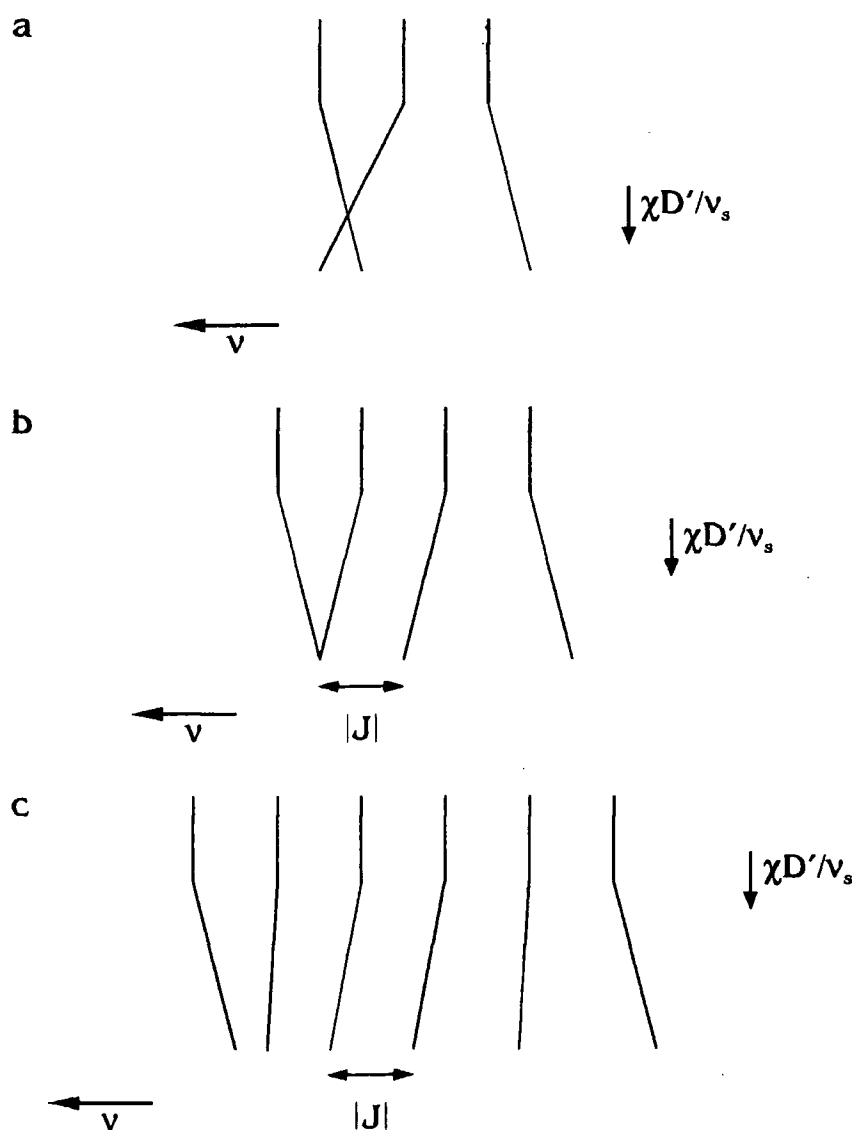


Figure 7.2.1 The effects of the second-order parameter $\chi D'/\nu_s$ on the spectra of a spin-1/2 nucleus I coupled to a quadrupolar nucleus S with spin quantum number $S = 1$ (a), $S = 3/2$ (b) and $S = 5/2$ (c).

It can be seen from figure 7.2.1 that as S increases overlap becomes less severe for a given value of the isotropic indirect coupling constant J . In addition, for given values of D' , χ and S , i.e. for any given compound, the overlap of lines becomes greater as the static field strength B_0 is decreased. This inverse proportionality of the magnitude of splitting observed to the applied magnetic field is explained simply by a decrease in the transferred second-order effect as the ratio of the quadrupolar to Zeeman interactions is reduced. The centre of gravity of the spectrum is invariant to second-order effects and therefore isotropic chemical shift values can be accurately determined. Furthermore, if no crossing over of lines is seen the average spacing gives the isotropic coupling constant.

No mention has been made thus far of the necessity to differentiate between splittings in the spectra caused by second-order quadrupolar effects and those caused by isotropic indirect coupling effects. In figure 7.2.1, second-order quadrupolar effects were considered only for cases where there was appreciable isotropic indirect coupling between the spin-1/2 and quadrupolar nuclei. Many examples exist where isotropic indirect coupling between a spin-1/2 and spin > 1 spin-pair is negligible, usually when the quadrupolar nucleus is small, and if this is the case the spectrum can be expected to adopt a totally different appearance. Figure 7.2.2 is a diagrammatic representation of the appearance of the spectrum, for a spin-1/2 nucleus coupled to a spin-3/2 nucleus, in the cases where indirect coupling is (a) negligibly small and (b) substantial.

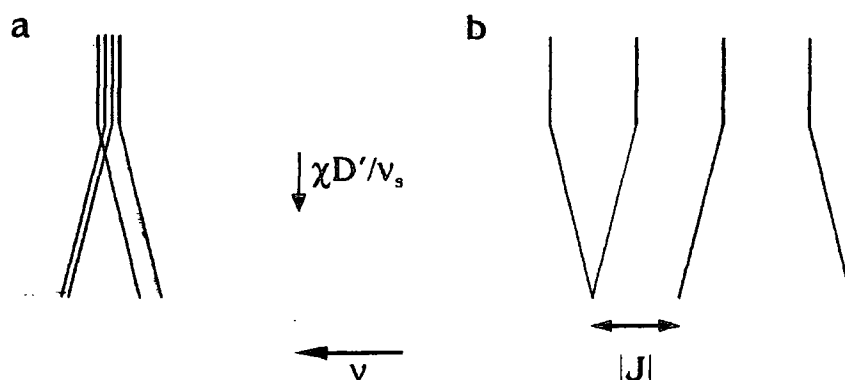


Figure 7.2.2 The effects of the magnitude of the isotropic indirect coupling constant, J , on the appearance of the spectrum of a spin-1/2 nucleus I coupled to a quadrupolar nucleus S with spin quantum number $S = 3/2$: (a) isotropic indirect coupling negligibly small, (b) significant isotropic indirect coupling.

As is apparent from figure 7.2.2, in such cases where the isotropic indirect coupling constant is expected to be small a symmetric doublet is predicted at high field-strengths. The isotropic chemical shift can still be accurately determined from these spectra since it is just given by the mid-point of the doublet.

In the preceding paragraphs, where we have been considering the appearance of spectra resulting from second-order quadrupolar effects (and indirect coupling effects), we have rather loosely referred to the separate components of the residual dipolar coupling induced multiplets as 'lines'. In actual fact these 'lines' do not possess a simple Lorentzian lineshape, but are in principle powder patterns. More often than not, as was the case for our systems, no such powder patterns are observed since they are broadened by effects such as field inhomogeneities and improper 'off-resonance' proton decoupling. However, more clearly defined powder patterns have been reported in spectra of nitrogen-containing compounds, arising from (^{13}C , ^{15}N) residual dipolar coupling.¹² Later in this chapter, where techniques are presented for calculating line positions and simulating spectra, when reference is made to line positions, what is really implied is the average band positions, i.e. the centres of gravity of the powder patterns. This concept is clarified when the results of

calculations performed to simulate theoretical powder patterns for residual dipolar coupling between the ^{13}C , $^{35,37}\text{Cl}$ spin-pair are presented in chapter 9, and between the ^{13}C , $^{79,81}\text{Br}$ spin-pair in chapter 10.

7.3 Theoretical Predictions of the Lineshapes for Spin-1/2 Nuclei Coupled to Quadrupolar Nuclei

A plausible explanation for the strange multiplicities observed in the signals arising from spin-1/2 nuclei in close proximity to quadrupolar nuclei has been presented in the previous section, and we have a list of the relevant parameters on which the magnitudes of the splittings observed are known to depend. Detailed theories have been developed¹³⁻¹⁵ to allow us to predict the second-order shifts observed in the spectra of the spin-1/2 (I) nucleus due to the second-order interaction with a quadrupolar spin (S), from a prior knowledge of these parameters, and hence the appearance of the spectrum. Conversely, estimations of the relevant parameters are possible from a well-resolved spectrum. However, these theories are very complex, time consuming to evaluate and therefore not particularly appropriate to everyday use. More recently more amenable theories have been developed that lead to simply applicable analytical equations, incorporating all the relevant parameters, and which therefore allow us to calculate lineshapes given a knowledge of the relevant parameters or vice-versa much more simply. The applicability of such theories is dependent on the value of the ratio R , introduced in the previous section. Three regimes can be envisaged; one when $\chi \ll \nu_s$, one when $\chi \approx \nu_s$ and one when $\chi \gg \nu_s$. We can characterise each of these regimes with respect to the value of R by stating they pertain to $R < 1$, $1 < R < 4$ and $R > 10$ respectively. For each of these regimes a different theory must be applied to obtain good agreement between experimental results and theoretical predictions. The accuracy of the predictions made using any given theory is found to rapidly fall away if it is applied in the wrong regime. What follows is an explanation of the derivation and application of these three theories. The raw theories give rise to cumbersome equations and so a number of assumptions are

necessary, some of which are based on previously acquired experimental data, to simplify them and make them more manageable.

7.3.1 "Normal" First-order Theory

In the limit of $\chi \ll \nu_s$, i.e. when $R \ll 1$, a "normal" first-order perturbation approach can be adopted.^{16,17} Here the quadrupole Hamiltonian is taken as a small perturbation of the Zeeman interaction.

The complete equation for the shift experienced (ν_m) of the lines in an I multiplet, relative to the unperturbed isotropic I frequency, produced by S eigenstates ($m = S, S-1, \dots, -S$) when one applies the first-order perturbation theory is given by:

$$\begin{aligned} \nu_m = & -mJ + (3\chi/20\nu_s)[S(2S-1)]^{-1} [S(S+1)-3m^2] \\ & [D(3\cos^2\beta^D-1+\eta\sin^2\beta^D\cos^22\alpha^D) \\ & -(\Delta J/3)(3\cos^2\beta^J-1+\eta\sin^2\beta^J\cos^22\alpha^J)] \end{aligned} \quad (7.3.1)$$

Consequently although, as was stated previously, the lineshapes of spin 1/2 nuclei experiencing the effect can be used to evaluate these parameters and hence lead to chemical information, the dependence on such a large number of terms implies that obtaining definitive information may prove arduous. Fortunately in practice certain simplifications are possible by applying a number of plausible assumptions. One such assumption, already mentioned in section 7.2, (which is reasonable for directly bonded nuclei) is that the unique axis of the J tensor is aligned with r_{IS} ,^{18,19} i.e. coaxiality of the J and D tensors so that $\alpha^D = \alpha^J$ and $\beta^D = \beta^J$. Thus D and ΔJ can be incorporated into a single effective coupling constant D' ($D' = D - \Delta J/3$). An equation for the combined effects of scalar and residual dipolar coupling can now be formulated:

$$\begin{aligned} \nu_m = & -mJ + (3D'\chi/20\nu_s)[S(2S-1)]^{-1} [S(S+1)-3m^2] \\ & [(3\cos^2\beta^D-1+\eta\sin^2\beta^D\cos^22\alpha^D)] \end{aligned} \quad (7.3.2)$$

If we further assume the asymmetry parameter of the EFG tensor is zero and there is co-axiality of the bond axis and the axis of the EFG tensor at the quadrupolar nucleus then $\beta' = \beta^D = 0$ and further simplifications are possible leading to equation 7.3.3.

$$\nu_m = -mJ + (3\chi D'/10\nu_s)[S(2S-1)]^{-1} [S(S+1)-3m^2] \quad (7.3.3)$$

On analysing equation 7.3.3, one finds it can be divided into two distinct parts. The first term ($-mJ$) dictates the multiplet structure of the I spin-1/2 resonance (quartet for coupling to $S = 3/2$, sextet for coupling to $S = 5/2$). The second term ($(3\chi D'/10\nu_s)[S(2S-1)]^{-1} [S(S+1)-3m^2]$) acts as a field-dependent perturbation of the former, and determines whether any overlap of lines causes the multiplet to apparently possess fewer lines than that predicted by the former term. We will define this perturbation of the I lines as a second-order shift Δ , where

$$\Delta = -(3\chi D'/10\nu_s) \quad (7.3.4)$$

Therefore the shifts (ν_m) experienced by the I lines as a consequence of the interaction with a quadrupolar nucleus S can be written as:

$$\nu_m = -mJ + [S(2S-1)]^{-1} [S(S+1)-3m^2] \Delta \quad (7.3.5)$$

Equation 7.3.5 gives us a means of probing the relevant NMR parameters of the system under study, the way it is used being dependent on the information available, or conversely allows us to predict the appearance of the spectrum from a knowledge of some of the NMR parameters. If χ is known, for instance from NQR experiments D , or more precisely D' , the "effective" dipolar coupling ($D' = D - \Delta J/3$) can be derived. More importantly, if both J and ΔJ can be expected to be negligible compared to D as is often the case, then these terms can be ignored, i.e. $D' = D$, and

D can be evaluated leading to the value of r_{IS} , the bond distance. For heavier nuclei, where the values of J and ΔJ may become significant compared to D , then if r_{IS} is known from X-ray diffraction studies information on the former two parameters may be available. The possibility of estimating the magnitude of ΔJ is particularly interesting, since there is no manifestation of this quantity in the solution state due to rapid molecular tumbling, and frequently it is of a magnitude so small that solid-state NMR studies fail to yield the necessary resolution to observe it.

So far the discussion has made no mention of the importance of the sign of the relevant interactions, which can have implications on the sense of the second-order shift. The signs of D and ν_s are dependent on the signs of the magnetogyric ratios. Neither γ_I or γ_S affect the sense of the shift providing D and D' have the same sign. As a rule of thumb, if bunching of the peaks occurs at low frequency then either χ is negative with D and D' having the same sign or, χ is positive and D and D' have opposite signs. If the sign of χ is known and r_{IS} is also known the sign of ΔJ can be obtained unambiguously. However, as is more usually the case, if the sign of χ is unknown a knowledge of r_{IS} leads to two values for ΔJ that are indistinguishable.

7.3.2 Application of "Normal" First-order Theory to (^{13}C , $^{35,37}\text{Cl}$) Residual Dipolar Coupling

The general theory presented in the previous sections is applicable to a spin- $1/2$ I nucleus coupling to a quadrupolar spin S , possessing any spin quantum number. If we now turn our attention to the instance of residual dipolar coupling investigated in chapter 9, namely that between chlorine and carbon nuclei, further simplifications to equation 7.3.5 are possible. Both isotopes of chlorine have spin quantum number equal to $3/2$ and therefore in the "high-field" regime, where $R < 1$, and assuming we are considering the combined effects of indirect and dipolar coupling interactions, equation 7.3.5 can be simplified to:

$$\nu_m = -mJ + (3\chi D'/10\nu_s) (5/4 - m^2) \quad (7.3.6)$$

For the ^{13}C , $^{35/37}\text{Cl}$ spin-pair J and ΔJ can be expected to be negligible compared with $3D$. Indeed relaxation studies conducted on simple chlorinated organic compounds revealed magnitudes of $J(^{13}\text{C}, ^{35/37}\text{Cl})$ in the region of 10-40 Hz.²⁰ This value is far smaller than not only the magnitude of D , but also the minimum linewidths presently attainable in ^{13}C CP/MAS spectra. Therefore, it is reasonable to neglect J and ΔJ^{21-23} (ΔJ being part of D' , contained in Δ) in equation 7.3.6, so that:

$$v_m = +(3\chi D/10v_s)(5/4 - m^2) \quad (7.3.7)$$

Normal first-order theory therefore predicts two spin-1/2 signals at $\pm (3\chi D/10v_s)$, i.e. a symmetric doublet having splitting given by:

$$s = \Delta v_{\pm 1/2} - \Delta v_{\pm 3/2} = (6\chi D/10v_s) \quad (7.3.8)$$

7.3.3 The Exact Approach and its Application to (^{13}C , $^{35,37}\text{Cl}$) Residual Dipolar Coupling

As the value of χ increases or the applied magnetic field strength becomes less the Zeeman interaction at the S nuclei may become smaller than the quadrupole interaction and the observed splittings display a tendency to deviate from the values calculated by equation 7.3.8. Here we are entering the regime of $\chi \approx \nu$, and the aforementioned perturbation treatment is no longer applicable.

Now it is necessary to return to exact calculations, from which a set of polynomial equations can be derived which can be used to predict the positions of the lines in the multiplet. The exact approach consists of carrying out a full-matrix diagonalisation of the complete Zeeman-quadrupole Hamiltonian for the S nucleus and averaging of the dipolar I,S coupling through a cycle of magic-angle spinning (repeated over thousands of different space orientations). The exact approach has been described¹³ and applied to the (^{13}C , $^{35,37}\text{Cl}$) dipolar and indirect coupling interactions.^{24,25} The necessity for more than one polynomial equation to describe the

lineshapes in this regime arises since it is in this regime that the transition from doublet through 2:1:1 triplet to asymmetric quartet occurs. A least squares fitting to a cubic polynomial equation, calculated by means of the exact theory is found to yield accurate results in the prediction of the appearance of signals in the MAS spectrum of the spin-1/2 nucleus for values of R in the range $1 < R < 3$. In this regime the appearance of the signal is still a doublet.

$$s = D(0.581 R + 0.033 R^2 - 0.021 R^3) \quad (R = \chi/\nu_s) \quad (7.3.9)$$

For slightly larger values of R (up to 4) the components of the spin-1/2 signal no longer appear as a doublet since the $\Delta\nu_{\pm 1/2}$ and $\Delta\nu_{\pm 3/2}$ lines start to diverge, and an asymmetric triplet with intensities in the ratio 2:1:1 if χ is positive and 1:1:2 if χ is negative (in the direction of increasing frequencies) is seen. The region of $3 < R < 4$ can be fitted to a cubic equation applied to the three components of the triplet:

$$\nu_1 = D(0.821 R - 0.307 R^2 + 0.051 R^3) \quad (7.3.10a)$$

$$\nu_2 = D(0.173 R^2 - 0.043 R^3) \quad (7.3.10b)$$

$$\nu_3 = D(-0.405 R + 0.066 R^2 - 0.004 R^3) \quad (7.3.10c)$$

where $\nu_{1,2}$ are the lines having relative intensity 1 and ν_3 is the one with relative intensity 2. The implications of the asymmetry of the lineshape should be fully appreciated since now, for the first time, the lineshape is sensitive to the sign of χ , and this gives us a means of its determination.

At values of $R > 4$ the lineshape adopted is a distorted quartet and therefore the possibility of accessing information regarding the sign of χ is still preserved. The relevant cubic equations for calculating the positions of the components of the quartet, derived from the exact approach are of the form:

$$v_1 = D(-1.473 + 1.274/R + 6.643/R^2 - 13.146/R^3) \quad (7.3.11a)$$

$$v_2 = D(1.731 - 3.096/R + 37.874/R^2 - 104.81/R^3) \quad (7.3.11b)$$

$$v_3 = D(0.247 + 3.736/R - 50.122/R^2 + 122.34/R^3) \quad (7.3.11c)$$

$$v_4 = D(-0.491 - 2.172/R + 7.160/R^2 - 7.420/R^3) \quad (7.3.11d)$$

7.3.4 "Inverse" First-order Theory: Application to (^{13}C , $^{79,81}\text{Br}$) Residual Dipolar Coupling

Although residual dipolar coupling between chlorine and carbon is unlikely ever to experience a value of R greater than 4, residual dipolar coupling between carbon and bromine could easily give rise to such a situation. In fact the magnitudes of the quadrupole coupling constants for bromine in simple brominated organic compounds may be so large that the agreement with experimental data achieved using equations 7.1.11 a-d becomes totally unsatisfactory. Values for χ for $^{79,81}\text{Br}$ typically lie in the region of 500 MHz, compared to 70 MHz for $^{35,37}\text{Cl}$.

Now, when the quadrupole coupling constant is much larger than the Zeeman interaction of S , first-order perturbation theory may be applied once again if we reverse the situation and consider the Zeeman term to be acting as a small perturbation of the quadrupole Hamiltonian. This theory has been developed^{26,27} and is referred to as 'inverse' first-order perturbation theory, to differentiate it from the normal first-order case. In this regime the simplified equations assuming once again negligible contributions from J and ΔJ , are:

$$v_{\pm 3/2} = \pm (3/2)D + 2Dv_s/\chi \quad (7.3.12a)$$

$$v_{\pm 1/2} = \pm (1/2)D - 2Dv_s/\chi \quad (7.3.12b)$$

7.3.5 Comparison of Line Positions Predicted by Derived Analytical Equations and Full-Matrix Diagonalisation

The exact theory involving full-matrix diagonalisation of the Zeeman quadrupole Hamiltonian can be applied at any value of R , and the equations derived

from either exact theory (polynomial equations), “normal” first-order theory or “inverse” first-order theory merely provide less time-consuming alternatives for evaluation of spectra. Lineshapes expected in the different regimes using the exact approach can be represented pictorially. Figure 7.3.1 is such a diagrammatic representation of the perturbation of the lines observed when only the dipolar interaction is considered as a mechanism for transmission of the effect. A positive quadrupole coupling constant is assumed and the transition from symmetric doublet through asymmetric 2:1:1 triplet to asymmetric quartet is clearly visible.

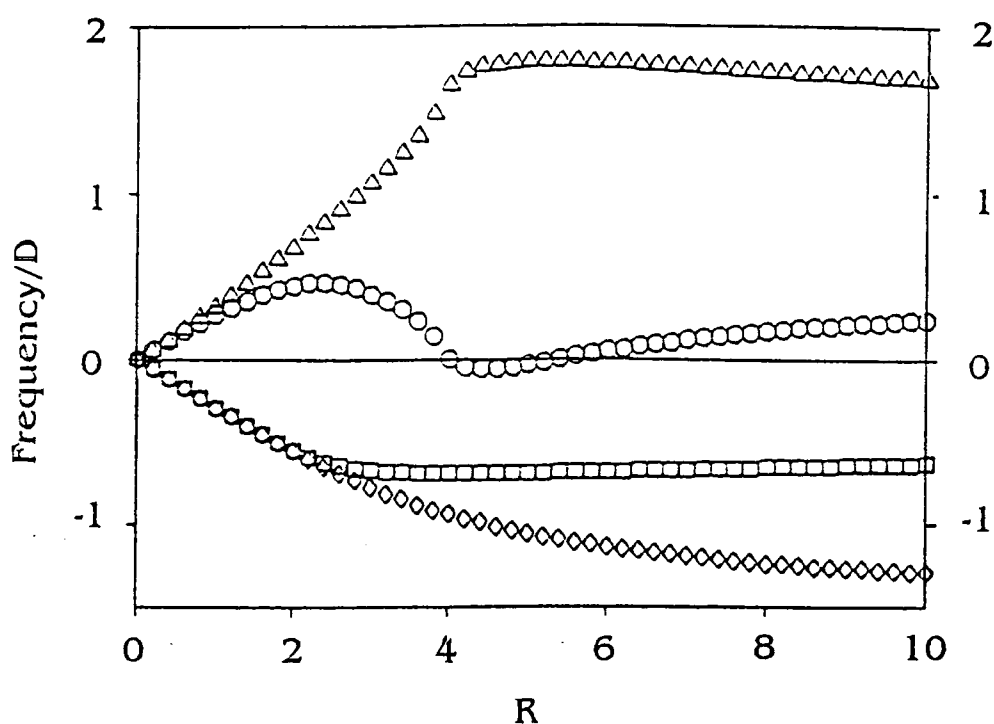


Figure 7.3.1 Line positions (in units of D) of a spin- $1/2$ I nucleus dipolar coupled to a spin- $3/2$ quadrupolar nucleus S as a function of the ratio R ($R = \chi/\nu_s$), as obtained by full matrix diagonalisation of the Zeeman-quadrupole Hamiltonian for positive χ and $\beta_D = 0$.²³

Furthermore, it is possible to compare the splittings/line positions calculated by the exact theory to those predicted by the equations derived for each regime corresponding to the situations where the “normal” first-order theory, the polynomial

equations or the “inverse” first-order theory are applicable. Figure 7.3.2 is a comparison of the calculated line positions obtained using full-matrix diagonalisation of the Zeeman quadrupole Hamiltonian, equation 7.3.8 and equation 7.3.9 for the regime $0 < R < 3$. Figure 7.3.3 similarly compares the results obtained using the exact approach to those predicted using equations 7.3.10 a, b and c for the regime $3 < R < 4$. Finally figure 7.3.4 shows the accuracy of equations 7.3.11 a, b, c and d in the regime $4 < R < 10$ compared to the full-matrix diagonalisation method and the results predicted using equations 7.3.12 a and b in the regime $R > 10$.

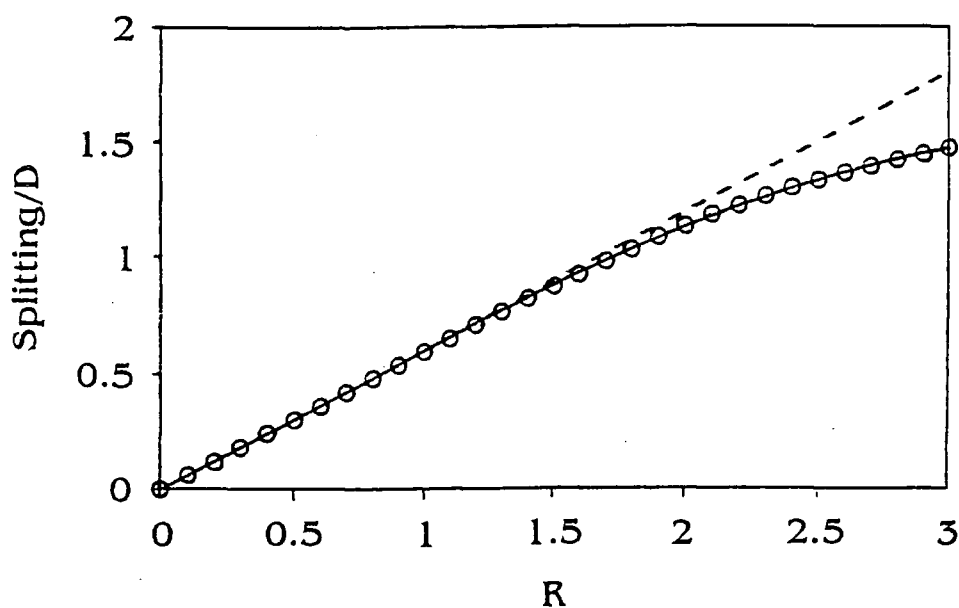


Figure 7.3.2 Comparison of the symmetric splitting predicted (in units of D) in the MAS NMR signal of a spin-1/2 nucleus dipolar coupled to a spin-3/2 nucleus as a function of R . Circles: values obtained by the exact calculations. Full line: values given by equation 7.3.9. Dashed straight line: result predicted by first-order theory.²³

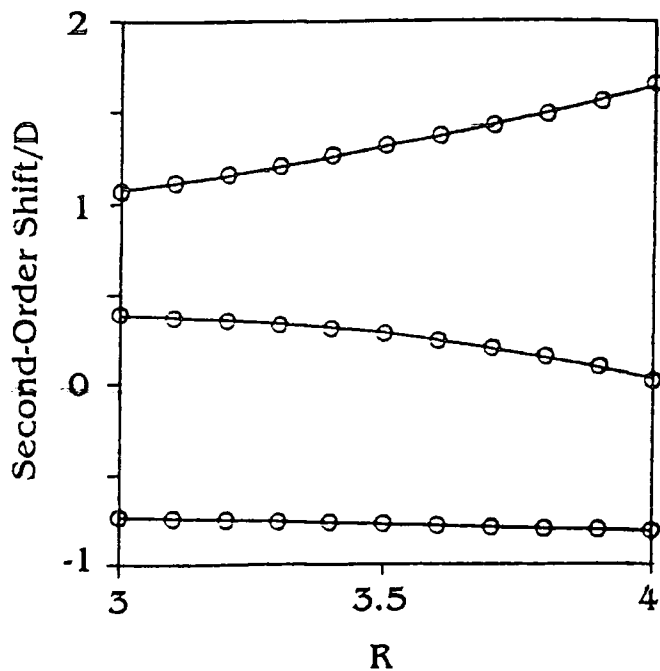


Figure 7.3.3 Comparison of second-order residual dipolar effects for spin-1/2, spin-3/2 coupling in the region $3 < R < 4$. Circles: Line positions calculated using exact approach. Full lines: Line positions predicted using the polynomial equations 7.3.10 a-c.²⁸

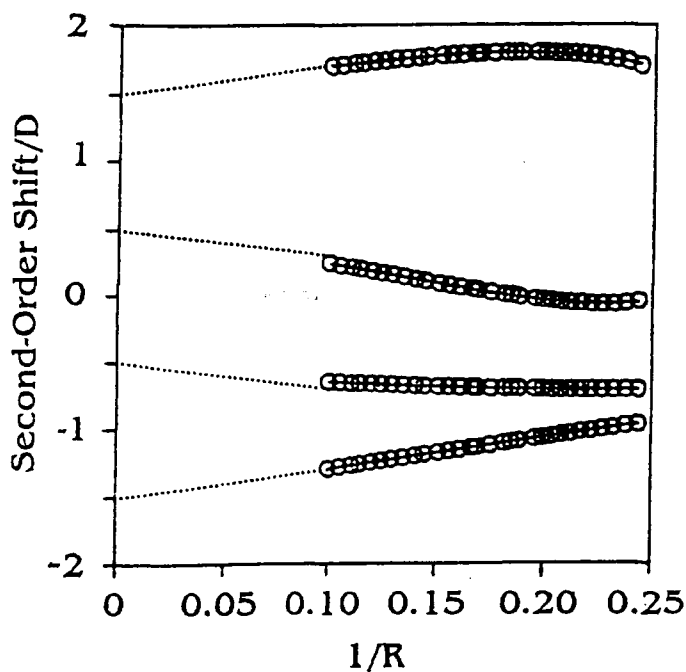


Figure 7.3.4 Comparison of second-order residual dipolar effects for spin-1/2, spin-3/2 coupling in the region $R > 4$. Circles: Results calculated using the exact approach. Solid lines: Positions of lines predicted using the polynomial equations 7.3.11 a-d. Dotted lines: The line positions predicted by "inverse" first-order theory.²⁸

7.3.6 The Effects of Anisotropy in Indirect Coupling

In the above diagrams the second-order shift is considered only in terms of D , which is fine provided no appreciable indirect coupling is present between the two nuclei in question, as is known to be the case in (^{13}C , $^{35,37}\text{Cl}$) residual dipolar coupling. However, for a bromine nucleus coupled to carbon nucleus larger values for J (and therefore ΔJ) can reasonably be expected^{20,28} and it is no longer possible to neglect the effect of J and its anisotropy on the lineshapes observed. Certain modifications to equations 7.3.12 a and b are needed to account for the role of these parameters in the transmission of the effect from the bromine nucleus to the carbon nucleus. The individual components of the asymmetric quartet are given by the equations:^{26,27}

$$v_{\pm 3/2} = \pm (0.75 J - 1.5 D') + 2(J + D')v_s/\chi \quad (7.3.13a)$$

$$v_{\pm 1/2} = \pm (0.8546 J + 0.5 D') - 2(J + D')v_s/\chi \quad (7.3.13b)$$

where once again $D' = D - \Delta J/3$ is the effective dipolar coupling constant (assuming coaxiality in D and J tensors). Now not only does the magnitude of the shifts depend on J , but the sense of the shifts depends on the relative signs of $(J + D')$, v_s and χ . Given the necessary information the possibility of determining the sign of J is realised.

7.4 "Self-decoupling"

In the case of residual dipolar coupling between ^{13}C and ^{127}I inverse first-order theory is again applicable since the iodine nucleus commonly possesses quadrupole coupling constants in excess of 1500 MHz in its compounds. The spin quantum number of the iodine nucleus is 5/2 and consequently the signal from the carbon directly bonded to the iodine would be expected to adopt the form of a 1:1:1:1:1:1 asymmetric sextet if no overlapping of lines was observed, which is reasonable given the information in figure 7.2.1. However, to the best of our knowledge, there are no

known cases of detailed analyses of complex bandshapes arising from residual dipolar coupling effects between carbon and iodine cited in the literature to date. This may be attributed to the difficulty in observing the effect due to properties intrinsic in the iodine nucleus. The expected multiplets are seen to collapse due to a phenomenon termed self-decoupling.^{29,30} Dynamic effects are thought to be responsible for such a collapse through two interconnected mechanisms. Rapid isotropic motion or certain geometries of rapid anisotropic motion may cause both either total or partial averaging of the dipolar and quadrupolar interactions and/or fast spin-lattice relaxation for the quadrupolar nucleus.

It is found that providing $D < \tau^{-1}$ (where τ is the correlation time for the motion) the motionally averaged splittings will be reduced to 1/9 of the value observed in the absence of motion. However, when molecular motion is fast and isotropic, complete collapse of the splittings will result.^{25,31}

The induction of short spin-lattice relaxation times for the quadrupolar nucleus by molecular motion³² can be paralleled with chemical exchange coalescence and is dependent on the rate of transition between the energy levels of the quadrupolar nucleus. For coupling to a spin-3/2 quadrupolar nucleus it is predicted that self-decoupling will be observed provided $2^{1/2}[p_{\pm 3/2, \pm 1/2}(\theta, \phi)]/\pi > s(\theta, \phi)$, where $p_{\pm 3/2, \pm 1/2}(\theta, \phi)$ is the transition rate between the states $|\pm 3/2\rangle$ and $|\pm 1/2\rangle$ of the ^{35,37}Cl nuclei, and θ and ϕ are the polar angles locating the position of the Z_{EFG} axis in the coordinate system.³¹ Although in principle $s(\theta, \phi)$ can be computed, discrete values of $p_{\pm 3/2, \pm 1/2}(\theta, \phi)$ cannot be obtained from NQR measurements on powder samples, and only access to a powder average value $\langle p_{\pm 3/2, \pm 1/2} \rangle$ is guaranteed. This latter factor is given directly by $[T_1(^{35}\text{Cl})]^{-1}$ and is therefore easily accessible from NQR experiments.

7.5 Coupling to (Several) Remote Quadrupolar Nuclei

In the case of (^{13}C , $^{35,37}\text{Cl}$) residual dipolar coupling, where only the dipolar coupling was been considered as a mechanism for the transmission of the quadrupolar effects it has so far been assumed that $\beta_D = 0$. This has been an adequate assumption for the case of directly bonded nuclei, but recently cases of residual dipolar coupling between non-bonded carbon and chlorine nuclei have been reported.³³ Now β_D may be non-zero, and such simplifications are not possible, so we can no longer neglect the angular dependent $(3 \cos^2 \beta^D - 1)$ term. Taking the case of a carbon nucleus experiencing residual dipolar coupling to the two quadrupolar isotopes of chlorine to which it is not directly bonded, in the regime $R < 1$, equation 7.3.8 would be modified thus:

$$s = \Delta v_{\pm 1/2} - \Delta v_{\pm 3/2} = (3 \cos^2 \beta^D - 1)(6\chi D/20v_s) \quad (7.3.14)$$

Similarly, in the regime $1 < R < 3$ the full polynomial equation (7.3.9) would become:

$$s = D [(3 \cos^2 \beta^D - 1) / 2] (0.581 R + 0.033 R^2 - 0.021 R^3) \quad (7.3.15)$$

and in the regime $3 < R < 4$:

$$v_1 = D [(3 \cos^2 \beta^D - 1) / 2] (0.821 R - 0.307 R^2 + 0.051 R^3) \quad (7.3.16a)$$

$$v_2 = D [(3 \cos^2 \beta^D - 1) / 2] (0.173 R^2 - 0.043 R^3) \quad (7.3.16b)$$

$$v_3 = D [(3 \cos^2 \beta^D - 1) / 2] (-0.405 R + 0.066 R^2 - 0.004 R^3) \quad (7.3.16c)$$

Hence the magnitude of the splitting now has a direct dependency on the angle β^D between the internuclear vector r and the Z_{EFG} axis of the quadrupole tensor at the chlorine nucleus. Similar complications arise when considering (^{13}C , $^{79,81}\text{Br}$) residual dipolar coupling in the series of brominated benzenes studied in chapter 10. For these

compounds (see table 8.2.1) we can envisage a whole host of different internuclear separations and angles β^D corresponding to different remote interactions between carbon and bromine nuclei at different sites around the ring³⁴. These include interactions between $^{79,81}\text{Br}$, and ^{13}C directly bonded to each other and $^{79,81}\text{Br}$ in *ortho*, *meta* and *para* positions relative to ^{13}C . In addition, due to the nature of the stacking of the aromatic rings in the crystal structure, it becomes necessary to consider interactions between ^{13}C and $^{79,81}\text{Br}$ in nuclei in different molecules. One other important point worthy of mention for residual dipolar coupling between remote nuclei in bromobenzenes, where ΔJ is expected to be appreciable, is that now, because the J and D tensors are not coaxial for non-bonded nuclei the effects of ΔJ can no longer be subsumed into an effective dipolar coupling constant D' .

The coupling of a ^{13}C nucleus to more than one quadrupolar nucleus, as described in the previous paragraph, itself poses some interesting questions. When there is more than one quadrupolar nucleus present to which a spin 1/2 nuclei may couple, the overall coupling pattern may just be considered as a convolution of the individual splittings, regardless of whether the quadrupolar nuclei are equivalent or not (assuming the quadrupolar nuclei are not themselves strongly coupled together). In the case of the brominated benzenes discussed in chapter 10 the principal effect is due to coupling to the directly-bonded bromine nucleus, with those couplings to remote bromine nuclei having only a minor effect on the form of the carbon-13 multiplet. In contrast, when the carbon nucleus is directly bonded to two or three quadrupolar nuclei, as is encountered for the chloroacetates investigated in chapter 9, each of these nuclei display large couplings and consequently have a large effect on the lineshapes. The form of the respective lineshapes when coupling to 2 or 3 quadrupolar nuclei is further discussed in chapter 9. A plethora of examples of coupling to two or more inequivalent quadrupolar nuclei^{33, 35-39} and even coupling to two different quadrupolar nuclei⁴⁰ have been reported in the literature.

The case of coupling to two different quadrupolar nuclei leads to another important point. The two cases of residual dipolar coupling considered in depth thus

far have placed no importance on the fact that there exists for both chlorine and bromine two quadrupolar isotopes. For each element the two isotopes are totally distinct entities. Therefore each isotope will possess its own unique properties and hence different values for the relevant parameters. In fact for the ^{35}Cl and ^{37}Cl isotopes it is found that they possess similar nuclear properties. The two natural abundances for ^{35}Cl and ^{37}Cl are 75.53 % and 24.47 % respectively. The values of Q (the quadrupole moment) for the two isotopes are -0.08165 (^{35}Cl)⁴⁰ and -0.06435 (^{37}Cl).⁴¹ Since the expected splitting, as calculated by first-order theory, is proportional to the combined factor $D'\chi/\nu_s$, and therefore independent of γ , if only the major isotope (^{35}Cl) is considered when performing the calculations the effects of the minor isotope on the appearance of the spectrum can be expected to be significant. To calculate the expected splittings more accurately one should use weighted averages of the relevant parameters corresponding to the individual isotopes. A similar situation exists for the two isotopes of bromine, but now the natural abundances of the two relevant isotopes of bromine are 50.5 % and 49.0 % for ^{79}Br and ^{81}Br respectively. In addition the most recent value of the ratio of the quadrupole moments $Q(^{81}\text{Br}) / Q(^{79}\text{Br}) = 0.833$.⁴¹ Once again, weighted averages of the relevant parameters should be used when performing the calculations.

7.6 Background of Residual Dipolar Coupling

Since the initial reports of residual dipolar coupling between ^{13}C and ^{14}N nuclei⁵⁻⁹ the attention paid to the effects communicated to spin-1/2 nuclei by contiguous quadrupolar nuclei has greatly increased from both theoretical and experimental points of view. It is now known that a great number of examples of this phenomenon exists between spin-pairs distributed all over the Periodic Table. One reason for the increased awareness is the better accessibility of new nuclei to study by NMR with the advent of higher-field spectrometers. One consequence of the increased commercially availability of spectrometers possessing greater static field

strengths has been to depose the ^{13}C , ^{14}N spin pair as the exemplary case of the phenomenon, since the effects are rarely observed even at what is considered a relatively low field by today's standards of 4.7 T. However, this spin-pair still provides the most rigorously investigated example of the effect, and (^{13}C , ^{14}N) residual dipolar coupling has been observed in ^{13}C CP/MAS spectra of a variety of ^{14}N -containing organic and biologically relevant compounds.^{7,8,42,43} Uses have included elucidation of structure through non-bonded ^{13}C , ^{14}N interactions,⁴⁴ unambiguous assignment of ^{13}C resonances,^{45,46} and acquisition of potential energy profiles in proton-exchanging systems³² as well as determination of the magnitude and sign of the ^{14}N quadrupole coupling constants.^{43, 47-51} Now the increased range of spin pairs displaying the phenomenon has meant it has been detected in many new materials, some of which are technologically important such as zeolites,⁵² surface-immobilized substrates⁵³ and silicon ceramics.^{37,54} These new spin pairs have included (^{13}C , ^2H),^{55,56} (^{13}C , ^{75}As),⁵⁷ (^{13}C , ^{59}Co),⁵⁸ (^{13}C , ^{23}Na),⁵⁹ (^{119}Sn , $^{35,37}\text{Cl}$),^{35,60,61} (^{119}Sn , ^{14}N),^{38,39} (^{31}P , $^{63,65}\text{Cu}$),⁶²⁻⁶⁶ (^{31}P , ^{27}Al),⁵³ (^{31}P , ^{14}N),⁶⁷ (^{31}P , ^{55}Mn),⁶⁸ (^{31}P , ^{59}Co),⁶⁹ (^{31}P , ^{93}Nb),⁶⁹ (^{31}P , $^{99,101}\text{Ru}$),⁶⁹ (^{113}Cd , ^{14}N),¹¹ (^{29}Si , ^{14}N),^{37,54} (^{29}Si , $^{35,37}\text{Cl}$),⁵⁹ (^{29}Si , ^{27}Al),⁵² (^1H , ^{14}N),⁷⁰ (^{195}Pt , $^{35/37}\text{Cl}$).⁷¹

The wide range of examples listed above gives an idea of the ubiquity of the phenomenon. However, the cases of residual dipolar coupling covered in this thesis, namely (^{13}C , $^{35/37}\text{Cl}$)²¹⁻²⁴ and (^{13}C , $^{79/81}\text{Br}$) effects,^{72,73} have only been observed relatively recently. The following chapters concentrate on investigations carried out for these two spin pairs,^{33,34} in addition to a brief account of work performed investigating the effects of ^{127}I on ^{13}C lineshapes in simple CP/MAS spectra. The occurrence of the phenomenon is reported for a variety of simple halogenated organic compounds, and experimental results are compared to theoretical calculations. The value of this body of work is twofold. Firstly that it can explain the occurrence of doublets, triplets and quartets in the solid-state spectra of halogenated compounds. Identification of the multiplets arising from residual dipolar coupling displayed by carbon nuclei directly bonded to halogen nuclei, or even those located at more remote

positions to halogen nuclei, can avoid a potential source of confusion. Solid-state spectra are notorious for giving rise to unexpected multiplicities due to effects such as non-equivalence of molecules in the unit cell and unique conformations lowering the effective symmetry, and if additional confusion can be avoided this can only be advantageous. Secondly, as discussed earlier, interesting dynamic phenomena are likely to lead to "self-decoupling" in favourable cases, especially for the $^{79/81}\text{Br}$ and ^{127}I nuclei. Frequently, broad resonances are observed in the carbon spectra for nuclei directly bonded to halogen nuclei, with no splittings apparent as a result of self-decoupling effects. At the extreme, resonances of carbons bonded to iodine have been known to broaden to such an extent so as to render them undetectable, so again a potential source of confusion can be avoided, although obviously, determination of associated nuclear parameters such as the sign of the quadrupole coupling constant from such spectra becomes impossible.

The prevalence of the self-decoupling phenomenon, rendering observation of the effect difficult, and the fact that many potentially ideal subjects having uncluttered spectra are liquids at room temperature, has meant that very few halogenated organic compounds have been identified that possess properties conducive to the observation of the effect. Consequently, despite the increasing volume of work being undertaken in the area of residual dipolar coupling only a limited number of reports have been published describing the phenomenon between ^{13}C and halogen spins.

References

1. H. S. Gutowski and B. R. McGarvey, *J. Chem. Phys.*, **21**, 1423 (1953).
2. T. L. Weeding and W. S. Veeman, *J. Chem. Soc., Chem Commun.*, 946 (1989).
3. S. Hayashi and K. Hayamizu, *Bull. Chem. Soc. Jpn.*, **63**, 913 (1990).
4. S. Hayashi and K. Hayamizu, *J. Phys. Chem. Solids*, **53**, 239 (1992).
5. E. Kundia and L. Alla, in *Proceedings of 20th Congress Ampere, Tallinn*, p. 92. Springer, Berlin (1979).
6. E. Lippmaa, M. Alla, H. Raude, R. Teelar, I. Heinmua, and E. Kundia, in *Proceedings of 20th Congress Ampere, Tallinn*, p. 87. Springer, Berlin (1979).
7. S. Opella, M. H. Frey and T. A. Cross, *J. Am. Chem. Soc.*, **101**, 5856 (1979).
8. C. J. Groombridge, R. K. Harris, K. J. Packer, B. J. Say and F. Tanner, *J. Chem. Soc., Chem. Commun.*, 174 (1980).
9. R. K. Harris and A. C. Olivieri, *Prog. Nucl. Magn. Reson. Spectrosc.*, **24**, 435 (1992).
10. K. Eichele, R. E. Wasylshen, J. F. Corrigan, S. Doherty, Y. Sun and A. J. Carty, *Inorg. Chem.*, **32**, 121 (1993).
11. K. Eichele and R. E. Wasylshen, *Angew. Chem. Int. Ed. Engl.*, **31**, 1222 (1992).
12. R. Challoner and R. K. Harris, *Solid State Nuclear Magnetic Resonance*, **88**, 888 (1994).
13. E. M. Menger and W. S. Veeman, *J. Magn. Reson.*, **46**, 257 (1982).
14. N. Zumbudyalis, P. M. Henrichs and R. H. Young, *J. Chem. Phys.*, **75**, 1603 (1991).
15. J. G. Hexem, M. H. Frey and S. J. Opella, *J. Chem. Phys.*, **77**, 3847 (1982).
16. A. C. Olivieri, L. Frydman and L. E. Diaz, *J. Magn. Reson.*, **75**, 50 (1987).
17. A. C. Olivieri, *J. Magn. Reson.*, **81**, 201 (1989).
18. P. N. Tutunjian and J. S. Waugh, *J. Magn. Reson.*, **49**, 155, (1982).
19. G. H. Penner, W. P. Power and R. E. Wasylshen, *Can. J. Chem.*, **66**, 1821 (1988).
20. V. Mlynarik, *Prog. NMR Spectrosc.*, **18**, 277 (1986), V. Mlynarik, *Org. Magn. Reson.*, **22**, 164 (1984), N. M. Sergejev, P. Sandor, N. D. Sergejeva and W. T. Raynes, *J. Magn. Reson.*, **A 115**, 174, (1995).

21. A. C. Olivieri, P. Cabildo, R. M. Claramunt J. E. Elguero and I. Sobrados, *J. Phys. Chem.*, **98** (20), 5211 (1994).
22. R. K. Harris, M. Sunnetcioglu, K. S. Cameron and F. G. Riddell, *Magn. Reson. Chem.*, **31**, 963 (1993).
23. R. M. Cravero, C. Fernandez, M. Gonzalez-Sierra and A. C. Olivieri, *J. Chem. Soc. Chem. Commun.*, 1253 (1993).
24. S. H. Alarcon, A. C. Olivieri and R. K. Harris, *Solid State NMR*, **2**, 325 (1993).
25. S. H. Alarcon, A. C. Olivieri, S. A. Carss, R. K. Harris, M. Zuriaga and G. Monti, *J. Magn. Reson.*, (in press).
26. A. C. Olivieri, *Solid State NMR*, **1**, 345 (1992).
27. A. C. Olivieri, *J. Magn. Reson.*, **A 101**, 313 (1993).
28. O. Yamamoto and M. Yanagisawa, *J. Chem. Phys.*, **67**, 3803 (1977).
29. H. W. Speiss, U. Haeberlen, and H. Zimmerman, *J. Magn. Reson.*, **25**, 55 (1977).
30. P. Jonsen, *J. Magn. Reson.*, **77**, 348 (1988).
31. J. F. Haw, R. A. Crook and R. C. Crosby, *J. Magn. Reson.*, **66**, 551 (1986).
32. A. C. Olivieri, *J. Chem. Soc. Perkin Trans.*, **2**, 85 (1990).
33. S. H. Alarcon, A. C. Olivieri, S. A. Carss and R. K. Harris, *Angew. Chem. Int. Ed. Engl.*, **33**(15/16), 1624 (1994).
34. A. E. Aliev, K. D. M. Harris, R. K. Harris, S. A. Carss and A. C. Olivieri, *J. Chem. Soc. Faraday Trans.*, (in press).
35. R. K. Harris, A. Sebald, D. Furlani, G. Tagliavini, *Organometallics*, **7**, 388 (1988).
36. R. K. Harris and A. Root, *Molec. Phys.*, **66**, 993 (1989).
37. A. C. Olivieri and G. R. Hatfield, *J. Magn. Reson.*, **94**, 535 (1991).
38. A. Lycka, J. Holecek, B. Schneider and J. Straka, *J. Organomet. Chem.*, **389**, 29 (1990).
39. D. C. Apperley, N. A. Davies, R. K. Harris, A. K. Brimah, S. Eller and R. D. Fischer, *Organometallics*, **9**, 2672 (1990); D. C. Apperley, N. A. Davies and R. K. Harris, *11th ISMAR Conf.*, Vancouver (July 1992).
40. A. Lycka, J. Holecek, A. Sebald and I Tkac, *J. Organomet. Chem.*, **409**, 331 (1991).

41. P. Pyykko, *Z. Naturforsch., Teil A* **47**, 189 (1992).
42. M.H. Frey and S. J. Opella, *J. Chem. Soc. Chem. Commun.*, 474 (1980).
43. A. C. Olivieri, L. Frydman M. Grasselli and L. E. Diaz, *Magn. Reson. Chem.*, **26**, 281 (1988).
44. C. J. Moreland, E. O. Stejskal, S. C. J. Summer, J. D. Memory, F. I. Carroll, G. A. Brine and P. S. Portoghese, *J. Magn. Reson.*, **83**, 173 (1989).
45. R. K. Harris and P. Jackson, *J. Phys. Chem. Solids*, **48**, 813 (1987).
46. L. Frydman, A. C. Olivieri, L. E. Diaz, A. Valasinas and B. Frydman, *J. Am. Chem. Soc.*, **110**, 5651 (1988).
47. J. G. Hexem, M. H. Frey and S. J. Opella, *J. Am. Chem. Soc.*, **105**, 5717 (1983).
48. A. M. Chippendale, A. Mathias, R. S. Aujla, R. K. Harris, K. J. Packer and B. J. Say, *J. Chem. Soc. Perkin Trans.*, **2**, 1357 (1983).
49. S. J. Opella, J. G. Hexem, M. H. Frey and T. A. Cross, *Phil. Trans. R. Soc. Lond.*, **A299**, 665 (1981).
50. A. Naito, S. Ganapathy and C. A. McDowell, *J. Magn. Reson.*, **48**, 367 (1982).
51. N. Okazaki, A. Naito and C. A. McDowell, *Chem. Phys. Lett.*, **100**, 15 (1983).
52. J. S. Hartman and B. L. Sheriff, *J. Phys. Chem.*, **95**, 7575 (1991).
53. P.-J. Chu, J. H. Lunsford and D. J. Zalewski, *J. Magn. Reson.*, **87**, 68 (1990).
54. A. C. Olivieri, *Z. Naturforsch., Teil A* **47**, 39 (1992).
55. S. D. Swanson, S. Ganapathy and R. G. Bryant, *J. Magn. Reson.*, **73**, 239 (1987).
56. P. Jonsen, S. F. Tanner and A. H. Haines, *Chem. Phys. Lett.*, **164**, 325 (1989).
57. D. L. Sastry, A. Naito and C. A. McDowell, *Chem. Phys. Lett.*, **146**, 422 (1988).
58. S. Aime, M. Botta, R. Gobetto and B. E. Hanson, *Inorg. Chem.*, **28**, 1196 (1989).
59. J. Böhm, D. Fenzke and H. Pfeifer, *J. Magn. Reson.*, **55**, 197 (1983).
60. D. C. Apperley, B. Haiping and R. K. Harris *Mol. Phys.*, **68**, 1277 (1989).
61. R. K. Harris, *J. Magn. Reson.*, **78**, 389 (1988).
62. A. C. Olivieri, *J. Am. Chem. Soc.*, **114**, 5758 (1992).

63. G. A. Bowmaker, B. W. Skelton, A. H. White and P. C. Healy, *J. Chem. Soc. Dalton Trans.*, 2825 (1988).
64. P. F. Barron, J. C. Dyason, L. M. Engelhardt, P. C. Healy and A. H. White, *Inorg. Chem.*, **23**, 3766 (1984).
65. J. C. Dyason, P. C. Healy, L. M. Engelhardt, C. Pakawatchai, V. A. Patrick, C. L. Raston, and A. H. White, *J. Chem. Soc. Dalton Trans.*, 831 (1985).
66. P. C. Healy, A. K. Whitakker, J. D. Kildea, B. W. Skelton and A. H. White, *Aust. J. Chem.*, **44**, 729 (1991).
67. W. P. Power, R. E. Wasylshen and R. D. Curtis, *Can. J. Chem.*, **67**, 454 (1989).
68. R. Gobetto, R. K. Harris and D. C. Apperley, *J. Magn. Reson.*, **96**, 119 (1992).
69. K. Eichele, R. E. Wasylshen, J. F. Corrigan, S. Doherty, Y. Sun and A. J. Carty, *Inorg. Chem.*, **32**, 121 (1993).
70. A. Naito, A. Root and C. A. McDowell, *J. Phys. Chem.*, **95**, 3578 (1991).
71. S. Hayashi and K. Hayamizu, *Magn. Reson. Chem.* **30**, 658 (1992).
72. B. Nagasaka, S. Takeda and N. Nakamura, *Chem. Phys. Lett.*, **222**, 486 (1994).
73. A. E. Aliev, K. D. M. Harris, P. J. Barrie and S. Camus, *J. Chem. Soc., Faraday Trans.*, **90**, 3729 (1994).

Chapter 8

Experimental Aspects

8.1 Nuclei of Interest

8.1.1 Magnetic Properties of the Nuclei

Naturally, observation of the carbon nucleus predominated in this body of work, and the magnetic properties of the ^{13}C nucleus have already been mentioned in table 3.1.1. However in addition to the carbon-13 spectra a small amount of ^{35}Cl NMR of certain chlorinated organic and inorganic compounds was carried out. Table 8.1.1 lists the fundamental NMR parameters of the chlorine-35 nucleus¹.

Nucleus	Spin, I	Natural Abundance (%)	Gyromagnetic Ratio, γ ($10^7\text{T}^{-1}\text{s}^{-1}$)	Receptivity ^a (Relative to ^1H)
^{35}Cl	3/2	75.53	2.6240	3.56×10^{-3}

^a Product of natural abundance and sensitivity

Table 8.1.1 NMR properties of chlorine-35 nucleus.

It is apparent from table 8.1.1 that the chlorine-35 nucleus has a natural abundance of 75% which, coupled to the value of its gyromagnetic ratio, means it possesses a receptivity approximately twenty times that of the carbon-13 nucleus. Furthermore, chemical shift ranges are large, and the value of its gyromagnetic ratio leads to a Larmor frequency that is high enough to be measured on a normal high-field spectrometer. Acquiring an NMR signal should therefore, in practice, be

relatively simple compared to carbon NMR, and lead to information that is of value in structural analysis. Indeed, strictly speaking, the simplicity side of things is borne out, as chlorine-35 NMR signals are generally instantly apparent upon application of a r.f. pulse. However, certain other factors, pertaining to the characteristics of the NMR signals acquired, conspire to make information retrieval difficult. Complications existing due to the presence of the nuclear quadrupole $S = 3/2$, a point discussed in chapter 7, make information retrieval all but impossible without the implementation of costly techniques such as DAS (Dynamic Angle Spinning)^{2,3} and DOR (Double Rotation),⁴ to suppress the quadrupolar interaction. For simple organic compounds this quadrupolar coupling overwhelms other interactions to such a degree that excessive spectral broadening allows little information to be gleaned from such spectra. For inorganic compounds the problems may not be so acute. For instance in NaCl the cubic symmetry of the nuclear site leads to a small value of the quadrupole coupling constant, negating such quadrupolar broadening, and sharp resonances are observed in the solid state.⁵ The main purpose of performing the ³⁵Cl NMR was simply to demonstrate the overwhelming effects that quadrupolar interactions usually have on spectra of simple organic compounds, and hence emphasise the value of being able to extract information relating to quadrupolar nuclei by observing residual dipolar coupling effects in NMR spectra of less problematic nuclei such as carbon-13.

One final experimental consideration concerns the tuning of the probe for observation of the chlorine-35 nucleus. It has been mentioned that the gyromagnetic ratio leads to operating frequencies that are of a suitable magnitude to allow observation. However, with our commercial probe, tuning was only just possible, (*i.e.* near the low frequency limit, given the capacitors supplied), in order to acquire the spectra.

Of more relevance to the subject of residual dipolar coupling is spectroscopic data relating to the nuclear quadrupole of the nuclei for which residual dipolar coupling to carbon-13 was investigated. Table 8.1.2 lists the magnetic properties of

the quadrupolar nuclei (all magnetic isotopes), whose second-order quadrupole effects are investigated.

Nucleus	Spin, I	Natural Abundance (%)	Quadrupole Moment (Barn)	Typical ^a Quadrupole Coupling Constant (MHz)
³⁵ Cl	3/2	75.53	-9.8	-70
³⁷ Cl	3/2	24.47	-8.2	-50
⁷⁹ Br	3/2	50.54	0.37	550
⁸¹ Br	3/2	49.46	0.31	450
¹²⁷ I	5/2	100	-0.79	1800

^a For compounds studied in this body of work.

Table 8.1.2 Spin properties of the quadrupolar nuclei investigated for second-order effects.¹

It is apparent that certain differences exist in the nuclear properties of the halogen nuclei contained in table 8.1.2. Firstly, iodine has a spin quantum number of 5/2 whereas the other nuclei have spin quantum numbers of 3/2. Secondly, the chlorine nuclei exhibit values of the quadrupolar moment and quadrupolar coupling constants that are negative, in contrast to those of the iodine and bromine nuclei. Thirdly, much larger quadrupolar coupling constants are observed for bromine and iodine compared to chlorine. All of these differences in nuclear characteristics are significant, as will become apparent, since their effects are relayed to the carbon nucleus, via residual dipolar coupling, and are therefore often manifest in spectral differences in the carbon spectra of these compounds.

8.2 Compounds

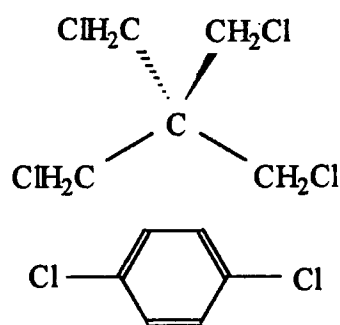
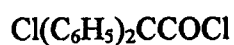
All of the compounds studied, with the exception of NaCl on which ^{35}Cl NMR was performed, can be classified as organic in nature. Compounds studied included sodium and potassium salts of mono-, di-, and tri- halogenated acetic acids, halogenated benzenes and related aromatic compounds, and a halogenated pyrazole derivative. Other halogenated compounds, that it was envisaged would possess the correct characteristics to display second-order quadrupolar effects, were also investigated, although the experiments were ultimately unsuccessful. Section 8.2.1 deals, in detail, with the structures and properties of the compounds examined.

8.2.1 Properties and Numbering of Compounds Investigated for Second-order Quadrupolar (SOQ) Effects

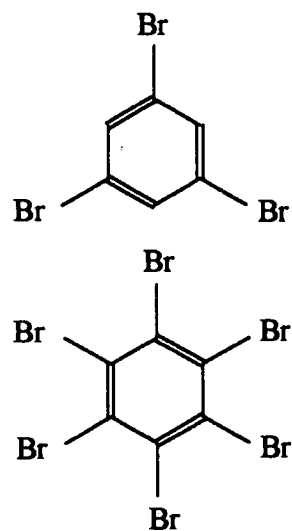
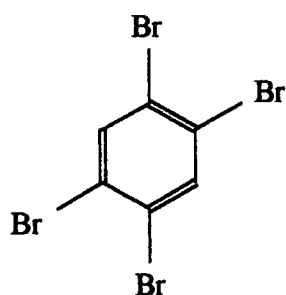
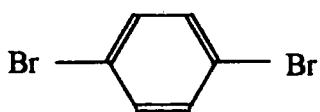
In order for second-order quadrupolar effects to be readily observable the compounds under investigation had to fulfil certain criteria. Firstly they had to be simple compounds, containing few carbon atoms so as not to obscure the resonances of interest, which alone represented an obstacle, since the majority of such simple chlorinated organic compounds are liquid at room temperature. Secondly their structures had to be as rigid as possible to prevent self-decoupling of the quadrupolar nucleus rendering observation of the SOQ effect impossible. The phenomenon of self-decoupling was more evident for the brominated and iodinated compounds, because of the larger quadrupolar coupling constants of bromine and iodine nuclei compared to those of chlorine nuclei. Consequently initial investigations centred on chlorinated compounds: chloroacetic acid salts, and in particular sodium chloroacetates. Subsequently a variety of simple aromatic compounds were studied. The chloroacetates investigated included sodium, potassium and lithium salts of the mono- di- and tri- chloroacetates. Each was a white crystalline compound that was ground into a powder for analysis. Numbering used for these systems was simply 1 and 2 for the carbonyl and the aliphatic carbons respectively. The halogenated aromatic compounds were numbered according to IUPAC convention.

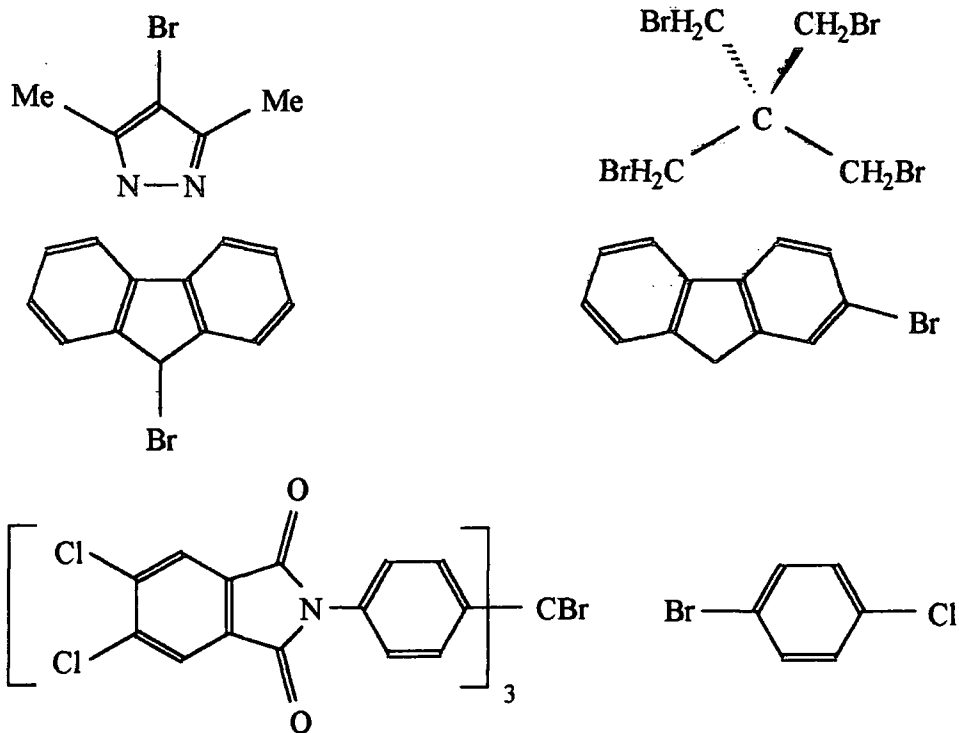
A full list of the compounds studied for second-order quadrupolar effects, some of which displayed the phenomenon and some of which did not, is contained in table 8.2.1.

Chlorinated Compounds



Brominated Compounds





Iodinated Compounds

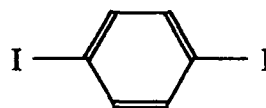


Table 8.2.1. Compounds investigated for second-order quadrupolar effects.

^{35}Cl NMR was performed on two compounds: NaCl and 3-chlorobenzoic acid.

8.3 Spectrometer Systems

A wide variety of solid-state spectrometers were used during the course of these studies which was brought about by the need to observe residual dipolar coupling effects at a variety of static field strengths. The three different static magnetic field strengths at which investigations were carried out were 4.7 T, 7.05 T

and 11.75 T. The respective spectrometers were for 4.7 T either on a Bruker CXP-200 spectrometer or, latterly, on a Chemagnetics CMX-200H spectrometer, both equipped with a wide-bore (89.5 mm) Oxford Instruments superconducting magnet, for 7.05 T a Varian VXR 300 and for 11.75 T a Bruker AMX-500.

The two chlorine-35 solid-state NMR spectra were obtained on the CMX-200H spectrometer.

8.4 Spectral Considerations

8.4.1 Solvents and Chemical Shift References

Where solution state work was carried out on these compounds, to compare against the isotropic chemical shifts in the solid-state, CDCl_3 was used as the solvent. Referencing was again internal using a value of 77 ppm for the ^{13}C signal.

In the solid-state chemical shifts were referenced externally with respect to the high frequency signal of adamantane at 38.4 ppm. Chlorine-35 solid-state NMR spectra were referenced to the resonance of 1 M NaCl solution at 0 ppm.

8.4.2 Spectral Parameters

Solid-state carbon-13 spectra recorded for the observation of SOQ effects were acquired at 50.33 MHz on the Chemagnetics 200H spectrometer, 75.43 MHz on the Varian VXR-300 and 125.76 MHz on the Bruker AMX-500. The cross-polarisation mode of operation was used in all cases except where the samples were devoid of protons, such as sodium trichloroacetate and hexabromobenzene. Spectral parameters for each particular experiment are given in the relevant figure captions contained in chapters 9 and 10. The variety of field strengths used had important implications on selection of the spinning speed in these spectra. At higher field strengths faster spinning speeds were needed to ensure that important bandshapes were not obscured by first-order spinning sidebands.

Chlorine-35 solid-state NMR spectra were acquired at a spectrometer frequency of 19.62 MHz. For both the sodium chloride and 3-chlorobenzoic acid samples spectra were acquired in the single-pulse mode of operation without proton decoupling. This was deemed sensible since NaCl contains no protons, and broadening due to the quadrupolar interaction in 3-chlorobenzoic acid was expected to far exceed any broadening from heteronuclear (^1H , $^{35,37}\text{Cl}$) dipolar interactions. A 5 μs pulse duration was used in conjunction with a 2 s recycle delay. Spectral widths of 50 kHz and 500 kHz were used for NaCl and 3-chlorobenzoic acid respectively.

8.5 Computer Lineshape Fitting and Simulations

Simulations of ^{13}C CP/MAS NMR bandshapes performed for both sodium monochloroacetate, in chapter 9, and the range of brominated benzenes, in chapter 10, were calculated using the exact approach presented by Menger et al.⁶ and Hexem et al.⁷

For the brominated systems the simulations were performed by considering ^{13}C influenced by ^{79}Br and ^{13}C influenced by ^{81}Br separately and then summing these sub-spectra according to the natural isotopic abundances of ^{79}Br and ^{81}Br . Digital resolution in these simulated spectra corresponds to 6 Hz i.e. 1001 points covering the spectral width of 6 kHz. The resultant powder patterns were then convoluted by a gaussian line-broadening function varying between 200 and 400 Hz, and compared to experimentally obtained spectra.

The usual simplifications implicit in the exact calculations for such systems, discussed in the previous chapter, were applied. Additionally, since it is known that $D^{81}/D^{79} = J^{81}/J^{79} = 1.078$, it is necessary only to consider D^{79} and J^{79} as independent variables in the simulations, since the values of D^{81} and J^{81} are easily derived using the above relation. The mechanics of the simulations involved considering *ca.* 200-1300 different combinations of D^{79} and J^{79} . The value of D^{79} was varied systematically over the range 960-1500 Hz. This particular range was

chosen by calculating values of D^{79} using a r_{CBr} distance of 1.7 - 2.0 Å (a good approximation using X-ray diffraction data) and assuming that $\Delta J^{79} = 0$, and therefore that $D'^{79} = D^{79}$. J^{79} was varied in 5 Hz increments over a range of approximately ± 80 Hz around the value $-|J^{79}|$, (with $|J^{79}|$ obtained from solution-state ^{13}C NMR and in the knowledge that J^{79} is negative). Using such a wide range of values for J^{79} was justified by the substantial uncertainties associated with the measurement of solution state (^{13}C , ^{79}Br) (and (^{13}C , ^{81}Br)) indirect coupling constants and the fact that the values in the solid state may differ from those seen for the same species in solution.

To our knowledge no cases of 2J , 3J , or 4J (^{13}C , $^{79,81}\text{Br}$) coupling constants have been reported in bromobenzenes and consequently for the remote interactions between ^{13}C nuclei and $^{79,81}\text{Br}$ nuclei situated in *ortho*, *meta* or *para* positions, as well as those in neighbouring molecules, we have assumed that $J^{79} = J^{81} = 0$ Hz and that $\Delta J^{79} = \Delta J^{81} = 0$ Hz (hence $D'^{79} = D^{79}$ and $D'^{81} = D^{81}$ for these interactions). The values of these remote dipolar couplings were determined from published crystal structures of 1,4-dibromobenzene,⁸ 1,3,5-tribromobenzene,⁹ 1,2,4,5-tetrabromo-benzene¹⁰ and hexabromobenzene.¹¹

References

1. R. K. Harris, *Nuclear Magnetic Resonance Spectroscopy*, John Wiley and Sons (1983).
2. A. Samoson, E. Lippmaa and A. Pines, *Mol. Phys.*, **65**, 1013 (1988).
3. A. Llor and J. Virtlet, *Chem. Phys. Lett.*, **152**, 248 (1988).
4. K. T. Müller, B. Q. Sun, G. C. Chingas, J. W. Zwanziger, T. Terao and A. Pines, *J. Magn. Reson.*, **86**, 470 (1990).
5. T. L. Weeding and W. S. Veeman, *J. Chem. Soc., Chem Commun.*, 946 (1989).
6. E. M. Menger and W. S. Veeman, *J. Magn. Reson.*, **46**, 257 (1982).
7. J. G. Hexem, M. H. Frey and S. J. Opella, *J. Chem. Phys.*, **77**, 3847 (1982).
8. U. Coratto and S. Bezzi, *Gazz. Chim. Ital.*, **72**, 318 (1942).
9. H. J. Milledge and L. M. Pant, *Acta Crystallogr.*, **13**, 285 (1960).
10. G. Gafner and F. H. Nerbstein, *Acta Crystallogr.*, **13**, 706 (1960).
11. E. Baharie and G. S. Pawley, *Acta Crystallogr., Sect. A*, **35**, 233 (1979).

Chapter 9

$(^{13}\text{C}, ^{35/37}\text{Cl})$ Residual Dipolar Coupling in Solid Sodium Chloroacetates

9.1 Introduction

The number of compounds found exhibiting the phenomenon of $(^{13}\text{C}, ^{35,37}\text{Cl})$ residual dipolar coupling in carbon MAS spectra can be expected to exceed that found exhibiting $(^{13}\text{C}, ^{79,81}\text{Br})$ and $(^{13}\text{C}, ^{127}\text{I})$ residual dipolar coupling. This is a reflection on the lower value of the quadrupole coupling constant for the two isotopes of chlorine compared to those of bromine and iodine, and the associated lesser inclination for chlorinated compounds to undergo the self-decoupling phenomenon. It is quite surprising therefore that the number of compounds which have been reported to display the phenomenon, such that clearly discernible splittings are observable in carbon-13 spectra, remains relatively low. One group of compounds that fulfill the required criteria are the chlorinated sodium acetates. Sodium mono- di- and tri- chloroacetate are well suited to the study of $(^{13}\text{C}, ^{35,37}\text{Cl})$ residual dipolar coupling since they are structurally very simple, and therefore have uncluttered ^{13}C spectra, are readily available and cheap. The fact that the carbon-13 NMR spectra of these compounds contain only two signals, well separated on the chemical shift scale, is a great advantage since it obviates the need to employ dipolar dephasing¹ techniques or the TOSS² pulse sequence to reduce the number of peaks in the spectrum, as has been necessary in the study of these effects for more structurally complex systems. Initial investigations carried out on the chloroacetates, at ambient temperatures, have yielded very interesting results. Clearly discernible splittings, of magnitudes in good agreement with those predicted by first-order perturbation theory and exact calculations, have been apparent in both the CH_2Cl and carboxyl carbon

signals in the CP/MAS spectra of sodium monochloroacetate, i.e. at both bonding and non-bonding distances. No such splittings have been observed in spectra of the trichloroacetate acquired at ambient temperatures. An ill-defined splitting on C1 has been observed in the ambient temperature spectrum of sodium dichloroacetate acquired at 4.70 T, but no such splitting has been observed in the analogous spectrum acquired at 7.05 T. However, by acquiring 7.05 T spectra of this compound at various low temperatures we have been able to study for the first time not only residual dipolar coupling of the ^{13}C nucleus to more than one $^{35,37}\text{Cl}$ nucleus, but also the onset of the self-decoupling phenomenon.

9.2 Variable-field Studies of Sodium Monochloroacetate

9.2.1 Experimental Results

The three static magnetic field strengths used in the investigations were 4.70, 7.05 and 11.75 T, corresponding to ^{13}C resonant frequencies of 50.33, 75.43 and 125.77 MHz respectively. Figure 9.2.1 shows the ambient temperature (293 K) ^{13}C CP/MAS spectra of sodium monochloroacetate obtained at the various field strengths. The effects of (^{13}C , $^{35,37}\text{Cl}$) residual dipolar coupling are clearly visible in these spectra and are manifest as unexpected multiplicities in the carbon signals. The form of the CH_2Cl carbon ($\delta_{\text{Ciso}} = 46.1$ ppm) can be seen to progress from a doublet displaying a narrow splitting through a doublet displaying a broader splitting to an asymmetric 1:2:2 triplet with decreasing field strength. The magnitudes of the splittings in the signals display the unusual property of an inverse proportionality to the applied magnetic field strength, a trait that allows us to recognise the occurrence of the residual dipolar coupling phenomenon. On closer examination of figure 9.2.1 it is apparent that the behaviour of the CH_2Cl signals is mirrored in the signals arising from the carboxyl carbon, occurring at approximately 176 ppm, in the spectra acquired at 4.70 T and 7.05 T. These signals are shown in expanded form in the insets to figure 9.2.1 (b) and (c).

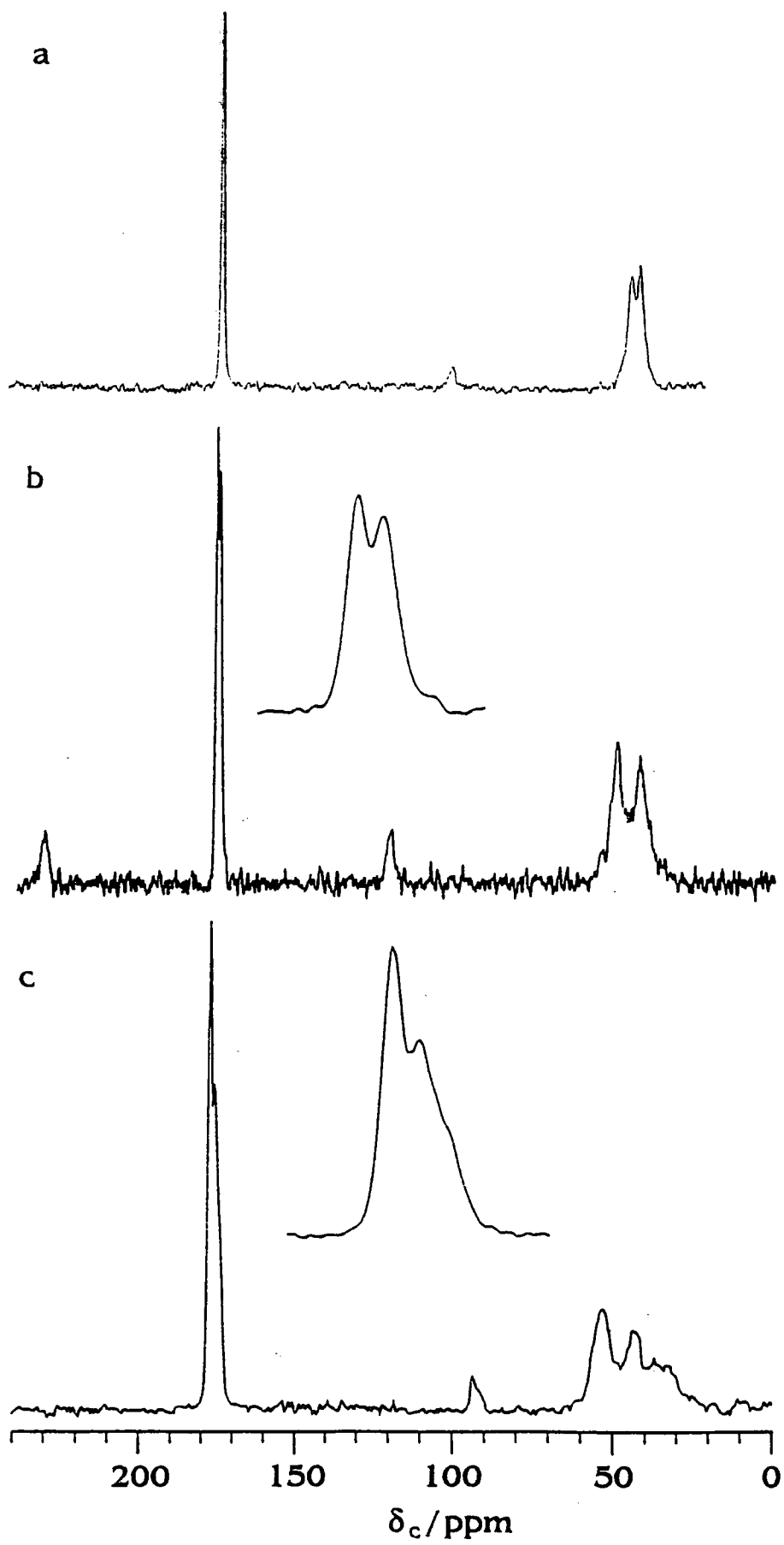


Figure 9.2.1 Carbon-13 CP/MAS spectra of sodium monochloroacetate at (a) 11.75 T, (previous page) (b) 7.05 T and (c) 4.70 T at ambient probe temperature (293 K). Spectral parameters: (a) Spectral width, 38 kHz; relaxation delay, 30 s; contact time, 3.5 ms; number of acquisitions, 1980; spinning speed, 9000 Hz. (b): Spectral width, 30 kHz; relaxation delay, 30 s; contact time, 3 ms; number of acquisitions, 1840; spinning speed, 4200 Hz. (c): Spectral width, 20 kHz; relaxation delay, 30 s; contact time, 3.5 ms; number of acquisitions, 2040; spinning speed, 4200 Hz. Asterisks are used to denote spinning sidebands.

At 11.75 T no splitting is observed in the carboxyl signal, which can be attributed to the fact that it is too small to be detected within the experimental linewidth of 140 Hz.

The doublet structure of the signals at the two highest field strengths occurs due to the overlap of the components arising from the $|\pm 3/2\rangle$ states (both shifted to lower frequencies) and overlap of the components arising from the $|\pm 1/2\rangle$ states of the $^{35,37}\text{Cl}$ nucleus (both shifted to higher frequencies). This overlap of the two pairs of components indicates that the (^{13}C , $^{35,37}\text{Cl}$) indirect coupling constant (J) in this compound is negligible (see figure 7.2.2). Due to the symmetric nature of the doublets obtained at 11.75 and 7.05 T it is impossible to access information pertaining to the sense of the second-order shifts, which would lead to a determination of the relative signs of the parameters χ , D , and D' . However, it is possible to glean such information by inspection of the 4.70 T spectrum, where the multiplet adopts an asymmetric character. Here the component of the triplet having double intensity (at high frequency) is due to overlap of the two lines arising from the $|\pm 1/2\rangle$ states of the $^{35,37}\text{Cl}$ nucleus, and the two components having single intensity (at low frequency) are due to the lines arising from the $|\pm 3/2\rangle$ states. To use a previously mentioned terminology "bunching" occurs at high frequency, and from this it is surmised that the sign of χ is negative.

Information regarding the experimentally observed line positions of each component of the multiplets at each of the static applied magnetic field strengths is contained in table 9.2.1. These are given with respect to TMS at 0 ppm. In this table, and throughout the remainder of the thesis C1 is used to identify the carboxyl carbon and C2 the CH_2Cl carbon.

B ₀ /T Carbon	11.75		7.05		4.7	
	C1 ^a	C2 ^b	C1 ^b	C2 ^b	C1 ^c	C2 ^c
Line	176.4	45.1	175.7	42.2	174.0 ^d	33.9
Positions (δ /ppm)		47.7	176.7	50.0	175.7	43.3
					177.3	53.2

^a Singlet.

^b 1:1 Doublets.

^c 1:1:2 Triplets.

^d Shoulder of the signal at $\delta = 175.7$ ppm.

Table 9.2.1 Line positions observed in the ¹³C CP/MAS spectra of sodium monochloroacetate.

9.2.2 Comparison of Experimentally Observed and Theoretically Predicted Splittings

9.2.2.1 Evaluation of Required Parameters

In chapter 7 various theories and equations were presented that enable one to predict the lineshapes expected in the ¹³C MAS spectrum of a carbon nucleus displaying residual dipolar coupling to ^{35,37}Cl nuclei, and hence perform comparisons between the form of the multiplets obtained experimentally and those predicted by the theories. As is implicit in the discussion contained in chapter 7, a pre-requisite to the feasibility of carrying out lineshape predictions using such theories is a knowledge of certain fundamental parameters concerning the system of interest. These parameters include, amongst others, the dipolar coupling constant D , or more precisely the effective dipolar coupling constant D' , between the chlorine and carbon nuclei, the internuclear separation r_{IS} and the angle β_D that the internuclear vector makes with the principal axis of the axially symmetric quadrupole tensor. The last of these parameters is particularly important for the instances of coupling between the non-bonded carboxyl and chlorine nuclei observed herein, since in this instance β_D can no longer be assumed to be zero, a point underlined in figure 9.2.2 that shows a typical chloroacetate geometry.

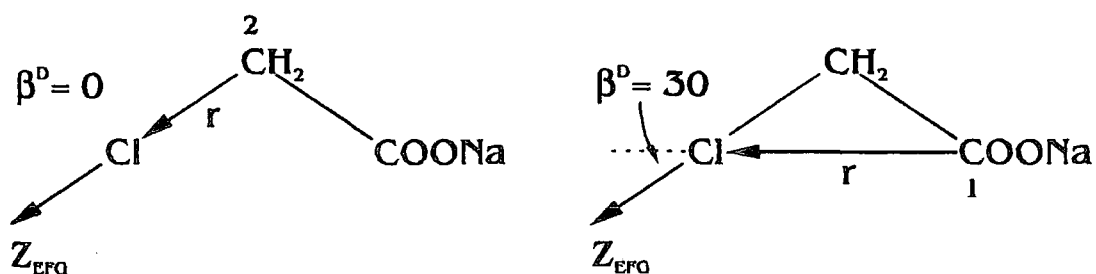


Figure 9.2.2 Relative orientations of the internuclear vector r and the $^{35,37}\text{Cl}$ Z_{EFG} axis for the carbon atoms C1 and C2.

From figure 9.2.2 it can be seen that for C2, the CH_2Cl carbon, β_D is assumed to be zero and for C1, the carboxyl carbon, β_D is taken as 30° . The values of the internuclear distances r_{IS} have previously been determined from X-ray diffraction studies: for C2 $r_{IS} = 1.77 \text{ \AA}$ and for C1 $r_{IS} = 2.74 \text{ \AA}$.^{3,4} From the values of the internuclear distances the dipolar coupling constants between the carbon and chlorine nuclei can be calculated for the two cases using $[D = (\mu_0/4\pi)\gamma_I\gamma_S/4\pi^2r^3]$. Consequently, for C2 D is estimated to be approximately 510 Hz and for C1 D is approximately 140 Hz. The large disparity in the magnitude of dipolar coupling constants for the two pairs of nuclei, when there is only approximately 1 \AA difference in the internuclear separation is a consequence of the r^{-3} dependence of D . In these chloroacetates the effective dipolar coupling constant D' is assumed to be equal in magnitude to D since it is well known that ΔJ for the ^{13}C , $^{35,37}\text{Cl}$, spin-pair in simple chlorinated organic compounds is negligible. Certain other parameters intrinsic to the quadrupolar nucleus are also needed. The quadrupole coupling constant is one such parameter which is known to lie in the vicinity of 70 MHz⁵ for chlorine nuclei in chlorinated organic compounds. Fortunately, the exact value of the ^{35}Cl quadrupole coupling constant in this compound has previously been determined by NQR experiments and is as follows: $\chi(^{35}\text{Cl}) = -67.8 \text{ MHz}$.⁶ From the most recent evaluation of the quadrupole moments of the two chlorine isotopes, $Q(^{37}\text{Cl})/Q(^{35}\text{Cl}) =$

0.788,⁷ it is possible to calculate that $\chi(^{37}\text{Cl}) = -53.4$ MHz. The Larmor frequencies of the two chlorine nuclei at the field strengths used to acquire the spectra shown in figure 9.2.1 are: $\nu_s(^{35}\text{Cl}) = 19.6$ MHz and $\nu_s(^{37}\text{Cl}) = 16.3$ MHz at 4.7 T, $\nu_s(^{35}\text{Cl}) = 29.4$ MHz and $\nu_s(^{37}\text{Cl}) = 24.5$ MHz at 7.05 T and $\nu_s(^{35}\text{Cl}) = 49.0$ MHz and $\nu_s(^{37}\text{Cl}) = 40.8$ MHz at 11.75 T. The evaluation of these parameters now allows us to calculate the value of the ratio R ($R = \chi/\nu_s$) at each static field strength and hence identify which of the simplified theories is the most applicable to calculate the expected line positions. It is important at this point to consider the effects of the natural abundance of each of the two quadrupolar non-radioactive isotopes of chlorine, which for our purposes are taken as $C(^{35}\text{Cl}) = 75.53$ and $C(^{37}\text{Cl}) = 24.47$. Consequently the isotopically weighted average values of R at the three field strengths implemented in the investigations are calculated to be 3.42 at 4.7 T, 2.28 at 7.05 T and 1.37 at 11.75 T.

9.2.2.2 Comparisons of Experimental and Predicted Results

For analysis of the line positions at 11.75 T, where $R = 1.37$, strictly speaking it is not appropriate to apply first-order perturbation theory. However, when one applies equation 7.3.14 [$s = \Delta\nu_{\pm 1/2} - \Delta\nu_{\pm 3/2} = (3 \cos^2 \beta^D - 1)(6\chi D/20\nu_s)$] one obtains values for the estimated splittings of 419 Hz and 72 Hz in C1 and C2 respectively. Although no splitting is observed in the signal from C1, this is to be expected, given that the $\omega_{1/2}$ of this peak is ~ 140 Hz. The value of the splitting predicted for C2, however, 419 Hz, compares moderately favourably with the experimentally observed value of 335 Hz.

Since we are not in the true first-order regime, i.e. χ is greater in magnitude than ν_s , to be more accurate one should apply equation 7.3.15, derived from the exact approach, [$s = D [(3 \cos^2 \beta^D - 1)/2](0.581 R + 0.033 R^2 - 0.021 R^3)$], to calculate the predicted splittings. Using this polynomial expression the splitting in C2 is now estimated to be 410 Hz, which is only marginally in better agreement with the experimental results (the non-observed splitting for C1 is calculated to be 70 Hz).

At 7.05 T, where $R = 2.27$, again although first-order perturbation theory is strictly inapplicable, yields values of splittings for C2 and C1 of 695 Hz and 119 Hz respectively. However, if equation 7.3.15 is used the predicted splitting for the doublet displays much better agreement with the experimental value. It predicts a splitting in C2 of 634 Hz and in C1 of 107 Hz, compared to the experimentally recorded values of 587 Hz and 75 Hz. Thus at 7.05 T the agreement between the splitting calculated using equation 7.3.15 and the experimentally observed splitting is much better than that between the splitting calculated using first-order theory and the experimental results. However, at 11.75 T the two simplified theories gave very similar predicted splittings. This is the behaviour that one would expect, since at the higher static field strength we are much closer to the regime of $R < 1$, where first-order perturbation theory is valid.

At 4.7 T $R = 3.42$, and neither first-order perturbation theory nor equation 7.3.15 are appropriate. Now a broad 1:1:2 triplet is expected on the basis of exact calculations. It is now appropriate to use equations 7.3.16 a-c, derived from the exact theory to predict the line positions. In figure 7.3.3 it was shown that the results obtained on predicted line positions using the three polynomial equations (7.3.10 a-c) display a very good agreement to the results obtained by the full-matrix diagonalisation method for the case when the angle between the vector r_{IS} and the Z_{EFG} axis of the quadrupole tensor at the $^{35,37}\text{Cl}$ (β^D) is equal to zero. These equations, derived from the exact theory, can be modified by insertion of the angular dependent term $[(3 \cos^2 \beta^D - 1)/2]$, to apply to the case where $\beta^D \neq 0$, and they then still show good agreement with those values predicted by full-matrix diagonalisation. The modified equations (7.3.16 a-c) predict the following line positions: $\nu_1 = -637$ Hz, $\nu_2 = -155$ Hz and $\nu_3 = +394$ Hz, which are indeed in good agreement with the experimentally observed line positions of $\nu_1 = -614$ Hz, $\nu_2 = -141$ Hz and $\nu_3 = +357$ Hz. For C1 this approach is found to yield even more accurate. The experimental values are: $\nu_1 = -111$ Hz, $\nu_2 = -25$ Hz and $\nu_3 = +55$ Hz and the predicted line positions using the polynomial equations are: $\nu_1 = -109$ Hz, $\nu_2 = -27$ Hz and $\nu_3 = +68$

Hz. Table 9.2.2 is a summary of the line positions observed experimentally and those calculated using the most applicable theory.

B_0/T R (χ/ν_s) Carbon	11.75 1.37		7.05 2.27		4.7 3.42	
	C1 ^a	C2 ^b	C1 ^b	C2 ^b	C1 ^c	C2 ^c
Experimental Line Positions / ppm	176.4 ^e	45.1	175.7	42.2	174.0 ^d	33.9
		47.7	176.7	50.0	175.7	43.3
					177.3	53.2
Calculated Line Positions / ppm	176.1	44.8	175.5	41.9	174.0	33.4
	176.7	48.0	176.9	50.3	175.7	43.0
					177.6	53.9

^a Singlet.

^b 1:1 Doublets.

^c 1:1:2 Triplets.

^d Shoulder of the signal at $\delta = 175.7$ ppm.

^e Splitting lost in natural linewidth.

Table 9.2.1 Comparisons of experimental line positions and those predicted using equations 7.3.14 (at 11.75 T), 7.3.15 (at 7.05 T), and 7.3.16 a-c (at 4.70 T) for sodium monochloroacetate.

It is worthy of mention that in each spectrum, as was discussed in chapter 7, each component of the multiplet is actually a powder pattern (or convolution of more than one powder pattern), broadened by factors such as field inhomogeneity and improper (off-resonance) proton decoupling. The true position of the lines, calculated using the various equations, lie at the centre of gravity of the powder patterns. However, the peak maxima obtained from experimental data may not coincide exactly with the centres of gravity of these powder patterns and consequently a significant degree of uncertainty is introduced into the positions of the experimentally observed line positions listed in table 9.2.1. Such a statement can be further clarified by

inspection of figure 9.2.3, which depicts theoretical lineshapes simulated using the computer program described in section 8.5.

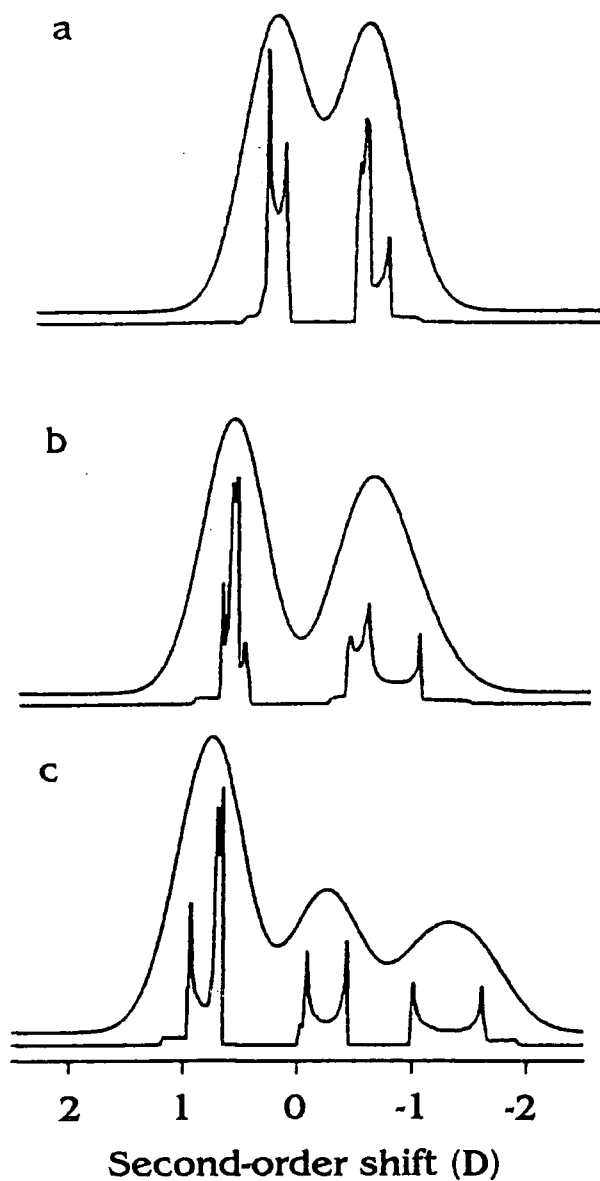


Figure 9.2.3

Theoretical lineshapes expected for ^{13}C MAS spectra affected by a single ^{35}Cl nucleus through residual dipolar coupling at (a) 11.75 T, (b) 7.05 T and (c) 4.70 T. Superimposed on the Pake-like powder patterns in each case is a Gaussian convoluted spectrum (broadening factor = $0.5D$). A quadrupole coupling constant of -70 MHz was assumed for each spectrum.

If the uncertainty in locating the true position of each line is estimated to be of the order of ± 30 Hz, this may account in part for the apparent poor agreement of experimentally obtained and calculated line positions in some cases.

9.3 Variable-field and Temperature Studies of Sodium Di- and Trichloroacetate

9.3.1 Predicted Appearance of Spectra

Where we are concerned with the form of the multiplets of the carbon signals in sodium dichloroacetate and sodium trichloroacetate we must now consider the effects of coupling to two and three equivalent chlorine nuclei respectively. At high fields, where $R < 3$ the situation can be paralleled to the cases of (^{13}C , $^{35,37}\text{Cl}$) residual dipolar coupling in sodium monochloroacetate at 7.05 T and 11.75 T, which gave symmetric doublets. Hence we would expect the experimental results to yield lineshapes consisting of convolutions of two and three such doublets for the dichloroacetate and the trichloroacetate, which assuming the chlorines in question are in equivalent positions, result in a symmetric 1:2:1 triplet and 1:3:3:1 quartet respectively. At lower field strengths however, for example at 4.7 T, where the lineshape for the monochloroacetate was a 1:1:2 triplet, more complex lineshapes are predicted due to the convolution of two and three such patterns.

9.3.2 75.43 MHz Variable-temperature Spectra of Sodium Di- and Trichloroacetate

Figure 9.3.1 shows the 75.4 MHz ^{13}C CP/MAS spectra obtained from sodium dichloroacetate ($R = 2.37$) at (a) 158 K and (b) ambient probe temperature, whereas figure 9.3.2 is the 75.4 MHz single-pulse ^{13}C MAS spectra of sodium trichloroacetate acquired at 163 K.

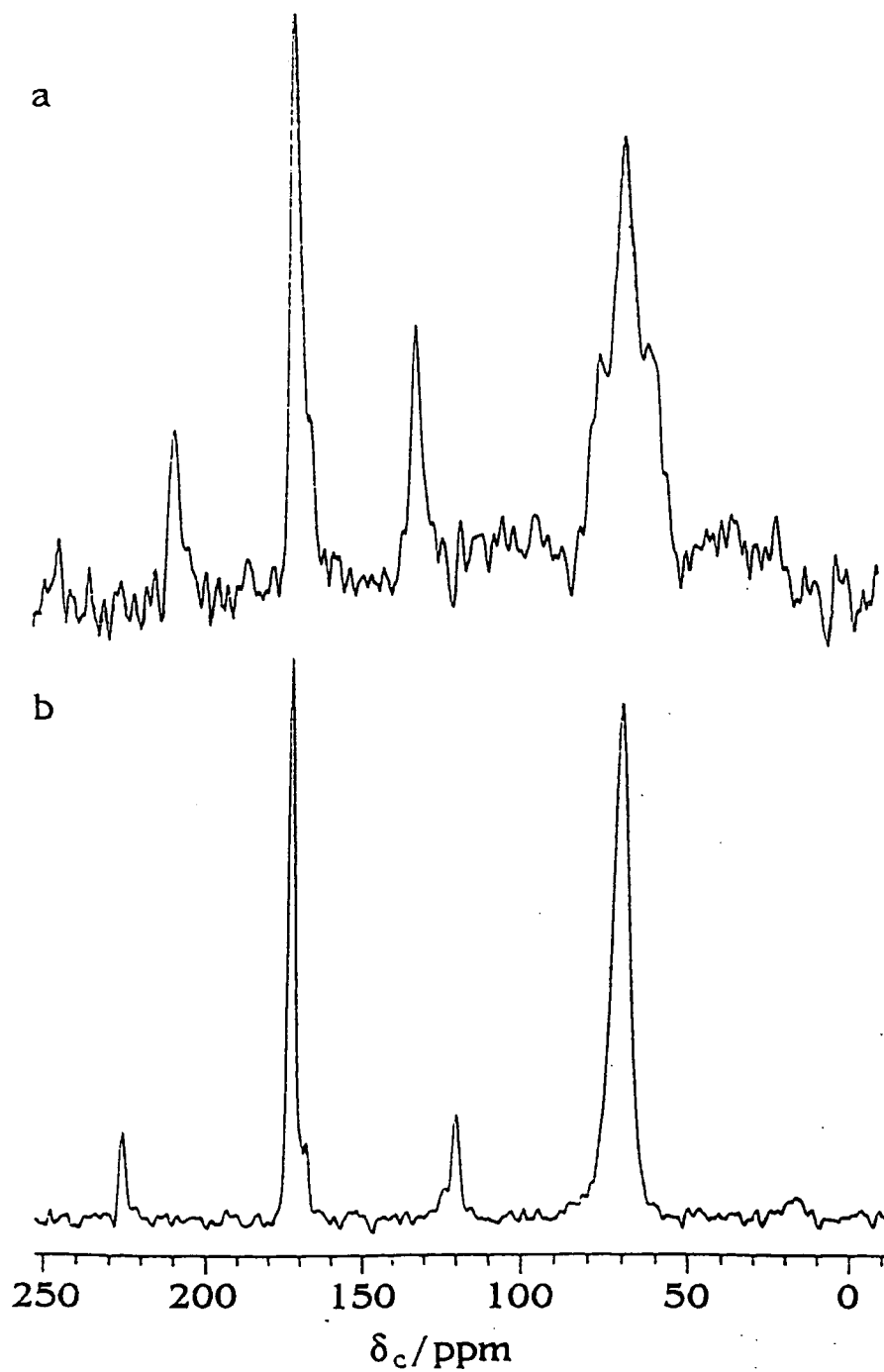


Figure 9.3.1 Variable-temperature ^{13}C CP/MAS spectra of sodium dichloroacetate at 75.43 MHz, recorded at (a) 158 K and (b) 293 K. Spectral parameters: Spectral width 20 kHz, recycle delay 300s, contact time 1 ms, MAS rate 2800 Hz, number of transients 12.

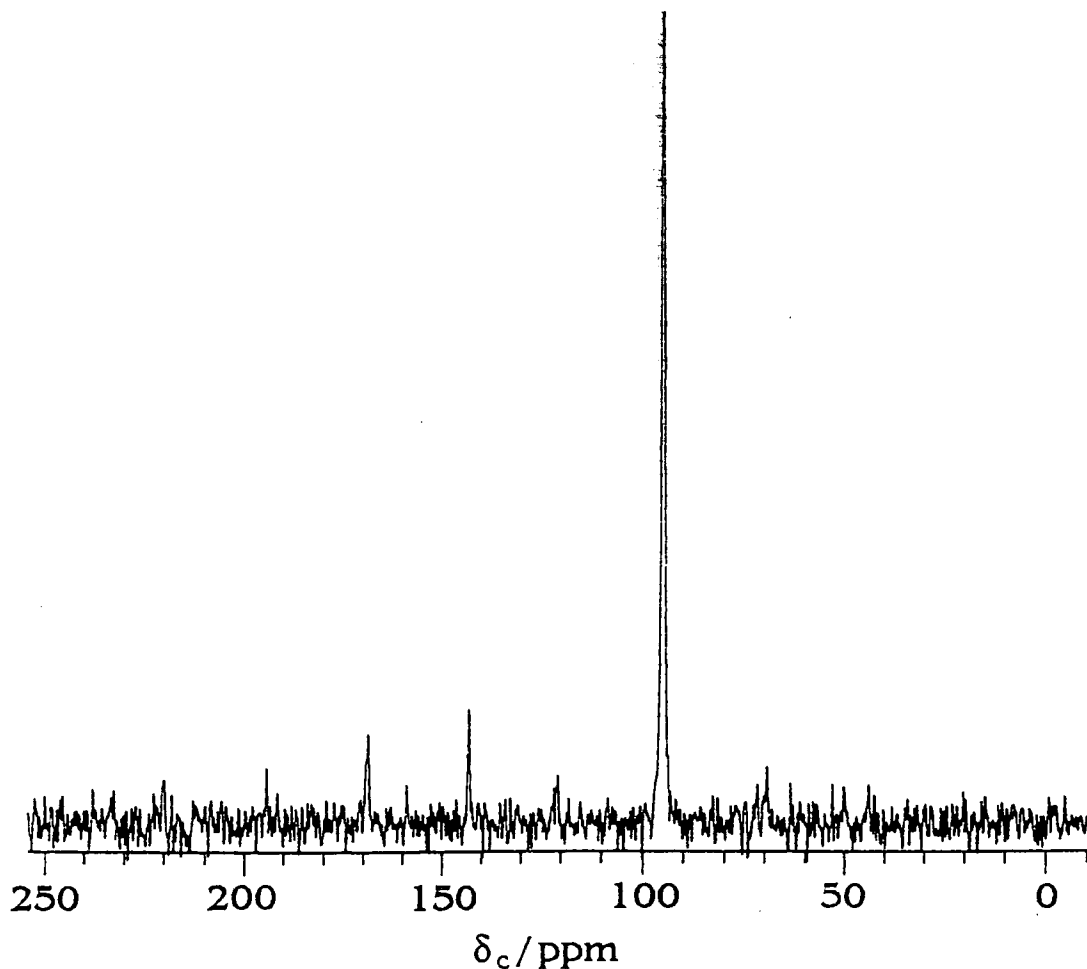


Figure 9.3.2 ^{13}C Single pulse MAS spectra of sodium trichloroacetate at 75.43 MHz, recorded at 163 K. Spectral parameters: Spectral width 20 kHz, recycle delay 60 s, MAS rate 1900 Hz number of transients 32.

It is evident that of all the spectra shown in figures 9.3.1 and 9.3.2 only the low-temperature spectrum of sodium dichloroacetate displays the expected signal multiplicities, and even in this case no multiplicity is observed for C1. The splitting in the 1:2:1 triplet for C2 (approximately 600 Hz) is of a comparable magnitude to that observed in the ambient temperature spectrum of the monochloroacetate recorded at the same field strength (see figure 9.2.1). The absence of a similar 1:2:1 triplet structure for the carboxyl carbon resonance of occurring at 172.3 ppm is to be expected given that the separation of components within the doublet in the analogous

carbon in the monochloroacetate at the same field strength was 75 Hz and that the experimental linewidth of the C1 resonance in figure 9.3.1 (a) is some 300 Hz.

In the spectrum of the trichloroacetate the predicted 1:3:3:1 quartet is not observed in either carbon signal even though the probe temperature is 163 K. At this temperature the linewidth of the CCl_3 carbon signal is 67 Hz. Further experiments were performed at temperatures of 203 K and 293 K, which resulted in reductions in linewidth of this signal to 37 Hz and 30 Hz respectively.

9.3.3 Motional Effects on (^{13}C , $^{35,37}\text{Cl}$) Residual Dipolar Coupling in Sodium Di- and Trichloroacetate

The presence of the predicted 1:2:1 triplet in the low temperature spectrum of sodium dichloroacetate and its disappearance at elevated temperatures is interpreted as meaning that some kind of temperature-dependent phenomenon must be occurring to nullify the effects of residual dipolar coupling. In chapter 7 two such effects were discussed, which act so as to either partially or totally suppress the residual dipolar coupling phenomenon. Both of them are associated with the presence of molecular motion(s) within the system and are therefore highly dependent on the temperature of the system. Since it is expected that rapid rotation about the C-C bond could occur very easily, especially for the threefold symmetric CCl_3 group, it is surmised that most probably either or both of these dynamic effects are causing a breakdown of the expected multiplicities. This argument is attested by the observed temperature dependence of the breakdown in multiplicity of the signals, since the rate of molecular motion is well known to increase as the temperature of the system is raised. As discussed in chapter 7 the residual dipolar coupling phenomenon can be removed by either averaging the relevant tensors involved in the (^{13}C , $^{35,37}\text{Cl}$) coupling and/or by shortening the T_1 of the chlorine nuclei (self-decoupling). The fact that the effect is more pronounced for the trichloroacetate, with a linewidth of only 67 Hz observed for the CCl_3 carbon resonance at 163 K compared to one of 300 Hz for the carbon of the CHCl_2 group in the dichloroacetate recorded at 158 K, is a result of the easier

rotation of the threefold symmetric CCl_3 group compared to that of the CHCl_2 group. Similarly, the rate of rotation about the C-C bond in the monochloroacetate, which displays easily discernible splittings at ambient probe temperature, must be significantly less than in the dichloroacetate.

9.3.4 50.33 MHz Spectra of Sodium Di- and Trichloroacetate

The dispersion of the components in the multiplets observed due to the residual dipolar coupling phenomenon is known to increase as the static field strength is decreased, a point highlighted in figure 9.2.1. Therefore it is not unreasonable to assume that it may be possible to observe the predicted multiplicities in the signals arising from both carbon nuclei in the dichloroacetate and the trichloroacetate if we were to acquire spectra at 4.7 T. These multiplets would be expected to be more complex than the 1:2:1 triplet and 1:3:3:1 quartet predicted at 7.05 T, since now it is necessary to consider the convolution of 2:1:1 asymmetric triplets and not just simple doublets. Figure 9.3.3 shows the ambient temperature 50.33 MHz CP/MAS spectrum of sodium dichloroacetate.

A more complicated spectrum is observed at this lower field than was seen at 7.05 T. The pattern expected, if residual dipolar coupling effects were in operation, would be that arising from a 1:1:2 convolution of 1:1:2 components. In our case, taking careful account of the position of the isotropic shift, this pattern equates to a 1:2:5:4:4 quintet. However, experimentally no such pattern is observed, with the C2 resonance possessing no discernible splittings and having a peak-width at half-height of approximately 500 Hz, and the C1 resonance displaying only one splitting (the first time an ambient temperature spectrum has yielded multiplicities for this compound). This observation of a splitting in the C1 resonance and lack of definition in the signal arising from C2 is very difficult to explain. At ambient temperature we would expect self-decoupling effects to dominate, manifest in the spectrum as a collapse of the expected multiplicities, as was the case in the spectrum recorded at 7.05 T.

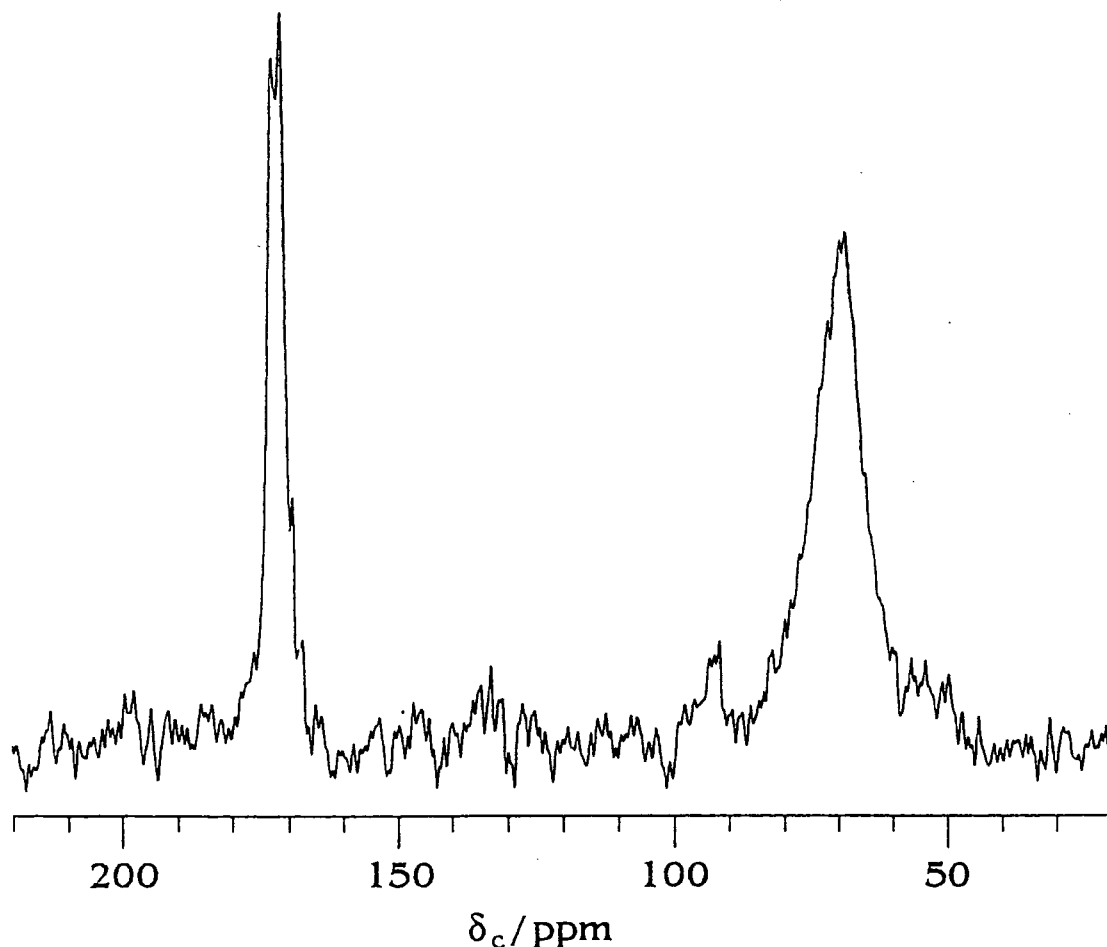


Figure 9.3.3 ^{13}C CP/MAS spectra of sodium dichloroacetate at 50.33 MHz, recorded 293 K. Spectral parameters: Spectral width 20 kHz, recycle delay 20s, contact time 3.0 ms, MAS rate 4200 Hz, number of transients 2664.

If our understanding of the self-decoupling phenomenon is correct the splitting in C1 must be due to another factor. One plausible explanation is that we are observing a crystallographic splitting, which remains unresolved due to larger linewidths in the 7.05 T spectrum. If the splitting was due to crystallographic inequivalence it would be expected that an increase in temperature for the system would not remove this splitting. However, if the splitting was indeed due to residual dipolar coupling a disappearance of the splitting would occur from an increase in the temperature of the system. Figure 9.3.4 is an identical spectrum to figure 9.3.3, but acquired at an elevated probe temperature of 363 K.

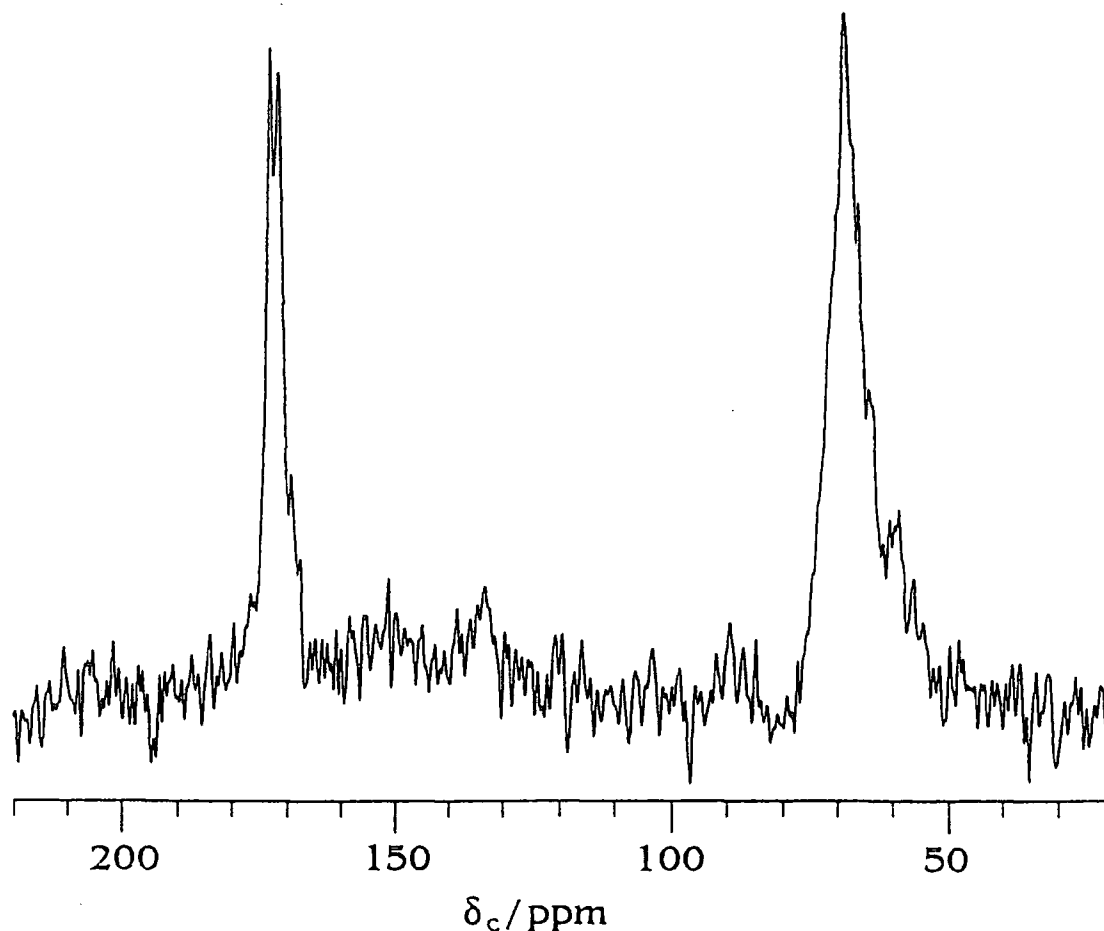


Figure 9.3.4 ^{13}C CP/MAS spectra of sodium dichloroacetate at 50.33 MHz, recorded 263 K. Spectral parameters as for figure 9.3.3, except number of transients 128.

Although no noticeable reduction in linewidth or change in appearance is observed for C1, which is indicative of the splitting not being due to the residual dipolar coupling phenomenon, a definitive explanation as to the cause of the effect cannot be made.

The spectrum of sodium trichloroacetate acquired using a static field strength of 4.7 T (see figure 9.3.5) is very similar in appearance to that obtained at 7.05 T, with very narrow resonances displaying no multiplicities, suggesting that the rotation of the CCl_3 group is much more rapid compared to that seen in the dichloroacetate. The broad hump centred on approximately 105 ppm is attributed to background signals from the probe.

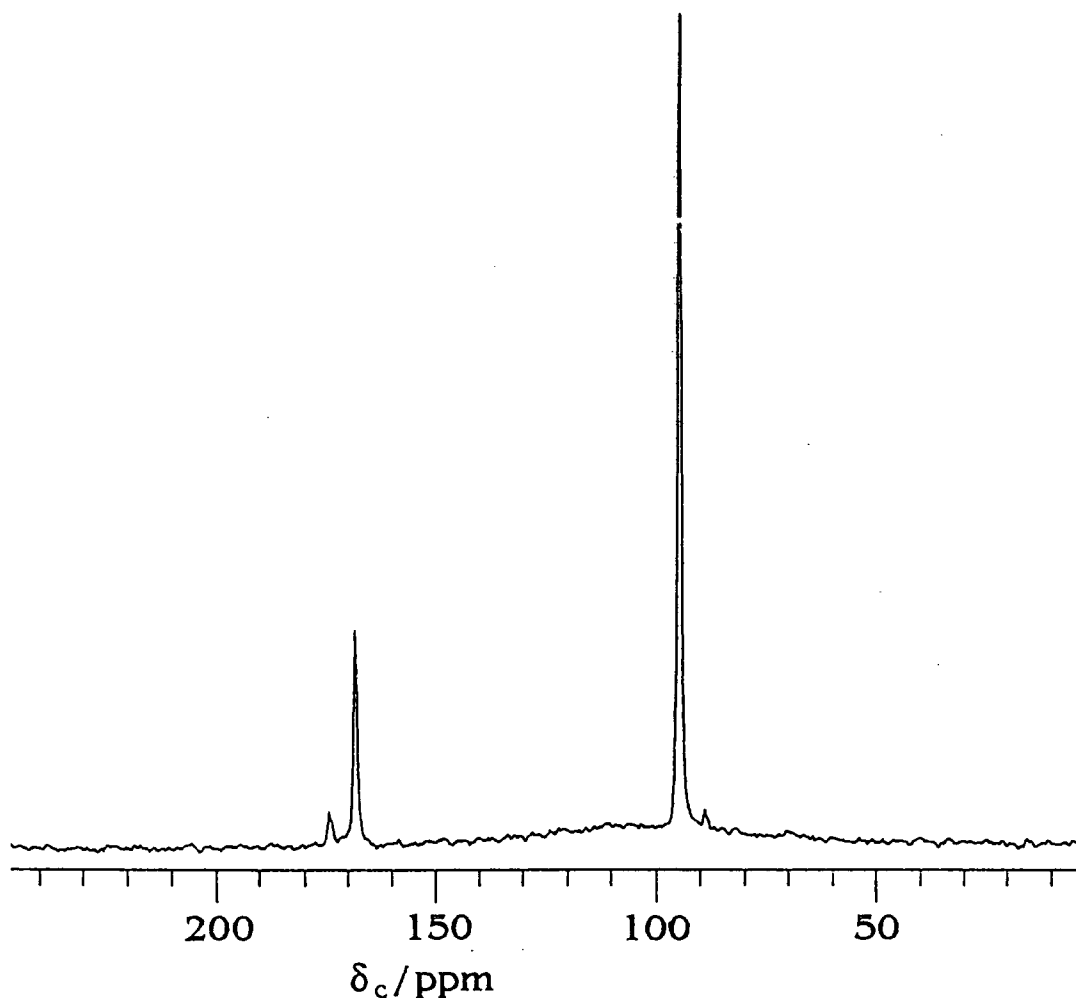


Figure 9.3.5 ^{13}C single-pulse MAS spectra of sodium trichloroacetate at 50.33 MHz, recorded at 293 K. Spectral parameters: Spectral width 20 kHz, recycle delay 30s, MAS rate 4000 Hz, number of transients 960.

9.3.5 Explanation of Absence of Expected Multiplicities in Spectra of Sodium Di- and Trichloroacetate

If we consider the rotation of the chloromethyl groups as a three-site jump reorientation about the C-C bond it is possible to make predictions, using data obtained from NQR experiments, as to whether the expected multiplicities would materialise in the signals, or whether the rate of motion would act so as to suppress these multiplicities. One question that remains is which of the two motion-assisted mechanisms is responsible for the breakdown in multiplet structure i.e. are the effects

observed due to averaging of the relevant tensors or the induction of short spin-lattice relaxation times for the chlorine nuclei, the self decoupling phenomenon.

As regards averaging of the quadrupolar and dipolar tensors, it was discussed in chapter 7 that two motional regimes can be envisaged: one where $D < \tau^{-1} < \chi$ and a faster one where $D, \chi < \tau^{-1}$ (where τ is the correlation time for the motion). In the first of these regimes the splittings are reduced to 1/9 of the expected (static) values. However, in the fast-motion regime splittings will be completely collapsed as has been observed for the "roundish" species hexamethylenetetramine⁸ and PCl_6^- anion.⁹ It is therefore possible, from a prior knowledge of the values of D, χ and τ^{-1} to ascertain whether multiplicities would be expected.

Molecular motions are also able to induce short spin-lattice relaxation times for the quadrupolar nuclei, which will lead to a self-decoupling phenomenon, giving complete collapse of all multiplicities due to residual dipolar coupling. It is predicted that self-decoupling will be observed providing $2^{1/2}[p_{\pm 3/2, \pm 1/2}(\theta, \phi)] / \pi > s(\theta, \phi)$, where $p_{\pm 3/2, \pm 1/2}(\theta, \phi)$ is the transition rate between the states $|\pm 3/2\rangle$ and $|\pm 1/2\rangle$ of the $^{35,37}\text{Cl}$ nuclei, and θ and ϕ are the polar angles locating the position of the Z_{EFG} axis in a suitable crystal fixed coordinate system.¹⁰ Table 9.3.1 lists the ^{35}Cl NQR for all three chloroacetates at variable temperature, along with the ^{35}Cl NQR spin-lattice relaxation times T_1 , measured at 'Ciudad Universitaria' by Drs. M. J. Zuriaga and G. A. Monti, from which the values the necessary parameter $2^{1/2}\langle p_{\pm 3/2, \pm 1/2} \rangle / \pi$ can be calculated.

Compound	T/K	$T_1 (^{35}\text{Cl}) / \text{s}$	$2^{1/2}\langle p_{\pm 3/2, \pm 1/2} \rangle / \pi / \text{s}^{-1}$	$\nu(^{35}\text{Cl}) / \text{MHz}$
1	155	0.113	4.0	34.624
	295	0.0205	22.0	33.974
2	155	0.0596	7.6	37.146
	220	0.0158	28.0	36.810
3	150	2.71×10^{-4}	1.7×10^3	38.035

Table 9.3.1 Variable-temperature NQR data for the three chloroacetates studied.¹¹

Table 9.3.2 lists the splittings, and where appropriate linewidths, of the signals observed in the ^{13}C NMR spectra of the three chloroacetates.

Compound	T/K	^{13}C Splittings Observed Carbon: s/Hz (B_0/T)
1	293	C1: 76 (7.05)
	293	C2: 590 (7.05)
	293	C2: 340 (11.75)
2	158	C2: 604 (7.05) $\omega_{1/2} = 300$ Hz
	203	C2: 604 (7.05) $\omega_{1/2} = 300$ Hz
	293	C2: Singlet (7.05) $\omega_{1/2} = 450$ Hz
3	163	C2: Singlet (7.05) $\omega_{1/2} = 30$ Hz
	293	C2: Singlet (4.7) $\omega_{1/2} = 70$ Hz

Table 9.3.3 Splittings and linewidths observed in ^{13}C NMR spectra of sodium mono-, di- and trichloroacetate.

For the monochloroacetate the values of $\nu(^{35}\text{Cl})$ compares favourably to those obtained in previous studies.⁶ Comparing the values obtained of the parameter $2^{1/2}\langle p_{\pm 3/2, \pm 1/2} \rangle / \pi$ and the splitting, s , in each case leads to the following results. For the monochlorinated acetate $2^{1/2}\langle p_{\pm 3/2, \pm 1/2} \rangle / \pi$ is substantially smaller than the observed

splittings for both C2 and C1 at both temperatures at which the experiments were conducted. Consequently internal motion will have a negligible effect on (^{13}C , $^{35,37}\text{Cl}$) splittings and we would expect to observe splittings of a magnitude predicted by first-order perturbation theory, or the polynomial equations derived from the exact approach. This is confirmed by the experimental results (see figure 9.2.1 c).

For the trichloroacetate it is known that rapid three-site jumps around the C-C bond can reasonably be expected. However, it is not envisaged that the rate of such motions will exceed 70 MHz and therefore result in a total collapse of the multiplet structure, but that the situation will be in the D , $\chi < \tau^{-1}$ regime and lead to a motionally averaged value of the expected splitting some 1/9 the value of that predicted for the static case. At 7.05 T the motionally averaged value can be calculated to be approximately 65 Hz for C2 and, given that the experimental linewidth is 30 Hz at this field strength, a 1:3:3:1 quartet would be expected to be clearly visible. At 4.7 T the expected pattern would be more complex due to the convolution of three asymmetric 2:1:1 triplets and the signal from C2 would be expected to display a linewidth of the order of 350 Hz. The absence of the theoretically predicted multiplicities at both magnetic field strengths and all temperatures is strongly indicative of self-decoupling. In addition the observed value of $2^{1/2}\langle p_{\pm 3/2, \pm 1/2} \rangle / \pi$ at 158 K is much larger than the splittings predicted for either the static case or the motionally averaged case, and consequently the idea that the collapse of the multiplets is caused by self-decoupling and not by averaging of the relevant tensors is further validated.

The variable-temperature 75.43 MHz ^{13}C MAS spectra for the dichloroacetate (see figure 9.3.1) are similarly interpreted to indicate the possibility of dynamic effects. At 158 K the value of $2^{1/2}\langle p_{\pm 3/2, \pm 1/2} \rangle / \pi$ is again smaller than the splitting expected in the signal from C2. The observation of a splitting of about 600 Hz implies that if motion is present in the system it must be slow compared to $D(^{13}\text{C}, ^{35,37}\text{Cl})$, since if it were faster only splittings of motionally averaged magnitudes would be observed. Unfortunately the value of $T_1(^{35}\text{Cl})$ for this compound was unable to be

measured at 293 K due to the broadness of the NQR lines, which is in itself an indication that T_1 is short, and consequently a value of $2^{1/2}\langle p_{\pm 3/2, \pm 1/2} \rangle / \pi$ was not so easily obtained. However, by extrapolation of the data contained in table 9.3.1 the value of this parameter was estimated to be of the order of 90 Hz. This is smaller than the expected static splitting of 600 Hz, but is not smaller than the motionally averaged value of 67 Hz, that would be expected if there was an appreciable increase in the rate of rotation of the CHCl_2 group at this elevated temperature. Hence we can conclude that self-decoupling effects may also be evident in sodium dichloroacetate. However, since the linewidth at room temperature is approximately 300 Hz, which is considerably larger than the magnitude of the predicted motionally averaged splitting we cannot discount the possibility that the singlet in the ^{13}C MAS spectrum acquired at 293 K contains a multiplicity that is buried under the linewidth. If this were the case then the collapse of the multiplet structure would be attributed to the presence of a small, motionally averaged, second-order shift.

9.4 Conclusions

Signals in the ambient temperature ^{13}C CP/MAS spectra of sodium mono- and dichloroacetate have been shown to display the phenomenon of ($^{13}\text{C}, ^{35,37}\text{Cl}$) residual dipolar coupling. Their appearance as symmetric doublets or 2:1:1 asymmetric triplets has been attributed to the following factors: The intermediate size of the $^{35,37}\text{Cl}$ quadrupole coupling constant, the small value of the ($^{13}\text{C}, ^{35,37}\text{Cl}$) isotropic indirect coupling constant, and the strength of the static magnetic field. The effects of residual dipolar coupling have been observed not only in the signals arising from the carbon directly bonded to the chlorine nucleus, but also in those arising from the adjacent carboxyl carbons. From comparisons with experimentally obtained data it has been demonstrated that first-order perturbation theory, and polynomial equations derived from the exact approach, can be used to predict the structures of the signals both at

bonding and non-bonding distances with a reasonable degree of confidence, provided the theories are correctly applied.

For sodium trichloroacetate a breakdown of the residual dipolar coupling phenomenon results in the collapse of the expected multiplicities. This has been shown to occur due to a fast spin-lattice quadrupole relaxation induced by rapid three-site jumps around the C-C bond, a conjecture supported not only by variable-temperature ^{13}C MAS NMR spectra recorded at various fields, but also by ^{35}Cl NQR T_1 measurements. For the monochloroacetate values of ^{35}Cl NQR T_1 have been found to be large enough to prevent the self decoupling phenomenon, which has been attributed to a slower rate of rotation of the monochloromethyl group compared to that displayed by the threefold symmetric trichloromethyl group. In the case of the dichloroacetate the multiplets observed at low temperatures in the spectra recorded at 7.05 T have been seen to collapse at ambient temperatures as a result of an increased rate of rotation of the dichloromethyl group. However, the natural linewidth of signals in the ambient temperature spectra have been too large to establish categorically whether the collapse is due to fast spin-lattice relaxation of the quadrupolar nucleus or motional averaging of the relevant tensors or a combination of the two effects.

9.5 Acknowledgements

I would like to thank Professor A. C. Olivieri at the 'Universidad Nacional de Rosario', Rosario, Argentina for the use of theories developed by him, introduced in chapter 7, without which the writing of this chapter would not have been possible, and for the spectral simulations conducted on the monochloroacetate presented in section 9.2. I am also extremely grateful to Drs. M. J. Zuriaga and G. A. Monti for the NQR measurements made at 'Ciudad Univeritaria', Córdoba, Argentina.

References

1. S. Opella and S. J. Frey, *J. Am. Chem. Soc.*, **101**, 5854 (1979).
2. W. T. Dixon, J. Schaefer, M. D. Sefcik, E. O. Stejskal and R. A. McKay, *J. Magn. Reson.*, **49**, 341 (1982).
3. M. Ichikawa, *Acta Crystallogr. Sect., B* **30**, 651 (1974).
4. D. Hadzi, I. Leban, B. Orel, M. Iwata and J. M. Williams, *J. Cryst. Mol. Struct.*, **9**, 117 (1979).
5. E. A. C. Luken, *Nuclear Quadrupole Coupling Constants*, Academic press. London, p. 187. (1969).
6. H. C. Allen, *J. Am. Chem. Soc.*, **74**, 6047 (1952).
7. P. Pyykko, *Z. Naturforsch. A* **47**, 189 (1992).
8. J. F. Haw, R. A. Crook and R. C. Crosby, *J. Magn. Reson.*, **66**, 551 (1986).
9. R. K. Harris and A. Root, *Molec. Phys.*, **66**, 993 (1989).
10. A. C. Olivieri, *J. Chem. Soc. Perkin Trans.*, **2**, 85 (1990).
11. S. H. Alarcon, A. C. Olivieri, S. A. Carss, R. K. Harris, M. Zuriaga and G. Monti, *J. Magn. Reson.*, (in press).

Chapter 10

$(^{13}\text{C}, ^{79,81}\text{Br}/^{127}\text{I})$ Residual Dipolar Coupling in Halogenated Aromatic and Related Compounds

10.1 Introduction

The increased propensity for bromine, and especially iodine, to undergo the self-decoupling phenomenon leads to a difficulty in locating compounds displaying residual dipolar coupling between carbon and these two nuclei. Indeed such is the magnitude of χ for the iodine nucleus (~ 1800 MHz) that to date no compounds have been identified that lead to the expected multiplets in carbon-13 MAS spectra of iodinated compounds. For the bromine nucleus the problem is less acute, although currently examples of compounds displaying $(^{13}\text{C}, ^{79,81}\text{Br})$ residual dipolar coupling have been restricted to those possessing a high degree of π -bonding such as aromatic and pyrazole derivatives.

10.2 $(^{13}\text{C}, ^{79,81}\text{Br})$ Residual Dipolar Coupling in 1,4-Dibromobenzene

10.2.1 Fundamental Parameters

Bromine quadrupole coupling constants in 1,4-dibromobenzene are 535.8 MHz for ^{79}Br and 447.6 MHz for ^{81}Br . This gives the value of $\chi(^{81}\text{Br})/\chi(^{79}\text{Br})$ as 0.835, which is in excellent agreement with the most recent ratio of the quadrupole moments, $[Q(^{81}\text{Br})/Q(^{79}\text{Br}) = 0.833]$.² These values are considerably larger than the corresponding Larmor frequencies $\nu_s(^{79}\text{Br}) = 50.11$ MHz and $\nu_s(^{81}\text{Br}) = 54.01$ MHz at 4.7 T, and consequently the values of $R (= \chi/\nu_s)$ at this field strength are 10.69 for ^{79}Br and 8.29 for ^{81}Br . Since the two bromine isotopes have similar nuclear properties, as was the case for the chlorine-35 and chlorine-37 nuclei, their separate

effects should not be distinguishable. Using relative natural abundances of 0.505 and 0.495 for ^{79}Br and ^{81}Br respectively leads to an isotopically weighted average of R of 9.50. By referring to figure 7.3.1, the expected form of the multiplet at this value of the parameter R predicted using the exact calculations, when considering only dipolar coupling as a mechanism for the transfer of the effect, is an asymmetric quartet.

10.2.2 50.33-MHz Experimental Results

An expansion of the 50.33 MHz ^{13}C CP/MAS spectrum of 1,4-dibromobenzene, recorded in the non-quaternary suppression mode of operation, is shown in figure 10.2.1.

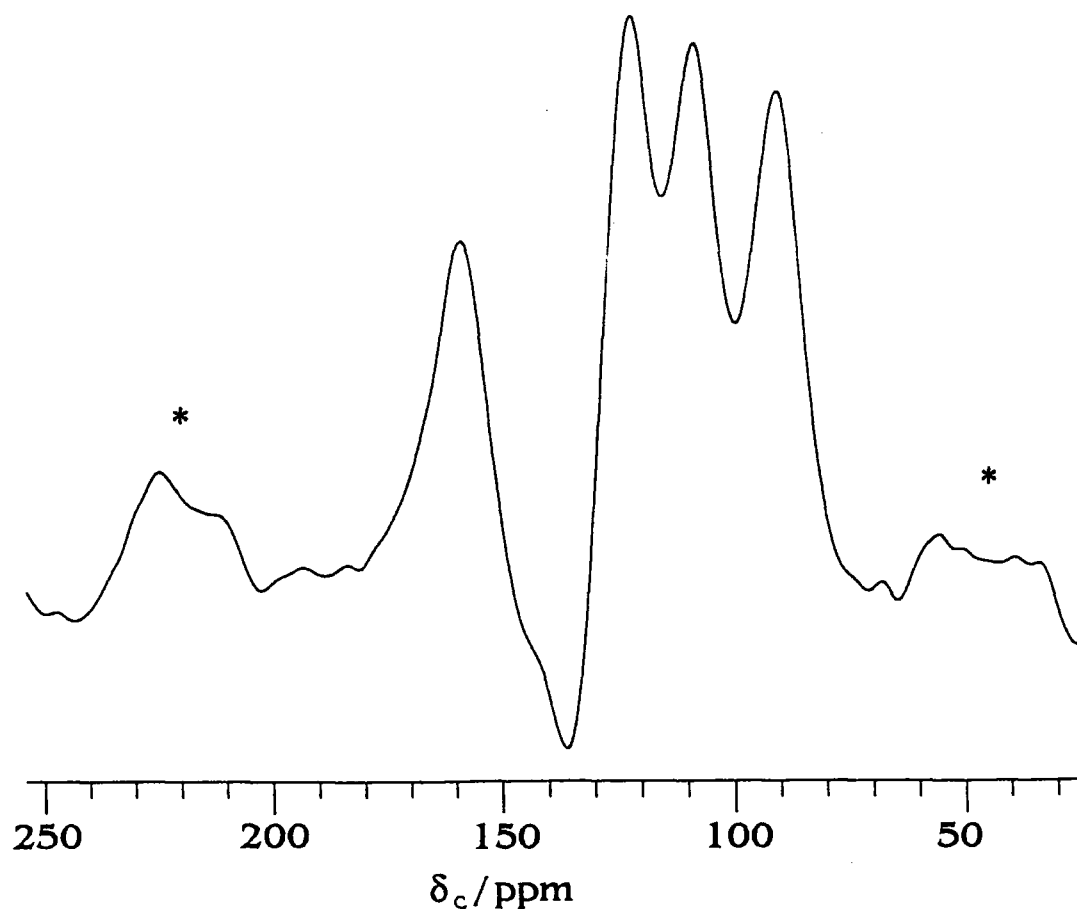


Figure 10.2.1 50.33 MHz ^{13}C NQS spectrum of 1,4-dibromobenzene. Operating conditions: Spectral width 20 kHz; pulse duration 4.0 μs ; contact time 3.0 ms; recycle delay 5 s; dephasing time 37 μs ; number of transients 908; spinning rate 4 kHz. The peaks marked with an asterisk are spinning sidebands.

The signals from the carbons directly bonded to the bromine nuclei are observed as a broad asymmetric quartet at a chemical shift $\delta = 121.2$ ppm. This isotropic chemical shift is in close agreement to that obtained for a solution in CDCl_3 of 121.58 ppm. The line positions of the individual components of the multiplet are -29.9, -11.0, +1.9 and +39.0 ppm (-1.50, -0.55, +0.10 and +1.96 kHz) with respect to the isotropic chemical shift. Recording the spectrum in the NQS mode of operation was imperative to suppress the C-H signals that would have otherwise obscured the multiplet for the C-Br signals. However, one interesting feature that is apparent from the spectrum shown in figure 10.2.1 is the peak displaying negative intensity at approximately -138 ppm. Having previously acquired a spectrum of this compound using the simple CP mode of operation it was known that this is at the shift of the C-H resonance. This feature of ^{13}C NQS (dipolar-dephasing) experiments has been observed before in compounds containing a limited number of protons and investigated at length.³ In a (^{13}C , ^1H) dipolar-dephasing experiment the ^{13}C spins initially dephase by transferring magnetisation, via dipolar coupling, to nearby protons, which essentially means protons that are directly bonded to the carbon nucleus in question. For a compound containing an abundance of protons a network of coupled proton spins exists. Once the magnetisation has been transferred from the carbon to the directly-bonded proton a further distribution of magnetisation is possible between the homonuclear-dipolar-coupled protons. Consequently the magnetisation for a proton-coupled carbon spin under these conditions exhibits an almost Gaussian decay to zero. However, if we consider a compound containing very few protons, a situation may arise where we have isolated ^1H , ^{13}C spin-pairs, trios or quartets. In such cases no such smooth Gaussian diminution of magnetisation is observed by transmission to the proton 'spin-bath' but an oscillation of magnetisation, back and forth between carbon nuclei and the proton(s) is set up, leading to a decay of magnetisation to zero which proceeds in a periodic oscillatory manner about zero. Consequently, depending on the particular dephasing time used in the experiment, ^{13}C signals may be observed having either positive or negative intensities.

In a variable dephasing-time experiment conducted on 1,4-dibromobenzene the C-H signal was found to become increasingly negative after a dephasing time of about 40 μs . The most suitable dephasing time, giving the optimum suppression of the C-H signal, was found to be one of 37 μs , the time used in the acquisition of the spectrum in figure 10.2.1. The only disadvantage associated with the occurrence of such a phenomenon is that the degree of inversion of the C-H signal dictates, to some extent, the position of the peak maximum for the component of the C-Br multiplet lying adjacent to it to lower frequency. Therefore, in making quantitative comparisons of experimentally observed and theoretically predicted line positions it should be appreciated that an associated degree of uncertainty exists.

10.2.3 Theoretical Predictions of Line Positions

For this brominated compound at this static magnetic field strength, yielding this value of R , there are two approaches, in addition to using exact calculations, that can be taken to predict the positions of the lines.

10.2.3.1 Inverse First-order Theory

If one applies inverse first-order perturbation theory, which takes into account the contribution to the residual dipolar coupling phenomenon from ΔJ , the relevant equations needed to calculate the predicted line positions are 7.3.13 a and b.

$$v_{\pm 3/2} = \pm (3/4 J - 3/2 D') + 2(J + D')v_s/\chi$$

$$v_{\pm 1/2} = \pm (1/4 + \pi/3\sqrt{3} J + 1/2 D') - 2(J + D')v_s/\chi$$

However, as it is necessary to average the parameters in these two equations according to the relative populations of ^{79}Br and ^{81}Br , this leads to:

$$\langle v_{\pm 3/2} \rangle = \pm [3/4 (p_{79} J_{79} + p_{81} J_{81}) - 3/2 (p_{79} D'_{79} + p_{81} D'_{81})] \\ + 2[p_{79} (J_{79} + D'_{79}) / R_{79} + p_{81} (J_{81} + D'_{81}) / R_{81}]$$

$$\langle v_{\pm 1/2} \rangle = \pm [1/4 + \pi/3\sqrt{3}](p_{79} J_{79} + p_{81} J_{81}) + 1/2 (p_{79} D'_{79} + p_{81} D'_{81}) \\ - 2[p_{79} (J_{79} + D'_{79}) / R_{79} + p_{81} (J_{81} + D'_{81}) / R_{81}]$$

where $J_{79,81}$ are the isotropic indirect coupling constants between $^{79,81}\text{Br}$ and ^{13}C , $D'_{79,81}$ are the corresponding effective dipolar coupling constants and $R_{79,81}$ are the ratios χ/v_s for $^{79,81}\text{Br}$. Since $J_{81}/J_{79} = D'_{81}/D'_{79} = \gamma_{81}/\gamma_{79} = 1.078$ and the fractional populations of the two bromine isotopes p_{79} and p_{81} are as given previously, the line positions for the four components of the ^{13}C multiplet predicted by inverse perturbation theory are calculated as (measured from its centre of mass): $1.002 J_{79} - 1.335 D'_{79}$, $-1.111 J_{79} - 0.742 D'_{79}$, $0.665 J_{79} + 0.296 D'_{79}$ and $-0.556 J_{79} + 1.781 D'_{79}$.

The best fit of the two adjustable parameters J_{79} and D'_{79} appearing in the expressions predicted by inverse first-order theory to the observed line positions is $J_{79} = -0.18 \pm 0.04$ kHz and $D'_{79} = 1.04 \pm 0.04$ kHz. These values give line positions corresponding to -1.57 , -0.57 , $+0.19$ and $+1.95$ kHz, which are in excellent agreement with the experimental results. Furthermore, the former of these two values compares favourably with those for $|J_{79}|$ obtained in solution from relaxation measurements conducted on 1,2-dibromobenzene and 1,3,5-tribromobenzene of 0.135 and 0.136 kHz respectively.⁴ However, from the present investigations it is possible to extract not only the magnitude, but also the sign of the (^{13}C , ^{79}Br) indirect coupling constant. The negative sign is consistent with the general trend expected for coupling between nuclei contained in groups 14 and 17 of the Periodic Table.⁵ Similarly, the value obtained for D'_{79} is close to the full dipolar coupling constant $D_{79} = 1.24$ kHz, obtained from calculations based on a C-Br internuclear separation of 1.827 Å (as derived from a rather old X-ray diffraction study of 1,4-dibromobenzene).⁶

It is worthy of mention that experimental ^{13}C line positions can only be fitted to the above equations if the quadrupole coupling constants of both bromine isotopes are assumed to be positive. This is in accordance with the sign previously determined¹

and in direct contrast to the positive values of χ observed for the two isotopes of chlorine. The sign of χ is immediately apparent from the sense of the asymmetric quartet, which shows signal bunching at low frequency, compared to the bunching at high frequency which was observed for the components of the multiplets for the ^{13}C signals in sodium monochloroacetate at 4.7 T. However, the above argument is only strictly applicable if D' is also assumed to be positive (i.e. provided $|D| > |\Delta J/3|$). Since the electronic environments in C-Cl and C-Br are expected to be similar, but the nuclear quadrupole moments have opposite signs,² the reversal in sign of χ is unsurprising.

10.2.3.2 Exact Theory

If the exact approach is used to calculate the expected line positions the values obtained are: $0.985 J_{79} - 1.326 D'_{79}$, $-1.065 J_{79} - 0.675 D'_{79}$, $0.606 J_{79} + 0.232 D'_{79}$ and $-0.527 J_{79} + 1.769 D'_{79}$. These are close to those calculated using inverse first-order theory. If we once again determine the best fit for the two parameters J_{79} and D'_{79} we find that they are computed to be: $J_{79} = -0.13 \pm 0.04$ kHz, $D'_{79} = 1.07 \pm 0.02$ kHz. This value of J_{79} is very close to those evaluated from the relaxation measurements of similar brominated aromatic compounds mentioned previously, and the new value of D'_{79} is nearer to the value of the full dipolar coupling constant in 1,4-dibromobenzene. Now the calculated line positions (from their centres of mass) are: -1.55, -0.58, +0.17 and +1.96 kHz, all within ± 0.07 kHz of the experimental results. This high degree of agreement of theoretically predicted line positions to those obtained experimentally can be further appreciated if one considers that the widths of the ^{13}C lines in figure 10.2.1 are *ca.* 0.5 kHz.

Since we now have an appreciable (^{13}C , ^{79}Br) indirect coupling constant (and therefore an appreciable (^{13}C , ^{81}Br) indirect coupling constant) it is not unreasonable to assume that there will be a corresponding anisotropy associated with the J tensor. In the above calculations the estimated value of D'_{79} is consistently lower than D (^{13}C , ^{79}Br). If this difference is attributed to the anisotropy in J , then ΔJ_{79} can be

calculated using the equation $D'_{79} = D_{79} - \Delta J_{79}/3$ to be + 0.51 kHz, with substantial uncertainty. Hence it can be surmised that, in the case of (^{13}C , $^{79,81}\text{Br}$) residual dipolar coupling, the quadrupolar effect is most likely transferred to the ^{13}C nucleus not only via dipolar coupling, but also via an appreciable anisotropy in indirect coupling.

10.2.3.3 Fitting to a Polynomial Expression

The final method of analysis available to us is to use the polynomial equations, presented in chapter 7, derived from the exact theory. If we use an effective dipolar coupling constant of 1.07 kHz, as derived from the exact approach, which takes into account the effects of ΔJ , the calculated line positions are as follows: -1.42, -0.72, +0.25 and +1.89 kHz from the isotropic chemical shift, which are in moderate agreement with the experimental results.

10.2.4 75.43 MHz Experimental Results

The ^{13}C NQS spectrum of 1,4-dibromobenzene was also recorded at 7.05 T. Figure 10.2.11, which shows a comparison of spectra recorded at 4.7 T and 7.05 T.

At a glance it is evident that the three low-frequency lines are more closely spaced and the high-frequency line occurs at slightly higher frequency in the 7.05 T spectrum compared to the 4.7 T spectrum. At this increased magnetic field strength the $^{79,81}\text{Br}$ isotopically weighted average of R is now 6.33 and, if one refers to figure 7.3.1, it is apparent that at this lower value of R this is the behaviour that would be expected. For the 7.05 T spectrum the experimentally observed line positions are -1.19, -0.54, +0.12, and +2.05 kHz with respect to the isotropic resonance.

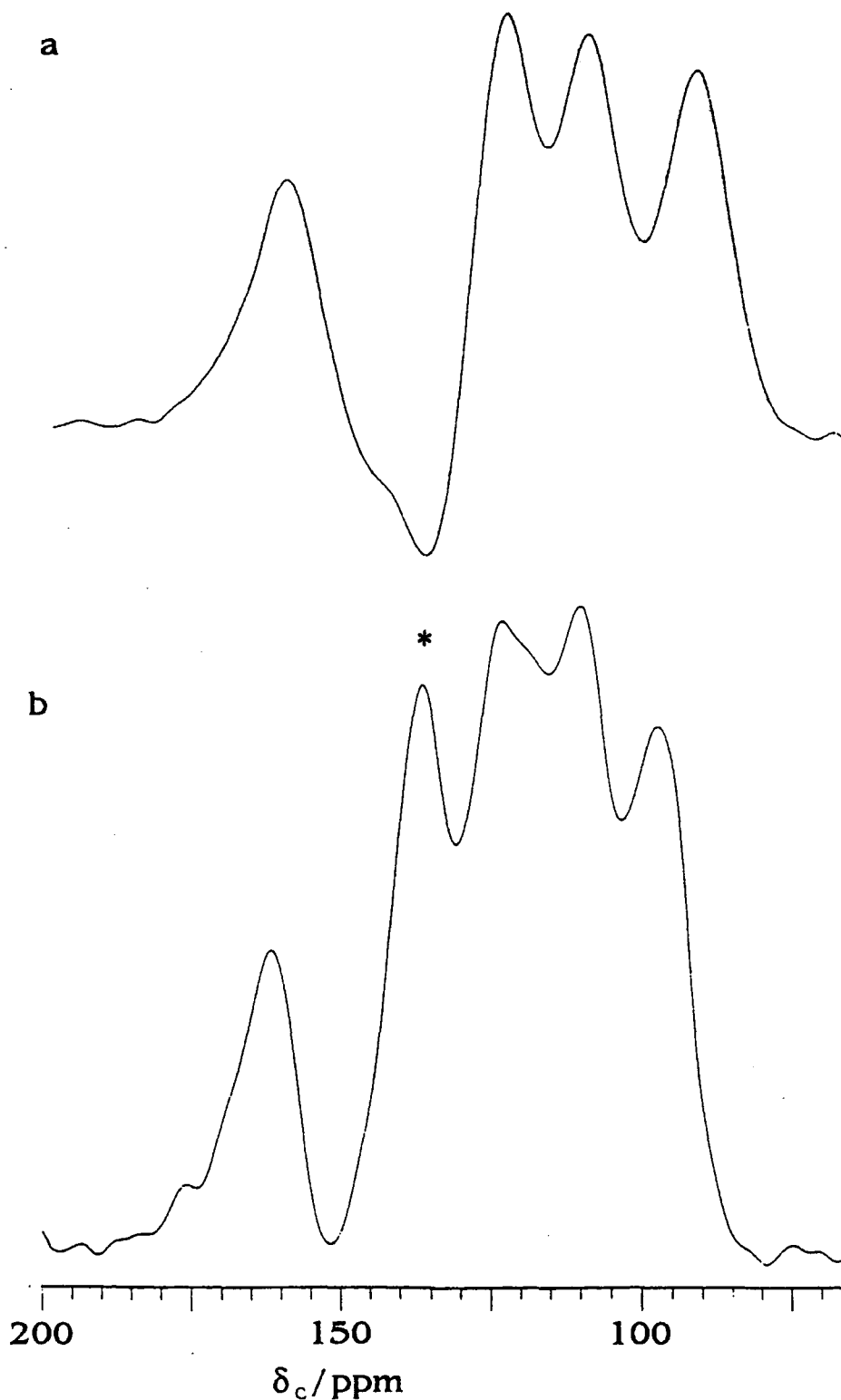


Figure 10.2.2 Comparison of (a) 50.33 MHz and (b) 75.43 MHz ^{13}C NQS spectra of 1,4-dibromobenzene. Operating conditions for (a) are the same as in figure 10.2.1; for (b): Spectral width 30 kHz; contact time 4.0 ms; recycle delay 10 s; number of transients 600; spinning rate 7.88 kHz. A Gaussian broadening of 200 Hz and 300 Hz was applied to (a) and (b) respectively prior to Fourier transformation. In (b) the peak indicated by an asterisk is due to incomplete suppression of the CH signals.

10.2.5 Theoretical Predictions of Line Positions

If the exact approach is used to calculate the line positions for the 7.05 T spectrum, the best fit is obtained for $D'_{79} = 1.03$ kHz and $J_{79} = -0.11$ kHz, with line positions predicted to lie in the following positions: -1.22, -0.49, +0.13, +2.05 kHz. These calculated positions are in excellent agreement with those observed experimentally, and furthermore the values of D'_{79} and J_{79} are in moderately good agreement to those calculated from the spectrum acquired at 4.7 T. If the polynomial equations are used to predict the line positions the computed values are -1.19, -0.70, +0.07 and +1.83 kHz, which again are in moderate agreement with the experimental results. Finally, if inverse first-order perturbation theory is applied the necessary equations are reduced to $1.114 J_{79} - 1.223 D'_{79}$, $-1.222 J_{79} - 0.854 D'_{79}$, $0.553 J_{79} + 0.184 D'_{79}$, $-0.444 J_{79} + 1.893 D'_{79}$. Using the values of D'_{79} and J_{79} obtained from the exact calculation yields line positions of -1.38, -0.75, +0.12, and +2.00 kHz.

10.2.6 Comparisons and Explanation of Accuracy of Fit for Experimental and Calculated Line Positions

Table 10.2.1 summarises the information listed in the previous sections concerning comparisons of experimentally observed line positions and those predicted theoretically using each of the different methods of calculation.

Line Positions Apparent from	Line Positions from Isotropic Resonance / kHz	
	4.7 T	7.05 T
Experimental Data	-1.50, -0.55, 0.10, 1.96	-1.19, -0.54, 0.12, 2.05
Exact Calculations	-1.55, -0.58, 0.17, 1.96	-1.22, -0.49, 0.13, 2.05
Inverse First-Order Theory	-1.57, -0.57, 0.19, 1.95	-1.38, -0.75, 0.12, 2.00
Polynomial Equations	-1.42, -0.72, 0.25, 1.89	-1.19, -0.70, 0.07, 1.83

Table 10.2.1 Comparison of the experimentally observed line positions and those predicted using the available methods of calculation.

From the data contained in table 10.2.1 it can be seen that at both magnetic field strengths the agreement between the experimental data and that those obtained by the exact calculations is excellent. At the lower field strength the fit of the experimentally observed line positions to those predicted using inverse first-order theory is also good. Consequently one can conclude that at 4.7 T inverse first-order theory provides not only a qualitative picture for the appearance of the asymmetric quartet but also relevant quantitative information. For the data acquired at the higher field strength of 7.05 T, the agreement between exact and inverse first-order theories is not as good. The disparity in line positions can be attributed to a partial breakdown of the inverse first-order theory at this magnetic field strength (lower value of R). Now inverse first-order theory is only able to provide us with a qualitative picture.

The agreement of the line positions calculated using the polynomial equations to the experimental positions is similarly not as good as would have been expected at either magnetic field strength, and so once again only a qualitative analysis is possible using this method of calculation.

10.2.7 Simulation of Theoretical Powder Patterns and Factors Affecting the Accuracy of the Simulation

From the exact calculations theoretical powder spectra were simulated using a computer program (ANYCHI), supplied by Prof. A. C. Olivieri. The details of how such simulations are carried out was discussed in section 8.5. Figure 10.2.3 is a comparison of the data obtained experimentally at 4.7 T, a spectrum simulated using the computer program, and a simulated spectrum convoluted with a Gaussian line-broadening factor.

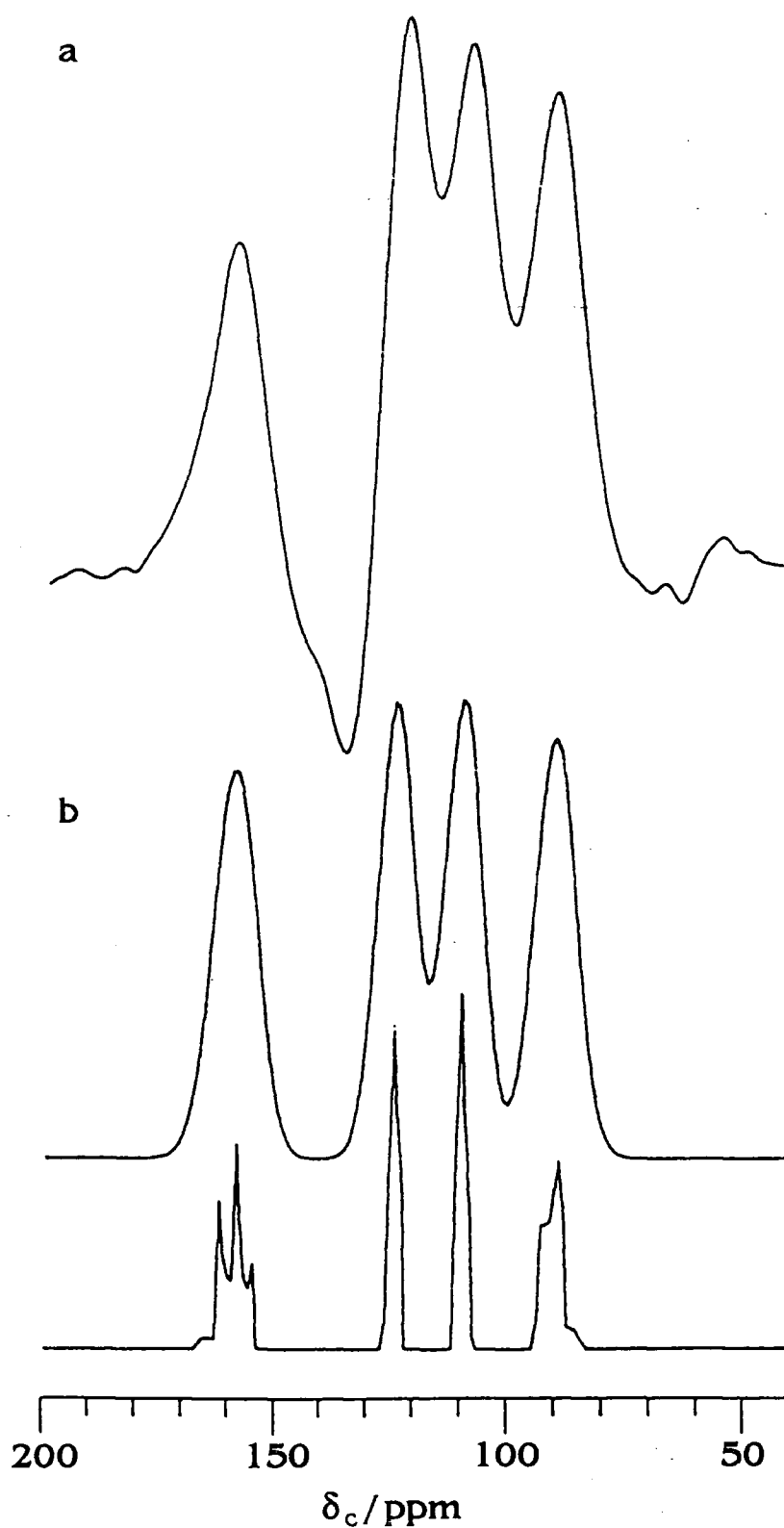


Figure 10.2.3 Comparison of (a) the 50.33 MHz ^{13}C NQS spectrum of 1,4-dibromobenzene shown in figure 10.2.1, (b) the theoretical powder spectrum obtained using the exact approach using $J(^{13}\text{C}, ^{79}\text{Br}) = -0.13$ kHz and $D'(^{13}\text{C}, ^{79}\text{Br}) = 1.07$ kHz and (c) a Gaussian convoluted powder spectrum (width parameter ≈ 200 Hz).

As can be seen from figure 10.2.3, when a Gaussian line-broadening function of $0.2 D'$ (approximately 200 Hz) is convoluted with the theoretically calculated powder pattern the resultant spectrum is very similar to that obtained experimentally. In part the application of a Gaussian broadening serves to take into account effects such as the intrinsic linewidth of each line contributing to the powder pattern, field inhomogeneity and improper (off-resonance) decoupling. However, there is another factor that in some instances can be accounted for by the application of a Gaussian broadening. In the previous chapter examples were given of residual dipolar coupling between non-bonded $^{35,37}\text{Cl}$ and ^{13}C nuclei for sodium monochloroacetate. Such intramolecular remote interactions can also be expected to be present in the brominated benzenes. For 1,4-dibromobenzene one can envisage a variety of interactions from remote bromine nuclei to any given C-Br carbon nucleus directly bonded to a bromine nucleus, all of which strictly speaking should be taken into consideration when performing exact calculations and bandshape simulations. These remote interactions will include the intramolecular interaction to the bromine nucleus *para* on the benzene ring and numerous intermolecular interactions from bromines in neighbouring molecules. As was discussed in chapter 7, for such remote interactions where the ^{13}C - $^{79,81}\text{Br}$ internuclear vector and the main axis of the EFG tensor are no longer coaxial, it is necessary to take into consideration the angle β_D that naturally complicates any calculations performed. From interpretation of the results obtained from exact calculations performed on 1,4-dibromobenzene, by Prof. K. D. M. Harris and Dr. A. E. Aliev, it was surmised that for this compound the remote interactions were not strong enough to cause critical bandshape changes and that these remote interactions could, in fact also be taken into account adequately by the application of a Gaussian line-broadening function, a point verified by the fact that the experimentally observed spectrum and Gaussian-broadened theoretical spectrum contained in figure 10.2.3 are so similar.

10.3 (^{13}C , $^{79,81}\text{Br}$) Residual Dipolar Coupling in 1,3,5-Tri-, 1,2,4,5-Tetra- and Hexabromobenzene - the Effects of Remote Interactions

In the case of more highly brominated aromatic derivatives such as 1,3,5-tribromobenzene, 1,2,4,5-tetrabromobenzene and hexabromobenzene it is envisaged the greater prevalence of bromine nuclei will result in stronger remote interactions, especially from the bromine nucleus in *ortho* and *meta* positions to the observed C-Br carbon. Consequently the effects of such remote interactions may well no longer be able to be accounted for by convolution of the bandshape, theoretically calculated using the exact approach arising from directly-bonded ^{13}C , $^{79,81}\text{Br}$ pairs, with a symmetric Gaussian lineshape, and it may now be necessary to incorporate the effects of the remote interactions explicitly into the exact calculations (and spectral simulations). Exact calculations and spectral simulations performed on these three compounds verified this postulate, since predictions of the positions of lines differed significantly when the effects of remote interactions were included explicitly in the calculations compared to when they were neglected. The actual simulations performed, that included remote interactions explicitly, incorporated only the largest of the remote interactions (about ten) since to include every single remote interaction detectable explicitly would have proved highly laborious. Consequently Gaussian broadening was still applied to the simulated spectra to take some account of the effects of those remote interactions that were not included explicitly in the calculation.

10.3.1 1,3,5-Tribromobenzene

Figure 10.3.1 compares the experimentally observed 50.33 MHz ^{13}C CP/MAS spectrum of 1,3,5-tribromobenzene recorded in the non-quaternary suppression mode of operation to spectra simulated from results obtained using the exact approach. In both of these spectral simulations the effects of only the strongest of the remote interactions have been considered.

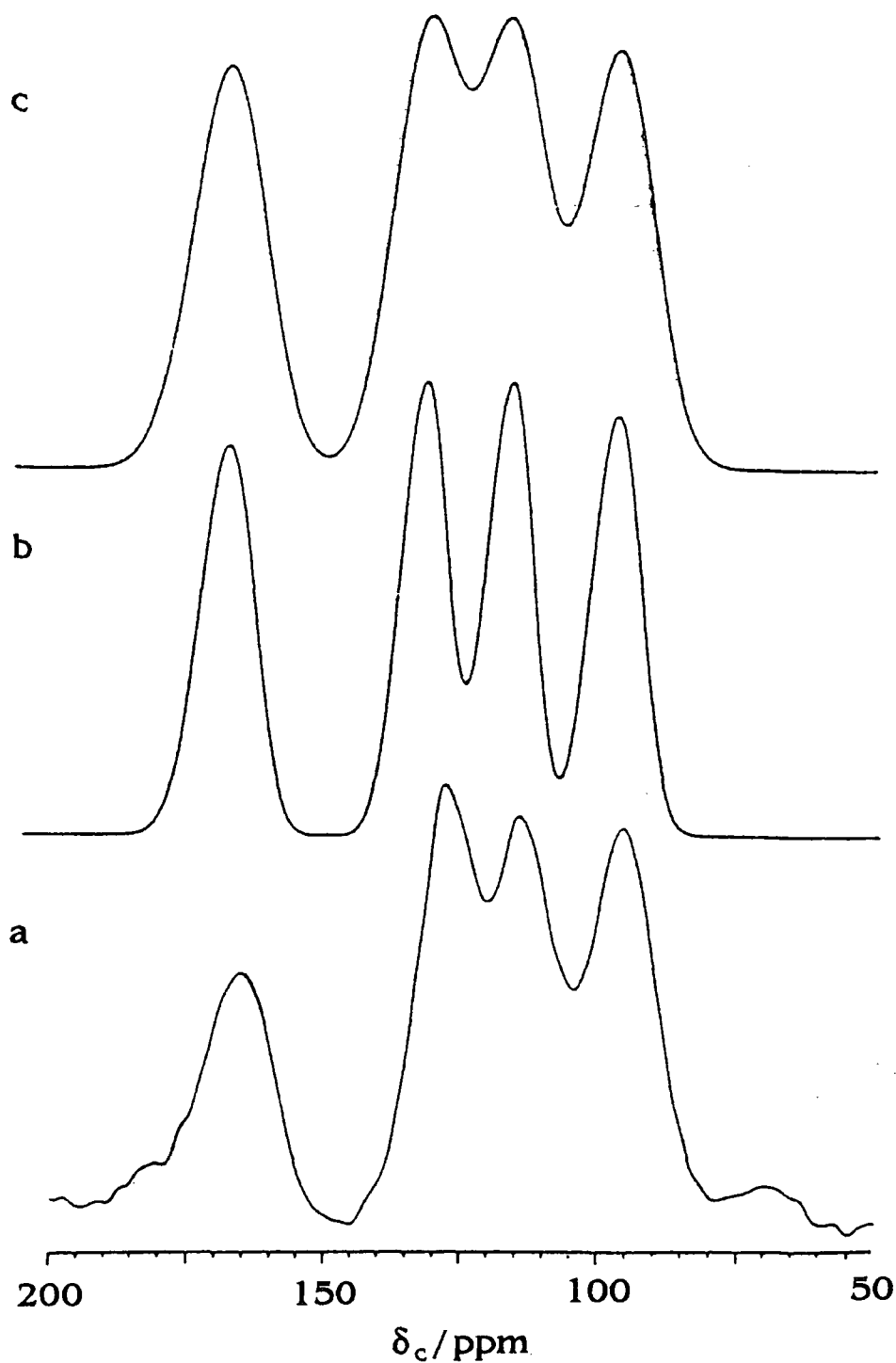


Figure 10.3.1 Comparison of (a) 50.33 MHz ^{13}C NQS spectrum of 1,3,5-tribromobenzene. (Operating conditions: Spectral width 20 kHz; pulse duration 4.2 μs ; contact time 10.0 ms; recycle delay 10 s; dephasing time 36 μs ; number of transients 6800; spinning rate 4.55 kHz), (b) bandshape simulation calculated using $\chi_{79} = 554$ MHz and $\chi_{81} = 468$ MHz, and (c) as (b) but with a Gaussian broadening of 320 Hz applied.

The expected asymmetric quartet is clearly defined and the simulated lineshape mirrors closely that obtained experimentally. The similarity in lineshape between the C-Br signals in this compound and those in the spectrum of 1,4-dibromobenzene, recorded at the same field strength, suggests that remote interactions do not play as critical a role as expected in the determination of the lineshape for 1,3,5-tribromobenzene, a hypothesis verified by Prof. K. D. M. Harris et al.⁷ from exact calculations performed both including and neglecting such interactions.

10.3.2 1,2,4,5-Tetrabromobenzene and Hexabromobenzene

Figures 10.3.2 and 10.3.3 are comparisons of the experimental and simulated data (simulated the same way as in figure 10.3.1, taking into account the effects of such remote interactions) for 1,2,4,5-tetrabromobenzene and hexabromo-benzene respectively.

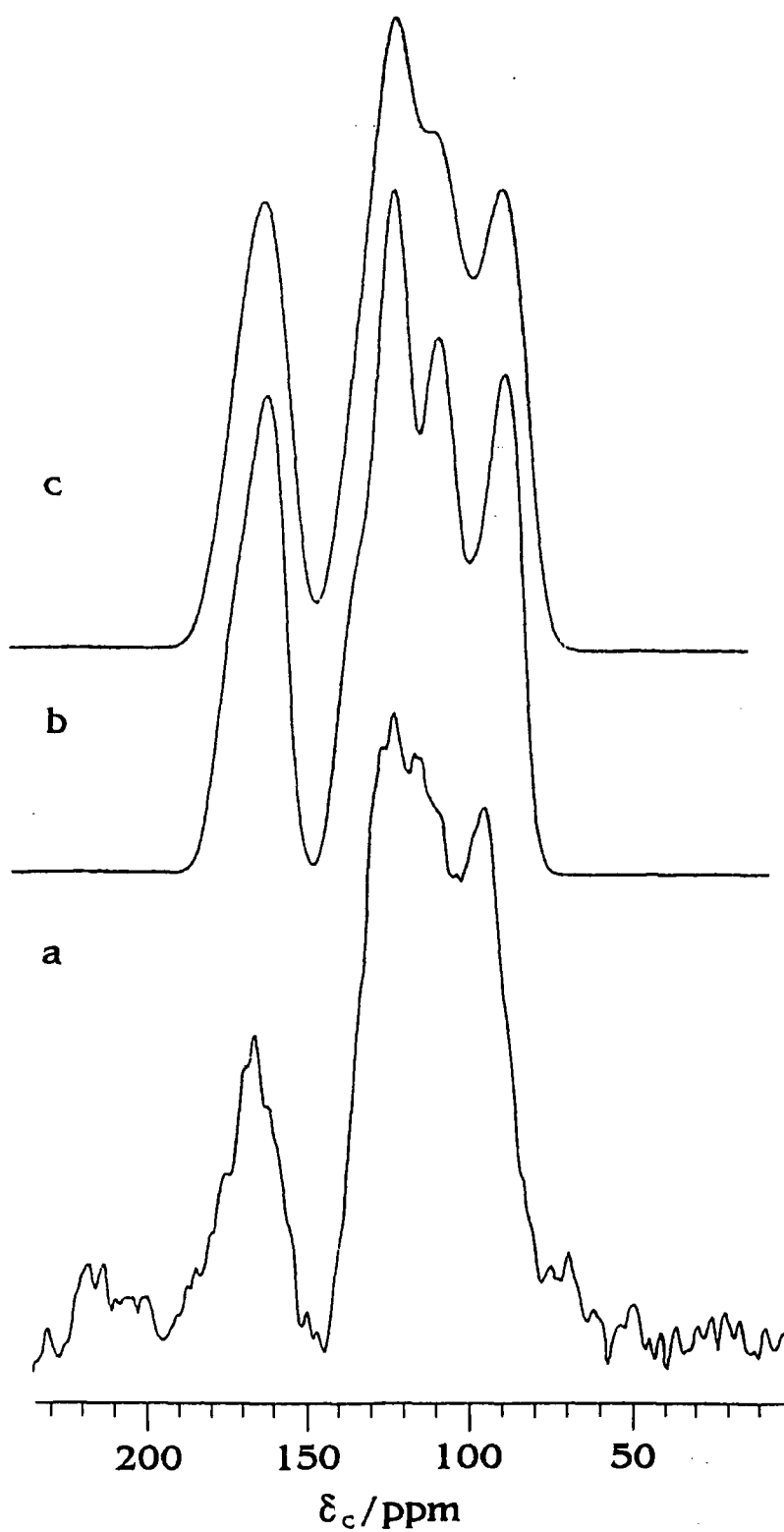


Figure 10.3.2 (a) 50.33 MHz High-resolution solid-state ^{13}C NMR spectrum (NQR with dipolar dephasing delay $36\ \mu\text{s}$) recorded at ambient probe temperature for 1,2,4,5-tetrabromobenzene, (b) bandshape calculated using $\chi_{79} = 574\ \text{MHz}$ and $\chi_{81} = 485\ \text{MHz}$, (c) as (b) but with a Gaussian broadening factor of 260 Hz applied.

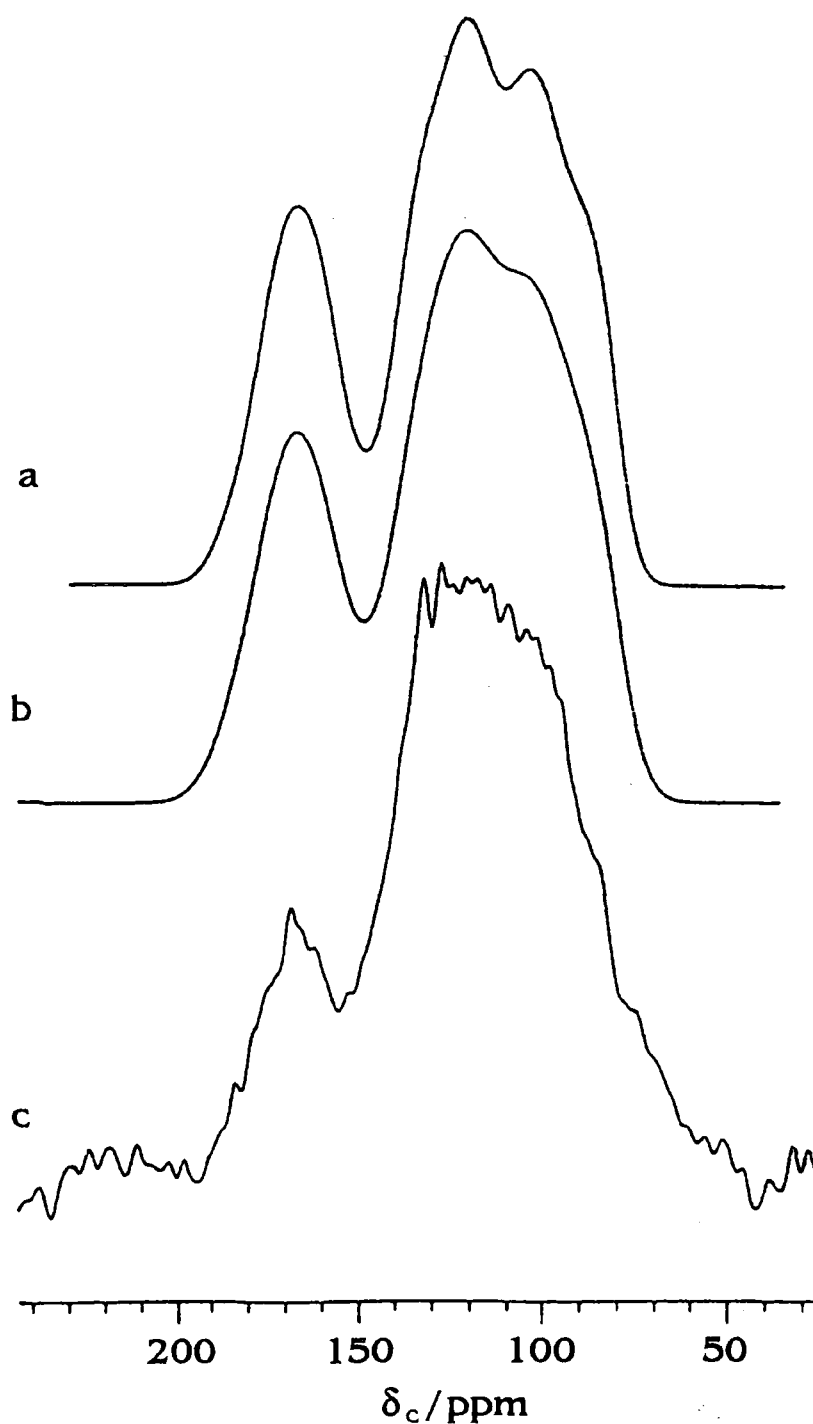


Figure 10.3.3 (a) 50.33 MHz High-resolution solid-state ^{13}C single-pulse NMR spectrum recorded at ambient probe temperature for hexabromobenzene, (b) bandshape simulated from exact approach using $\chi_{79} = 605$ MHz and $\chi_{81} = 506$ MHz and a Gaussian broadening of 340 Hz applied (c) as (b) but with no Gaussian broadening applied.

Once again in both cases the simulated spectra closely resemble the experimental data. From the experimental spectra it is apparent that bunching of signals at low frequency is still occurring, even though the components of the multiplet within this region of the spectrum are less easy to discern than for the di- and tri-brominated analogues. In fact, in the case of hexabromobenzene the resonances remain almost unresolved. Remote interactions have been calculated to have a substantial influence over the positions of the lines in the ^{13}C CP/MAS spectrum for 1,2,4,5-tetrabromobenzene,⁷ and although such calculations have not been performed for hexabromobenzene, a similar behaviour is expected. The major influence amongst the non-bonded bromine nuclei has been found to arise from the *ortho* bromine. The strength of the dipolar interaction between a C-Br carbon and an *ortho* bromine has been calculated to be of a magnitude some two and a half times that between any other carbon-remote bromine spin-pair.

10.4 Other Brominated Compounds

Although a great number of other brominated organic compounds were investigated to see if such (^{13}C , $^{79,81}\text{Br}$) residual dipolar coupling effects were manifest in their ^{13}C CP/MAS spectra, very few gave rise to observation of the phenomenon. Spectra from two other compounds found to exhibit the phenomenon are shown in the following sections.

10.4.1 4-Bromo-3,5-dimethylpyrazole

Figure 10.4.1 shows expansions of the relevant regions of the 7.05 T (a) and 4.7 T (b) ^{13}C NQS spectra of 4-bromo-3,5-dimethylpyrazole. In these spectra the large signal at ~ 150 ppm arises from the two unsuppressed C-Me resonances.

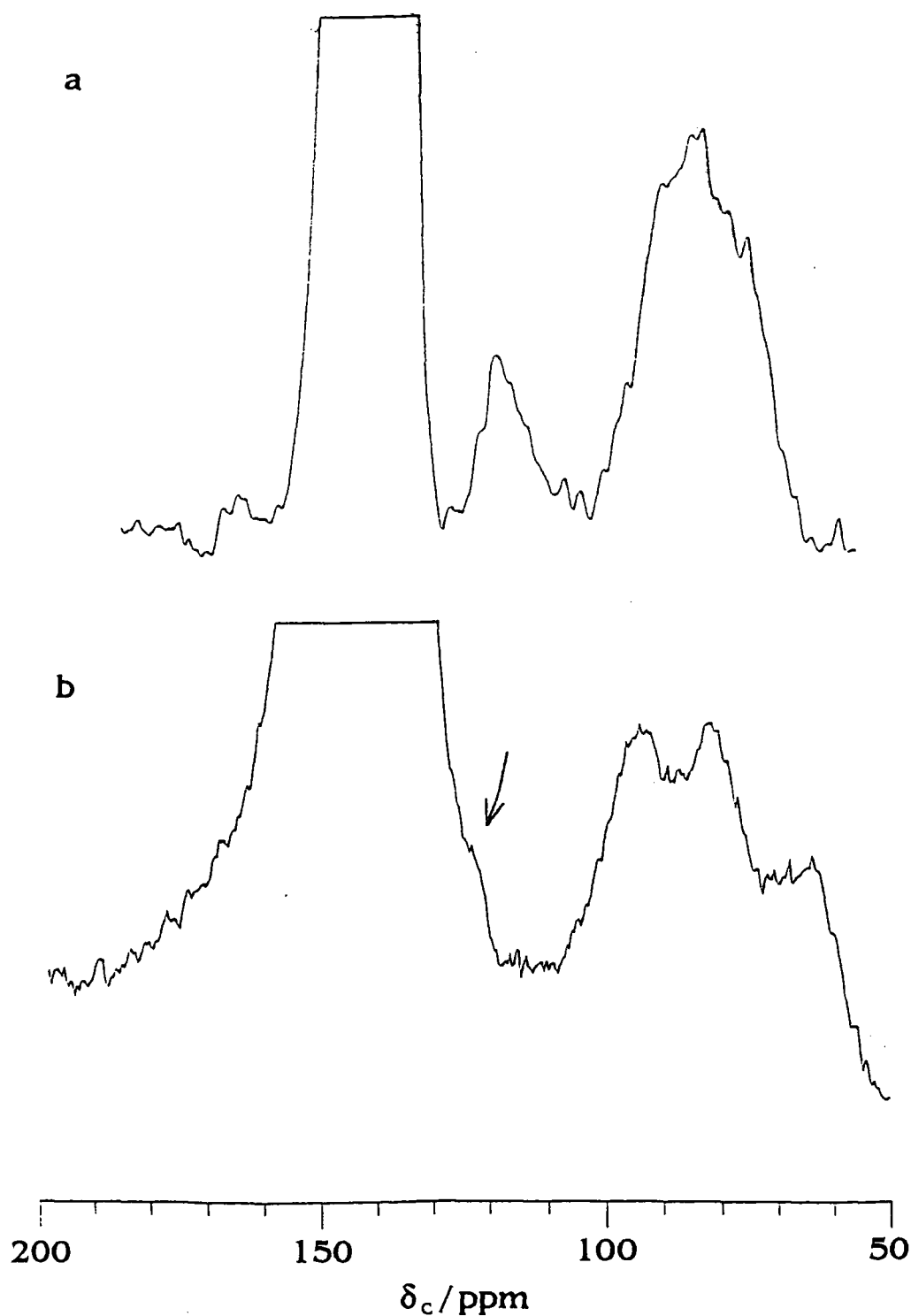


Figure 10.4.1 (a) 75.43 MHz and (b) 50.33 MHz ^{13}C NQS spectra of 4-bromo,-3,5-dimethylpyrazole. Operating conditions: (a) Spectral width 30 kHz; contact time 15.0 ms; recycle delay 30 s; number of transients 1888; spinning rate 11.7 kHz. (b) Spectral width 20 kHz; contact time 2.0 ms; recycle delay 5 s; number of transients 9840; spinning rate 5.7 kHz. The high frequency component of the quartet in the 50.33 MHz spectrum appears as a shoulder on the C-Me resonance and is indicated by the arrow.

As was observed for the brominated aromatic derivatives, an asymmetric quartet is observed at both field strengths, with the components bunching at low frequency, indicative of a positive quadrupole coupling constant. The dispersion of lines is, as expected, less at the higher field strength. In the 4.7 T spectrum the line positions are 65.3, 83.6, 95.5 and 138.9 ppm, with the last component appearing as a shoulder on the intense C-Me signal at 138.9 ppm. The average of the four shifts is 95.8 ppm, which is close to the solution-state value seen for the C-Br resonance at 93.84 ppm (recorded in CDCl_3). Furthermore, the deviations of the individual components from the centre of mass of the multiplet (-1.54, -0.61, -0.01 and +2.17 kHz) are similar to those quoted for 1,4 dibromobenzene at 4.7 T (-1.50, -0.55, +0.10 and +1.96 kHz), suggesting similar values of J and D' for the two compounds. The similarity of the estimated values of D' for the two compounds is also consistent with the finding that the literature value of the C-Br bond distance, determined from X-ray diffraction studies, is 1.87 Å,⁸ in fair agreement to the C-Br bond distance of 1.83 Å in 1,4 dibromobenzene.

10.4.2 1-Bromo-4-chlorobenzene

The final example of residual dipolar coupling is probably the most interesting, since it combines effects of (^{13}C , $^{35,37}\text{Cl}$) and (^{13}C , $^{79,81}\text{Br}$) residual dipolar coupling in the same molecule. Figure 10.4.2 is the 50.33 MHz ^{13}C NQS CP/MAS spectrum of 1-bromo-4-chlorobenzene.

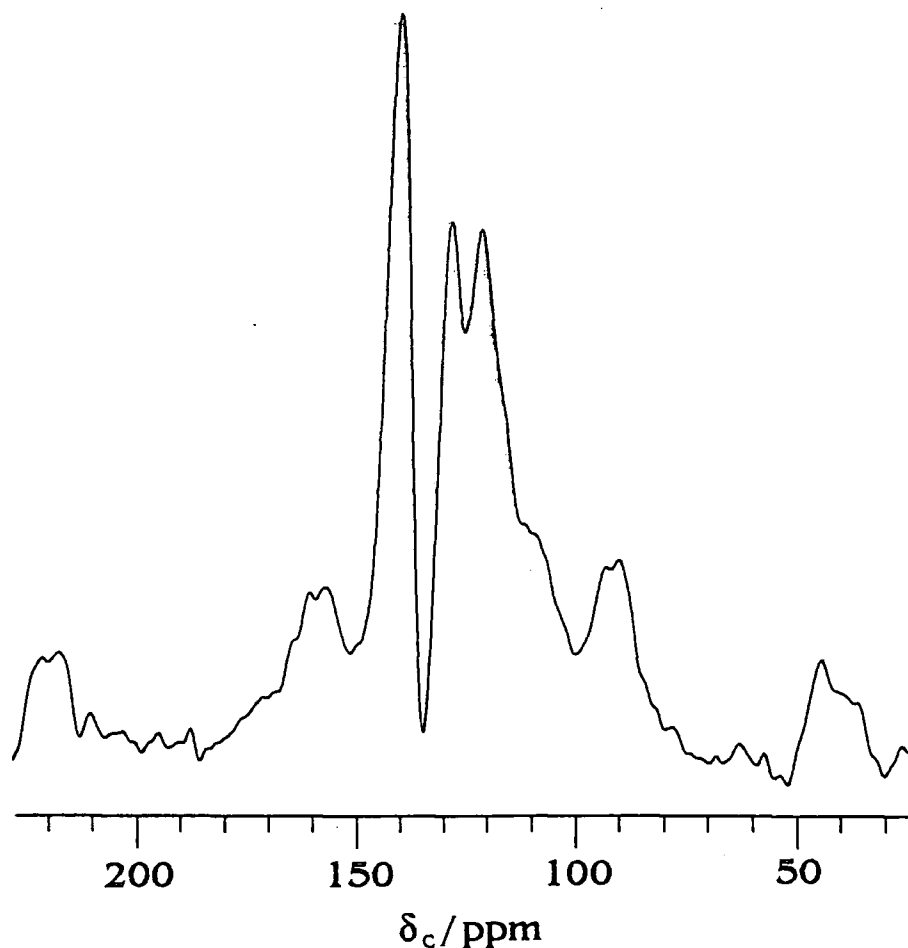


Figure 10.3.4 50.33 MHz ^{13}C NQS spectrum of 1-bromo4-chlorobenzene. Operating conditions: Spectral width 20 kHz; pulse duration 4.0 μs ; contact time 3.0 ms; recycle delay 5 s; number of transients 1532; spinning rate 4.8 kHz

The 2:1:1 triplet arising from the C-Cl carbon is clearly visible, having its components at 140.7, 129.0 and 121.9 ppm respectively, whereas for the C-Br asymmetric quartet only three of the components are visible at 158.7, 109.9, and 92.4 ppm, the third being obscured by the signals at 129.0 and 121.9 arising from the C-Cl carbon. The positions of the three visible components of the C-Br resonance parallel relatively closely what was found for the same components in the simple brominated benzenes at the same field strength (160.2, 110.2 and 91.3 ppm for 1,4-dibromobenzene), and the splittings observed in the C-Cl resonance (11.7 and 7.1 ppm, high frequency to low frequency) are not too dissimilar to those seen for the C-Cl signal in the spectrum of sodium monochloroacetate recorded at 4.7 T (9.9 and 9.4 ppm).

It is important to point out that in this compound the two carbon nuclei (C-Cl and C-Br) are, of course, chemically inequivalent and therefore their multiplets will not share a common isotropic shift. It would be expected that the isotropic shift of the signal from the chlorinated carbon will occur to higher frequency than that of the brominated carbon, a facet that is visible from figure 10.3.4.

This spectrum is also useful as it serves as a good illustration as to the effects the sign of the quadrupole coupling constant has on the sense of the second-order shift. Bunching occurs at high frequency for the C-Cl resonance (double intensity peak at high frequency) due to the negative value of χ for chlorine, and at low frequency for the C-Br resonance since the bromine nucleus possesses a positive χ .

10.5 Unfavourable Cases: Motion-induced Suppression of Predicted Multiplets

10.5.1 Sodium Monobromoacetate

When initial attempts were made to attempt to detect the residual dipolar coupling phenomenon between the ^{13}C , $^{79,81}\text{Br}$ spin-pair a logical starting point seemed to be to record the ^{13}C CP/MAS spectrum of sodium monobromoacetate, since favourable results had been achieved in investigations carried out on the analogous chlorinated compound. Unfortunately, however, as was the case for a large number of brominated compounds investigated, the carbon-13 signal of the C-Br carbon was found to be a singlet, displaying none of the multiplicities predicted. Figure 10.5.1 is the 50.33 MHz ^{13}C CP/MAS spectrum of sodium monobromoacetate.

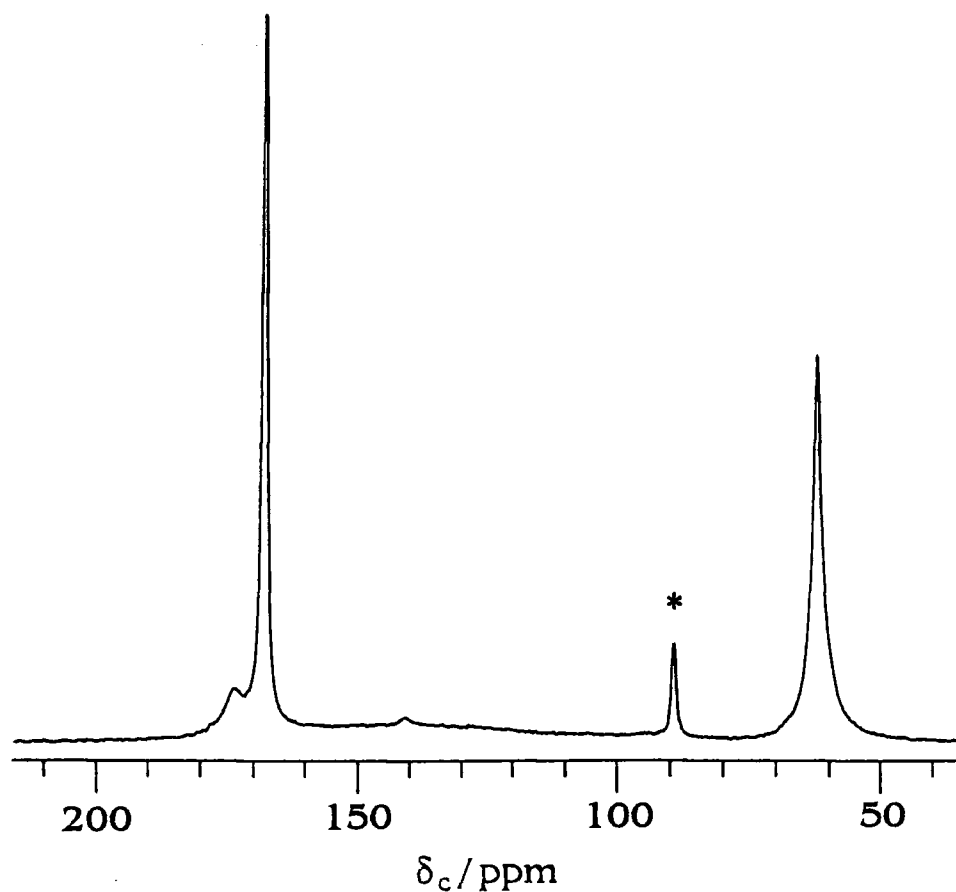


Figure 10.5.1 50.33 MHz ^{13}C CP/MAS spectrum of sodium monobromoacetate. Operating conditions: Spectral width 20 kHz; pulse duration 4.8 μs ; contact time 2.0 ms; recycle delay 5 s; number of transients 12260; spinning rate 4 kHz. The peak marked with an asterisk is a spinning sideband, and the small resonance at 174.0 ppm is thought to arise from a small impurity of the free acid.

The signal from the C-Br carbon is located at 62.8 ppm, and displays a Lorentzian lineshape having a linewidth of approximately 90 Hz. The rise in the baseline centred around approximately 140 ppm is attributed to background signals arising from the probe/stator.

10.5.2 1-Bromoadamantane

The 50.33 MHz ^{13}C CP/MAS spectrum of 1-bromoadamantane is shown in figure 10.5.2. Again, this compound contains few inequivalent carbon nuclei and should give rise to an uncluttered spectrum.

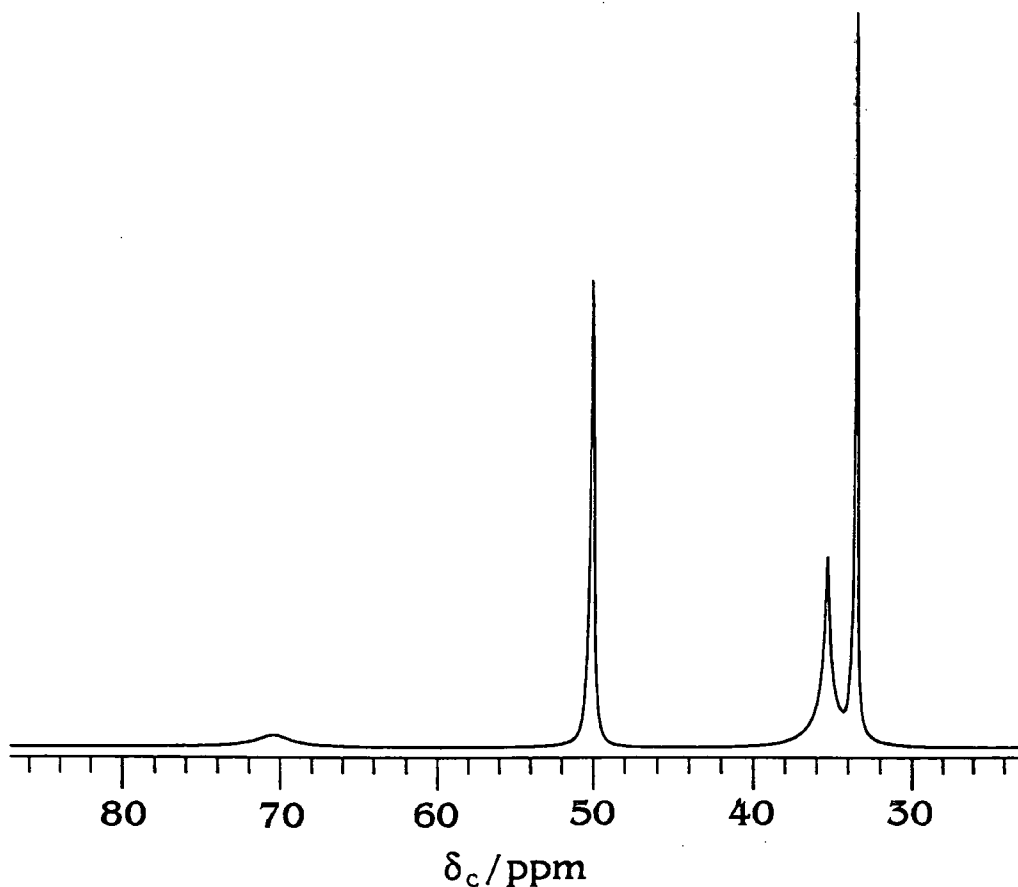


Figure 10.5.2 50.33 MHz ^{13}C CP/MAS spectrum of 1-bromoadamantane. Operating conditions: Spectral width 20 kHz; pulse duration 4.0 μs ; contact time 5.0 ms; recycle delay 20 s; number of transients 2848; spinning rate 4 kHz.

Once again the C-Br resonance at 70.4 ppm is a Lorentzian lineshape, possessing a width at half height of 120 Hz. This resonance has a much lower apparent intensity than the peak from the C-Br carbon in sodium bromoacetate, but this is only a consequence of the increased number of equivalent carbon nuclei in 1-bromoadamantane.

It is surmised that in both of these compounds self-decoupling effects are the cause for the breakdown of the expected multiplets. In both compounds it is impossible to know whether the phenomenon is due to a fast quadrupole spin-lattice relaxation caused by rapid three-site jumps around the C-C bond in the case of the

bromoacetate and by an overall molecular motion in the case of 1-bromoadamantane, in much the same way as was observed for sodium trichloroacetate, or by motional averaging of the relevant tensors, since linewidths are broad.

10.6 Iodinated Compounds

As was mentioned in the introduction at the start of this chapter to date no iodinated compounds have been identified which give rise to the phenomenon of (^{13}C , ^{127}I) residual dipolar coupling. The iodine nucleus possesses spin quantum number $5/2$, which means that if residual dipolar coupling effects were apparent we would expect to see a sextet of lines making up the predicted multiplet. The ^{13}C CP/MAS spectrum of sodium iodoacetate is shown in figure 10.6.1.

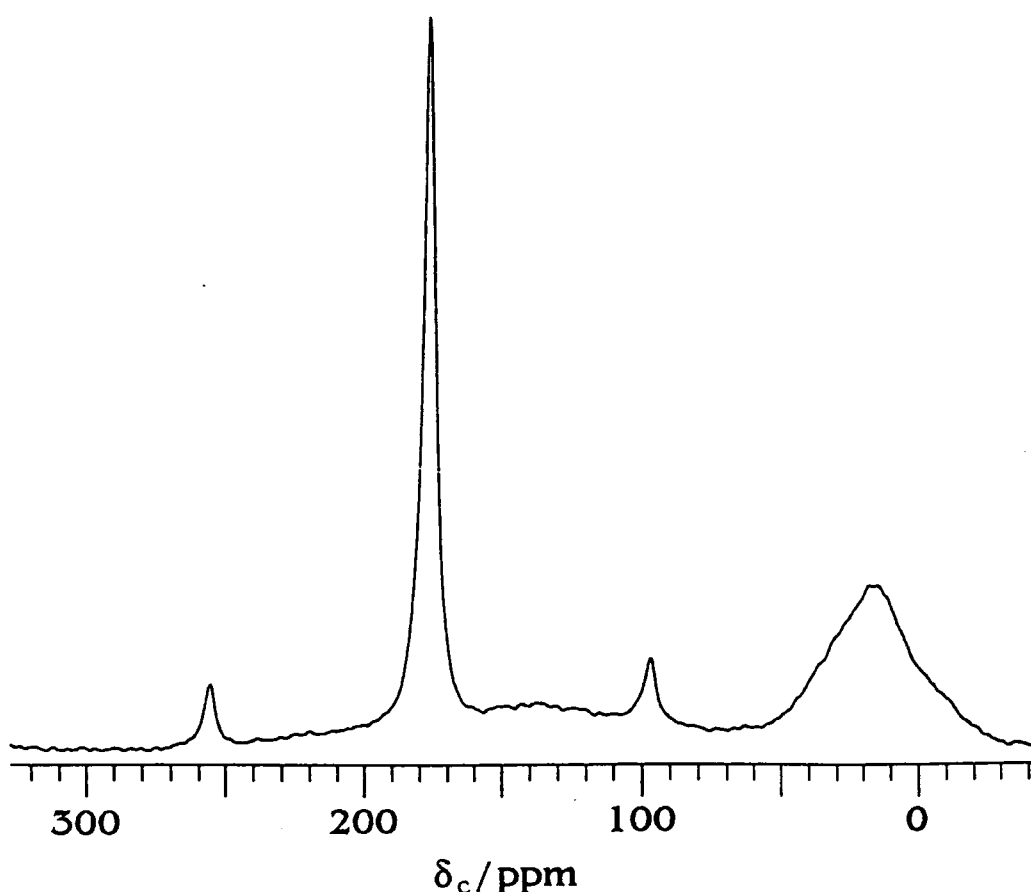


Figure 10.6.1 50.33 MHz ^{13}C CP/MAS spectrum of sodium monoiodoacetate. Operating conditions: Spectral width 20 kHz; pulse duration 4.8 μs ; contact time 2.0 ms; recycle delay 5 s; number of transients 2812; spinning rate 4 kHz.

The resonance from the C-I carbon appears not as an asymmetric hextet, but as a very broad non-Lorentzian signal at 18.2 ppm, with a frequency spread of greater than *ca.* 2 kHz. A similar shape of C-I signal was obtained from a ^{13}C CP/MAS spectrum of 1,4-diiodobenzene. It is known that the value of χ for ^{127}I is of the order of 1800 MHz⁹ and that $|J(^{13}\text{C}, ^{127}\text{I})|$ for iodobenzene is 145 Hz.⁴ A typical value for the C-I bond distance is 2.095 Å,¹⁰ which equates to a dipolar coupling constant D , of 0.66 kHz. As was evident in spectra of sodium trichloroacetate and sodium monobromoacetate it is likely that fast quadrupolar relaxation of the iodine nucleus is causing a breakdown of residual dipolar coupling. This effect has already been studied for the ^{13}C , ^{127}I spin-pair in trans-diiodoethylene.¹¹

One interesting facet of the spectrum of sodium monoiodoacetate is that self-decoupling effects appear to be less severe than they were for the corresponding bromo- compound. The C-I resonance is far broader than the analogous C-Br signal. This is surprising given the fact that the quadrupole coupling constant for ^{127}I is some three times that seen for $^{79,81}\text{Br}$. It may be that this is a reflection of slower rotation of the CH_2I group compared to the CH_2Br group as a consequence of steric effects.

10.7 Conclusions

It has been shown that in contrast to the case of (^{13}C , $^{35,37}\text{Cl}$) residual dipolar coupling, where signals in the ^{13}C CP/MAS spectra of sodium chloroacetate were seen to adopt the form of a symmetric doublet or 2:1:1 asymmetric triplet depending on the static field strength, the effects of (^{13}C , $^{79,81}\text{Br}$) residual dipolar coupling result in asymmetric quartets for the C-Br signals at both 4.7 T and 7.05 T. This reflects the larger magnitude of the quadrupole coupling constant for the two bromine isotopes (~ 500 MHz) compared to the two chlorine isotopes (~ 60 MHz) and the fact that a significant (^{13}C , $^{79,81}\text{Br}$) isotropic J -coupling exists. Furthermore, the bunching of lines at low frequency in ^{13}C CP/MAS spectra of brominated compounds is indicative of a reversal in sign of the quadrupole coupling constant compared to

chlorine (negative for $^{35,37}\text{Cl}$, positive for $^{79,81}\text{Br}$). The application of inverse first-order perturbation theory to the case of 1,4-dibromobenzene can result in predictions of line positions displaying good agreement with the experimental results, and serves as an indication of the increased importance of ΔJ effects for the ^{13}C , $^{79,81}\text{Br}$ spin-pair compared to the ^{13}C , $^{35,37}\text{Cl}$ spin-pair. Evaluation of the (^{13}C , ^{79}Br) isotropic indirect coupling constant is now possible from 'best-fit' methods of data analysis along with determination of its sign, leading to estimations of the elusive parameter ΔJ .

Similar lineshapes are adopted by the ^{13}C signals from carbon nuclei directly bonded to bromine nuclei in CP/MAS spectra of more highly brominated benzenes and 4-bromo-3,5-dimethylpyrazole, which indicates similar values of the relevant parameters for these compounds. For the former compounds lineshape simulations have been carried out using exact theory, and these simulations have displayed a close resemblance to experimentally recorded spectra. They have been carried out taking into consideration a number of remote interactions, which have been shown to be of increased importance for these more highly brominated benzenes, especially 1,2,4,5-tetrabromobenzene and hexabromobenzene. In some cases, such as 1,4-dibromobenzene, where remote interactions are weak and no discernible improvement in fit is observed between experimental and simulated bandshapes when the remote interactions are included explicitly in the simulation, their effects can be accounted for by the application of a Gaussian linebroadening factor. However, in other cases (e.g. 1,2,4,5-tetrabromobenzene) significantly better agreement between experimental and simulated bandshapes is obtained when the effects of remote interactions are accounted for in the simulation rather than by subsuming their effects into a Gaussian broadening factor. In the case of 1,2,4,5-tetrabromobenzene this can be traced to the influence of a dominant remote interaction with the bromine nucleus in the *ortho* position.

While the results presented in this chapter have focused on the assessment of the magnitudes and signs of the relevant fundamental NMR parameters for compounds of known structure, it is easy to envisage that conversely, in principle, a

prior knowledge of the values of these fundamental parameters could lead to a determination of molecular structure. However, a pre-requisite to such structure determination is a knowledge of ΔJ , and given its inherent inaccessibility it is doubtful whether such feats would be possible. Unfortunately, to date no compounds have yet been identified that display long-range residual dipolar coupling effects for the ^{13}C , $^{79,81}\text{Br}$ spin-pair.

All attempts to observe residual dipolar coupling for the ^{13}C , ^{127}I spin-pair have been blighted by the willingness of the iodine nucleus to undergo self-decoupling due to fast quadrupole relaxation.

10.8 Acknowledgements

Special thanks go to Prof. A. C. Olivieri for the use of his theories and computer bandshape simulation program (ANYCHI), and to Prof. K. M. Harris and Dr. A. E. Aliev who carried out the spectral simulations and calculations pertaining to the strengths of remote interactions in brominated benzenes presented in this chapter.

References

1. P. Bucci, P. Cecchi and A. Colligani, *J. Am. Chem. Soc.* **86**, 2513 (1963).
2. P. Z. Pyykko, *Z. Naturforsch., Teil A* **47**, 189 (1992).
3. R. H. Newman, *J. Magn. Reson.*, **86**, 176 (1990) and references cited therein.
4. V. Mlynárik, *Prog. Nucl. Magn. Reson. Spectrosc.* **18**, 277 (1986).
5. C. J. Jameson, in *Multinuclear NMR*, edited by J. Mason, Chapt. 4. Plenum Press, New York (1987).
6. U. Croatto and S. Bezzi, *Gazz. Chim. Ital.* **72**, 318 (1942).
7. A. E. Aliev, K. D. M. Harris, R. K. Harris, S. A. Carss and A. C. Olivieri, *J. Chem. Soc. Faraday Trans.* (in press).
8. M. K. Ehlert, S. J. Rettig, A. Storr, R. C. thompson and J. Trotter, *Can. J. Chem.* **70**, 2160 (1992).
9. G. K. Semin, S. I. Gushchin, V. I. Stanko, E. V. Bryukhova and N. G. Iroshnikova, *Dokl. Akad. Nauk SSSR*, **281**, 1126 (1985).
10. F. H. Allen, O. Kennard, D. G. Watson, L. Brammer, A. G. Orpen and R. Taylor, *J. Chem. Soc., Perkin Trans. 2*, S1 (1987).
11. H. W. Speiss, U. Haeberlen, and H. Zimmerman, *J. Magn. Reson.* **25**, 55 (1977).

Appendix

The Board of Studies in Chemistry at Durham University requires that each postgraduate research thesis contains details of:

- (i) All research conferences attended and papers presented by the author during the authors residence as a postgraduate student;
- (ii) All publications accepted, submitted or in preparation;
- (iii) Any period of work away from the Board's laboratories;
- (iv) All research colloquia, research seminars and lectures arranged by the Department of Chemistry.

(i) Papers Presented and Research Conferences Attended

Oral Presentations

High-resolution Fluorine-19 Spectra of Organic Solids, Royal Society of Chemistry's Autumn Meeting, Pre-doctoral Symposium, University of Sheffield, 5 September 1995.

High-resolution Fluorine-19 Spectra of Organic Solids, Royal Society of Chemistry's 12th International Meeting on NMR Spectroscopy, UMIST, Manchester, 2-7 July 1995.

Solid-state ^{19}F NMR of Proton-containing Solids, Durham University Third Year Graduate Colloquia, 10 May 1995.

Solid-state ^{19}F NMR of Proton-containing Solids, North-East Universities Postgraduate Chemistry Symposium 1995, University of Durham, 5 April 1995.

Poster Presentations

*Effects of (^{13}C , Cl) and (^{13}C , Br) Interactions on Solid-state ^{13}C NMR Spectra, ISMAR, Sydney, July 1995.

Effects of (^{13}C , Cl) and (^{13}C , Br) Interactions on Solid-state ^{13}C NMR Spectra, Royal Society of Chemistry's 12th International Meeting on NMR Spectroscopy, UMIST, Manchester, 2-7 July 1995.

High-resolution Fluorine-19 Spectra of Organic Solids, 36th Experimental Nuclear Magnetic Resonance Conference, Marriott Copley Place, Boston MA (USA) 26-30 March 1995.

Solid-state NMR Investigations of Residual Dipolar Coupling and Scalar Coupling in Carbon-Halogen Systems, 36th Experimental Nuclear Magnetic Resonance Conference, Marriott Copley Place, Boston MA (USA) 26-30 March 1995.

*Residual Dipolar Effects on ^{13}C MAS Spectra Arising From Halogen Nuclei, 35th Experimental Nuclear Magnetic Resonance Conference, Asilomar, CA, 11-14 April 1994.

Residual Dipolar Effects on ^{13}C MAS Spectra Arising From Halogen Nuclei, ICI Poster Competition, University of Durham, December 1993.

* Presented by Prof. R.K. Harris.

(ii) Publications

Carbon-13 NMR Investigations of Three Fluorinated Steroids,
S. A. Carss, R. K. Harris and R. A. Fletton, *Magn. Reson. Chem.*, **33**, 501 (1995).

High-resolution Fluorine-19 NMR Spectra of Solid Fluorinated Organic Compounds,
S. A. Carss, R. K. Harris, P. Holstein, B. J. Say and R. A. Fletton, *J. Chem. Soc., Chem. Commun.*, 2407 (1994).

^{19}F NMR of Proton Containing Solids,
S. A. Carss, U. Scheler, R. K. Harris, P. Holstein and R. A. Fletton, *Magn. Reson. Chem.*, (in press).

The Use of a ^1H - ^{19}F Double-resonance High-speed MAS Probe,
U. Scheler, P. Holstein, S. A. Carss and R. K. Harris, *Chemagnetics Application Note* (May 1995).

High-resolution Fluorine-19 Solid-state NMR of Materials Containing Both Fluorine and Hydrogen,
R. K. Harris, S. A. Carss, R. D. Chambers, P. Holstein, A. P. Minoja and U. Scheler, *Bull. Magn. Reson.*, (in press).

Effects of $^{35}\text{Cl}/^{37}\text{Cl}$, ^{13}C Residual Dipolar Coupling on the Variable-temperature ^{13}C CP/MAS NMR Spectra of Solid, Chlorinated Sodium Acetates,
S. H. Alarcon, A. C. Olivieri, S. A. Carss and R. K. Harris, *Angew. Chem. Int. Ed. Engl.*, **33**(15/16), 1624 (1994).

Residual Dipolar ($^{35,37}\text{Cl}$, ^{13}C) Coupling in Solid Sodium Chloroacetates: A Combined Variable-temperature ^{35}Cl NQR and Variable-field ^{13}C MAS NMR study,
S. H. Alarcon, A. C. Olivieri, S. A. Carss, R. K. Harris, M. Zuriaga and G. Monti,
Magn. Reson. Chem., (in press).

$^{79/81}\text{Br}$ Effects in the High-resolution ^{13}C NMR Spectra of Solid Bromoaromatic Compounds: Dipolar and Indirect ($^{79/81}\text{Br}$, ^{13}C) Interactions Studied by 'Inverse' First-order Perturbation Theory,
S. H. Alarcon, A. C. Olivieri, S. A. Carss and R. K. Harris, *Magn. Reson. Chem.*, **33**, 603 (1995).

Second-order Quadrupolar Effects for Directly Bonded and Remote ^{13}C - $^{79/81}\text{Br}$ Spin Pairs in High-Resolution ^{13}C NMR Spectra of Solids,
A. E. Aliev, K. D. M. Harris, R. K. Harris, S. A. Carss and A. C. Olivieri, *J. Chem. Soc., Faraday Trans.*, **91**, (1995) (in press).

(iii) Research Conducted Outside the Department

One Week's Research at Glaxo Research and Development Ltd., Greenford Road Greenford, 26 February - 2 March 1993.

(iv) Colloquia, Seminars and Lectures Given by Invited Speakers

1992

- October 15 Dr. M. Glazer, Oxford University, & Dr. S. Tarling, Birkbeck College, London
It Pays To Be British! The Chemists Role as an Expert Witness in Patent Litigation.
- October 20 Dr. H. E. Bryndza, Du Pont Central Research
Synthesis, Reactions and Thermochemistry of Metal (Alkyl) Cyanide Complexes and Their impact on Olefin Hydrocyanation Catalysis
- October 22 *Prof. A. Davies, University College London
The Ingold-Albert Lecture. The Behaviour of Hydrogen as a Pseudometal
- October 28 *Dr. J. K. Cockcroft, University of Durham
Recent Developments in Powder Diffraction
- October 29 Dr. J. Emsley, Imperial College London
The Shocking History of Phosphorus

- November 4 Dr. T. P. Kee, University of Leeds
Synthesis and Co-ordination Chemistry of Silylated Phosphites
- November 5 *Dr. C. J. Ludman, University of Durham
Explosions, A Demonstration Lecture
- November 11 Prof. D. Robins, Glasgow University
Pyrrolizidine Alkaloids: Biological Activity, Biosynthesis and Benefits
- November 12 Prof. M. R. Truter, University College, London
Luck and Logic in Host-Guest Chemistry
- November 18 Dr. R. Nix, Queen Mary College, London
Characterisation of Heterogeneous Catalysts
- November 25 Prof. Y. Vallee, University of Caen
Reactive thiocarbonyl Compounds
- November 25 Prof. L. D. Quin, University of Massachusetts, Amherst
Fragmentation of Phosphorus Heterocycles as a Route to Phosphoryl
Species with Uncommon Bonding
- November 26 Dr. D. Humber, Glaxo Greenford
AIDS- The Development of a Novel Series of Inhibitors of HIV
- December 2 Prof. A. F. Hegarty, University College Dublin
Highly Reactive Enols Stabilised by Steric Protection
- December 2 Dr. R. A. Aitken, University of St. Andrews
The Versatile Cycloaddition of $\text{Bu}_3\text{P} \cdot \text{CS}_2$
- December 3 *Prof. P. Edwards, Birmingham University
The SCI Lecture: What is Metal?
- December 9 *Dr. A. N. Burgess, ICI Runcorn
The structure of Perfluorinated Inonomer Membranes
- 1993
- January 20 Dr. D. C. Clary, University of Cambridge
Energy Flow in Chemical Reactions
- January 21 *Prof. L. Hall, Cambridge
NMR- Window to the Human Body
- January 27 Dr. W. Kerr, University of Strathclyde
Development of the Pauson-Khand Annulation Reaction:
Organocobalt Mediated Synthesis of Natural and Unnatural Products

- January 28 *Prof. J. Mann, University of Reading
Murder, Magic and Medicine
- February 3 Prof. M. S. Roberts, University of Exeter
Enzymes in Organic Synthesis
- February 10 *Dr. D. Gillies, University of Surrey
NMR and Molecular Motion in Solution
- February 11 Prof. S. Knox, Bristol University
The Tiden Lecture: Organic Chemistry at Polynuclear Metal Centres
- February 17 Dr. W. R. Kemmitt, University of Leicester
Oxatrimethylenemethane Metal Complexes
- February 18 Dr. I. Fraser, ICI Wilton
Reactive Processing of Composite Materials
- February 22 *Prof. D. M. Grant, University of Utah
Single Crystals, Molecular Structure and Chemical-Shift Anisotropy
- February 24 Prof. C. J. M. Stirling, University of Sheffield
Chemistry on the Flat Reactivity of Ordered Systems
- March 10 Dr. P. K. Baker, University College of North Wales, Bangor
'Chemistry of Highly Versatile 7-Coordinate Complexes'
- March 11 *Dr. R. A. Y. Jones, University of East Anglia
The Chemistry of Wine Making
- March 17 Dr. R. J. K. Taylor, University of East Anglia
Adventures in Natural Product Synthesis
- March 24 Prof. I. O. Sutherland, University of Liverpool
Chromogenic Reagents for Cations
- May 13 *Prof. J. A. Pople, Carnegie-Mellon University, Pittsburgh
The Boys-Rahman Lecture: Applications of Molecular Orbital Theory
- May 21 Prof. L. Weber, University of Bielefeld
Metallo-phospha Alkenes as Synthons in Organometallic Chemistry
- June 1 Prof. J. P. Konopelski, University of California Santa Cruz
Synthetic Adventures with Enantiomerically Pure Acetals
- June 2 Prof. F. Ciardelli, University of Pisa
Chiral Discrimination in the Stereospecific Polymerisation of Alpha Olefins

- June 7 Prof. R. S. Stein, University of Massachusetts
Scattering Studies of Crystalline and Liquid Crystalline Polymers
- June 16 Prof. A. K. Covington, University of Newcastle
Use of Ion Selective Electrodes as Detectors in Ion Chromatography
- June 17 Prof. O. F. Nielsen, H. C. Ørsted Institute, University of Copenhagen
Low-frequency IR- and Raman Studies of Hydrogen Bonded Liquids
- September 13 Dr. A. D. Schluter, Freie Universitat, Berlin, Germany
Synthesis and Characterisation of Molecular Rods and Ribbons
- September 13 Dr. K. J. Wynne, Office of Naval Research, Washington
Polymer Surface Design for Minimal Adhesion
- September 14 Prof. J. M. DeSimone, University of North Carolina
Homogeneous and Heterogeneous Polymerisations in Environmentally
Responsible Carbon Dioxide
- September 28 Prof. H. Ila, North Eastern Hill University, India
Synthetic Strategies for Cyclopentanoids via Oxoketene Dithioacetals
- October 4 Prof. F. J. Feher, University of California, Irvine
Bridging the Gap Between Surfaces and Solution with Sessilquioxanes
- October 14 Dr. P. Hubberstey, University of Nottingham
Alkali Metals: Alchemist's Nightmare, Biochemist's Puzzle and
Technologist's Dream
- October 20 Dr. P. Quayle, University of Manchester
Aspects of aqueous ROMP Chemistry
- October 21 Prof. R. Adams, University of South Carolina
Chemistry of Metal Carbonyl Cluster Complexes: Development of
Cluster Based Alkyne Hydrogenation Catalysts
- October 27 *Dr. R. A. L. Jones, Cavendish Laboratory, Cambridge
Perambulating Polymers
- November 10 *Prof. M. N. R. Ashfold, University of Bristol
High Resolution Photofragment Translational Spectroscopy: A New
Way to Watch Photodissociation
- November 17 *Dr. A. Parker, Rutherford Appleton Laboratory, Didcot
Applications of Time Resolved Resonance Raman Spectroscopy to
Chemical and Biochemical Problems
- November 24 Dr. P. G. Bruce, University of St. Andrews
Structure and Properties of Inorganic Solids and Polymers

- November 25 *Dr. R. P. Wayne, University of Oxford
The Origin and Evolution of the Atmosphere
- December 1 Prof. M. A. McKervey, Queen's University, Belfast
Synthesis and Applications of Chemically Modified Calixarenes
- December 8 Prof. O. Meth-Cohn, University of Sunderland
Friedel's Folly Revisited- A Super Way to Fused Pyridines
- December 16 Prof. R. F. Hudson, University of Kent
Close Encounters of the Second Kind
- 1994
- January 26 *Prof. J. Evans, University of Southampton
Shining Light on Catalysts
- February 2 *Dr. A. Masters, University of Manchester
Modelling Water Without Using Pair Potentials
- February 9 Prof. D. Young, University of Sussex
Chemical and Biological Studies on the Coenzyme Tetrahydrofolic Acid
- February 16 Prof. K. P. Theopold, University of Delaware
Paramagnetic Chromium Alkyls: Synthesis and Reactivity
- February 23 Prof. P. M. Maitlis, University of Sheffield
Across the Border: From Homogeneous to Heterogeneous Catalysis
- March 2 Dr. C. Hunter, University of Sheffield
Noncovalent Interaction between Aromatic Molecules
- March 9 *Prof. R. Wilkinson, Loughborough University of Technology
Nanosecond and Picosecond Laser Flash Photolysis
- March 10 Prof. S. V. Ley, University of Cambridge
New Methods for Organic Synthesis
- March 25 Dr. J. Dilworth, University of Essex
Technetium and Rhenium Compounds with Applications as Imaging Agents
- April 28 *Prof. R. J. Gillespie, McMaster University, Canada
The Molecular Structure of some Metal Fluorides and Oxofluorides:
Apparent Exceptions to the VSEPR Model

- May 12 Prof. D. A. Humphreys, McMaster University, Canada
Bringing Knowledge to Life
- October 5 *Prof. N. L. Owen, Brigham Young University, Utah
Determining Molecular Structure-The INADEQUATE NMR Way
- October 19 Prof. N. Bartlett, University of California
Some Aspects of (AgII) and (AgIII) Chemistry
- October 26 *Dr. G. Rumbles, Imperial College
Real or Imaginary 3rd Order Non-Linear Optical Materials
- November 2 Dr. P. G. Edwards, University of Wales, Cardiff
The Manipulation of Electronic and Structural Diversity in Metal
Complexes - New Ligands for New Properties
- November 9 Dr. G. Hogarth, University College, London
New Vistas in Metal Imido Chemistry
- November 16 Prof. M. Page, University of Huddersfield
Four Membered Rings and B-Lactamase
- November 23 Dr. J. Williams, University of Loughborough
New Approaches to Asymmetric Catalysis
- November 30 Prof. P. Parsons, University of Reading
Applications of Tandem Reactions in Organic Synthesis
- December 7 *Prof. D. Briggs, ICI and University of Durham
Surface Mass Spectrometry
- 1995
- January 25 Dr. D. A. Roberts, Zeneca Pharmaceuticals
The Design and Synthesis of Inhibitors of the Renin-Angiotensin
System
- February 1 *Dr. T. Cosgrove, Bristol University
Polymers do it at Interfaces
- February 8 Dr. D. O'Hare, Oxford University
Synthesis and Solid State Properties of Poly- Oligo- and Multidecker
Metallocenes
- March 1 Dr. M. Rosseinsky, Oxford University
Fullerene Intercalation Chemistry

April 26 Dr. M. Schroder, University of Edinburgh
Redox Active Macrocyclic Complexes: Rings, Stacks and Liquid
Crystals

May 24 Dr. P. Beer, Oxford University
Anion Complexation Chemistry

* Indicates lectures attended.

